

# Loop Formulation in Low Dimensional Supersymmetric Models on the Lattice

Inauguraldissertation  
der Philosophisch-naturwissenschaftlichen Fakultät  
der Universität Bern

vorgelegt von  
**Kyle Steinhauer**  
von Riggisberg BE

2014

Leiter der Arbeit:

**Prof. Dr. Urs Wenger**

Albert Einstein Center for Fundamental Physics  
Institut für theoretische Physik, Universität Bern



# Loop Formulation in Low Dimensional Supersymmetric Models on the Lattice

Inauguraldissertation  
der Philosophisch-naturwissenschaftlichen Fakultät  
der Universität Bern

vorgelegt von  
**Kyle Steinhauer**  
von Riggisberg BE

2014

Leiter der Arbeit:  
**Prof. Dr. Urs Wenger**

Albert Einstein Center for Fundamental Physics  
Institut für theoretische Physik, Universität Bern

Von der Philosophisch-naturwissenschaftlichen Fakultät  
angenommen.

Bern, 13.8.2014

der Dekan:

Prof. Dr. Silvio Decurtins



## ABSTRACT

The spontaneous breakdown of supersymmetry in quantum field theories is a non-perturbative phenomenon of great interest. The fact that such theories have a vanishing Witten index makes straightforward numerical simulations suffer from a sign problem. The fermion loop and bosonic bond formulation allowed for a sign problem free simulation of supersymmetric quantum mechanics with a highly efficient Monte Carlo simulation by the so called worm algorithm. In this thesis we derive the fermion loop formulation for the two-dimensional  $\mathcal{N} = 1$  Wess-Zumino model. Analogously to the case of a free Majorana fermion we show that the sign of the fermion determinant is under perfect control and a worm algorithm is simulating the fermionic degrees of freedom with great success. This allows for a non-perturbative study of the model even in the phase where supersymmetry is spontaneously broken. We present results of the critical point of spontaneous supersymmetry breaking in the thermodynamic and continuum limit and investigate the mass spectrum which shows the Goldstino emerging as a massless mode in the supersymmetry-broken phase. We then follow the same procedure for the supersymmetric nonlinear  $O(N)$  sigma model. The fermion loop structure which is depending on the choice of  $N$  is discussed in detail. Since this model suffers from sign problems, results are only presented in the phase quenched scenario for  $N = 2$ . At last we consider the bond and loop formulation of supersymmetric matrix quantum mechanics that are obtained by dimensional reduction of  $d$ -dimensional super  $U(N)$  Yang-Mills theories. We show that the formulation allows for a separate investigation of different sectors of the partition function corresponding to the different number of fermions winding around the temporal direction. We combine the fermion loop formulation with a transfer matrix approach and present a method how transfer matrix elements can be efficiently calculated for large  $N$  in certain sectors.



# Contents

<b>Introduction</b>	<b>9</b>
<b>1. Loop formulation of a free Majorana fermion in two dimensions</b>	<b>15</b>
1.1. Continuum model . . . . .	15
1.2. Discretisation . . . . .	16
1.2.1. The lattice . . . . .	16
1.2.2. Lattice action . . . . .	17
1.3. Fermion loop formulation . . . . .	18
1.3.1. Wilson projectors . . . . .	18
1.3.2. Hopping Expansion . . . . .	19
1.4. Contributions to the partition function . . . . .	19
1.4.1. Loops . . . . .	19
1.4.2. Mass terms . . . . .	23
1.4.3. $Z$ in the loop formulation . . . . .	24
1.5. Correlation function . . . . .	24
1.6. The sign of a configuration . . . . .	25
1.6.1. Topological classes . . . . .	25
1.6.2. Partition function and boundary conditions . . . . .	26
1.7. Observables . . . . .	27
1.8. Worm algorithm . . . . .	28
1.8.1. Basic idea . . . . .	28
1.8.2. Algorithm for the free Majorana fermion . . . . .	29
1.8.3. Vertices in $Z$ . . . . .	30
1.8.4. Local updates . . . . .	31
<b>2. Boson bond formulation of <math>\phi^4</math>-theory</b>	<b>35</b>
2.1. Bond formulation of $\phi^4$ -model . . . . .	35
2.1.1. Correlation function . . . . .	36
2.2. Worm algorithm . . . . .	36
<b>3. <math>\mathcal{N} = 1</math> <math>D = 2</math> WESS-ZUMINO MODEL</b>	<b>39</b>
3.1. Motivation . . . . .	39
3.2. Continuum model . . . . .	40
3.2.1. Witten index . . . . .	42
3.2.2. $\mathbb{Z}_2$ and supersymmetry . . . . .	43
3.3. Discretisation . . . . .	45
3.3.1. Supersymmetric continuum limit . . . . .	45
3.3.2. Bosonic lattice action . . . . .	46

3.3.3.	Fermionic lattice action . . . . .	48
3.4.	Renormalisation . . . . .	49
3.5.	Hopping expansion . . . . .	50
3.5.1.	Boson bond formulation . . . . .	50
3.5.2.	Fermion loop expansion . . . . .	52
3.6.	Critical point . . . . .	54
3.6.1.	Dimensionless coupling and continuum limit . . . . .	54
3.6.2.	Towards simulation . . . . .	55
3.6.3.	The bosonic field and the $\mathbb{Z}_2$ symmetry . . . . .	56
3.6.4.	Partition function $Z_{\mathcal{L}_{ij}}$ and $\mathbb{Z}_2$ symmetry . . . . .	58
3.6.5.	Witten index . . . . .	60
3.6.6.	Determination of the critical coupling . . . . .	61
3.6.7.	Thermodynamic limit . . . . .	66
3.6.8.	Continuum limit . . . . .	68
3.6.9.	Chiral condensate . . . . .	70
3.6.10.	A Ward identity of supersymmetry . . . . .	70
3.7.	Masses in the system . . . . .	74
3.7.1.	Supersymmetric phase . . . . .	74
3.7.2.	Supersymmetry broken phase . . . . .	76
3.7.3.	Goldstino and Goldstino-amplitude . . . . .	80
3.7.4.	Thermodynamic limit of lowest the mass states . . . . .	82
3.7.5.	Continuum limit of masses at constant renormalised coupling $f^R$ . . . . .	84
3.8.	Conclusion and outlook . . . . .	88
<b>4.</b>	<b>Supersymmetric Nonlinear <math>O(N)</math> sigma Model</b>	<b>91</b>
4.1.	Motivation . . . . .	91
4.2.	Continuum model . . . . .	92
4.3.	Partition function and constraints . . . . .	93
4.4.	Discretisation . . . . .	95
4.4.1.	Partition function and constraints on the lattice . . . . .	95
4.4.2.	Lattice derivative . . . . .	95
4.4.3.	Bosonic lattice action . . . . .	96
4.4.4.	Fermionic lattice action . . . . .	97
4.5.	Hopping expansion . . . . .	98
4.5.1.	The constraint $\phi\psi = 0$ . . . . .	99
4.5.2.	Bosonic bond formulation . . . . .	99
4.5.3.	Fermion loop formulation . . . . .	101
4.6.	Contributions to the partition function . . . . .	106
4.6.1.	Fermionic contributions for $O(2)$ . . . . .	107
4.6.2.	Fermionic contributions for $O(3)$ . . . . .	108
4.6.3.	Bosonic contribution from $\phi\psi = 0$ for $O(2)$ . . . . .	109
4.6.4.	Bosonic contribution from $\phi\psi = 0$ for $O(3)$ . . . . .	110
4.6.5.	$Z$ in the bond/loop formulation for $O(2)$ . . . . .	110
4.6.6.	$Z$ in the bond/loop formulation for $O(3)$ . . . . .	111



4.7. Graphical Representation for small $N$ . . . . .	111
4.7.1. $N = 2$ . . . . .	112
4.7.2. $N = 3$ . . . . .	113
4.8. Partition function and boundary conditions . . . . .	114
4.9. Observables . . . . .	115
4.10. Sign problem in the bond/loop formulation . . . . .	116
4.11. Flavour integration . . . . .	117
4.12. Numerical results for $N=2$ . . . . .	117
4.12.1. Fermionic constraints and sings . . . . .	118
4.12.2. Critical point . . . . .	120
4.12.3. Masses . . . . .	123
4.12.4. Uncertain phase diagram . . . . .	126
4.13. Conclusion and outlook . . . . .	126
<b>5. Fermion sectors in Matrix-theory</b>	<b>129</b>
5.1. Motivation . . . . .	129
5.2. Continuum model . . . . .	130
5.2.1. Yang-Mills and adjoint fermion in $d$ dimensions . . . . .	130
5.2.2. Spin structure and SUSY . . . . .	131
5.2.3. Dimensional reduction . . . . .	131
5.3. Discretised $4d$ $\mathcal{N} = 1$ super Yang-Mills reduced to $1d$ . . . . .	134
5.3.1. Continuum model . . . . .	134
5.3.2. Lattice . . . . .	134
5.3.3. Boson lattice action . . . . .	135
5.3.4. Fermion lattice action . . . . .	136
5.4. Fermion loop formulation . . . . .	137
5.4.1. Hopping expansion . . . . .	138
5.4.2. Gauge link . . . . .	141
5.5. Fermion transfer matrix . . . . .	142
5.5.1. Basic idea . . . . .	143
5.5.2. Enlarging and generalising the toy model . . . . .	148
5.5.3. Transfer matrix of dimensionally reduced $4d$ $\mathcal{N} = 1$ super Yang-Mills	150
5.5.4. Including the gauge link . . . . .	152
5.6. Boson bond formulation . . . . .	154
5.7. Bond-Loop formulation . . . . .	155
5.8. Explicit calculations . . . . .	156
5.8.1. Explicit time slice interaction matrix for $SU(2)$ . . . . .	157
5.8.2. Zero fermions propagating in time . . . . .	158
5.8.3. One fermion propagating in time . . . . .	159
5.8.4. All fermions are propagating in time . . . . .	159
5.8.5. All but one fermions are propagating in time . . . . .	160
5.9. Conclusion and Outlook . . . . .	160
<b>Acknowledgement</b>	<b>163</b>

<b>A. Numerical data</b>	<b>165</b>
A.1. Ising-suszeptibility . . . . .	165
A.2. Binder cummulant . . . . .	166
<b>B. Monte Carlo</b>	<b>167</b>
B.1. Markov Chain . . . . .	167
B.2. Importance sampling . . . . .	168
B.3. Metropolis algorithm . . . . .	168
<b>C. Data and error analysis</b>	<b>169</b>
C.1. Correlated data . . . . .	169
C.2. Binning analysis . . . . .	170
C.3. Jackknife analysis . . . . .	170
C.4. Cumulative distribution . . . . .	171
C.5. Systematic error estimate . . . . .	171
C.6. Fitting correlated data . . . . .	173
<b>D. Grassmann integrals</b>	<b>175</b>
D.1. Grassmann variables calculus . . . . .	175
D.2. Delta function in a grassmann integral . . . . .	175
<b>E. Flavour integration in the supersymmetric nonlinear <math>O(2)</math> sigma model</b>	<b>177</b>
E.1. Flavour integrated partition function . . . . .	177
E.2. Two-point function . . . . .	179

# Introduction

Physics is the science of studying and analysing nature and all its phenomena. One field of physics is dealing with the smallest constituents of our universe which are commonly referred to as the elementary particles. The efforts in creating a mathematical framework that accommodates those particles and successfully describes their interactions among one another, led to what is nowadays known as the Standard Model of particle physics [1–3]. It is a quantum field theory that includes three fundamental forces observed in nature, the electromagnetic interaction, the weak interaction and the strong interaction. Despite the fact that the Standard Model can be celebrated as a very powerful theory with strong predictive power and for which also high precision tests<sup>1</sup> can be made, it fails explaining several fundamental observations. The theory of gravitation is for example not accommodated in the Standard Model. It does also not contain any suitable dark matter candidate, can not explain the observed expansion of the universe and does not account for the oscillating neutrino masses. On a technical basis the Standard Model suffers from the hierarchy problem [6, 7], which comes from the fact that the bare Higgs mass parameter<sup>2</sup> receives large quantum corrections from loop diagrams and therefore needs to be incredibly fine-tuned in order to create an effective mass compatible with the expected and now even experimentally confirmed mass of around 125 GeV [8, 9]. The hierarchy problem is also known as the naturalness problem or the fine-tuning problem. It becomes clear that a new theory needs to be constructed which describes the physics beyond the Standard Model while still performing equally well in explaining the phenomena the Standard Model already describes with great success.

One solution to solve many of the just mentioned problems is the introduction of a concept called supersymmetry which extends the symmetries of the Standard Model in a particular way.

In theoretical physics a quantity, this may be a physically measurable observable or a mathematical expression, is symmetric if it is unchanged after a corresponding symmetry transformation. There are many symmetries which are incorporated in mathematical models in order to successfully describe various phenomena. One of the most important symmetries in the Standard Model is the  $SU(3)_c \times SU(2)_L \times U(1)_Y$  gauge symmetry. The  $SU(3)_c$  group is for example shuffling the colour states of a quark flavour among themselves and the  $SU(2)_L$  is mixing the left handed weak doublets. Enforcing an additional symmetry in the Standard Model is highly restricted by the Coleman-Mandula no-go theorem [10]. However, there is one solution how to circumvent the no-go theorem and to

---

<sup>1</sup>Note that high precision tests are also used to search for new physics, e.g. the muon  $g - 2$  [4], low energy tests [5].

<sup>2</sup>The gauge bosons are protected from such corrections by local gauge symmetry and the fermions from chiral symmetry.

extend the Poincaré symmetry non-trivially. This can only be achieved by adding anti-commuting generators which are spinors themselves. Those generators are the generators of supersymmetry which exchanges integer spin particles, called bosons, and half-integer spin particles, called fermions, into one another. Supersymmetry is not only emerging somehow naturally from extending the Poincaré group but is also able to solve many of the problems that are encountered when solely relying on the Standard Model. It solves the hierarchy problem because the quantum corrections of the bosonic loops cancel exactly with the fermionic ones. Note that this is true for almost all ultraviolet divergences in many supersymmetric quantum field theories. Supersymmetry can further provide a dark matter candidate and is well suited for constructing grand unification models<sup>3</sup> [11]. Unlike any other internal symmetries of the Standard Model, supersymmetry is linked to space time transformations. After performing two successive supersymmetry transformations on a field, we obtain the same field evaluated at a different space time coordinate. What is then remarkable is that by imposing local supersymmetry we are forced to introduce additional fields that follow Einstein’s theory of general relativity. Such a theory is called supergravity.

Supersymmetry is therefore indeed one of the most promising concepts currently available to incorporate all the success of the Standard Model and offering a description for many beyond Standard Model phenomena.

Historically the idea of supersymmetry in quantum field theory was initialised by [12–15], which then led to the work of Wess and Zumino [16], who created four dimensional explicitly supersymmetric quantum field theories. The concept of supersymmetry arose afterwards in many other theories like supersymmetric gauge theories, superstring theories and supersymmetric sigma models. Concerning extensions of the Standard Model, the Minimally Supersymmetric Standard Model (MSSM<sup>4</sup>) made its way to the currently possibly most attractive candidate to explain beyond Standard Model physics by stabilising the weak scale, allowing for gauge coupling unification and providing a dark matter candidate.

Despite its mathematical beauty and its ability to free our current models from incompatibility with certain phenomena, supersymmetry is suffering from one big flaw. In a supersymmetric theory a particle has the same mass as its super-partner<sup>5</sup>, but this degeneracy of mass is not observed in nature. So if supersymmetry is a symmetry of a theory successfully describing our world, it must be spontaneously broken [18] at some energy scale. The spontaneous breakdown of a symmetry is in general a fundamental concept appearing already in the Standard Model, e.g. chiral symmetry breaking, Higgs-mechanism, which are experimentally confirmed. In the case of supersymmetry there exist different types of spontaneous supersymmetry breaking, but they all suffer from the fact that non of them are compatible with phenomenological observations<sup>6</sup>. This is why in order to stick to a phenomenologically compatible model, soft-breaking terms are added to the

---

<sup>3</sup>Theories that at high energy unify the electromagnetic, weak and strong interaction to one unified force.

<sup>4</sup>For more details see [17].

<sup>5</sup>This is because the momentum operator commutes with the supercharge. Applying a supercharge  $Q$  on a state leaves  $P_\mu P^\mu = m^2$  invariant.

<sup>6</sup>No Goldstino has been observed. There is also no charged scalar particle lighter than the electron.

MSSM. These break supersymmetry explicitly but let us still keep the cancellations of the quadratic divergent correction to the scalar mass and in general let us preserve most of the features that initially motivated supersymmetry. This scenario of softly broken supersymmetry in the MSSM is currently tested and searched for at the Large Hadron Collider.

Spontaneous symmetry breaking and other interesting phenomena are perturbatively not accessible. Euclidean lattice field theories<sup>7</sup> in combination with numerical simulations have shown to be a highly successful concept allowing non-perturbative access to physics of many interesting models, where the most important is surely quantum-chromo-dynamics, short QCD. Independent whether supersymmetry is indeed realised in nature at some higher energy scale or not, it remains highly interesting to study also supersymmetric theories non-perturbatively by using the lattice. In this way more can be learned about dynamical supersymmetry breaking and maybe even some predictions can be made about the soft-breaking terms in the MSSM. The desire to formulate a discretised version of a supersymmetric quantum field theory, and thereby also deliver a non-perturbative definition, immediately runs into complications. Already the Poincaré symmetry is broken by the lattice discretisation and since supersymmetry is an extension thereof, it is obvious that a discretisation also breaks supersymmetry. This becomes also clear when considering the anti-commutator of the supersymmetry charge operator with its adjoint which is proportional to the infinitesimal translation operator, but on the lattice there are no infinitesimal operators. Equivalently the Leibniz rule [20–22] does not hold for the lattice difference operator. The Poincaré symmetry however, is fully restored in the continuum limit as an accidental symmetry. This is due to the intact remnant subgroup of discrete rotations and finite translations on the lattice. For supersymmetry this is not the case and obtaining a supersymmetric continuum limit without generally being confronted with an enormous fine-tuning problem was and still is a diligently pursued task. However, a lot of work has been done on this topic, allowing us nowadays to investigate theories that have a supersymmetric continuum limit. In certain models for example, it is possible to simply add one counter term in order to restore supersymmetry in the continuum, e.g. super Yang-Mills theory with one supersymmetry in four dimensions. Other solutions for theories with more supersymmetries are based on the idea of preserving one or more supersymmetries on the lattice such that the others arise accidentally in the continuum. The two approaches following this idea are orbifolding methods and twisted formulations. For two neat summaries on lattice supersymmetry see [23, 24].

In numerical simulations of lattice field theories based on Monte Carlo methods we often encounter the so called sign problem. A sign problem is related to the fact that the numerical method fails to evaluate the integral (partition function) of a highly oscillating integrand (Boltzmannfactor) due the strong cancellation between negative and positive contributions which creates an actual signal that is lower than the precision of the method. This can sometimes be avoided by finding a suitable mathematical formulation or algorithm which is free of any, or only suffers mildly, of a sign problem. When considering numerical simulations of theories that allow for spontaneous supersymmetry

---

<sup>7</sup>For more details see [19]

breaking, the sign problem seems to arise inevitably due to the vanishing of the Witten index. If supersymmetry is broken spontaneously, the Goldstino [25] is causing additional problems in a straightforward numerical treatment<sup>8</sup>.

In this thesis we want to take a closer look at three different supersymmetric models in low dimensions in order to study many of the mentioned non-perturbative dynamics. We will lay special focus on establishing the loop formulation of the fermionic degrees of freedom in order to try to find a sign problem free formulation and to efficiently simulate the model using a so called worm or fermion open string algorithm. The loop formulation is based on the exact hopping expansion of the fermionic action and forms a natural decomposition of the partition function into bosonic and fermionic contributions. The worm algorithm is based on the work of Prokof'ev and Svistunov [26] which presented the idea of updating closed path configurations through the motion of end points of disconnected paths in classical statistical models. Based on this concept further work [27] showed that also relativistic fermions can be efficiently simulated in that way. This formulation already allowed for numerical investigations of supersymmetry quantum mechanics [28] and has found wide use in non-supersymmetric theories.

In a first chapter we will familiarise the reader with the basic idea of the fermion loop formulation and the worm algorithm. This will be done by using a simple example of a free Majorana fermion living on a two dimensional torus with Euclidean metric. In addition we present the boson bond formulation allowing for the also discussed worm algorithm for the boson fields. Afterwards we will discuss three models for which we will create the fermion loop formulation and for which we will also present numerical data. These models are investigated in this theses in the following way.

In the second chapter we consider the  $\mathcal{N} = 1$  two-dimensional Wess-Zumino model [16]. This model is of special interest since its Witten index [29] is zero, which allows for spontaneous supersymmetry breaking. A lot of effort [30–33] has been put into the research of the analytic properties of the model and even numerical results [34, 35] are already present that we can at least qualitatively compare with. We will use Wilson's discretisation for the fermion and also the boson in order to obtain a supersymmetric continuum limit without fine tuning [36]. The fermion loop formulation will allow us, analogously to the case of the free Majorana fermion in chapter one, to obtain perfect control of the sign of each configuration contributing to the partition function. A detailed analysis of the critical point and the mass spectrum is possible with a yet unseen precision in that model.

In the third chapter we investigate supersymmetric nonlinear  $O(N)$  sigma-models [37, 38] in two dimensions. Those models show many interesting features like asymptotic freedom (for  $N > 2$ ) and chiral symmetry breaking that leads to mass generation. These properties have already analytically been studied [39, 40] and specially for the  $N = 3$  case also numerically investigated [41]. We will again establish a fermion loop and boson bond formulation which is valid for arbitrary  $N$ . Unlike in chapter two, where we analysed the

---

<sup>8</sup>The Goldstino is the Goldstone particle(fermionic) arising due to the spontaneous breakdown of supersymmetry and creates a zero mode in the fermion matrix.

$\mathcal{N} = 1$   $D = 2$  Wess-Zumino model, the reformulation does not show to be free from any sign problems. We will highlight the difference that exist between  $N = 2$  and  $N > 2$  and will provide first results for  $N = 2$  in the phase quenched scenario.

In the fourth chapter we will consider supersymmetric Yang-Mills quantum mechanics. By dimensional reduction of all compactified spatial dimensions of a super  $U(N)$  Yang-Mills theory we will obtain a quantum mechanical system with one time like dimension. Models of this kind are interesting because in their large- $N$  limit they can be seen as low energy effective theories [42] describing a stack of  $N$  D-branes [43] in string theory. The strongly coupled large- $N$  limit might also describe weakly coupled super gravity via the AdS/CFT correspondence [44, 45]. We will discretise the time like dimension and use Wilson's discretisation for the fermionic degrees of freedom before deriving the fermion loop formulation. The fact that the partition function can be written as a product of transfer matrices can be combined with the fermion loop formulation. This will allow us to split up the partition function into sectors corresponding to contributions from configurations in which a different number of fermions are winding around the system. We will present first analytic results for a restricted choice of sectors for the model with 4 supercharges. What we present can easily be generalised to the more interesting model with 16 supercharges. Some first numerical investigations are ongoing [46], but are not part of this thesis.





# 1. Loop formulation of a free Majorana fermion in two dimensions

In this chapter we focus on a detailed explanation on how to reformulate the partition function of a free Majorana fermion, living on a two-dimensional lattice using Wilson fermions, in a way that the partition function becomes a sum over fermion loop configurations. This forms one of the basic concepts that will be used throughout this thesis and will in general be called the fermion loop formulation.

Additionally we explain what a worm algorithm is and show how to use it in the loop formulation of the free Majorana fermion. One of the main reasons why a reformulation in terms of fermion loops is desired is the fact that the loop formulation is mostly very amenable to the worm algorithm.

The chapter is structured as follows. First we introduce the continuum model, then we regulate the theory by discretising it with the lattice. We will use Wilson fermions to solve the doubling problem. After this the hopping expansion of the Boltzmann factor is calculated in order to express the partition function as a sum of closed fermion loop configurations. The weight of a fermion loop configuration contributing to the partition function will be calculated explicitly followed by a discussion of the overall sign of the contributions. After this we explain the basic concept of the worm algorithm and illustrate it in more detail for the free Majorana fermion.

## 1.1. Continuum model

The lagrangian density  $\mathcal{L}(x)$  for a Majorana particle, where the interaction terms are switched off, is

$$\mathcal{L}(x) = \frac{1}{2} \bar{\psi}(x) (\gamma^\mu \partial_\mu + m) \psi(x), \quad (1.1)$$

in two-dimensional Euclidean spacetime. The field  $\psi$  is a two component real Majorana spinor with entries  $\psi^\alpha$ , where  $\alpha = 1, 2$  is the Dirac index. The charge conjugation matrix arising in  $\bar{\psi} = \psi^T \mathcal{C}$  has the properties

$$\mathcal{C} \gamma_\mu \mathcal{C}^{-1} = -\gamma_\mu^T = -\gamma_\mu^*, \quad \mathcal{C}^\dagger = -\mathcal{C}^{-1} \quad \text{and} \quad \mathcal{C} = -\mathcal{C}^T, \quad (1.2)$$

where the Dirac-Gamma matrices  $\gamma_\mu$  satisfy the anti-commutation relation  $\{\gamma_\mu, \gamma_\nu\} = 2\delta_{\mu\nu} \mathbb{1}_{2 \times 2}$ . We choose a basis such that  $\gamma_0 = \sigma_1$ ,  $\gamma_1 = \sigma_3$  and the charge conjugation matrix is  $\mathcal{C} = -i\sigma_2$ . The explicit form of  $\sigma$ -matrices is

$$\sigma_1 = \begin{pmatrix} 0 & 1 \\ 1 & 0 \end{pmatrix}, \quad \sigma_2 = \begin{pmatrix} 0 & -i \\ i & 0 \end{pmatrix} \quad \text{and} \quad \sigma_3 = \begin{pmatrix} 1 & 0 \\ 0 & -1 \end{pmatrix}, \quad (1.3)$$

## 1. Loop formulation of a free Majorana fermion in two dimensions

Further we have  $\gamma_5 = i\gamma_0\gamma_1$  and denoted the bare mass of field with  $m$ . In order to obtain the action we will need to perform the integral over both dimensions

$$S(\psi) = \int dx_0 \int dx_1 \mathcal{L}[\psi(x)], \quad (1.4)$$

where we used  $x = (x_0, x_1)$ . When talking about the system at a finite temperature we refer to a finite temporal extent  $\beta$  of the first dimension, where  $\beta$  is the inverse temperature  $1/T$  if the fermions have anti-periodic boundary conditions in  $x_0$ . The partition function can be written as

$$Z = \int \mathcal{D}\psi e^{-S(\psi)}. \quad (1.5)$$

## 1.2. Discretisation

In this section we introduce the lattice which is functioning as a regulator of our just introduced quantum field theory of a free Majorana fermion. We discretise the continuum action using Wilson's derivative to account for the fermion doubling problem. This is a standard procedure and rich disquisitions on this exist in almost any text book on lattice field theory, e.g. [19].

### 1.2.1. The lattice

Let us introduce a lattice following closely common notational conventions from [19]. Consider a lattice  $\Lambda$  of extent  $L_0 \times L_1$  lattice spacings  $a$  which can be defined as

$$\Lambda = \{x = (x_0, x_1) \in a\mathbb{Z}^2 \mid 0 \leq x_\mu \leq a(L_\mu - 1)\}, \quad (1.6)$$

where  $\mu = 0, 1$ . The unit vector in dimensions  $\mu$  is denoted by  $\hat{\mu}$ . The integral over all spacetime points in the action is replaced by a sum

$$\int_0^\beta dx_0 \int dx_1 \rightarrow a^2 \sum_x, \quad (1.7)$$

where  $\beta = aL_0$  corresponds to the inverse temperature. A field variable defined in continuous spacetime to be  $f(x)$  will get replaced by a lattice field variable  $f_x$ , where the subscript denotes the lattice site. The measure in the partition function can then be defined by

$$\int \mathcal{D}\psi = \prod_{x,\alpha} \int d\psi_x^\alpha. \quad (1.8)$$

For a field variable defined on all sites of the lattice we can define the boundary conditions to be

$$\begin{aligned} \text{periodic:} \quad & f_{x+a\hat{\mu}L_\mu} = f_x \\ \text{anti-periodic:} \quad & f_{x+a\hat{\mu}L_\mu} = -f_x. \end{aligned}$$

For bosonic fields we will always stick to periodic boundary conditions whereas for the fermions we allow the anti-periodic possibility. This means introducing

$$\psi_{i,x+a\hat{\mu}L_\mu} = (-1)^{\alpha_\mu} \psi_{i,x}, \quad (1.9)$$

where we introduced  $\alpha_\mu$ , denoting if the boundary condition in direction of  $\mu$  is periodic  $\alpha_\mu = 0$  or anti-periodic  $\alpha_\mu = 1$ . In order to take care of the fermion doubling problem we will use the Wilson derivative

$$\hat{\partial}_\mu^{\mathcal{W}}(r) = \hat{\partial}_\mu^S - \frac{ra}{2} \Delta^{\mathcal{W}}, \quad (1.10)$$

in which we have the symmetric derivative

$$[\hat{\partial}_\mu^S]_{xy} = \frac{1}{2a}(\delta_{x+\hat{\mu},y} - \delta_{x-\hat{\mu},y}) \quad (1.11)$$

and the additional Wilson term

$$\Delta^{\mathcal{W}} = \frac{ra}{2} \sum_{\nu=0}^{d-1} \hat{\partial}_\nu^+ \hat{\partial}_\nu^-, \quad (1.12)$$

where  $\hat{\partial}_\nu^+$  is the forward derivative and  $\hat{\partial}_\nu^-$  is the backward derivative

$$[\hat{\partial}_\nu^+]_{xy} = \frac{1}{a}(\delta_{x+\hat{\nu},y} - \delta_{x,y}) \quad (1.13)$$

$$[\hat{\partial}_\nu^-]_{xy} = \frac{1}{a}(\delta_{x,y} - \delta_{x-\hat{\nu},y}). \quad (1.14)$$

The Wilson parameter  $r$  is in the interval  $0 < r \leq 1$  and for convenience we will in the following set  $r$  and  $a$  to one.

### 1.2.2. Lattice action

With this introduced concept we can now go ahead and write down the discretised action of our model in eq.(1.1) which is

$$\hat{S} = \frac{1}{2} \sum_x \psi_x^T \mathcal{C} D_{xy} \psi_y = \frac{1}{2} \sum_x \psi_x^T \mathcal{C} (\hat{\partial}^S - \Delta^{\mathcal{W}} + m)_{xy} \psi_y, \quad (1.15)$$

in which we have, when setting  $a$  and  $r$  to one,

$$\begin{aligned} (\hat{\partial}^S - \Delta^{\mathcal{W}})_{xy} &= \gamma^\mu [\hat{\partial}_\mu^S]_{xy} - \frac{1}{2} \sum_{\nu=0}^{d-1} [\hat{\partial}_\nu^+]_{xz} [\hat{\partial}_\nu^-]_{zy} + m \delta_{xy} \\ &= \frac{1}{2} \sum_\mu \gamma^\mu (\delta_{x+\hat{\mu},y} - \delta_{x-\hat{\mu},y}) - \frac{1}{2} \sum_\nu (\delta_{x+\hat{\nu},y} + \delta_{x-\hat{\nu},y} - 2\delta_{x,y}) + m \delta_{xy} \\ &= (2 + m) \delta_{x,y} - \frac{1}{2} \sum_\mu [(1 - \gamma^\mu) \delta_{x+\hat{\mu},y} + (1 + \gamma^\mu) \delta_{x-\hat{\mu},y}]. \end{aligned} \quad (1.16)$$

Note that here we omitted writing the Dirac indices  $D_{xy}^{\alpha\beta}$ , which give rise to the Dirac structure via  $\gamma_\mu^{\alpha\beta}$ . Writing down the full fermion action on the lattice then yields

$$\hat{S} = \frac{1}{2} \sum_x \left\{ M_x \psi_x^T \mathcal{C} \psi_x - \psi_x^T \mathcal{C} \sum_\mu \left[ \frac{1}{2} (1 - \gamma^\mu) \delta_{x+\hat{\mu},y} + \frac{1}{2} (1 + \gamma^\mu) \delta_{x-\hat{\mu},y} \right] \psi_y \right\}, \quad (1.17)$$

where the mass monomer term is  $M_x = (2 + m_x)$ , where the mass is actually not site dependent but we will keep this dependence for the ongoing calculations in order to illustrate that the following works just fine with a site dependent weight.

### 1.3. Fermion loop formulation

#### 1.3.1. Wilson projectors

After establishing the fermionic lattice action, let us introduce Wilson projectors

$$\mathcal{P}_{\pm\mu} = \frac{1}{2} (1 \mp \gamma_\mu) , \quad (1.18)$$

which satisfy the relations

$$\mathcal{P}_{\pm\mu} \mathcal{P}_{\pm\mu} = \mathcal{P}_{\pm\mu} , \quad (1.19)$$

$$\mathcal{P}_{+\mu} \mathcal{P}_{-\mu} = \mathcal{P}_{-\mu} \mathcal{P}_{+\mu} = 0. \quad (1.20)$$

Using these projectors we can rewrite the action above as

$$\hat{S}_F = \frac{1}{2} \sum_x \left\{ M_x \psi_x^T \mathcal{C} \psi_x - \psi_x^T \mathcal{C} \sum_\mu (\mathcal{P}_{+\mu} \psi_{x+\hat{\mu}} + \mathcal{P}_{-\mu} \psi_{x-\hat{\mu}}) \right\} . \quad (1.21)$$

In the following we will quickly show that the orientation of the hop is not important for Majorana fermions. This can be seen by considering

$$\psi_x^T \mathcal{C} \mathcal{P}_\mu \psi_{x+\mu} = - (\psi_x^T \mathcal{C} \mathcal{P}_{+\mu} \psi_{x+\hat{\mu}})^T \quad (1.22)$$

$$= - \psi_{x+\hat{\mu}}^T (\mathcal{C} \mathcal{P}_{+\mu})^T \psi_x. \quad (1.23)$$

By the use of the appropriate relations of the projector

$$\mathcal{P}_{\pm\mu}^T = \mathcal{P}_{\pm\mu} , \quad \text{since } \gamma_\mu^T = \gamma_\mu \quad (1.24)$$

$$\mathcal{C}^T = -\mathcal{C} \quad (1.25)$$

$$\mathcal{P}_{+\mu} \mathcal{C} = \mathcal{C} \mathcal{P}_{-\mu} , \quad \text{since } \gamma_\mu \mathcal{C} = -\mathcal{C} \gamma_\mu , \quad (1.26)$$

one can see that

$$(\mathcal{C} \mathcal{P}_{\pm\mu})^T = \mathcal{P}_{\pm\mu}^T \mathcal{C}^T = -\mathcal{P}_{\pm\mu} \mathcal{C} = -\mathcal{C} \mathcal{P}_{\mp\mu}. \quad (1.27)$$

This relation can now be used to simplify eq.(1.23) further to

$$- \psi_{x+\hat{\mu}}^T (\mathcal{C} \mathcal{P}_{+\mu})^T \psi_x = - \psi_{x+\hat{\mu}}^T \mathcal{P}_{+\mu}^T \mathcal{C}^T \psi_x \quad (1.28)$$

$$= \psi_{x+\hat{\mu}}^T \mathcal{C} \mathcal{P}_{-\mu} \psi_x , \quad (1.29)$$

which shows that the direction of the so called hops is irrelevant for a Majorana fermion. The just derived fact, that  $\psi_{x+\mu}^T \mathcal{C} \mathcal{P}_\mu \psi_x = \psi_{x+\mu}^T \mathcal{C} \mathcal{P}_{-\mu} \psi_x$  can now be used in eq.(1.21) to combine the identical hops, giving rise to a factor of two which gets cancelled by the overall prefactor of 1/2. Working this out properly yields

$$\hat{S} = \frac{1}{2} \sum_x \psi_x^T \mathcal{C} M_x \psi_x - \sum_{x,\mu} \psi_x^T \mathcal{C} \mathcal{P}_{+\mu} \psi_{x+\hat{\mu}} . \quad (1.30)$$

### 1.3.2. Hopping Expansion

Let's consider the expansion of the Boltzmann factor

$$\exp(-\hat{S}) = \prod_x \left(1 - \frac{1}{2} \psi_x^T \mathcal{C} M_x \psi_x\right) \prod_{x,\mu} \left(1 + \psi_x^T \mathcal{C} \mathcal{P}_{+\mu} \psi_{x+\hat{\mu}}\right), \quad (1.31)$$

which is exact, since all higher order terms vanish due to the Grassmann-nature of  $\psi$  D.1. This can be rewritten as

$$\exp(-\hat{S}) = \prod_x \left[ \sum_{m(x)=0}^1 \left(-\frac{1}{2} \psi_x^T \mathcal{C} M_x \psi_x\right)^{m(x)} \right] \prod_{x,\mu} \left[ \sum_{h(x,\mu)=0}^1 \left(\psi_x^T \mathcal{C} \mathcal{P}_{+\mu} \psi_{x+\hat{\mu}}\right)^{h(x,\mu)} \right], \quad (1.32)$$

where we will call  $m(x) \in \{0, 1\}$  and  $h(x, \mu) \in \{0, 1\}$  the occupation numbers. If we talk about a configuration we will refer to a configuration of fixed occupation numbers, some of them set to one and some to zero. Due to the Grassmann-nature of the fields a lot of configurations do not contribute in the Grassmann integral. We want to find a constraining equation for the occupation numbers such that any configuration not fulfilling that equation is also not contributing to the partition function. There are only two possibilities per site to create a configuration with a generally non-vanishing contribution. Either a site is saturated by a mass monomer term or a fermion is hopping through that site. The formal condition the occupation numbers need to fulfil in order to create a non-zero contribution is

$$m(x) + \frac{1}{2} \sum_{\mu=0}^1 [h(x, \mu) + h(x - \hat{\mu}, \mu)] = 1 \quad \forall x. \quad (1.33)$$

This tells us that only self avoiding and closed loops survive the Grassmann integration. Sites which do not have two fermion links connected to them must be occupied by a mass term. The partition function can now be expressed by a sum over all configurations  $\{c\}$  which have closed, self-avoiding and non backtracking loops  $\Omega = \Omega_1, \Omega_2, \dots$  where all sites not part of a loop, i.e.  $\Lambda \setminus \Omega$  are occupied by a mass term

$$Z = \sum_{\{c\}} W^M(\Lambda \setminus \Omega) \prod_{\Omega_i \in c} W^F(\Omega_i), \quad (1.34)$$

where  $W^M$  and  $W^F$  are the weights to the partition function coming from the monomer terms and the loop terms, respectively. In the next section it is our goal to calculate those contributions exactly.

## 1.4. Contributions to the partition function

### 1.4.1. Loops

The contribution of a closed loop has already been computed in [47–50] and we will follow closely the concept of [47, 48]. The important features of the loops are that they are closed, self-avoiding and due to

$$\mathcal{P}_{+\mu} \mathcal{P}_{-\mu} = 0, \quad (1.35)$$

they are also not back-tracking. Now we calculate the fermionic contribution to the weight in the partition function and will explain the determination of the sign of a contribution

### 1. Loop formulation of a free Majorana fermion in two dimensions

in more detail.

Let our fermion pass through a set of  $L$  sites  $\Omega = \{x_0, x_1, \dots, x_{L-1}\}$  and as a simplification assume that no boundaries are crossed. We introduce the variable  $n_l$  which denotes the lattice unit vector connecting the site  $x_l$  with its neighbour  $x_{l+1}$  along the loop, i.e.  $n_l = \pm \hat{\mu}$  with  $\hat{\mu} = \hat{0}, \hat{1}$ . Since the fermion loop is closed we have  $n_L = n_0$ . If we now look at the Grassmann integration of a fermion loop we can write

$$\prod_{x \in \Omega} \int d\psi_x^1 d\psi_x^2 \cdot \prod_{l=0}^{L-1} \psi_{x_l}^T \mathcal{C} \mathcal{P}_{n_l} \psi_{x_{l+1}}, \quad (1.36)$$

with  $\mathcal{P}$  being the modified Wilson-projector, where the sign is already incorporated by

$$\mathcal{P}_n = \frac{1}{2}(\mathbb{1}_{2 \times 2} - \not{n}), \quad (1.37)$$

since  $n = \pm \hat{\mu}$  and  $\not{n} = n^\rho \gamma_\rho$ . We now need to perform the integral

$$\int d\psi_x^1 d\psi_x^2 \psi_x \psi_x^T \mathcal{C} = \int d\psi_x^1 d\psi_x^2 \begin{pmatrix} \psi_x^1 \\ \psi_x^2 \end{pmatrix} \begin{pmatrix} \psi_x^1 & \psi_x^2 \end{pmatrix} \mathcal{C} = \mathbb{1}_{2 \times 2}, \quad (1.38)$$

that can be used to simplify eq.(1.36) such that we are left with the calculation of

$$\int d\psi_{x_0}^1 d\psi_{x_0}^2 \psi_{x_0}^T \mathcal{C} \mathcal{X} \psi_{x_0}, \quad (1.39)$$

where  $\mathcal{X}$  is the product of projector operators, i.e.

$$\mathcal{X} = \prod_{l=0}^{L-1} \mathcal{P}_{n_l}. \quad (1.40)$$

The integral in eq.(1.39) can be solved and it, dropping the site index and introducing Greek letters for component-wise summation, shows us that

$$\begin{aligned} \int d\psi^1 d\psi^2 \psi^T \mathcal{C} \mathcal{X} \psi &= \int d\psi^1 d\psi^2 (\psi^T)_\alpha \mathcal{C}^{\alpha\beta} \mathcal{X}_{\beta\rho} (\psi)^\rho \\ &= (\mathcal{C}^{2\alpha} \mathcal{X}_{\alpha 1} - \mathcal{C}^{1\beta} \mathcal{X}_{\beta 2}) \\ &= -\mathcal{X}_{11} - \mathcal{X}_{22} = -\text{Tr } \mathcal{X}. \end{aligned} \quad (1.41)$$

The minus sign in front of the trace is the minus sign occurring due to having a closed fermion loop. Note that no site on the path of the fermion loop is exquisite, i.e. there is no starting or ending point, we could have chosen any site which is part of the loop in 1.39. We have now performed the Grassmann integration and are left with the evaluation of  $\text{Tr } \mathcal{X}$ .

Any part of the loop where there is a straight line there will be a multiplication of identical projectors, and since

$$\mathcal{P}_n \mathcal{P}_n = \mathcal{P}_n, \quad (1.42)$$

the product of the projectors only depends on the reduced fermion loop, in which every site is a corner and any straight line is reduced to just one link in that direction. In the

case of a fermion which is winding itself around the torus without any corners on its path we can already write down the contribution to the partition function

$$\text{Tr } \mathcal{X} = \text{Tr } \mathcal{P}_{n_0}^L = \text{Tr } \mathcal{P}_{n_0} = 1. \quad (1.43)$$

So let's now consider the reduced fermion loop in which all straight lines are reduced to just one, formally this means  $n_l \neq n_{l+1} \forall l \in \Omega$ . Let us introduce the  $\pi/2$  spinor rotation matrix

$$\mathcal{R}_{n,m} = e^{\frac{\pi}{8}[\not{n}, \not{m}]} \quad (1.44)$$

and demand that the unit vectors are orthogonal, i.e.  $n \cdot m = 0$ . With the introduced rotation matrix we now want to show that any Wilson projector can be rotated into another one. This will then allow us to write the product of projectors simply as a product of rotations matrices and one single projector. Evaluating the anti-commutator yields

$$[\not{n}, \not{m}] = -2i\sigma(n, m)\gamma_5, \quad (1.45)$$

where

$$\sigma(n, m) = n_0 m_1 - n_1 m_0 \in \{-1, +1\}. \quad (1.46)$$

The two rotation matrix can now be written in terms of trigonometric functions in the form

$$\begin{aligned} \mathcal{R}_{n,m} = e^{\frac{\pi}{8}[\not{n}, \not{m}]} &= e^{\frac{\pi}{4}i\sigma(n,m)\gamma_5} = \cos\left(\frac{\pi}{4}\right) \mathbb{1}_{2 \times 2} - i\sigma(n, m)\gamma_5 \sin\left(\frac{\pi}{4}\right) \\ &= \frac{1}{\sqrt{2}} (\mathbb{1}_{2 \times 2} - i\sigma(n, m)\gamma_5), \end{aligned} \quad (1.47)$$

where the inverse is simply

$$\mathcal{R}_{n,m}^{-1} = \frac{1}{\sqrt{2}} (\mathbb{1}_{2 \times 2} + i\sigma(n, m)\gamma_5), \quad (1.48)$$

which makes it obvious that  $\mathcal{R}_{n,m}^{-1} = \mathcal{R}_{m,n}$ . Let us now show that with the rotation matrix we can rotate any projector  $\mathcal{P}_m$  into another one

$$\begin{aligned} R_{n,m} \mathcal{P}_m R_{n,m}^{-1} &= \frac{1}{\sqrt{2}} (\mathbb{1}_{2 \times 2} - i\sigma(n, m)\gamma_5) \frac{1}{2} (\mathbb{1}_{2 \times 2} - \not{m}) \frac{1}{\sqrt{2}} (\mathbb{1}_{2 \times 2} + i\sigma(n, m)\gamma_5) \\ &= \frac{1}{4} (\mathbb{1} + i\sigma\gamma_5 - \not{m} - i\sigma\not{m}\gamma_5 - i\sigma\gamma_5 - \sigma^2\gamma_5^2 + i\sigma\gamma_5\not{m} + \sigma^2\gamma_5\not{m}\gamma_5) \\ &= \frac{1}{2} (\mathbb{1}_{2 \times 2} - i\sigma(n, m)\not{m}\gamma_5), \end{aligned} \quad (1.49)$$

where in the last step we used the properties of the Dirac algebra, essentially the fact that  $\gamma_5^2 = \mathbb{1}_{2 \times 2}$  and  $\{\gamma_\mu, \gamma_5\} = 0$ , as well as  $\{\gamma_\mu, \gamma_\nu\} = 2\delta_{\mu\nu}\mathbb{1}_{2 \times 2}$  and  $\text{Tr } \gamma_\mu = 0$ . In a next step we make use of  $\gamma_5 = i\gamma_0\gamma_1$  to obtain

$$R_{n,m} \mathcal{P}_m R_{n,m}^{-1} = \frac{1}{2} (\mathbb{1}_{2 \times 2} - \sigma(n, m)(m_0\gamma_1 + m_1\gamma_0)). \quad (1.50)$$

Writing  $\sigma(n, m)$  as  $n_0 m_1 + n_1 m_0$  explicitly and using  $n \cdot m = 0$  we get

$$\begin{aligned} R_{n,m} \mathcal{P}_m R_{n,m}^{-1} &= \frac{1}{2} (\mathbb{1}_{2 \times 2} - (n_1 m_0^2 \gamma_1 + n_0 m_1^2 \gamma_0)) \\ &= \frac{1}{2} (\mathbb{1}_{2 \times 2} - \not{n}) = \mathcal{P}_n. \end{aligned} \quad (1.51)$$

### 1. Loop formulation of a free Majorana fermion in two dimensions

We now showed that  $\mathcal{P}_m$  can be rotated into  $\mathcal{P}_n$ . So any combination of  $\mathcal{P}_n \mathcal{P}_m$  can be written as

$$\begin{aligned}
\mathcal{P}_n \mathcal{P}_m &= \mathcal{R}_{n,m} \mathcal{P}_m \mathcal{R}_{n,m}^{-1} \mathcal{P}_m \\
&= \frac{1}{\sqrt{2}} (\mathbb{1}_{2 \times 2} - i\sigma\gamma_5) \frac{1}{2} (\mathbb{1}_{2 \times 2} - \eta\hbar) \frac{1}{\sqrt{2}} (\mathbb{1}_{2 \times 2} + i\sigma\gamma_5) \frac{1}{2} (\mathbb{1}_{2 \times 2} - \eta\hbar) \\
&= \frac{1}{4} (\mathbb{1}_{2 \times 2} - \eta\hbar - i\sigma\gamma_5 + i\sigma\gamma_5\eta\hbar) \\
&= \frac{1}{\sqrt{2}} \frac{1}{\sqrt{2}} (\mathbb{1}_{2 \times 2} - i\sigma\gamma_5) \frac{1}{2} (\mathbb{1}_{2 \times 2} - \eta\hbar) \\
&= \frac{1}{\sqrt{2}} \mathcal{R}_{n,m} \mathcal{P}_m .
\end{aligned} \tag{1.52}$$

This shows us, that any product of Wilson projectors along the path of a fermion loop can be replaced by

$$\text{Tr} \left\{ \prod_{l=0}^{L-1} \mathcal{P}_{n_l} \right\} = \text{Tr} \left\{ \frac{1}{\sqrt{2}} \mathcal{R}_{n_0, n_1} \frac{1}{\sqrt{2}} \mathcal{R}_{n_1, n_2} \dots \mathcal{P}_{n_{L-1}} \right\} , \tag{1.53}$$

where the factors of  $1/\sqrt{2}$ , appearing for every corner can be taken out of the trace

$$\text{Tr} \left\{ \prod_{l=0}^{L-1} \mathcal{P}_{n_l} \right\} = 2^{-(L-1)/2} \text{Tr} \left\{ \mathcal{R}_{n_0, n_1} \mathcal{R}_{n_1, n_2} \dots \mathcal{P}_{n_{L-1}} \right\} . \tag{1.54}$$

Let us include a unit matrix

$$\mathbb{1}_{2 \times 2} = \mathcal{R}_{n_{L-1}, n_0} \mathcal{R}_{n_{L-1}, n_0}^{-1} = \mathcal{R}_{n_{L-1}, n_0} \mathcal{R}_{n_0, n_{L-1}} , \tag{1.55}$$

in front of the only remaining Wilson projector, such that

$$\text{Tr} \left\{ \prod_{l=0}^{L-1} \mathcal{P}_{n_l} \right\} = 2^{-(L-1)/2} \text{Tr} \left\{ \mathcal{R}_\Theta \mathcal{R}_{n_0, n_{L-1}} \mathcal{P}_{n_{L-1}} \right\} , \tag{1.56}$$

in which the total rotation matrix, defined to be

$$\mathcal{R}_\Theta = \mathcal{R}_{n_0, n_1} \mathcal{R}_{n_1, n_2} \dots \mathcal{R}_{n_{L-1}, n_0} \mathcal{R}_{n_0, n_{L-1}} , \tag{1.57}$$

is counting the total angle  $\Theta$  created by adding up all rotations in the product above. Starting at the initial link  $n_0$  we follow a consecutive series of rotations by  $\pi/2$  which are either clockwise if  $\sigma(n, m) = -1$  or anti-clockwise if  $\sigma(n, m) = 1$ . We introduce the number of clockwise rotations  $N_\circ$  and  $N_\circlearrowright$  accordingly for anti-clockwise rotations. It is then clear that the total angle obtained by all rotations along the fermion loop is

$$\Theta = \frac{\pi}{2} (N_\circ - N_\circlearrowright) . \tag{1.58}$$

So the total rotation matrix can be written as

$$\mathcal{R}_\Theta = \left( e^{-i\frac{\pi}{4}(\mp 1)\gamma_5} \right)^{|N_\circ - N_\circlearrowright|} \tag{1.59}$$



Since the loops are self-avoiding, non-backtracking and closed, there are only two possibilities for  $|N_{\cup} - N_{\cap}|$ . For loops which are winding around the lattice  $\Theta$  must be zero, yielding

$$\mathcal{R}_{\Theta=0} = \mathbb{1}_{2 \times 2}. \quad (1.60)$$

For loops which are not crossing any boundaries the total angle is  $\pm 2\pi$ , therefore the total rotation matrix is

$$\mathcal{R}_{\Theta=\pm 2\pi} = \left( e^{-i\frac{\pi}{4}(\mp 1)\gamma_5} \right)^4 = \cos(\pi)\mathbb{1}_{2 \times 2} \pm i\gamma_5 \sin(\pi) = -\mathbb{1}_{2 \times 2}. \quad (1.61)$$

It is now clear that in the trace over all projectors, the total rotation matrix is only contributing with a sign. We are left with the calculation of

$$\begin{aligned} \text{Tr} \{ \mathcal{R}_{n_0, n_{L-1}} \mathcal{P}_{n_{L-1}} \} &= \text{Tr} \left\{ \frac{1}{\sqrt{2}} (\mathbb{1}_{2 \times 2} - i\sigma(n_0, n_{L-1})\gamma_5) \frac{1}{2} (\mathbb{1}_{2 \times 2} - \not{n}_{L-1}) \right\} \\ &= \frac{1}{2\sqrt{2}} \text{Tr} \{ \mathbb{1}_{2 \times 2} - \not{n}_{L-1} - i\sigma\gamma_5 + i\sigma\gamma_5 \not{n}_{L-1} \} \\ &= \frac{1}{\sqrt{2}} \end{aligned} \quad (1.62)$$

All the results can now be collected and the trace of all projectors is

$$\text{Tr} \mathcal{X} = (-1)^\nu 2^{-L/2}, \quad (1.63)$$

where  $\nu \in \{0, 1\}$  stands for the number of total rotations of the loop. This is true for what we called a reduced loop, a loop which only consists of corners. If we generalise the result for a generic geometry of a loop, the number of links no longer correspond to the number of corners in the loop. Since we have seen that consecutively following identical projectors only contribute with the identity matrix, we can simply write down the trace of a general loop geometry by

$$\text{Tr} \mathcal{X} = (-1)^\nu 2^{-n_c/2}, \quad (1.64)$$

where  $n_c$  denotes the number of corners in the loop. We now performed all essential steps in order to write down the contribution of the fermion loop

$$W^F(\Omega) = \prod_{x \in \Omega} \int d\psi_x^1 d\psi_x^2 \cdot \prod_{l=0}^{L-1} \psi_{x_l}^T \mathcal{C} \mathcal{P}_{n_l} \psi_{x_{l+1}} = -(-1)^{\nu(\Omega)} 2^{-\frac{n_c(\Omega)}{2}}, \quad (1.65)$$

where the additional minus sign comes from the Grassmann integration.

#### 1.4.2. Mass terms

Sites which are not part of a fermion loop need to be saturated by a mass monomer term  $M_x$ , i.e. have occupation number  $m_x = 1$ . The corresponding weight from these sites is

$$\int d\psi_x^1 d\psi_x^2 \left( -\frac{M_x}{2} \right) \psi_x^T \mathcal{C} \psi_x = M_x, \quad (1.66)$$

where we used that, dropping the site index,

$$\int d\psi^1 d\psi^2 \psi^T \mathcal{C} \psi = \int d\psi^1 d\psi^2 (\psi^1, \psi^2) \begin{pmatrix} 0 & 1 \\ -1 & 0 \end{pmatrix} \begin{pmatrix} \psi^1 \\ \psi^2 \end{pmatrix} = -2, \quad (1.67)$$

### 1. Loop formulation of a free Majorana fermion in two dimensions

where the factor of two comes from the commutation rule of the Grassmann numbers  $\psi^1\psi^2 - \psi^2\psi^1 = 2\psi^1\psi^2$  and the minus sign from

$$\int d\psi^1 \int d\psi^2 \psi^1\psi^2 = - \int d\psi^1 \int d\psi^2 \psi^2\psi^1 = - \int d\psi^1 \psi^1 = -1. \quad (1.68)$$

#### 1.4.3. $Z$ in the loop formulation

All weights are now derived and we can write down the partition function from eq.(1.34) as

$$Z = \sum_{\{c\}} \prod_{x \in \{\Lambda \setminus \Omega\}} M_x \prod_{\Omega_i \in c} -(-1)^{\nu(\Omega_i)} 2^{-\frac{n_c(\Omega_i)}{2}}. \quad (1.69)$$

At first sight it might seem cumbersome to determine the overall sign of a configuration in the partition function above, since every loop  $\Omega_i$  in the configuration  $\{c\}$  may actually change the sign of the configuration. However, after discussion the correlation function we will present an elegant way of determining the overall sign of a contribution from a given configuration.

### 1.5. Correlation function

In this section we will discuss the fermion correlation function in the loop formulation. The fermionic correlator can be defined as the two-point function

$$C_{xy} = \langle \psi_x \bar{\psi}_y \rangle = \frac{1}{Z} \int \mathcal{D}\psi \psi_x \bar{\psi}_y \exp \left[ -\hat{S}(\psi) \right]. \quad (1.70)$$

The only configurations generating a generally non-vanishing contribution to  $C_{xy}$  are those that fulfil

$$m(z) + \frac{1}{2} \sum_{\mu} [h(z, \mu) + h(z - \hat{\mu}, \mu)] + \frac{1}{2} (\delta_{z,x} + \delta_{z,y}) = 1 \quad \forall z, \quad (1.71)$$

Since there is a  $\psi$  at site  $x$  and a  $\bar{\psi}$  at site  $y$  the equation is identical to eq.(1.33) except at the sites  $x$  and  $y$ . The only possibility to create a non-vanishing contribution to  $C_{xy}$  is therefore a self-avoiding non-backtracking open fermion string starting with one end at  $x$  and the other at  $y$ . We will now calculate the contribution of a configuration that fulfils eq.(1.71).

With the results from the previous section, where we discussed the contributions of the fermion loops to the partition function, it is easy to see that the contribution of a fermion open string, starting at  $x_0$  and ending at  $x_L$  with  $x_0 \equiv x$  and  $x_L \equiv y$ , is

$$W^S = \prod_{x \in \tilde{\Omega}} \int d\psi_x^1 d\psi_x^2 \cdot \psi_{x_0} \left[ \prod_{l=0}^{L-1} \psi_{x_l}^T \mathcal{C} \mathcal{P}_{n_l} \psi_{x_{l+1}} \right] \psi_L^T \mathcal{C} = (-2)^{-n_c/2} \mathcal{R}_{\Theta} \mathcal{P}_{\pm\mu}, \quad (1.72)$$

where  $\tilde{\Omega}$  is the set of all sites along the open fermion string including its endpoints,  $\mathcal{R}_{\Theta}$  is the rotation matrix introduced in eq.1.59 and  $\Theta$  is the total angle obtained by all rotations along the fermion open string up until the last link. The projector  $\mathcal{P}_{\pm\mu}$  connects the second last site with the last one  $y$  in the adequate direction  $\pm\hat{\mu}$ . Each corner is contributing with  $1/\sqrt{2}$ , therefore  $n_c$  is the number of corners along the fermion string. Integrating

out also the other Grassmann fields on all other sites gives us the correlator in the loop formulation

$$C_{xy} = \langle \psi_x \bar{\psi}_y \rangle = \frac{1}{Z} \sum_{\{c\}} \left\{ \left[ \prod_{x \in \{\Lambda \setminus \Omega\}} M_x \right] \left[ \prod_{\Omega_i \in c} W^F(\Omega_i) \right] W^S \right\}, \quad (1.73)$$

where  $\Omega_i$  is the set of all sites in a closed fermion loop.

As we will shortly see it is the fermion worm algorithm which is not only updating the configurations contributing to the partition function but also in every updating step generating a configuration contributing with a matrix, of the form seen in eq.(1.72), to the correlator.

## 1.6. The sign of a configuration

In this section we discuss the sign of a contribution coming from a configuration of closed fermion loops. The weight contributing to the partition function is given by eq.(1.69). The sign of a contribution is solely given by the number of rotations of the loops and the boundary conditions. In the first subsection we show that the partition function can be split up into topological sectors corresponding to the winding number of the fermion around the dimensions of the Euclidean torus. These will turn out to hold all information about the number of rotations and therefore also the sign. In the second subsection we then discuss the effect of different boundary conditions. This section is derived from [47, 51].

### 1.6.1. Topological classes

The sign of a contribution from a configuration  $c$  to the partition function is

$$- \prod_{\Omega_i \in c} (-1)^{\nu(\Omega_i)}, \quad (1.74)$$

where  $\nu(\Omega_i)$  is the number of rotations of the loop  $\Omega_i$ . Every loop configuration that may occur falls in one of the topological sectors  $\mathcal{L}_{ij}$  with  $i, j \in \{0, 1\}$ , where  $i$  is the number of times the fermion winds itself around the first dimension modulo two and the index  $j$  is the equivalent for the second dimension. For example,  $\mathcal{L}_{01}$  is the sector in which an even number of fermions are winding around the first dimension and an odd number in the second. Any two loops in the same class can be transformed into each other by local transformations. Further there exists no sequence of local transformations which bring a configuration from one class in any other. A local transformation is a change of the occupation numbers around a single plaquette in which eq.(1.33) is never violated. Since local transformations can not change the number of rotations, all configurations in the same topological class have contributions with the identical sign. In fig.(1.1) we illustrate a representative configuration of each class. Let us for simplicity consider only one single fermion loop. For example, consider a simple fermionic loop in  $\mathcal{L}_{00}$ . Since it is not winding around any direction it must have  $\nu = 1$  and together with the minus sign coming from closing the fermion loop, give a total contribution which is positive. Consider also a loop in  $\mathcal{L}_{01}$ , which is winding once around the second dimension and therefore  $\nu = 0$ , it then comes with a total contribution which is negative. However, if we would add a second

### 1. Loop formulation of a free Majorana fermion in two dimensions

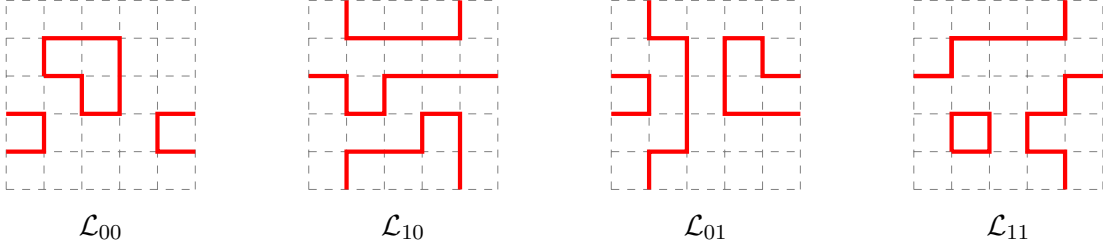


Figure 1.1.: An example of four different configurations falling into the topological classes  $\mathcal{L}_{ij}$

loop winding around the same dimension, creating an additional minus, we are again in  $\mathcal{L}_{00}$  with purely positive contributions. These kinds of considerations can be made for all topology classes finding that, with periodic boundary conditions, all contributions from configurations in  $\mathcal{L}_{00}$  are positive and all in  $\mathcal{L}_{10}$ ,  $\mathcal{L}_{01}$  and  $\mathcal{L}_{11}$  are negative. We state that, keeping all boundary conditions periodic for now, the partition function can be written as

$$Z_{pp} = Z_{\mathcal{L}_{00}} - Z_{\mathcal{L}_{10}} - Z_{\mathcal{L}_{01}} - Z_{\mathcal{L}_{11}}, \quad (1.75)$$

where the subscript  $pp$  stands for periodicity in both dimensions.. We now established a classification serving as a global criterion to determine with which sign a configuration is contributing to the partition function.

When a fermion loop is winding around a dimension the boundary conditions come into play and can change the sign of the contribution. In the next subsection we discuss the effect of those in more detail.

#### 1.6.2. Partition function and boundary conditions

Recall that we already defined the boundary conditions for a field living on every site of the lattice in eq.(1.9). The fermions are allowed to have either periodic or anti-periodic boundary conditions, which is controlled by  $\alpha(\mu)$ , as introduced in eq.(1.9). When calculating the contribution to the partition function we found that the periodic-periodic partition function  $Z_{pp}$  can be written as

$$Z_{pp} = Z_{\mathcal{L}_{00}} - Z_{\mathcal{L}_{10}} - Z_{\mathcal{L}_{01}} - Z_{\mathcal{L}_{11}}. \quad (1.76)$$

If we now impose anti-periodic boundary conditions in direction  $\mu$  there is an additional minus sign for contributions from the sector in which an odd number of fermions are actually winding around that anti-periodic dimension. Of course if there are anti-periodic boundary conditions in both dimensions the minus signs combine to a plus in the case of  $Z_{\mathcal{L}_{11}}$ . We can write the generic partition function in the following way

$$Z_{\alpha} = Z_{(\alpha_0, \alpha_1)} = Z_{\mathcal{L}_{00}} + (-1)^{1+\alpha_0} Z_{\mathcal{L}_{10}} + (-1)^{1+\alpha_1} Z_{\mathcal{L}_{01}} + (-1)^{1+\alpha_0+\alpha_1} Z_{\mathcal{L}_{11}}. \quad (1.77)$$

In this work we are predominantly interested in case where  $\alpha = (0, 0)$ , which refers to a system with periodic boundary conditions in both dimensions for which we just write  $Z_{pp} = Z_{(0,0)}$ . The other case which is of interest is the one where only one dimension is anti-periodic, i.e.  $\alpha = (1, 0)$ . These boundary conditions are also known as thermal boundary conditions, which let us interpret the inverse length of the anti-periodic dimension with the

temperature of the system. The notation for this partition function will be  $Z_{ap} = Z_{(1,0)}$  and it is

$$Z_{ap} = Z_{\mathcal{L}_{00}} + Z_{\mathcal{L}_{10}} - Z_{\mathcal{L}_{01}} + Z_{\mathcal{L}_{11}}. \quad (1.78)$$

We would like to add here again that counting the winding number in a certain dimension around the torus in order to obtain the topological class  $\mathcal{L}_{ij}$ , amounts to counting the number of fermion lines crossing the boundary of that dimension modulo two.

## 1.7. Observables

We use the common definition for the expectation value of an observable  $\mathcal{O}$

$$\langle \mathcal{O} \rangle = \frac{1}{Z} \int \mathcal{D}\psi \mathcal{O} e^{-S(\psi)}. \quad (1.79)$$

Let us express the partition function as a sum over all configurations  $c$  and write the expectation value of an observable as

$$\langle \mathcal{O} \rangle = \frac{1}{\sum_{\{c\}} W_c} \sum_{\{c\}} \mathcal{O} W_c, \quad (1.80)$$

where  $W_c$  simply denotes the Boltzmann weight of the configuration  $c$ . Since we can divide the partition function into topological sectors appearing with a given sign, we want to define expectation values also in the those topological sectors. It will show itself useful to introduce a notation, already used in [48], to write

$$\langle \langle \mathcal{O} \rangle \rangle_{\mathcal{L}_{ij}} = \sum_{\{c\} \in \mathcal{L}_{ij}} \mathcal{O} W_c, \quad (1.81)$$

which is the expectation value of the non-normalised observable in a given sector  $\mathcal{L}_{ij}$ . A very simple observable is  $Z$ , which is simply 1 for any configuration in the partition function  $Z$  and therefore its non-normalised expectation value is trivially

$$Z = \langle \langle 1 \rangle \rangle_{\text{all sectors}} \quad (1.82)$$

We can now ask for the partition function in a topological sector, namely  $Z_{\mathcal{L}_{ij}}$ , which is

$$Z_{\mathcal{L}_{ij}} = \langle \langle 1 \rangle \rangle_{\mathcal{L}_{ij}}. \quad (1.83)$$

A general observable  $\mathcal{O}$  in a system with boundary conditions  $\alpha$  can now be written using eq.(1.77) and the just introduced notation as

$$\langle \mathcal{O} \rangle_{\alpha} = \frac{\langle \langle \mathcal{O} \rangle \rangle_{\mathcal{L}_{00}} + (-1)^{1+\alpha_0} \langle \langle \mathcal{O} \rangle \rangle_{\mathcal{L}_{10}} + (-1)^{1+\alpha_1} \langle \langle \mathcal{O} \rangle \rangle_{\mathcal{L}_{01}} + (-1)^{1+\alpha_0+\alpha_1} \langle \langle \mathcal{O} \rangle \rangle_{\mathcal{L}_{11}}}{Z_{\mathcal{L}_{00}} + (-1)^{1+\alpha_0} Z_{\mathcal{L}_{10}} + (-1)^{1+\alpha_1} Z_{\mathcal{L}_{01}} + (-1)^{1+\alpha_0+\alpha_1} Z_{\mathcal{L}_{11}}}. \quad (1.84)$$

Let us write down the explicit expectation values of an observable in a system with periodic boundary conditions in both dimensions

$$\langle \mathcal{O} \rangle_{pp} = \frac{\langle \langle \mathcal{O} \rangle \rangle_{\mathcal{L}_{00}} - \langle \langle \mathcal{O} \rangle \rangle_{\mathcal{L}_{10}} - \langle \langle \mathcal{O} \rangle \rangle_{\mathcal{L}_{01}} - \langle \langle \mathcal{O} \rangle \rangle_{\mathcal{L}_{11}}}{Z_{\mathcal{L}_{00}} - Z_{\mathcal{L}_{10}} - Z_{\mathcal{L}_{01}} - Z_{\mathcal{L}_{11}}} \quad (1.85)$$

## 1. Loop formulation of a free Majorana fermion in two dimensions

and with thermal boundary conditions

$$\langle \mathcal{O} \rangle_{ap} = \frac{\langle \langle \mathcal{O} \rangle \rangle_{\mathcal{L}_{00}} + \langle \langle \mathcal{O} \rangle \rangle_{\mathcal{L}_{10}} - \langle \langle \mathcal{O} \rangle \rangle_{\mathcal{L}_{01}} + \langle \langle \mathcal{O} \rangle \rangle_{\mathcal{L}_{11}}}{Z_{\mathcal{L}_{00}} + Z_{\mathcal{L}_{10}} - Z_{\mathcal{L}_{01}} + Z_{\mathcal{L}_{11}}} \quad (1.86)$$

Note that when talking about an expectation value of a given sector in  $Z$ , we mean

$$\langle Z_{\mathcal{L}_{ij}} \rangle_Z = \frac{\langle \langle 1 \rangle \rangle_{\mathcal{L}_{ij}}}{\langle \langle 1 \rangle \rangle_Z} = \frac{Z_{\mathcal{L}_{ij}}}{Z}, \quad (1.87)$$

which in the plots in the result section will be also called  $Z_{\mathcal{L}_{ij}}$  to avoid introducing additional notation.

In appendix C we show which estimator is used to estimate expectation values when dealing with a statistical system and how to create correct error estimates for functions which depend on expectation values by using the Jackknife method. Additionally we show what is done if the data are correlated.

## 1.8. Worm algorithm

The worm algorithm is based on the work of Prokof'ev and Svistunov [26] which presented the idea of updating closed path configurations through the motion of end points of disconnected paths. In [27] it is shown that the fermion loop formulation is highly suited to numerically simulate a relativistic fermion by the worm algorithm. The predominant reason of the algorithms success is the fact that it can essentially eliminate critical slowing down and allows for simulations in the massless limit. Motivated by these facts we will in following chapters try to formulate our models' degrees of freedom in a way that they can be simulated efficiently by such an algorithm. In this section we discuss the algorithm in more detail for the free Majorana fermion. This should then serve as a basic concept for other models, for which mostly only small adaptation will need to be made.

The goal of this section is to explain the basic idea of the worm algorithm and to discuss it in more detail for the just derived loop formulation of the free Majorana fermion living on a two-dimensional lattice.

### 1.8.1. Basic idea

The main goal of the worm algorithm is to efficiently sample configurations contributing to the partition function, which correspond to closed loop configurations. The peculiarity of the idea is to leave the closed loop configuration and enter the configuration space of the two-point functions and after “moving” around in the configuration space of two-point functions, return back to a closed loop configuration. Like this we will not only have performed a generally non-local update of configurations contributing to the partition function but also sampled configurations contributing to the two-point function. In fig. 1.2 we illustrate this procedure which can be summarised as follows

- (I) Start with a closed loop configuration, i.e. occupation numbers fulfil eq.(1.33). Open up a loop and obtain an open string, this amounts to break eq.(1.33) and fulfil eq.(1.71).
- (II) Move open string around, i.e. sample configurations that fulfil eq.(1.71).
- (III) Close loop and obtain new closed loop configuration, i.e. break eq.(1.71) and fulfil eq.(1.33).

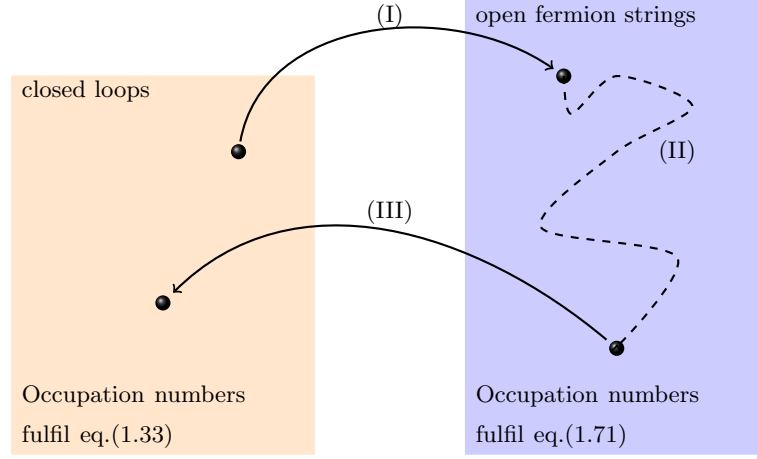


Figure 1.2.: Sketching the basic idea of the worm algorithm.

### 1.8.2. Algorithm for the free Majorana fermion

In this subsection we describe the algorithm in more detail for the case of our free Majorana fermion living on a two-dimensional lattice. We start with a closed fermion loop configuration that fulfils eq.(1.33). We then ask to insert a Majorana spinor pair  $\bar{\psi}$  and  $\psi$  onto a site  $x$  on the lattice, explicitly breaking the present configuration. In the following we will talk about the inserted  $\bar{\psi}_x$  as the tail of the worm, whereas  $\psi_x$  will be referred to as the head of the worm. What is essential though is that by inserting head and tail onto the lattice, we entered a configuration space which is no longer contributing to  $Z$  but is now contributing to the configuration space of the two-point functions, i.e. the occupation numbers fulfil eq.(1.71). We then propose to move, i.e. shift by one lattice spacing, the head around the lattice, creating a contribution to the two-point function after every shift of the head. If the head is shifted along a link with no fermion line we create a fermionic link and if there exists already a fermionic link, we delete it. This moving around is done until the head falls again onto the tail. We then ask to remove the head and tail from the lattice and enter again the configuration space of the closed fermion loops. Generally a new configuration contributing to  $Z$  will be created in this way. In fig. 1.3 we illustrates the flow diagram of the algorithm.

As we will shortly see when explaining the individual updating steps in more detail, it can be of use to even enter an non-physical configuration space which does not contribute to any physical observable. Steps like this though are only used to create a more effective update procedure, simplify detailed balance equations or simply enhance code readability

### 1. Loop formulation of a free Majorana fermion in two dimensions

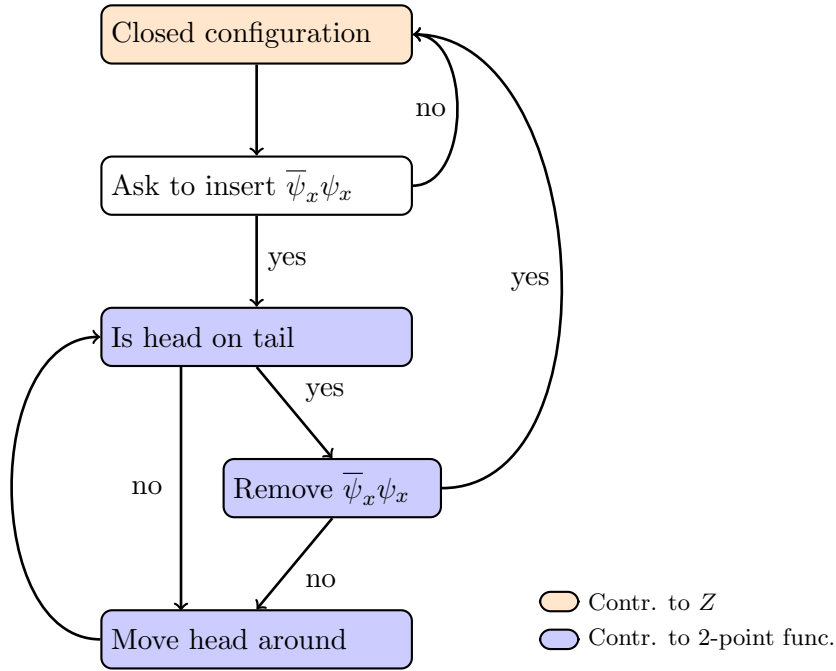


Figure 1.3.: Flow diagram of a possible worm algorithm

and testing. Note also, that what is presented here is one of the simplest ideas of a worm algorithm, there exist highly diverse algorithms based on similar and identical ideas. One is of course free to perform countless adaptations, e.g. moving head and tail simultaneously, inserting two head and tail pairs.

In the next subsection we discuss the weights of vertices that can arise in configurations contributing to the partition function. This will show itself useful in order to explain the local updating steps of the algorithm later on.

#### 1.8.3. Vertices in $Z$

Let us write down all possible vertices that can occur in a configuration contributing to the partition function, similar to [27, 50]. These are illustrated in fig.(1.4) with their corresponding weights. They can be viewed as the fundamental building blocks of a configuration in  $Z$ , where the only constraint to fulfil is eq.(1.33). Any contribution can be, except of an overall sign which is encoded in the topology classes, broken down to local weights. For the free Majorana fermion these are  $w_M = M_x$  for the mass monomer terms,  $w_F = 1$  for fermion lines and  $w_C = 1/\sqrt{2}$  for fermion lines forming a corner.

In the next subsection we will explain the local updates that are performed when shifting the head around the lattice. This will be done by using the vertices and local weights explained in this section.



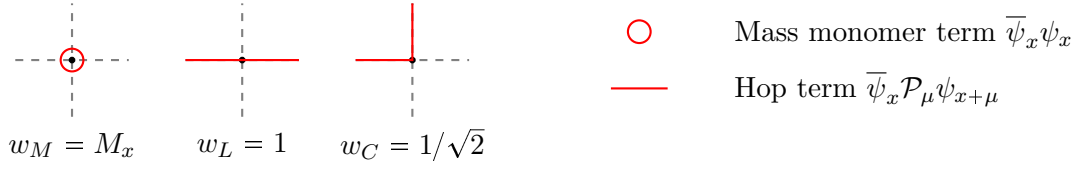


Figure 1.4.: All possible vertices, upon rotations of  $\pi/2$ , which are appearing in configurations contributing to  $Z$ .

#### 1.8.4. Local updates

Any change that the update performs is based on proposing a new configuration  $\chi'$  based on the old one  $\chi$ . This is done with a normal Metropolis update procedure, based on a Monte Carlo update step, where the proposed change is accepted if the action is decreased, i.e. the Boltzmann factor is increased. If on the other hand the Boltzmann factor is decreased, we only accept the proposed change with a probability equal to the ratio of the Boltzmann factors. The proposition probabilities (how likely is it that we propose  $\chi'$ ) and the acceptance probabilities (how likely is it that we accept the proposed  $\chi'$ ) must be such, that the algorithm is ergodic and satisfies detailed balance. These two key features are closer explained in B. The formula, which can be found in [19], to calculate the acceptance probability  $p_A(\chi \rightarrow \chi')$ , to get from a configuration  $\chi$  to a configuration  $\chi'$ , is given by

$$p_A(\chi \rightarrow \chi') \propto \min \left\{ 1, \frac{p_c(\chi' \rightarrow \chi)w(\chi')}{p_c(\chi \rightarrow \chi')w(\chi)} \right\} \quad (1.88)$$

where  $p_c(\chi \rightarrow \chi')$  is an arbitrary probability distribution for the proposed change of the configuration  $\chi$  to  $\chi'$  and  $w$  is the weight of the configuration, i.e the local Boltzmann factor. The formula above creates  $p_A$  in such a way that it compensates for  $p_c$ . Having this in mind we can now start writing down the actual updating steps of the worm algorithm. In order to have a more pedagogical approach we will look at the easiest but most fundamental step of the updating procedure, namely the shift of the head. In fig. 1.5 we illustrate that movement. The head of the worm is marked with a blue square box ( $\square$ ) and is sitting on site  $x$ . We then propose any neighbouring site with the probability  $p_c$ . Since there are four options available to which we can shift the head, we set this probability to  $1/4$ . In fig. 1.5 we proposed to change the configuration from  $\chi$  to  $\chi'$ . Since we use the

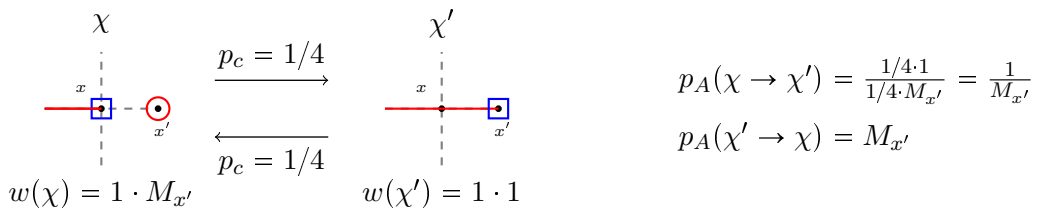


Figure 1.5.: Showing a normal shift of the head from one site to another.

same probability for  $\chi' \rightarrow \chi$ , they cancel out in the final acceptance probability. In the configuration  $\chi$  we have the head on site  $x$  and on the site  $x'$ , to which we propose to move the head to, exists a mass monomer term with weight  $M_{x'}$ . In the new configuration  $\chi'$  a fermion line is drawn from  $x$  to  $x'$  and the mass monomer term is removed. The site

### 1. Loop formulation of a free Majorana fermion in two dimensions

$x'$  is now saturated by an incoming fermion line, contributing with  $\bar{\psi}$ , and the head with  $\psi$ . The complete update step then finally reads: starting with  $\chi$ , we propose  $\chi'$  with the probability of  $p_c(\chi \rightarrow \chi')$  and then check whether this new state is accepted by picking a random number  $r \in [0, 1]$  and accept  $\chi'$  if  $r < p_A(\chi \rightarrow \chi')$ . The same works analogously the other way round from  $\chi' \rightarrow \chi$ . The exact weights can be also written off in fig. 1.5. There are of course other updating procedures which correspond to other parts of the flow diagram in fig. 1.3, but they all work strictly according to eq.(1.88). Nevertheless, we would like to highlight some update steps in more detail.

First we want to introduce the concept of so called artificial states. An artificial state, as the name explains already, is a state which is not real in the sense that it does not contribute to anything physical. We can therefore also assign an artificial weight  $w_A$  to artificial states, and will see that no physical quantity is depending on the choice of  $w_A$ . The best way to illustrate the use of artificial states is with an example. We can let the head of the worm hop into an already existing fermion line. When doing so we create a site which has three fermion lines attached to it, something which is not allowed since it does not survive the Grassmann integral and is not anymore in the two-point function configuration space. In fig. 1.6 we show exactly such a shift and the corresponding acceptance probability. With this trick we assure that the update procedure can break up

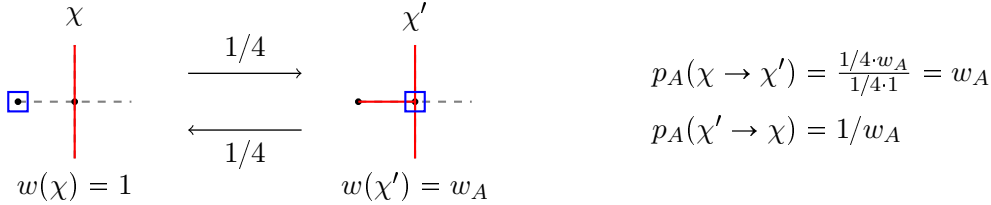


Figure 1.6.: Showing a shift of the head in to and out of an artificial configuration where three fermion lines meet at one site

parts of an already existing fermion loop and still stay completely local. With completely local updates we refer to updates shifting the head only by one lattice spacing. There is a site in  $\chi'$  that can get proposed in the next step, but to which a shift of the head would leave a site behind at which four fermion lines meet. This is indeed proposed, again for the sake of symmetric  $p_c$ , but the weight of that new configuration is set to zero. If the artificial state, introduced in fig. 1.6, was not included, an update procedure from configuration  $\chi \rightarrow \chi''$ , as illustrated in fig. 1.7, would need to be performed in one step. There we propose the change with the probability of  $1/8$  and jump directly from one state in the two-point configuration space to another. This of course is no problem at all, it is simply a matter of taste. Since we try to stick to completely local updates and want to keep  $p_c = 1/4$  at all times, we stick to the scenario which makes use of artificial states. If the update, illustrated in fig. 1.7, is done by inserting an artificial state as shown in fig. 1.6 we must of course reproduce the same transition probability and the artificial weight

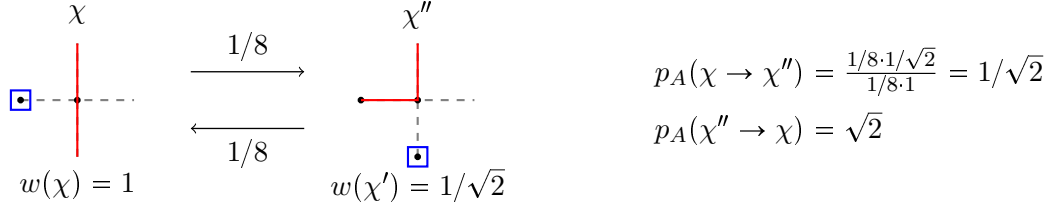


Figure 1.7.: Showing a shift of the head not entering an artificial state, but directly proposing a state in the two-point configuration space

must drop out. This can be shown by

$$\begin{aligned}
 p_A(\chi \rightarrow \chi'') &= p_A(\chi \rightarrow \chi') p_A(\chi' \rightarrow \chi'') = \frac{p_c(\chi' \rightarrow \chi) w(\chi') p_c(\chi'' \rightarrow \chi') w(\chi'')}{p_c(\chi \rightarrow \chi') w(\chi) p_c(\chi' \rightarrow \chi'') w(\chi')} \\
 &= \frac{p_c(\chi' \rightarrow \chi) p_c(\chi'' \rightarrow \chi') w(\chi'')}{p_c(\chi \rightarrow \chi') p_c(\chi' \rightarrow \chi'') w(\chi)} \\
 &= \frac{1}{\sqrt{2}},
 \end{aligned}$$

where we saw that  $w(\chi') = w_A$  drops out. In the last step we used that all  $p_c = 1/4$  and inserted the corresponding weights. Note that the factor of  $1/\sqrt{2}$  comes from the fact that the new configuration has a corner in the fermion loop.

There is one last step which is worth discussing in a bit more detail as well. This should not be presented as a problem, it should be rather seen as a technical aspect which can be solved in many ways. It is the point in the algorithm where the head and tail get placed onto the lattice and the first shift of the head takes place, or of course the other way round. We choose a probability  $\alpha$  which is the probability to remove the head and the tail from the lattice if they are on the same site. What is so special in that case is the fact that  $p_c$  is not symmetric anymore, i.e.  $p_c(\chi \rightarrow \chi') \neq p_c(\chi' \rightarrow \chi)$  when opening or closing the fermion worm. Since we want to propose every site with the probability of  $1/4$  it is important to account for that in  $p_A$ . In fig. 1.8 we present such a case, where head and tail are on the same site. We represent the tail by a green filled rectangle (■) in our vertex cartoons. If we now perform an update from  $\chi \rightarrow \chi'$  we have  $p_c(\chi \rightarrow \chi') = (1 - \alpha)/4$ ,

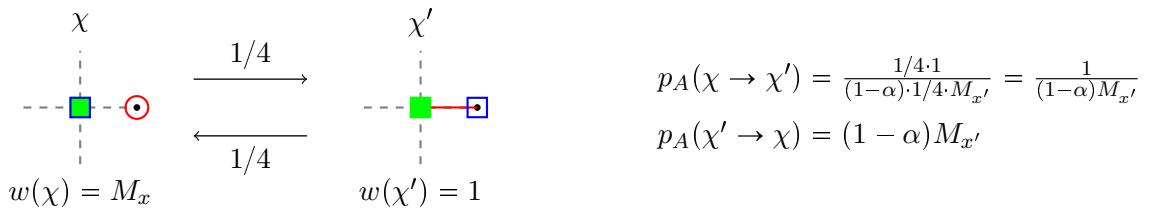


Figure 1.8.: Showing the opening and closing of the fermion worm. Head and tail get removed from the lattice with a probability of  $\alpha$ , therefore it takes  $1 - \alpha$  to open up and  $1/4$  to select a given site.

because we first ask if we want to remove head and tail with probability  $\alpha$  and then, if not removed, propose the actual shift to  $x'$ . The same principle needs to be applied when putting the head and tail onto the lattice and when removing it. This is because also in

### 1. Loop formulation of a free Majorana fermion in two dimensions

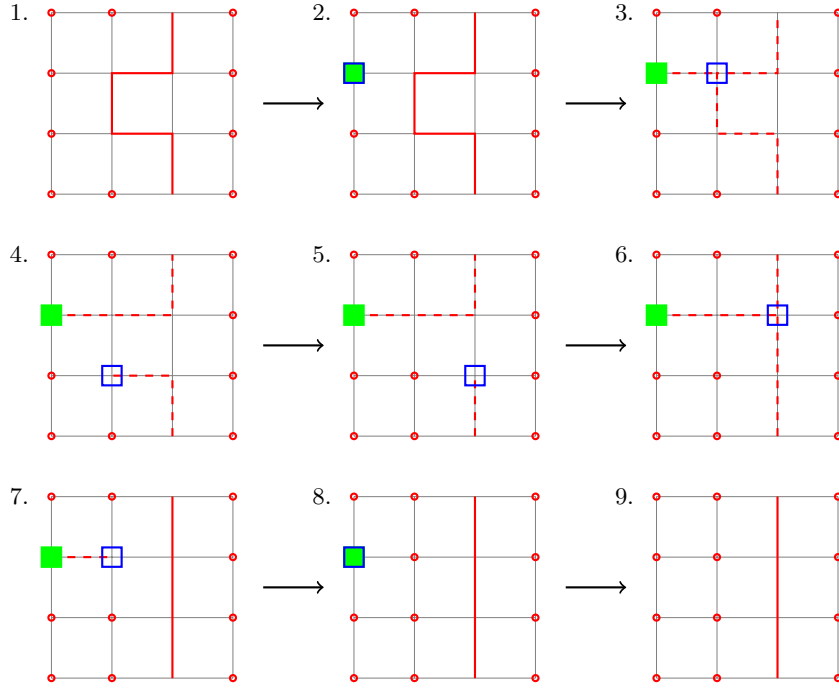


Figure 1.9.: A possible sequence of updating steps for a  $4 \times 4$  lattice. There are two artificial states, namely figure 3 and 6. Figure 1 and 9 are contributing to  $Z$ , whereas figures 2,4,5,7 and 8 are contributions to the two-point function.

that scenario,  $p_c$  is not symmetric. If we choose a site  $x$  to place our head and tail we take  $p_c(\chi \rightarrow \chi') = 1$ , whereas the probability to propose the removal from the lattice is  $p_c(\chi' \rightarrow \chi) = \alpha$ .

As a last note let us conclude that the choice of artificial weights and probabilities is truly a choice. A nice feature of this fact is that we can vary all artificial weights and all proposition probabilities and our physical observables must stay the same, it therefore forms a great tool for testing the code. The more important feature though is the fact that these probabilities and weights can be tuned in a model and parameter dependent way, such that CPU-time is reduced and the algorithm is working as efficiently as possible. Let us present a complete updating step with the worm algorithm to conclude this chapter. In fig. 1.9 we illustrate a sequence of updating procedures starting and ending with a configuration contributing to  $Z$ . In this figure we used a dashed line(---) to make clear which fermion links are actually part of the worm, whereas a solid line(—) marks the closed fermion loop. Monomer sites are again labelled with a red circle ( $\circ$ ), Head of the worm with ( $\square$ ) and tail with ( $\blacksquare$ ).

## 2. Boson bond formulation of $\phi^4$ -theory

The goal of this section is to understand how a bosonic bond formulation can be constructed for a simple boson lattice action. This reformulation can then be used to efficiently simulate the system with a so called worm algorithm that is working in principle like the one explained before for the free Majorana fermion.

The main motivation for establishing such a formulation is that simulations are possible with hardly any critical slowing down and an extraordinary high precision in measuring observables such as the two point function.

We will restrict ourselves to the  $\phi^4$ -model, which is extensively investigated, e.g. [52]. Reformulations in terms of closed loops have already been successfully simulated with a worm algorithm, e.g. see [53, 54].

In all models investigated in this work we will construct a boson bond formulation. However, as will be shown these seem less amenable to a worm-like update due to fluctuating signs. Therefore we will not discuss the algorithm in such detail as it was done for the fermion. For a more detailed and complete discussion of a worm algorithm based on the bond formulation of the  $\phi^4$ -theory we refer to [55]

### 2.1. Bond formulation of $\phi^4$ -model

The lattice action of the  $\phi^4$ -model in two-dimensional Euclidean space-time can, following [52], be written as

$$\hat{S} = \sum_x \left[ -\kappa \phi_x \sum_{\mu=0}^1 \phi_{x+\hat{\mu}} + V(\phi_x) \right], \quad (2.1)$$

where

$$V(\phi_x) = \frac{m^2}{2} \phi_x^2 + \frac{\lambda}{4} \phi_x^4. \quad (2.2)$$

The partition function can be defined as

$$Z = \int \mathcal{D}\phi \exp \left[ -\hat{S}(\phi) \right] = \prod_x \int d\phi_x \exp \left[ -\hat{S}(\phi) \right]. \quad (2.3)$$

We now expand the exponential of the hopping term  $\phi_x \phi_{x+\hat{\mu}}$  to all orders, giving us

$$Z = \prod_x \int d\phi_x \exp[-V(\phi_x)] \prod_{\mu=0}^1 \left( \sum_{n(x,\hat{\mu})}^{\infty} \frac{(\kappa \phi_x \phi_{x+\hat{\mu}})^{n(x,\hat{\mu})}}{n(x,\hat{\mu})!} \right), \quad (2.4)$$

where  $n(x, \mu) \in \mathbb{N}_0$  is called the occupation number between site  $x$  and site  $x + \hat{\mu}$ . Let us define the term configuration to correspond to a fixed set of bosonic bond numbers  $n(x, \hat{\mu})$ . The partition function can be build up by summing over all possible configurations  $\{c\}$ , i.e. combinations of  $n(x, \hat{\mu})$ . We can now define the total bosonic occupation number

## 2. Boson bond formulation of $\phi^4$ -theory

of a site  $x$ . It is telling us how many powers of  $\phi_x$  are present in a given configuration. The total number of powers is

$$N(x) = \sum_{\mu=0}^1 [n(x, \hat{\mu}) + n(x - \hat{\mu}, \hat{\mu})] . \quad (2.5)$$

It can be used to rewrite the partition function as

$$Z = \left[ \prod_x \prod_{\mu=0}^1 \left( \sum_{n(x, \hat{\mu})}^{\infty} \frac{\kappa^{n(x, \hat{\mu})}}{n(x, \hat{\mu})!} \right) \right] \prod_x Q(N(x)) , \quad (2.6)$$

where we introduced the site weight

$$Q(N_x) = \int d\phi_x \phi^{N(x)} \exp[-V(x)] = \int d\phi_x \phi^{N(x)} \exp \left[ -\frac{m^2}{2} \phi_x^2 - \frac{\lambda}{4} \phi_x^4 \right] . \quad (2.7)$$

From this integral we already see that  $N(x)$  must be even for all  $x$ , otherwise the integrand is zero. Translating this fact into the bond language we state that the sum of bonds connected to a site  $x$  must be even. Note that it will be convenient to sometimes write

$$Z = \sum_{\{c\}} \left[ \prod_x \prod_{\mu} \frac{\kappa^{n(x, \hat{\mu})}}{n(x, \hat{\mu})!} \right] \left[ \prod_x Q(N(x)) \right] , \quad (2.8)$$

where the sum over  $\{c\}$  is the sum over all configurations, i.e. different bond occupation numbers  $n(x, \mu)$  satisfying the constraint that  $N(x)$  is even  $\forall x$ .

In the next section we will now define the boson correlator in the just derived bond formulation.

### 2.1.1. Correlation function

The boson correlator is defined as the two-point function

$$C_{xy} = \langle \phi_x \phi_y \rangle = \frac{1}{Z} \int \mathcal{D}\phi \phi_x \phi_y \exp \left[ -\hat{S}(\phi) \right] , \quad (2.9)$$

If we add this insertion of  $\phi_x \phi_y$  in the bond formulation above we can simply modify the total occupation numbers  $N(x) = N(x) + 1$  and  $N(y) = N(y) + 1$ . Note that this means that the sum of all attached bonds to one of those sites must be odd in order to give an even occupation number and non-vanishing site weights

$$\int d\phi_x \phi_x^{N(x)+1} \exp[-V(\phi_x)] \quad \text{and} \quad \int d\phi_y \phi_y^{N(y)+1} \exp[-V(\phi_y)] . \quad (2.10)$$

## 2.2. Worm algorithm

The hopping expansion of the exponential of the bosonic kinetic term allowed us to reformulate the theory in terms of what we called occupation numbers  $n(x, \hat{\mu})$ . The worm algorithm for the boson bond formulation is working in the exact same fashion as for the fermion loop formulation. Let us, yet not in such detail as before, highlight the steps performed in the algorithm in order to update a system, i.e. create a new contribution to  $Z$ . When talking about the change in energy we refer to the ratio of the Boltzmann weights of the new configuration divided by the old one, analogously to  $w(\chi')/w(\chi)$  in eq.(1.88). The basic algorithm steps then are

1. Start with a valid configuration in  $Z$  by considering a fixed set of  $n(x, \hat{\mu})$  obeying the rule  $N(x) = \text{even} \forall x$
2. Propose to put a  $\phi_x \phi_x$  term onto the lattice. The change in energy of this action is

$$Q(N_x + 2)/Q(N_x) \quad (2.11)$$

and if accepted  $N(x) = N(x) + 2$ .

3. Ask to move one source  $\phi_x$  (called head) to a neighbouring site  $x + \hat{\mu}$ . Add or remove a bosonic bond between site  $x$  and  $x + \hat{\mu}$ . The change in energy when adding a bond is

$$\frac{\kappa}{n(x, \hat{\mu}) + 1} \frac{Q(N(x + \hat{\mu}) + 2)}{Q(N(x + \hat{\mu}))} \quad (2.12)$$

since there is a new bond(+1) and an additional power from the relocated source(+1) at site  $x + \hat{\mu}$ . If a bond is removed(-1) when relocating the source(-1) from  $x$  to  $x + \hat{\mu}$  the change in energy is

$$\frac{n(x, \hat{\mu})}{\kappa} \frac{Q(N(x) - 2)}{Q(N(x))}, \quad (2.13)$$

and all other  $Q$  weights stay the same and therefore cancel out. Redo this relocation until the head falls back onto the tail at  $x$ .

4. Take away the sources  $\phi_x \phi_x$ . The change in energy is

$$Q(N_x)/Q(N_x + 2) \quad (2.14)$$

and we again have a new contribution to the partition function.

Each action of course must be proposed and detailed balance condition must hold by correctly applying eq.(1.88) in each Metropolis update step. Note that when putting the sources  $\phi_x \phi_x$  on the lattice we leave the configuration space contributing to the partition function and enter the configuration space of the two-point functions to which we get a contribution after each shift of  $\phi_x$ . After taking the  $\phi_x \phi_x$  off the lattice we have a generally obtained new configuration contributing to  $Z$ .





### 3. $\mathcal{N} = 1$ $D = 2$ WESS-ZUMINO MODEL

In this chapter we study the spontaneous supersymmetry breaking of the  $\mathcal{N} = 1$  Wess-Zumino model in two dimensions and deliver a detailed symmetry phase diagram as well as the mass spectrum. The lattice serves us as a regulator and we use the Wilson fermion discretisation to describe the Majorana fermion and to remove the doublers. The use of Wilson fermions [56] serves the additional purpose of applying the already established fermion loop formulation for a Majorana fermion which can be used to efficiently simulate the fermionic degrees of freedom with a worm algorithm.

#### 3.1. Motivation

Spontaneous supersymmetry breaking and the corresponding phase transition is an interesting non-perturbative phenomenon which we want to study by considering the  $\mathcal{N} = 1$  Wess-Zumino model [16, 57] in two dimensions. It is one of the simplest models that allows for a spontaneous supersymmetry breaking. The model has a vanishing Witten index [29], which is a necessary but not sufficient condition for spontaneous supersymmetry breaking. The expected supersymmetry breaking pattern has already been analysed in [30] and was confirmed [31] by using Monte Carlo methods. More recent work was done in the Hamiltonian formulation [32, 58] giving lower bounds on the ground state energy and determining the transition point. In [33] exact renormalisation group methods are used and found a supersymmetry broken phase with a Goldstino, the Goldstone fermion [25] from the spontaneously broken supersymmetry. Further non-perturbative investigations [34] were done using Wilson derivatives for fermions and bosons, guaranteeing a supersymmetric continuum limit [36]. Recently a detailed analysis [35] of the phase diagram has been conducted using the SLAC derivative with a HMC<sup>1</sup>-algorithm. They have further determined masses of both, the boson and fermion field, and presented a renormalised symmetry phase diagram in the continuum for the  $\mathcal{N} = 1$  Wess-Zumino model on a two-dimensional Euclidean torus.

The lattice in general provides a convenient setup to perform detailed non-perturbative numerical investigations, however, in a system which exhibits spontaneous supersymmetry breaking, straightforward Monte Carlo simulations are not possible due to a fermion sign problem related to the vanishing of the Witten index. Using the Wilson fermion discretisation and performing a hopping expansion, one can formulate the partition function as a sum over closed fermion loop configurations which can be simulated very efficiently using the open fermion string algorithm [27]. In addition, the fermion loop formulation can provide a way to circumvent the sign problem [59]. This motivates us in deriving the loop

---

<sup>1</sup>Hybrid-Monte-Carlo

### 3. $\mathcal{N} = 1$ $D = 2$ WESS-ZUMINO MODEL

formulation of the  $\mathcal{N} = 1$  Wess-Zumino model with the Wilson discretisation.

Discretising the system generally breaks (or at least partially) supersymmetry explicitly, though a perturbative proof exists [36] that if a Wilson derivative is also used for the boson, the lattice Ward identities are equivalent to their continuum counterparts when sending the lattice spacing to zero. Therefore the supersymmetric continuum limit is recovered without fine tuning. This is supporting us again in the choice of Wilson derivatives. However, this comes at a cost of breaking the  $\mathbb{Z}_2$  symmetry explicitly that will only be restored completely when sending the lattice spacing to zero. Note that other discretisations that do not break the  $\mathbb{Z}_2$  symmetry are being used, such as the SLAC derivative used in [35] which creates a manifestly  $\mathbb{Z}_2$ -symmetric but non-local action. It is interesting to compare the two discretisations but also to consider further suitable techniques, e.g. domain wall fermions [60, 61].

We will now discuss the two-dimensional  $\mathcal{N} = 1$  Wess-Zumino model and discretise the model using Wilson derivatives [56] for the fermions and bosons. A hopping expansion of the Boltzmann factor of the fermionic part of the action will lead us to the fermion loop formulation, allowing us to write the partition function as a sum over all closed fermion loop configurations. These will then be simulated with a worm algorithm. In addition we also calculate the hopping expansion of the bosonic part of the action in order to create a boson bond formulation, being generally also amenable to an efficient simulation via worm algorithm. However, due to a sign problem in the bond formulation related to the use of the Wilson derivative, we will stick to the ordinary formulation and simulate the bosonic field with a Metropolis algorithm. With this setup we will then determine the critical point at which the symmetries break spontaneously and investigate the phase diagram of the bosonic and fermionic masses. It will be of special interest to see the mass degeneracy in the supersymmetric phase and to check the existence of a Goldstino in the broken one.

## 3.2. Continuum model

The two-dimensional on shell  $\mathcal{N} = 1$  Wess-Zumino model [16, 57] can be described by the continuum action in Euclidean spacetime

$$S = \int_0^\beta dx_0 \int dx_1 \left\{ \frac{1}{2} \partial_\mu \phi \partial^\mu \phi + \frac{1}{2} \bar{\psi} [\not{\partial} + P''(\phi)] \psi + \frac{1}{2} [P'(\phi)]^2 \right\}, \quad (3.1)$$

where  $\psi = \psi(x)$  is a real two component Majorana spinor. An entry is labelled with  $\psi^\alpha(x)$ , with  $\alpha = 1, 2$  being the Dirac index. The charge conjugation matrix arising in  $\bar{\psi} = \psi^T \mathcal{C}$  has the properties

$$\mathcal{C} \gamma_\mu \mathcal{C}^{-1} = -\gamma_\mu^T = -\gamma_\mu^*, \quad \mathcal{C}^\dagger = -\mathcal{C}^{-1} \quad \text{and} \quad \mathcal{C} = -\mathcal{C}^T, \quad (3.2)$$

and the  $\gamma_\mu$  matrices fulfil the anti-commutation relation  $\{\gamma_\mu, \gamma_\nu\} = 2\delta_{\mu\nu} \mathbf{1}_{2 \times 2}$ . The real scalar field is denoted by  $\phi = \phi(x)$  and  $P'(\phi)$  and  $P''(\phi)$  are the derivative and second derivative of the superpotential  $P(\phi)$  with respect to  $\phi$ , i.e.

$$P'(\phi) = \frac{\partial P(\phi)}{\partial \phi} \quad \text{and} \quad P''(\phi) = \frac{\partial^2 P(\phi)}{\partial \phi^2}. \quad (3.3)$$

We will address the specific choice of the superpotential below. The action in eq.(3.1) is invariant under a supersymmetry transformation  $\delta$ , which transforms  $\phi$ ,  $\psi$  and  $\bar{\psi}$  as follows,

$$\delta\phi = \bar{\epsilon}\psi, \quad \delta\psi = (\not{\partial}\phi - P')\epsilon, \quad \delta\bar{\psi} = 0, \quad (3.4)$$

where  $\epsilon$  is a constant Majorana spinor. Note that this supersymmetry only holds if the system has purely periodic boundary conditions, even for the fermionic fields in the temporal direction  $x_0$ . Like in [34], we choose the superpotential to be

$$P(\phi) = \frac{1}{3}g\phi^3 - \frac{m^2}{4g}\phi, \quad (3.5)$$

which is also called the minimal interacting superpotential. This form of the potential leads to an action with the Witten index being zero [29], which allows for spontaneous supersymmetry breaking. With the chosen superpotential we can now specify

$$P'(\phi) = g\phi^2 - \frac{m^2}{4g} \quad \text{and} \quad P''(\phi) = 2g\phi. \quad (3.6)$$

From the choice of such a superpotential a new symmetry of the action in eq.(3.1) emerges, it is now invariant under a discrete  $\mathbb{Z}_2$  chiral symmetry

$$\phi \rightarrow -\phi, \quad \psi \rightarrow \gamma_5\psi \quad \text{and} \quad \bar{\psi} \rightarrow -\bar{\psi}\gamma_5, \quad (3.7)$$

where  $\gamma_5$  is defined as

$$\gamma_5 = i\gamma_0\gamma_1 \quad (3.8)$$

and fulfils the anticommutation relation  $\{\gamma_5, \gamma_\mu\} = 0$ . With the above mentioned choice we can write our action as

$$S = \int d^2x \left\{ \frac{1}{2}\partial_\mu\phi\partial^\mu\phi + \frac{1}{2}\bar{\psi}(\not{\partial} + 2g\phi)\psi - \frac{m^2}{4}\phi^2 + \frac{g^2}{2}\phi^4 \right\}, \quad (3.9)$$

where the scalar potential allows for a spontaneous  $\mathbb{Z}_2$ -symmetry breaking and in the quenched case simply forms an ordinary  $\phi^4$ -theory. In fig. 3.1 the form of the scalar potential

$$\frac{[P'(\phi)]^2}{2} = \frac{1}{2} \left( g^2\phi^4 - \frac{m^2}{2}\phi^2 \right) + \text{const.} \quad (3.10)$$

is illustrated. There exist two classical minima at  $\phi_0 = \pm m/(2g)$ .

### 3. $\mathcal{N} = 1$ $D = 2$ WESS-ZUMINO MODEL

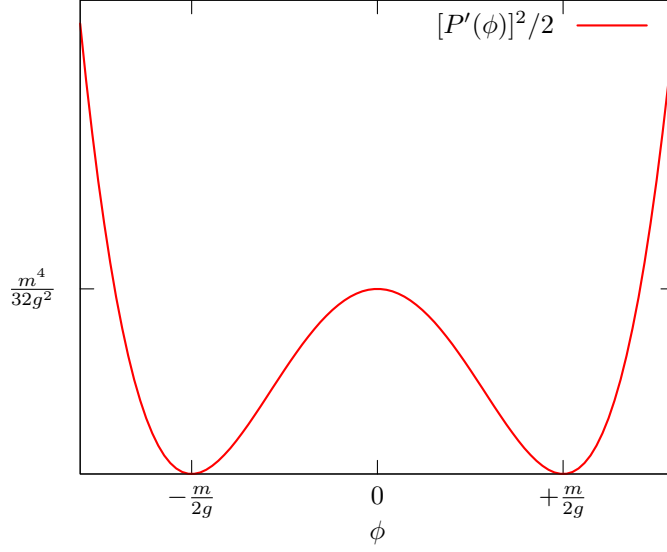


Figure 3.1.: This figure shows the classical form of the potential  $[P'(\phi)]^2/2$ , allowing for spontaneous symmetry breaking.

Note that it can be useful to shift the bosonic field  $\phi \rightarrow \phi - m/(2g)$  in order to work with a manifestly  $\mathbb{Z}_2$ -broken continuum action

$$S = \int d^2x \left\{ \frac{1}{2} \partial_\mu \phi \partial^\mu \phi + \frac{1}{2} \bar{\psi} \not{\partial} \psi + \bar{\psi} \psi g \phi + \frac{m^2}{2} \phi^2 + m g \phi^3 + \frac{g^2}{2} \phi^4 \right\}, \quad (3.11)$$

as it is done in [36]. The two models, the shifted and the non-shifted one, share the same point in terms of  $m$  and  $g$  where the symmetry breaks spontaneously, hence many results obtained in the shifted formulation can also be used for the action in eq.(3.9).

The partition function of the action  $S(\phi, \psi)$  from eq.(3.9) is

$$Z = \int \mathcal{D}\phi \int \mathcal{D}\psi \exp[-S(\phi, \psi)] \quad (3.12)$$

$$= \int \mathcal{D}\phi \exp[-S_B(\phi)] \int \mathcal{D}\psi \exp[-S_F(\phi, \psi)], \quad (3.13)$$

where we split up the action into a purely bosonic action  $S_B$  and fermionic action  $S_F$  which are of the form

$$S_B(\phi) = \int d^2x \left\{ \frac{1}{2} \partial_\mu \phi \partial^\mu \phi - \frac{m^2}{4} \phi^2 + \frac{g^2}{2} \phi^4 \right\}, \quad (3.14)$$

$$S_F(\phi, \psi) = \int d^2x \left\{ \frac{1}{2} \bar{\psi} (\not{\partial} + 2g\phi) \psi \right\}. \quad (3.15)$$

In the following we will now take a closer look at the Witten index and the Pfaffian before discretising the system and calculating the bosonic and fermionic lattice actions.

#### 3.2.1. Witten index

The Witten index [29] is defined as

$$W = \text{Tr} \left[ (-1)^{N_F} e^{-\beta H} \right], \quad (3.16)$$

where  $N_F$  is the fermion number operator. The formula above is a shortened notation for counting all existing ground states in the system. If a ground state is bosonic ( $N_F = 0$ ) it comes with a plus sign whereas if it is fermionic ( $N_F = 1$ ) it appears with a minus. In other words

$$W = n_B - n_F, \quad (3.17)$$

where  $n_B$  and  $n_F$  stand for the number of bosonic and fermionic ground states. The Witten index can be considered as a tool to determine whether supersymmetry can be spontaneously broken or not. If  $W \neq 0$  supersymmetry can not be broken. Note that this is a necessary but not sufficient condition, mathematically

$$W \neq 0 \Leftrightarrow \text{SUSY unbroken}, \quad (3.18)$$

$$W = 0 \Leftarrow \text{SUSY broken}. \quad (3.19)$$

With our choice of the superpotential in eq.(3.5) the Witten index is zero as can be seen as follows. The bosonic degrees of freedom always have periodic boundary conditions (b.c.), whereas the fermion can have either periodic b.c.  $\psi(x_0 = \beta) = \psi(x_0 = 0)$  or anti-periodic b.c.  $\psi(x_0 = \beta) = -\psi(x_0 = 0)$  in the temporal direction. Integrating out the Majorana fermion yields the (indefinite) Pfaffian  $\text{Pf}\mathcal{M}$  of the Majorana Dirac operator  $\mathcal{M}$ , appearing in

$$S_F(\phi, \psi) = \bar{\psi} \mathcal{M} \psi = \int d^2x \frac{1}{2} \bar{\psi} (\not{\partial} + 2g\phi) \psi. \quad (3.20)$$

The partition function with periodic b.c. for the fermion in both directions, denoted by  $Z_{pp}$ , is proportional to the Witten index,

$$Z_{pp} = \int \mathcal{D}\phi \exp[-S_B(\phi)] \int \mathcal{D}\psi \exp[-\bar{\psi} \mathcal{M}_{pp}(\phi) \psi] \quad (3.21)$$

$$= \int \mathcal{D}\phi \exp[-S_B(\phi)] \text{Pf}[\mathcal{M}_{pp}(\phi)] \quad (3.22)$$

$$\propto W. \quad (3.23)$$

Under a  $\mathbb{Z}_2$  symmetry transformation, where the bosonic field transforms as  $\phi \rightarrow -\phi$ , one finds

$$S_B(\phi) \rightarrow S_B(\phi) \quad \text{and} \quad \text{Pf}\mathcal{M}_{pp} \rightarrow -\text{Pf}\mathcal{M}_{pp}, \quad (3.24)$$

which tells us that for any bosonic field configuration that is contributing to  $Z_{pp}$ , there exists another one with exactly the same contribution but an opposite sign, hence yielding  $W = 0$ . The vanishing of the Witten index indicates that one is allowed to expect a bosonic and fermionic ground state which are related to one another by the supersymmetry transformation. However, in the case of thermal boundary conditions  $Z_{ap}$  (meaning anti-periodic b.c. for the fermions in temporal direction) the supersymmetry is broken by the finite temperature of the system and one finds

$$S_B(\phi) \rightarrow S_B(\phi) \quad \text{and} \quad \text{Pf}\mathcal{M}_{ap} \rightarrow +\text{Pf}\mathcal{M}_{ap}. \quad (3.25)$$

### 3.2.2. $\mathbb{Z}_2$ and supersymmetry

In order to understand the phases of the  $\mathcal{N} = 1$  Wess Zumino model better we would like to list some key features of the symmetry breaking pattern.

### 3. $\mathcal{N} = 1$ $D = 2$ WESS-ZUMINO MODEL

- With the given superpotential from eq.(3.5) the model enjoys a  $\mathbb{Z}_2$  symmetry which in the quenched scenario is identical to the well known  $\phi^4$ -theory that shows to have a  $\mathbb{Z}_2$  symmetric phase and a phase in which the  $\mathbb{Z}_2$  symmetry is spontaneously broken [52, 62]. This spontaneous symmetry breaking also appears in the full  $\mathcal{N} = 1$  Wess Zumino model and the value of the critical point is depends on the two parameters  $g$  and  $m$ , i.e.  $f = g/m$ .
- As previously shown the model has a Witten index that is zero, which is a necessary condition for spontaneous supersymmetry breaking.
- Both symmetries, the  $\mathbb{Z}_2$  and the supersymmetry are closely related. If the  $\mathbb{Z}_2$ -symmetry is spontaneously broken the system chooses to reside in one of two minima, either the one where  $\langle\phi\rangle = +m/(2g)$  or the other with  $\langle\phi\rangle = -m/(2g)$ . In the infinite volume the probability of tunnelling between those two vacua vanishes and the system selects one supersymmetric ground state. Therefore the model is supersymmetric in the  $\mathbb{Z}_2$ -broken phase. At the critical point where the  $\mathbb{Z}_2$  symmetry is restored the supersymmetry is expected to break spontaneously due to the degenerate ground state with  $\langle\phi\rangle = 0$ .

Let us summarise the phases of the  $\mathcal{N} = 1$  Wess Zumino model in a naive sketch in fig. 3.2, showing the expected symmetry phase diagram.

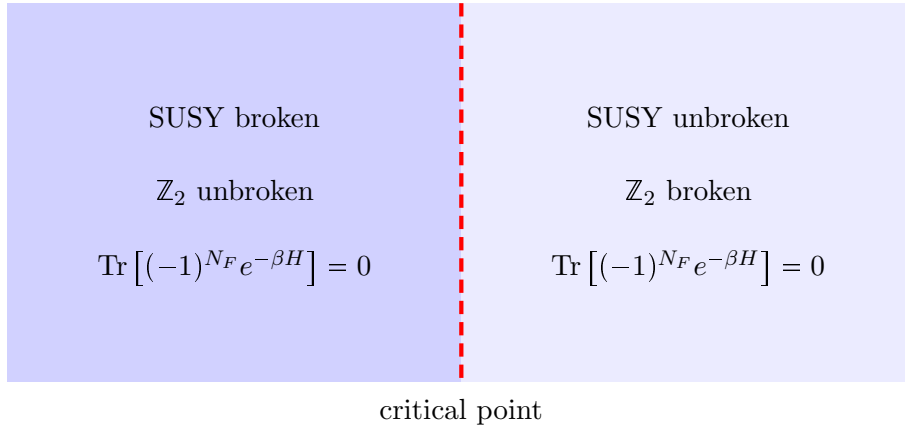


Figure 3.2.: Sketch of the expected symmetry phase diagram in the infinite volume.

Note that the Witten index is always zero since the number of ground states does not change. However, in the supersymmetric phase one ground state is spontaneously selected and the other one is inaccessible in the infinite volume limit. Despite still having two ground states in the action, an operator proportional to the Witten index, measuring  $n_b - n_f$ , would yield  $\pm 1$  in the supersymmetric phase in the infinite volume limit<sup>2</sup>.

<sup>2</sup>Note that this should be understood analogously to the  $\mathbb{Z}_2$  symmetry in a two-dimensional Ising model. The action enjoys a  $\mathbb{Z}_2$  symmetry but the ground state does not. Any simulation in the infinite volume limit would give a spin expectation value of  $\pm 1$  at zero temperature.

### 3.3. Discretisation

We introduce a two-dimensional lattice analogously to section 1.2.1 representing our discretised Euclidean space-time. The issue of recreating a supersymmetric theory when the lattice spacing is sent to zero forms a challenging problem that is strongly connected to the renormalisation of the theory. This is discussed a bit further in the section below by giving a summary of the work done in [36]. Afterwards we will then calculate the boson and fermion lattice actions explicitly based on this discretisation that reaches the supersymmetric continuum limit without fine tuning.

#### 3.3.1. Supersymmetric continuum limit

The goal of this section is to summarise and briefly discuss the results from [36], where Golterman and Pechter present a discretised action of the two-dimensional  $\mathcal{N} = 1$  Wess-Zumino model which is local and is guaranteed to have a supersymmetric continuum limit. This is done by considering Ward identities of supersymmetry in the continuum and to find a lattice action of the model such that the lattice Ward identities lead to their continuum counterparts when sending the lattice spacing to zero. It is explicitly shown that these identities satisfy the continuum Ward identities up to one loop in perturbation theory in the continuum limit. Up to terms of  $\mathcal{O}(a)$  this must be true to all orders of perturbation theory because all divergences of the model appear at the one loop level and can therefore be renormalised by supersymmetric counterterms. This comes from the fact that the theory is super-renormalisable. Note that on the lattice the superficial degree of divergence of a Feynman diagram may be different from the one in the continuum and there are generally additional divergent diagrams as compared to the continuum. Therefore they present a careful analysis of the divergent Feynman diagrams that occur at the one loop level and calculate the supersymmetric counterterms that are needed to renormalise the theory. The finite diagrams are all identical to their continuum counterparts when  $a \rightarrow 0$  due to the theorem of Reisz [63]

It is shown that the local action leading the Ward identities on the lattice to the correct continuum identities for  $a \rightarrow 0$  is the one with Wilson fermions and also a Wilson term for the bosons, i.e. Wilson bosons [64]. This is the discretisation that we will perform in the next section and which has also been used in [34]. One might ask oneself what happens if we only use the Wilson derivative for the fermionic degrees of freedom and treat the bosons with a symmetric derivative. It then turns out that extra lattice terms make the continuum limit of the lattice Ward identities no longer equivalent to the actual continuum Ward identities. This can be fixed by adding adequate extra terms which turn out to be exactly those that occur when using the Wilson derivative for both fields.

In a section 3.4 we will also use the results from [36] in order to renormalise the bare mass in our system which gets a divergent correction from the boson one loop self energy diagram.

### 3. $\mathcal{N} = 1$ $D = 2$ WESS-ZUMINO MODEL

#### 3.3.2. Bosonic lattice action

We use the symmetric lattice derivative operator

$$[\hat{\partial}_\mu^S]_{xy} = \frac{1}{2} (\delta_{x+\hat{\mu},y} - \delta_{x-\hat{\mu},y}) \quad (3.26)$$

and the Wilson term, already introduced in eq.(1.12),

$$[\Delta^{\mathcal{W}}]_{xy} = \frac{ra}{2} \sum_{\mu=0}^1 [\hat{\partial}_\mu^+]_{xz} [\hat{\partial}_\mu^-]_{zy}, \quad (3.27)$$

where  $\hat{\partial}_\mu^+$  is the forward and  $\hat{\partial}_\mu^-$  is the backward derivative. The lattice spacing  $a$  is set to one for convenience. The discretised bosonic part of the action in eq.(3.9) should then, identical to [34, 36], be

$$\hat{S}_B = \frac{1}{2} \left\{ -\phi_x [(\hat{\partial}^S)^2]_{xy} \phi_y + \hat{P}'_x \hat{P}'_x \right\}. \quad (3.28)$$

The Wilson term is then added in the potential

$$\hat{P}'_x = g\phi_x^2 - \frac{m^2}{4g} - [\Delta^{\mathcal{W}}]_{xy} \phi_y. \quad (3.29)$$

In prospect of creating a bosonic bond formulation we will need to know the explicit form of the bosonic action and determine all prefactors of all terms. Let us start by calculating the first term of  $\hat{S}_B$  explicitly

$$-\phi_x [(\hat{\partial}^S)^2]_{xy} \phi_y = -\phi_x [\hat{\partial}_\mu^S]_{xz} [\hat{\partial}_\mu^S]_{zy} \phi_y \quad (3.30)$$

$$= -\phi_x \frac{1}{4} \sum_{\mu} (\delta_{x+\hat{\mu},z} - \delta_{x-\hat{\mu},z}) (\delta_{z+\hat{\mu},y} - \delta_{z-\hat{\mu},y}) \phi_y \quad (3.31)$$

$$= -\phi_x \frac{1}{4} \sum_{\mu} (\delta_{x+2\hat{\mu},y} + \delta_{x-2\hat{\mu},y} - 2\delta_{xy}) \phi_y \quad (3.32)$$

$$= \phi_x^2 - \frac{1}{4} \phi_x \sum_{\mu} (\phi_{x+2\hat{\mu}} + \phi_{x-2\hat{\mu}}). \quad (3.33)$$

We are now left with the calculation of the squared lattice potential

$$\begin{aligned} \hat{P}'_x \hat{P}'_x &= \left( g\phi_x^2 - \frac{m^2}{4g} - [\Delta^{\mathcal{W}}]_{xy} \phi_y \right) \left( g\phi_x^2 - \frac{m^2}{4g} - [\Delta^{\mathcal{W}}]_{xy} \phi_y \right) \\ &= g^2 \phi_x^4 - \frac{m^2}{2} \phi_x^2 + \frac{m^4}{16g^2} \underbrace{-2g\phi_x^2 [\Delta^{\mathcal{W}}]_{xy} \phi_y}_A + \cancel{\frac{m^2}{2g} [\Delta^{\mathcal{W}}]_{xy} \phi_y} \xrightarrow{0} + \underbrace{[\Delta^{\mathcal{W}}]_{xy} \phi_y [\Delta^{\mathcal{W}}]_{xz} \phi_z}_B. \end{aligned}$$

Since we are computing an action we can get rid of the constant term  $m^4/(16g^2)$  and what is left is the calculation of the terms in  $A$ , containing one power of  $r$  and  $B$ , containing terms with two powers of  $r$ . In the following we will set  $r = 1$  for convenience, finding

$$\begin{aligned} A &= -2g\phi_x^2 [\Delta^{\mathcal{W}}]_{xy} \phi_y \\ &= -2g\phi_x^2 \frac{1}{2} \sum_{\mu} (\delta_{x+\hat{\mu},y} + \delta_{x-\hat{\mu},y} - 2\delta_{x,y}) \phi_y \\ &= -g\phi_x^2 \phi_{x+\hat{0}} - g\phi_x^2 \phi_{x-\hat{0}} - g\phi_x^2 \phi_{x+\hat{1}} - g\phi_x^2 \phi_{x-\hat{1}} + 4g\phi_x^3 \\ &= 4g\phi_x^3 - g\phi_x^2 \sum_{\mu} (\phi_{x+\hat{\mu}} + \phi_{x-\hat{\mu}}) \end{aligned} \quad (3.34)$$



and

$$\begin{aligned}
 B &= [\Delta^{\mathcal{W}}]_{xy} \phi_y [\Delta^{\mathcal{W}}]_{xz} \phi_z \\
 &= \frac{1}{2} \sum_{\mu} (\delta_{x+\hat{\mu},y} + \delta_{x-\hat{\mu},y} - 2\delta_{xy}) \frac{1}{2} \sum_{\nu} (\delta_{x+\hat{\nu},z} + \delta_{x-\hat{\nu},z} - 2\delta_{xz}) \phi_y \phi_z \\
 &= \frac{1}{4} (\delta_{x+\hat{0},y} + \delta_{x-\hat{0},y} + \delta_{x+\hat{1},y} + \delta_{x-\hat{1},y} - 4\delta_{xy}) \\
 &\quad \times (\delta_{x+\hat{0},z} + \delta_{x-\hat{0},z} + \delta_{x+\hat{1},z} + \delta_{x-\hat{1},z} - 4\delta_{xz}) \phi_y \phi_z \\
 &= 5\phi_x^2 + \frac{1}{2} \phi_{x-\hat{0}} \phi_{x+\hat{0}} + \frac{1}{2} \phi_{x-\hat{1}} \phi_{x+\hat{1}} \\
 &\quad + \frac{1}{2} \phi_{x+\hat{0}} \phi_{x+\hat{1}} + \frac{1}{2} \phi_{x+\hat{1}} \phi_{x-\hat{0}} + \frac{1}{2} \phi_{x-\hat{0}} \phi_{x-\hat{1}} + \frac{1}{2} \phi_{x+\hat{0}} \phi_{x-\hat{1}} \\
 &\quad - 2\phi_x (\phi_{x+\hat{0}} + \phi_{x-\hat{0}} + \phi_{x+\hat{1}} + \phi_{x-\hat{1}}) \\
 &= 5\phi_x^2 + \frac{1}{2} \phi_{x-\hat{0}} \phi_{x+\hat{0}} + \frac{1}{2} \phi_{x-\hat{1}} \phi_{x+\hat{1}} \\
 &\quad + \frac{1}{2} \phi_{x+\hat{0}} \phi_{x+\hat{1}} + \frac{1}{2} \phi_{x+\hat{1}} \phi_{x-\hat{0}} + \frac{1}{2} \phi_{x-\hat{0}} \phi_{x-\hat{1}} + \frac{1}{2} \phi_{x+\hat{0}} \phi_{x-\hat{1}} \\
 &\quad - 2\phi_x \sum_{\mu} (\phi_{x+\hat{\mu}} + \phi_{x-\hat{\mu}}), \tag{3.35}
 \end{aligned}$$

where we can, due to the fact that we are summing over all sites in the action, rewrite the expression in a symmetrised way

$$B = 5\phi_x^2 + \frac{1}{4} \phi_x \sum_{\mu} (\phi_{x+2\hat{\mu}} + \phi_{x-2\hat{\mu}}) + \frac{1}{2} \phi_x \sum_{ij} \phi_{x+\kappa_{ij}} - 2\phi_x \sum_{\mu} (\phi_{x+\hat{\mu}} + \phi_{x-\hat{\mu}}). \tag{3.36}$$

We just introduced  $\kappa_{ij} = (-1)^i \hat{0} + (-1)^j \hat{1}$ , with  $i, j \in \{0, 1\}$  for notational convenience. Note that the factor of  $1/2$  in front of the next to nearest neighbour interaction term arises due to the fact that in the symmetrised version each term arises twice when performing the sum over all sites. The explicit form of the lattice potential squared is now

$$\begin{aligned}
 \hat{P}'_x \hat{P}'_x &= g^2 \phi_x^4 + 4g\phi_x^3 + \left(5 - \frac{m^2}{2}\right) \phi_x^2 - g\phi_x^2 \sum_{\mu} (\phi_{x+\hat{\mu}} + \phi_{x-\hat{\mu}}) + \\
 &\quad + \frac{1}{4} \phi_x \sum_{\mu} (\phi_{x+2\hat{\mu}} + \phi_{x-2\hat{\mu}}) + \frac{1}{2} \phi_x \sum_{ij} \phi_{x+\kappa_{ij}} - 2\phi_x \sum_{\mu} (\phi_{x+\hat{\mu}} + \phi_{x-\hat{\mu}}). \tag{3.37}
 \end{aligned}$$

Respecting also the overall factor of  $1/2$  in eq.(3.28), the bosonic lattice action can be put together by adding the lattice potential squared to the kinetic term and we find

$$\hat{S}_B = \sum_x \left[ V(\phi_x) - \frac{g}{2} \phi_x^2 \sum_{\mu} (\phi_{x+\hat{\mu}} + \phi_{x-\hat{\mu}}) + \frac{1}{4} \phi_x \sum_{ij} \phi_{x+\kappa_{ij}} - \phi_x \sum_{\mu} (\phi_{x+\hat{\mu}} + \phi_{x-\hat{\mu}}) \right], \tag{3.38}$$

where  $V(\phi_x)$  is

$$V(\phi_x) = \frac{g^2}{2} \phi_x^4 + 2g\phi_x^3 + \left(3 - \frac{m^2}{4}\right) \phi_x^2. \tag{3.39}$$

The next to nearest neighbour interaction terms

$$\phi_x \sum_{\mu} (\phi_{x+2\hat{\mu}} + \phi_{x-2\hat{\mu}}) \tag{3.40}$$

### 3. $\mathcal{N} = 1$ $D = 2$ WESS-ZUMINO MODEL

dropped out when adding the square of the potential to the kinetic term and we are finally left with three different interaction terms in eq.(3.38). Note that the Wilson term in the potential is responsible for the explicit breaking of the  $\mathbb{Z}_2$  symmetry at finite lattice spacings. The terms that break the symmetry explicitly are all terms arising in  $A = -2g\phi_x^2[\Delta^{\mathcal{W}}]_{xy}\phi_y$ . Note though that all these are proportional to  $ra$  and therefore the action is  $\mathbb{Z}_2$ -symmetric when  $a \rightarrow 0$ .

#### 3.3.3. Fermionic lattice action

We now turn to the explicit form of the fermionic lattice action. The fermionic part of the continuum action is

$$S_F = \int d^2x \frac{1}{2} \bar{\psi} [\not{D} + P''(\phi)] \psi. \quad (3.41)$$

The discretised version can be written as

$$\hat{S}_F = \frac{1}{2} \psi_x^T \mathcal{C} K_{xy} \psi_y, \quad (3.42)$$

where

$$K_{xy} = \gamma^\mu [\hat{\partial}_\mu^S]_{xy} + P''_{xy} \quad (3.43)$$

and the second derivative of the potential on the lattice takes the form

$$P''_{xy} = 2g\phi_x \delta_{xy} - [\Delta^{\mathcal{W}}]_{xy} \quad (3.44)$$

which includes the Wilson term  $\Delta^{\mathcal{W}}$  in order to take care of the fermion doublers. With our specific choice of the super potential in eq.(3.5) the full fermion lattice action can now simply be written as

$$\hat{S}_F = \frac{1}{2} \psi_x^T \mathcal{C} \left[ \gamma^\mu [\hat{\partial}_\mu^S]_{xy} + P''_{xy} \right] \psi_y \quad (3.45)$$

$$= \frac{1}{2} \psi_x^T \mathcal{C} \left[ \gamma^\mu [\hat{\partial}_\mu^S]_{xy} + 2g\phi_x \delta_{xy} - [\Delta^{\mathcal{W}}]_{xy} \right] \psi_y \quad (3.46)$$

$$= \frac{1}{2} \psi_x^T \mathcal{C} \left[ \gamma^\mu \frac{1}{2} (\delta_{x+\hat{\mu},y} - \delta_{x-\hat{\mu},y}) + 2g\phi_x \delta_{xy} - \frac{1}{2} \sum_{\mu} (\delta_{x+\hat{\mu},y} + \delta_{x-\hat{\mu},y} - 2\delta_{xy}) \right] \psi_y, \quad (3.47)$$

where again  $a$  and  $r$  are set to one. The derivatives, which manifest themselves as combinations of Kronecker-deltas here, can be written in a more compact form

$$\hat{S}_F = \frac{1}{2} \psi_x^T \mathcal{C} \left[ (2 + 2g\phi_x) \delta_{xy} - \frac{1}{2} \sum_{\mu} ((1 - \gamma_\mu) \delta_{x+\hat{\mu},y} + (1 + \gamma_\mu) \delta_{x-\hat{\mu},y}) \right] \psi_y. \quad (3.48)$$

We replace the term  $2 + 2g\phi_x$  with  $M(\phi_x)$  and will call  $\psi_x^T \mathcal{C} M(\phi_x) \psi_x$  the monomer term. With this notation the action reads

$$\hat{S}_F = \frac{1}{2} \psi_x^T \mathcal{C} \left[ M(\phi_x) \delta_{xy} - \frac{1}{2} \sum_{\mu} ((1 - \gamma_\mu) \delta_{x+\hat{\mu},y} + (1 + \gamma_\mu) \delta_{x-\hat{\mu},y}) \right] \psi_y. \quad (3.49)$$

and is up to the actual form of  $M(\phi_x)$  identical to the free Majorana fermion discussed in section 1.2.2.

We now discretised the system and established the boson and fermion lattice actions. In the next section we discuss the renormalisation of the bare mass when performing the continuum limit.

### 3.4. Renormalisation

The continuum limit of the model is obtained by sending the lattice spacing to zero, i.e.  $a \rightarrow 0$ . When sending the lattice spacing to zero the cut-off goes to infinity and we need a renormalisation procedure in order to obtain finite results for physical quantities. In [36] we find a list of all divergent loop diagrams, which in the continuum appear all at one loop level since the theory is super renormalisable. On the lattice the superficial degree of freedom is different from the continuum and the divergence is maximally pushed to the two loop level. However, this is not the case for our discretisation and we can add counter terms  $\delta$  that cancel the one loop divergences. In the following we will focus on the renormalisation of the bare mass  $m$  and denote the renormalised quantity with a superscript  $m^R$ .

The boson one loop self energy correction of the bare mass is diverging when sending the lattice spacing to zero. This divergent one loop diagram is shown in fig. 3.3.

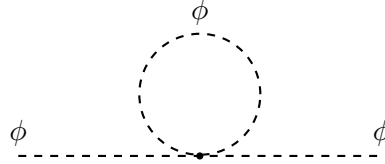


Figure 3.3.: Divergent one loop self energy of  $\phi$

By logarithmic renormalisation the mass parameter can be made finite. Hence, like in [35], we add an appropriate counter term  $\delta_{m^2}$  which includes only the 1PI part of the diagram shown in fig. 3.3. The renormalised mass  $(m^R)^2$  is then defined by

$$(m^R)^2 = m^2 + 2g^2\delta_{m^2} \quad (3.50)$$

where, as shown in [36],

$$\delta_{m^2} = \frac{1}{L_0 L_1} \sum_{k_0=1}^{L_0} \sum_{k_1=1}^{L_1} \frac{1}{K^2(k_\mu) - \square(k_\mu)}, \quad (3.51)$$

with

$$K(k_\mu) = m + \sum_{\mu} \left( 1 - \cos \left( \frac{2\pi k_\mu}{L_\mu} \right) \right), \quad (3.52)$$

coming from the Wilson derivative of the boson and

$$\square(k_\mu) = - \sum_{\mu} \sin^2 \left( \frac{2\pi k_\mu}{L_\mu} \right) \quad (3.53)$$

### 3. $\mathcal{N} = 1$ $D = 2$ WESS-ZUMINO MODEL

from the symmetric lattice derivative in Fourier space. For the sake of completeness we like to mention that  $\phi^2$  gets corrections from a divergent tadpole diagram and therefore an additional counter term would be needed to render the theory completely finite. As realised in [36], the complete renormalisation of the theory can be achieved by modifying the potential from eq.(3.6) by

$$\hat{P}'_x + \frac{g}{2\pi} \log(\mu a), \quad (3.54)$$

where  $\mu$  is an arbitrary scale factor.

## 3.5. Hopping expansion

In this section we expand the Boltzmann factor of the boson and fermion action and derive a bond representation for the bosonic degrees of freedom and a fermion loop formulation for the fermionic degrees of freedom. The hopping expansion is of particular interest since it is amenable to the worm algorithm. The derivation of the loop formulation is already done in section 1.3 for the free Majorana fermion and does not need much work to be adapted to the two-dimensional Wess Zumino model. In the case of the bosonic field variables all the terms of the expansion need to be considered, as already shown in section 2.1. Due to the Wilson term arising in  $\hat{P}'\hat{P}'$ , we will see that the bosonic bond representation of the two-dimensional Wess Zumino model suffers from a sign problem. Let us nevertheless still illustrate the construction of the bosonic bond representation before turning to the fermion loop formulation.

### 3.5.1. Boson bond formulation

We start by considering the pure bosonic lattice action from eq.(3.38), which is

$$\hat{S}_B = \sum_x \left[ V(\phi_x) - \frac{g}{2} \phi_x^2 \sum_{\mu} (\phi_{x+\hat{\mu}} + \phi_{x-\hat{\mu}}) + \frac{1}{4} \phi_x \sum_{ij} \phi_{x+\kappa_{ij}} - \phi_x \sum_{\mu} (\phi_{x+\hat{\mu}} + \phi_{x-\hat{\mu}}) \right] \quad (3.55)$$

where  $V(\phi_x)$  is

$$V(\phi_x) = \frac{g^2}{2} \phi_x^4 + 2g\phi_x^3 + (3 - \frac{m^2}{4})\phi_x^2. \quad (3.56)$$

In the action above all interaction terms are written in a symmetric way. However, when considering the bond formulation it is more useful to write the action in a way such that each interaction, corresponding to a specific bond, is only occurring once when performing the sum over all sites. Writing down the action in such a way leads to

$$\hat{S}_B = \sum_x \left[ V(\phi_x) - \frac{g}{2} \phi_x^2 \sum_{\mu} (\phi_{x+\hat{\mu}} + \phi_{x-\hat{\mu}}) + \frac{1}{2} \phi_x \sum_j \phi_{x+\kappa_{0j}} - 2\phi_x \sum_{\mu} \phi_{x+\hat{\mu}} \right], \quad (3.57)$$

lets us read off the corresponding bond weights easily. Note that the second term in eq.(3.57) generates two different kinds of interactions on a given bond connecting  $x$  and  $x+\hat{\mu}$ , namely  $\phi_x^2 \phi_{x+\hat{\mu}}$  and  $\phi_x \phi_{x+\hat{\mu}}^2$ . When talking about a bond we will refer to an interaction between two sites occurring in the formula above. There exist two bonds connecting nearest neighbour sites, two diagonal bonds and four bonds corresponding to the  $\phi_x^2 \phi_{x+\mu}$

interaction, which we will refer to as triangular bonds. A graphical representation of all these bonds in fig.3.4.

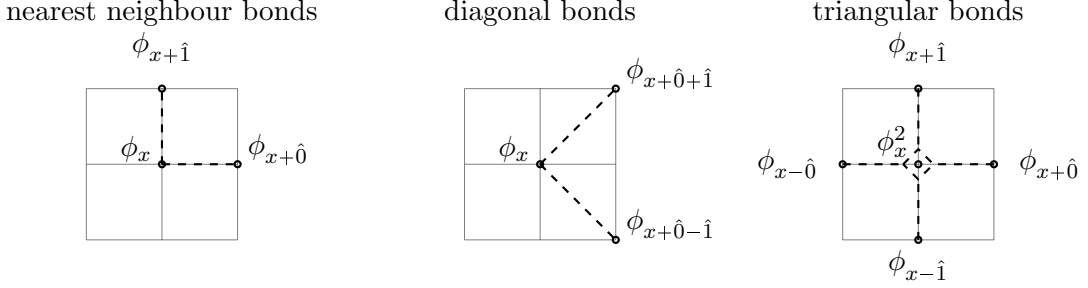


Figure 3.4.: In this figure we illustrate all bonds corresponding to interactions with the boson field on site  $x$ .

When we expand the bosonic Boltzmann factors  $\exp(-\hat{S}_B)$ , we get

$$\begin{aligned} \exp(-\hat{S}_B) = & \prod_x \prod_\mu \left( \sum_{n(x, \hat{\mu})=0}^{\infty} 2^{n(x, \hat{\mu})} \frac{(\phi_x \phi_{x+\hat{\mu}})^{n(x, \hat{\mu})}}{n(x, \hat{\mu})!} \right) \\ & \prod_x \prod_\mu \left( \sum_{d(x, \kappa_{0\mu})=0}^{\infty} \left( -\frac{1}{2} \right)^{d(x, \kappa_{0\mu})} \frac{(\phi_x \phi_{x+\kappa_{0\mu}})^{d(x, \kappa_{0\mu})}}{d(x, \kappa_{0\mu})!} \right) \\ & \prod_x \prod_\mu \left( \sum_{t(x, \pm\hat{\mu})=0}^{\infty} \left( \frac{g}{2} \right)^{t(x, \pm\hat{\mu})} \frac{(\phi_x^2 \phi_{x\pm\hat{\mu}})^{t(x, \pm\hat{\mu})}}{t(x, \pm\hat{\mu})!} \right) \prod_x e^{-V(\phi_x)}, \quad (3.58) \end{aligned}$$

where  $n(x, \hat{\mu})$  is the bond occupation number at site  $x$  in direction of  $\hat{\mu}$  and  $d(x, \kappa_{0\mu})$  for the number of diagonal bonds in direction  $\hat{\kappa}_{0\mu} = \hat{0} + (-1)^\mu \hat{1}$ . The bond occupation number  $t(x, \pm\hat{\mu})$  stands for the number of triangular bonds in direction  $\pm\hat{\mu}$ , these are different bonds and we simply shortened the notation above by writing  $\pm\hat{\mu}$  where actually two separate terms, one for each bond, would be correct. From eq.(3.58) we can read of the weight of each bond. The nearest neighbour bonds contribute with a weight of  $w(n(x, \hat{\mu})) = 2$ , the diagonal bonds with  $w(d(x, \hat{\kappa}_{0\mu})) = -1/2$  and the triangular bonds with  $w(t(x, \hat{\mu})) = g/2$ . We can now write down the complete bosonic site occupation number

$$\begin{aligned} N^B(x) = & \sum_\mu [n(x, \hat{\mu}) + n(x - \hat{\mu}, \hat{\mu}) + d(x, \hat{\kappa}_{0\mu}) + d(x + \hat{\kappa}_{1\mu}, \hat{\kappa}_{0\mu}) \\ & + 2t(x, \pm\hat{\mu}) + t(x \pm \hat{\mu}, \mp\hat{\mu})], \quad (3.59) \end{aligned}$$

which is the total number of bonds which are connected to that one site  $x$ . Note that we shortened the notation by meaning  $t(x, \pm\hat{\mu}) = t(x, +\hat{\mu}) + t(x, -\hat{\mu})$  and  $t(x \pm \hat{\mu}, \mp\hat{\mu}) = t(x + \hat{\mu}, -\hat{\mu}) + t(x - \hat{\mu}, +\hat{\mu})$ , which are all the possible triangular bonds connected to the site  $x$ . The factor of two in front of  $t(x, \pm\hat{\mu})$  comes from the fact that the triangular bond involves a factor of  $\phi_x^2$ , which rises the number of powers of the field by two. With this

### 3. $\mathcal{N} = 1$ $D = 2$ WESS-ZUMINO MODEL

formulation we can now write down a local weight

$$W^B(x) = Q(N^B(x)) \left[ \prod_{\mu} \frac{2^{n(x, \hat{\mu})}}{n(x, \hat{\mu})!} \frac{\left(\frac{-1}{2}\right)^{d(x, \hat{\kappa}_{0\mu})}}{d(x, \hat{\kappa}_{0\mu})!} \frac{\left(\frac{g}{2}\right)^{t(x, \pm \hat{\mu})}}{t(x, \pm \hat{\mu})!} \right] \quad (3.60)$$

where the only part that needs to be calculated for a given  $N^B(x)$  is

$$Q(N^B(x)) = \int_{-\infty}^{\infty} d\phi_x \phi_x^{N^B(x)} e^{-V(\phi_x)}. \quad (3.61)$$

The total boson weight  $W_{tot}^B$  of one specific configuration of the partition function can be calculated by simply performing the product over all local weights, i.e.

$$W_{tot}^B = \prod_x W^B(x). \quad (3.62)$$

The contributions from the bosonic part of the action to the partition function can be written as

$$Z_B = \sum_{\text{all bond conf.}} \prod_x W^B(x), \quad (3.63)$$

where the sum over all bond configurations is the sum over all integers for every bond occupation number from zero to infinity.

We now established a formulation in which we can calculate the contribution to the partition function from the bosonic part of the action by performing a sum over all possible bond occupation numbers and integrating out each  $\phi_x$  separately on every site. The formulation is now ready to be simulated by a worm-like algorithm explained in section 2.2. However, a sign problem arises when dealing with the diagonal bonds. This is because every diagonal bond contributes with a negative weight of  $w(d(x, \hat{\kappa}_{0\mu})) = -1/2$  and therefore local changes in the diagonal bonds change the overall sign of the contribution to the partition function, resulting in a fluctuating sing. Further  $Q(N^B(x))$  is also not guaranteed to be positive. Note that using a symmetric derivative for the bosonic field would resolve these problems, however this would force us to fine tune our model to reach a supersymmetric continuum limit.

#### 3.5.2. Fermion loop expansion

Following the concept of section 1.3, we introduce Wilson projectors

$$\mathcal{P}_{\pm\mu} = \frac{1}{2} (1 \mp \gamma_{\mu}) \quad (3.64)$$

and use the steps in eq.(1.22) to eq.(1.28) in order to rewrite eq.(3.48) and find

$$\hat{S}_F = \sum_x \left( \frac{1}{2} M(\phi_x) \psi_x^T \mathcal{C} \psi_x - \sum_{\mu} \psi_x^T \mathcal{C} \mathcal{P}_{+\mu} \psi_{x+\mu} \right). \quad (3.65)$$

The exponential  $\exp[-\hat{S}_F(\psi, \phi)]$  can now be expanded and is exact after the first order, due to the nilpotency of the Grassmann variables. The hopping expansion then takes the

following form

$$\exp \left[ -\hat{S}_F(\psi, \phi) \right] = \exp \left[ -\sum_x \left( \frac{1}{2} M(\phi_x) \psi_x^T \mathcal{C} \psi_x - \sum_{\mu} \psi_x^T \mathcal{C} \mathcal{P}_{+\mu} \psi_{x+\hat{\mu}} \right) \right] \quad (3.66)$$

$$= \prod_x \left( 1 - \frac{1}{2} M(\phi_x) \psi_x^T \mathcal{C} \psi_x \right) \prod_{x, \mu} (1 + \psi_x^T \mathcal{C} \mathcal{P}_{+\mu} \psi_{x+\hat{\mu}}) . \quad (3.67)$$

Let us rewrite the expansion as

$$\begin{aligned} \exp \left[ -S_F(\bar{\psi}, \psi, \phi) \right] &= \prod_x \left[ \sum_{m(x)=0}^1 \left( -\frac{1}{2} M(\phi_x) \psi_x^T \mathcal{C} \psi_x \right)^{m(x)} \right] \\ &\times \prod_{x, \mu} \left[ \sum_{h(x, \hat{\mu})=0}^1 \left( \psi_x^T \mathcal{C} \mathcal{P}_{\hat{\mu}} \psi_{x+\hat{\mu}} \right)^{h(x, \hat{\mu})} \right] , \end{aligned} \quad (3.68)$$

where  $m(x) \in \{0, 1\}$  is the site occupation number telling us if a site is saturated by a monomer term or not, and  $h(x, \hat{\mu}) \in \{0, 1\}$  a bond occupation number, which is doing the same for the hopping term. The Grassmann integral only gives non zero values when having exactly one copy of  $\psi_x^T \mathcal{C}$  and  $\psi_x$  at each site  $x$ , this can be mathematically expressed in terms of a constraining equation for the just introduced occupation numbers

$$m(x) + \frac{1}{2} \sum_{\mu=0}^1 [h(x - \hat{\mu}, \hat{\mu}) + h(x, \hat{\mu})] = 1 \quad \forall x . \quad (3.69)$$

Essentially we reformulated our models' degrees of freedom in terms of occupation numbers  $m(x)$  and  $h(x, \hat{\mu})$  and can now describe any fermionic configuration with those variables.

This hopping expansion of the Wess Zumino model is almost identical to the one of the free Majorana fermion explained in section 1.3.2. The only difference is that here the monomer term contributes with  $M = 2 + 2g\phi$  instead of  $M = m + 2$ . The partition function can now be described by a sum over all loop configurations  $\{c\}$  which have closed, self-avoiding and non backtracking loops  $\Omega = \Omega_1, \Omega_2, \dots$ , where all sites not part of a loop, i.e.  $\Lambda \setminus \Omega$ , are occupied by a mass monomer term. This results in

$$Z = \int \mathcal{D}\phi \exp[-\hat{S}_B(\phi)] \sum_{\{c\}} W^M(\Lambda \setminus \Omega) \prod_{\Omega_i \in \{c\}} W^F(\Omega_i) , \quad (3.70)$$

where  $W^M$  and  $W^F$  are the weights contributing to the partition function coming from the monomer terms and the loop terms, respectively. The contribution from the Dirac algebra structure for a given geometrically fixed loop  $\Omega_i$  is identical to the one of the free Majorana which was derived in section 1.4, namely

$$W^F(\Omega_i) = -(-1)^{\nu(\Omega_i)} 2^{-\frac{n_c(\Omega_i)}{2}} , \quad (3.71)$$

where  $\nu(\Omega_i)$  is the number of total rotations and  $n_c(\Omega_i)$  the number of corners along the loop  $\Omega_i$ . The weight coming from the monomer terms can be straightforwardly adapted and one finds  $M(\phi_x) = 2 + 2g\phi_x$ . Note that in general  $M(\phi)$  might also be negative,

### 3. $\mathcal{N} = 1$ $D = 2$ WESS-ZUMINO MODEL

however, this is not the case in the parameter region we are interested in<sup>3</sup>. The partition function with explicit weights from the fermionic terms in the action then has the following form

$$Z = \int \mathcal{D}\phi \exp[-\hat{S}_B(\phi)] \sum_{\{c\}} \left[ \prod_{x \in \{\Lambda \setminus \Omega\}} (2 + 2g\phi_x) \prod_{\Omega_i \in \{c\}} \left( -(-1)^{\nu(\Omega_i)} 2^{-\frac{n_c(\Omega_i)}{2}} \right) \right]. \quad (3.72)$$

The sign of a contribution from a fermion loop configuration is identical to the case of the free Majorana fermion, discussed in detail in section 1.6. The observables follow the same description as explained in section 1.7 and the closed loop configuration can analogously to section 1.8 be updated by a worm algorithm.

In the following we will now use the loop formulation in order to investigate the phase diagram and determine the critical coupling at which supersymmetry breaks spontaneously. This will be followed by measuring the masses of the fermion and boson in both, the supersymmetry broken and unbroken phase.

## 3.6. Critical point

In this section we will discuss the phase diagram of the two-dimensional  $\mathcal{N} = 1$  Wess-Zumino model by considering numerical results and investigations of the critical point which is separating the supersymmetric phase from the supersymmetry-broken phase. In section 3.7 we will then complete the discussion by showing the mass spectrum in both phases.

### 3.6.1. Dimensionless coupling and continuum limit

The coupling  $g$  of our two-dimensional system as well as the mass, have the dimension of an inverse lattice unit

$$[g] = [m] = a^{-1}. \quad (3.73)$$

In order to have a dimensionless quantity in which we can express the critical point of the system we are choosing the dimensionless coupling

$$f = g/m. \quad (3.74)$$

Ultimately we are interested in the value of the renormalised (super-script  $R$ ) coupling at the critical (sub-script  $c$ ) point in the continuum limit which is defined as

$$f_c^R = \lim_{a \rightarrow 0} \frac{g}{m^R} \Big|_c, \quad (3.75)$$

and is separating the supersymmetry-broken phase from the supersymmetric phase. In the formula above  $m^R$  is the renormalised mass that was discussed in section 3.4. Since

---

<sup>3</sup>In the  $\mathbb{Z}_2$ -symmetric phase  $\langle \phi \rangle = 0$  and therefore  $\langle M(\phi) \rangle = 2$  and in the  $\mathbb{Z}_2$ -broken phase, where  $\langle \phi \rangle = \pm m/(2g)$ , we find  $\langle M(\phi) \rangle = 2 \pm m$ . The interesting regime, i.e. critical point, is far away from  $m = 2$  for even coarse lattices, making a negative monomer weight incredibly unlikely. In our simulation no negative weight was encountered.



the coupling  $g$  has the dimension of a lattice spacing we will use  $g \rightarrow 0$  in order to send the lattice spacing to zero. The continuum limit of an observable  $\mathcal{O}$  is then defined as

$$\lim_{g \rightarrow 0} \mathcal{O}|_{\xi=\text{fixed}} , \quad (3.76)$$

where  $\xi$  is some physical quantity or situation that is kept fixed when sending  $g \rightarrow 0$ , e.g. considering the system at the critical point.

### 3.6.2. Towards simulation

When talking about data from a numerical simulation we will specify the statistics by the number of complete sweeps. A complete sweep is defined as

#### Boson update

10 sweeps through the lattice, visiting every site  $x$  and updating the bosonic field variable  $\phi_x$  with a standard Metropolis algorithm.

#### Fermion update

1 fermion update with the worm algorithm. This means explicitly breaking the fermion loop configuration, moving one source around the lattice and sampling configurations of the two-point function until the sources are both on the same site and are removed. This was also graphically illustrated in fig. 1.9.

If not stated otherwise, the thermalisation consists of one tenth of the total number of complete sweeps. Since the worm algorithm is a very effective updating procedure it showed itself convenient to have more bosonic updates than fermionic ones. Recall that if we were able to create a bosonic bond formulation without a sign problem, we could most likely speed up simulations enormously and simulate even at the critical point with hardly any critical slowing down.

Since on the lattice the  $\mathbb{Z}_2$  symmetry is never intact with the chosen discretisation, there is actually no real phase transition which we can observe in a computer simulation. Note that even with a  $\mathbb{Z}_2$  symmetric action, a  $\mathbb{Z}_2$ -broken phase only exists in the infinite volume limit. We will in the following still sometimes refer to the term phase transition even though something like pseudo phase transition would be most likely more adequate when talking about systems with finite lattice spacings and finite volume. Luckily the phase in which a symmetry is restored shows only small explicit symmetry violations at even coarse lattices, making the discretised system amenable to standard procedures to determine the critical point. In section 3.8 we will discuss possible solutions to this explicit  $\mathbb{Z}_2$  symmetry breaking.

In a first step we will now investigate some fundamental quantities of the system such as the expectation value of the bosonic field and the vacuum structure of the topological sectors of the partition function. This then enables us to determine the exact vacuum states and will fortify the phase diagram sketched in fig. 3.2. Afterwards we determine the critical coupling of the spontaneous symmetry breaking before measuring the mass spectrum.

### 3. $\mathcal{N} = 1$ $D = 2$ WESS-ZUMINO MODEL

Note that the discussed symmetry phase diagram is already non-perturbatively investigated in [35].

#### 3.6.3. The bosonic field and the $\mathbb{Z}_2$ symmetry

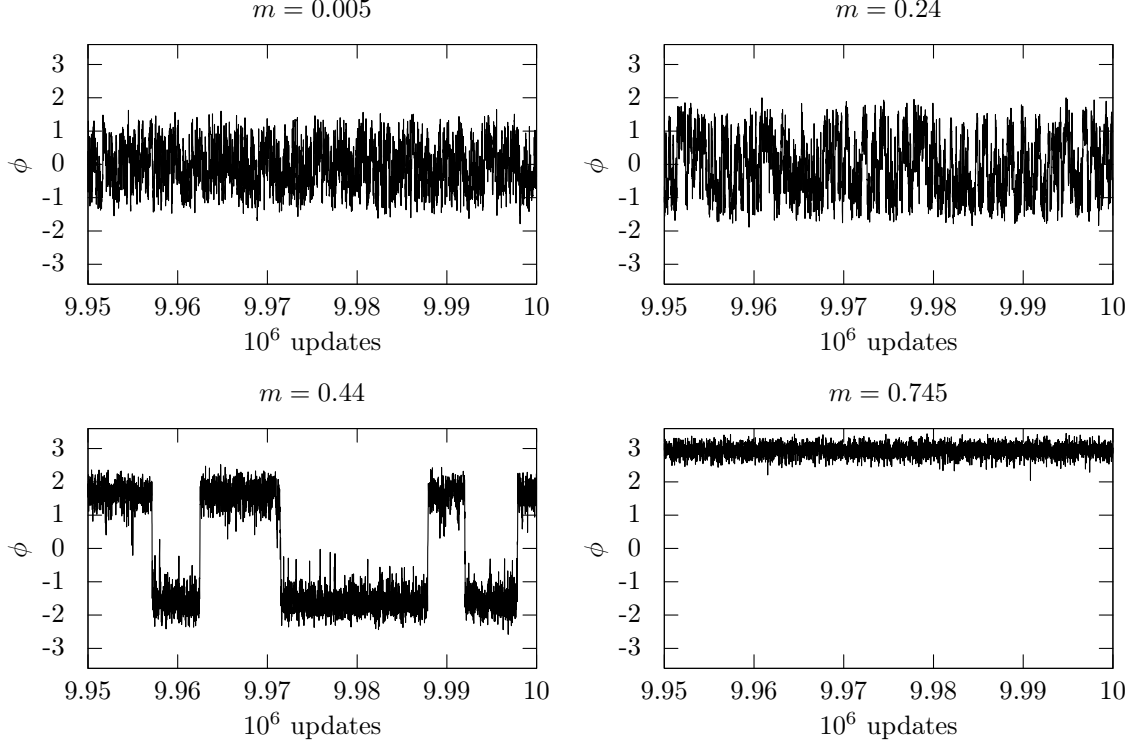


Figure 3.5.: Here the Monte-Carlo history is shown for the observable  $\phi$  for various bare masses  $m$  at a coupling of  $g = 0.125$ . From top left to bottom right these refer to  $f = 25$ ,  $f = 0.52083$ ,  $f = 0.2840$  and  $f = 0.16779$ .

In order to understand the  $\mathbb{Z}_2$  symmetry breaking we are investigating the behaviour of the bosonic field  $\phi$  in the symmetric as well as in the broken phase. Let us define the observable of interest to be the expectation value  $\langle \phi \rangle$  where  $\phi$  is the volume averaged bosonic field

$$\phi = \frac{1}{V} \sum_x \phi_x. \quad (3.77)$$

In fig. 3.5 we show the Monte-Carlo history of the observable  $\phi$  for various bare masses  $m$  at fixed coupling  $g = 0.125$  on a lattice with a volume of  $8 \times 8$ . The Monte-Carlo time window which is shown consists of  $5 \cdot 10^4$  complete sweeps. In the two plots in the upper panel we get an expectation value of  $\langle \phi \rangle \simeq 0$  for both masses. The system is here in the  $\mathbb{Z}_2$ -symmetric phase. Note that, as mentioned already above, the expectation value only needs to be zero in the continuum limit due to the explicit symmetry breaking at finite lattice spacings. In the lower panel we go to larger  $m$  and surpass the critical point and end up in the  $\mathbb{Z}_2$ -broken phase. In the lower panel of fig. 3.5 on the left hand side we see the bosonic field fluctuating between the two expected minima  $\langle \phi \rangle \simeq \pm m/(2g)$ . Note that this effect only vanishes in the thermodynamic limit where the two minima are completely

separated and the system chooses to reside in one of them. If we go to even higher bare masses, as shown in the lower right panel of fig. 3.5, we see that the algorithm does not tunnel to the negative minimum  $-m/(2g)$  in that time frame. When increasing the mass of the system the algorithm is fluctuating less and less between the two minima, eventually never reaching the other minimum in a reasonable time.

Investigating the Monte-Carlo histories at different dimensionless couplings  $f = g/m$

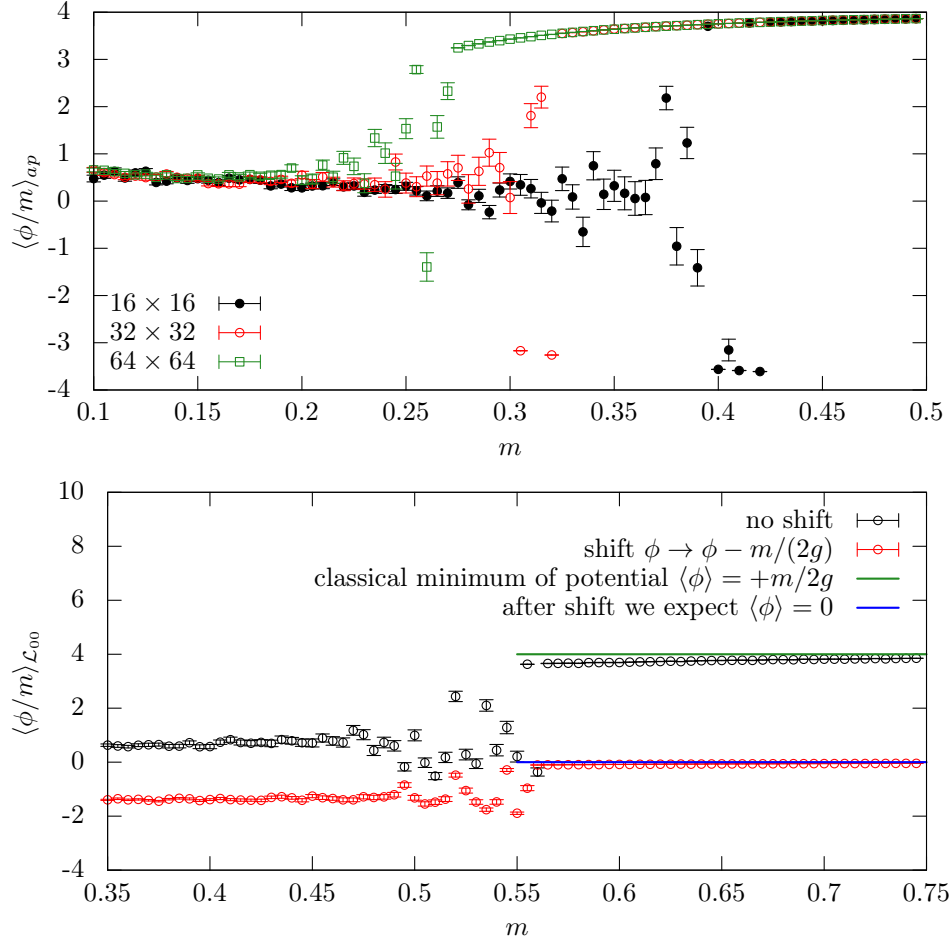


Figure 3.6.: In the upper panel we show  $\langle \phi/m \rangle_{ap}$  for three different lattice volumes at  $g = 0.125$ . In the lower panel we show  $\langle \phi/m \rangle_{\mathcal{L}_{00}}$  from a  $8 \times 8$  lattice at  $g = 0.125$ . Once the data are shown coming from a simulation using the potential which is  $\mathbb{Z}_2$ -symmetric in the continuum and the other data come from an action where the bosonic field is shifted by  $-m/(2g)$ . The statistics consists of  $10^6$  complete sweeps.

gives us a first insight of the two existing phases of the discrete  $\mathbb{Z}_2$  symmetry. Note that for large masses in the  $\mathbb{Z}_2$ -broken phase we can mostly choose in which minimum the Metropolis algorithm takes us by setting the initial field value to the positive or negative minimum of the continuum potential, i.e.  $\phi_x = \pm m/(2g)$ . Another observation that was made is that due to the Wilson term for the bosonic fields, one minimum of the potential is slightly shifted and therefore one vacuum state is preferred over the other. Note that this effect vanishes when letting  $a \rightarrow 0$ , but already at intermediate lattice spacings is very small, e.g. hardly detectable for  $g = 0.125$  shown in fig. 3.5.

### 3. $\mathcal{N} = 1$ $D = 2$ WESS-ZUMINO MODEL

In fig. 3.6 in the upper panel we can observe the behaviour of  $\langle \phi/m \rangle_{ap}$  at fixed coupling  $g = 0.125$  for three different lattice volumes. The tunnelling between the two different ground states in the  $\mathbb{Z}_2$ -broken phase is increasingly suppressed as we enlarge the volume. In the lower panel of fig. 3.6 we show  $\langle \phi/m \rangle_{\mathcal{L}_{00}}$  for two scenarios. In a first simulation we used the discretised version of the action in eq.(3.9) which has a  $\mathbb{Z}_2$ -symmetric potential in the continuum. A second simulation is performed with a shifted field  $\phi \rightarrow \phi - m/(2g)$ , corresponding to the continuum action in eq.(3.11). In one case the classical minimum of the potential is expected at  $\langle \phi \rangle = m/(2g)$  and therefore also at  $\langle \phi/m \rangle = 1/(2g)$ . This agrees nicely with the numerical observation in both simulations. We used a positive bosonic field configuration in the Metropolis algorithm in order to wind up in the positive minimum.

#### 3.6.4. Partition function $Z_{\mathcal{L}_{ij}}$ and $\mathbb{Z}_2$ symmetry

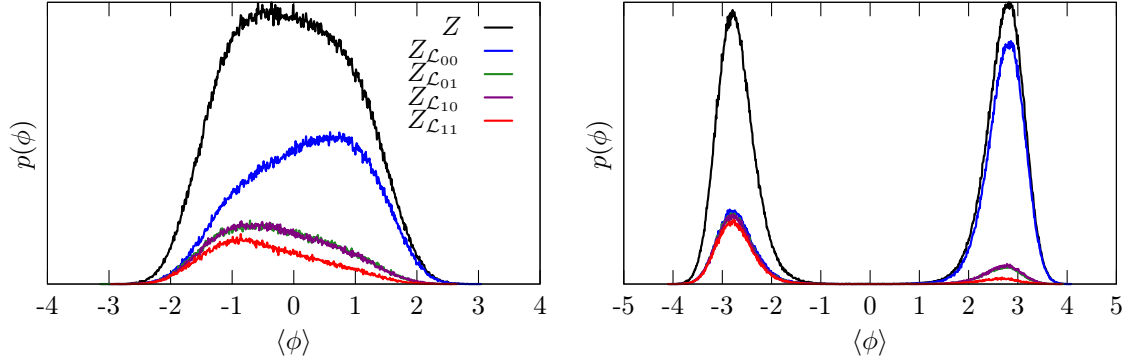


Figure 3.7.: These histograms show data from  $10^7$  updates for a  $8 \times 8$  lattice at fixed coupling  $g = 0.0625$  for two different dimensionless couplings  $f > f_c$  (left) and  $f < f_c$  (right).

Here we illustrate how the topological sectors of the partition function behave in the  $\mathbb{Z}_2$ -symmetric and broken phase. We recall the separation of the partition function  $Z$  into the four sectors  $Z_{\mathcal{L}_{00}}, Z_{\mathcal{L}_{10}}, Z_{\mathcal{L}_{01}}$  and  $Z_{\mathcal{L}_{11}}$ , which correspond to the contributions from configurations with a topology associated with the number of odd fermion loops winding around the directions of the two dimensional torus. This was discussed in detail in section 1.6.1. In fig. 3.7 results are shown for the two phases for an  $8 \times 8$  lattice at fixed coupling  $g = 0.0625$ , i.e. fixed lattice spacing. This time we construct a histogram over  $10^7$  complete sweeps, showing the partition function  $Z$  and the partition function  $Z_{\mathcal{L}_{ij}}$  depending on  $\langle \phi \rangle$ . After performing that many updates we can identify the histogram with the probability distribution  $p_{Z_{\mathcal{L}_{ij}}}(\phi)$ . In fig. 3.7 on the left we are at  $f > f_c$  where the  $\mathbb{Z}_2$  symmetry is intact and we find  $\langle \phi \rangle_Z = 0$ . Crossing the critical point and entering the regime of  $f < f_c$  we enter the phase where the  $\mathbb{Z}_2$  symmetry is spontaneously broken. This can be seen in fig. 3.7 on the right where we can identify the two peaks with the two minima. The system in the  $\mathbb{Z}_2$ -broken phase has two classical minima at  $\langle \phi \rangle = \pm m/(2g)$ , corresponding well to the observed peaks. From this probability distributions we see that in the case where the system is in the negative minimum  $\langle \phi \rangle = -m/(2g)$  all topological sectors arise

with the same probability, i.e.

$$Z_{\mathcal{L}_{00}} \simeq Z_{\mathcal{L}_{10}} \simeq Z_{\mathcal{L}_{01}} \simeq Z_{\mathcal{L}_{11}} \simeq Z/4. \quad (3.78)$$

This vacuum is called the fermionic ground state, where  $Z_{pp} = -Z_{pa}$ . On the other hand we see that if  $\langle\phi\rangle = +m/(2g)$  the system shows itself to be predominantly in the topological sector  $\mathcal{L}_{00}$  and therefore we have

$$Z \simeq Z_{\mathcal{L}_{00}} \quad \text{and} \quad Z_{\mathcal{L}_{10}} \simeq Z_{\mathcal{L}_{01}} \simeq Z_{\mathcal{L}_{11}} \simeq 0. \quad (3.79)$$

The system is then in the bosonic ground state where no odd number of fermion loops are winding around any dimension and we therefore find  $Z_{pp} = +Z_{pa}$ . We now saw that there are two minima in the  $\mathbb{Z}_2$ -broken phase corresponding not only to the classical minima of the potential where the bosonic field acquires the value  $\pm m/(2g)$ , but which also show to be two distinct vacua in terms of the fermion loop structure. Let us for now summarise the indicated phase structure based on the observed  $\mathbb{Z}_2$  symmetry breaking pattern, we conclude that in the continuum limit

- $\mathbb{Z}_2$ -symmetric phase

$$\langle\phi\rangle = 0 \quad \text{Vacuum tunnelling even when } V \rightarrow \infty \ (Z_{pp} \simeq 0),$$

$\implies$  Supersymmetry broken

- $\mathbb{Z}_2$ -broken phase, only when  $V \rightarrow \infty$

$$- \langle\phi\rangle = +m/(2g) \quad \text{Bosonic Vacuum } (Z_{pp} \simeq Z_{ap})$$

$$- \langle\phi\rangle = -m/(2g) \quad \text{Fermionic Vacuum } (Z_{pp} \simeq -Z_{ap})$$

$\implies$  Supersymmetry unbroken

At finite volume the  $\mathbb{Z}_2$  symmetry is always intact (of course besides the explicit breaking from the Wilson term) and spontaneous supersymmetry breaking is induced by tunnelling between the ground states. Since our observations show that  $Z_{pp} \simeq 0$  in the  $\mathbb{Z}_2$ -symmetric phase we will refrain from using  $\langle\mathcal{O}\rangle_{pp}$  because

$$\langle\mathcal{O}\rangle_{pp} = \frac{\langle\langle\mathcal{O}\rangle\rangle_{\mathcal{L}_{00}} - \langle\langle\mathcal{O}\rangle\rangle_{\mathcal{L}_{10}} - \langle\langle\mathcal{O}\rangle\rangle_{\mathcal{L}_{01}} - \langle\langle\mathcal{O}\rangle\rangle_{\mathcal{L}_{11}}}{Z_{\mathcal{L}_{00}} - Z_{\mathcal{L}_{10}} - Z_{\mathcal{L}_{01}} - Z_{\mathcal{L}_{11}}} \quad (3.80)$$

can not be accurately determinable due to the division by approximately zero<sup>4</sup>. Instead we will mostly consider  $\langle\mathcal{O}\rangle_{ap}$ , which is an observable in a system which is only supersymmetric in the thermodynamic limit.

---

<sup>4</sup> Note that an observable  $\langle\mathcal{O}\rangle_{pp}$  is in general well defined and finite, since the numerator vanishes with the denominator.

## 3.6.5. Witten index

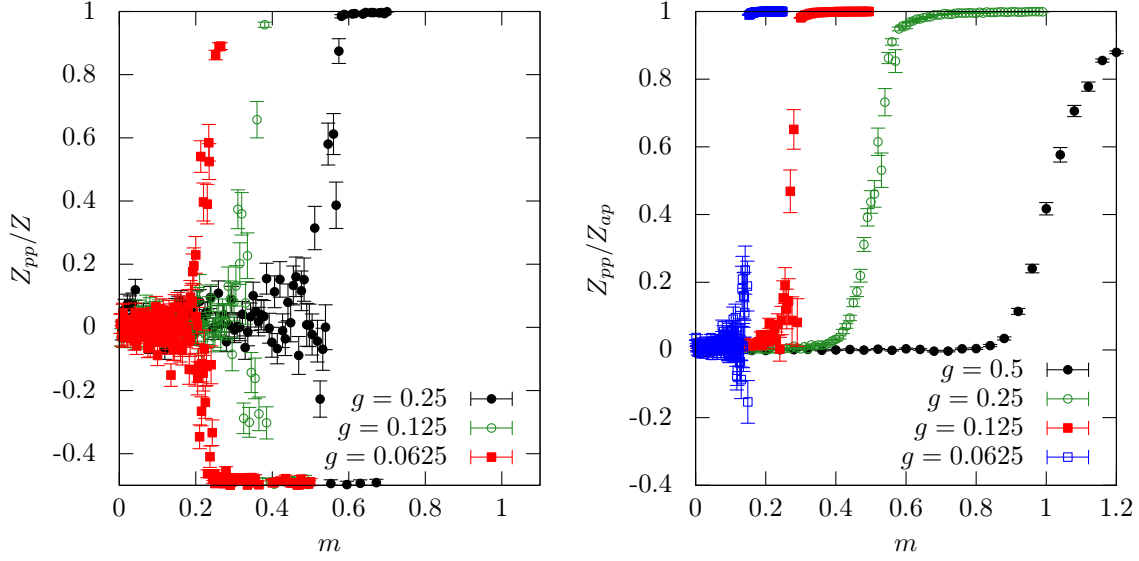


Figure 3.8.: On the left we show  $Z_{pp}(m)$  at a fixed volume of  $16 \times 16$  for  $g = 0.25$  and two smaller couplings. The simulation was thermalised by starting with a negative boson field configuration. On the right side we show  $Z_{pp}/Z_{ap}(m)$  at fixed physical volume  $gL = 4$  which correspond to  $L_x = 8, 16, 32, 64$ . The temporal extent is fixed to  $L_t = 128$  and the thermalisation was started with a positive boson configuration

As shown in section 3.2.1 the partition function with periodic boundary conditions in both dimensions  $Z_{pp}$  is proportional to the Witten index  $W$ . In fig. 3.8 on the left side we observe the behaviour of  $Z_{pp}(m)$  for various couplings  $g = 0.25, 0.125$  and  $0.0625$  at a fixed lattice volume of  $16 \times 16$ . The point on the bare mass scale where we enter the regime of  $Z_{pp}(m_c) = 0$  corresponds to the critical point  $m_c$ . With decreasing coupling the critical mass  $m_c$ , where the phase transition occurs, decreases as well. Around the critical point we see the system tunnelling between the two minima which gives us large error bars and uncertain predictions about the  $\mathbb{Z}_2$  symmetry. Specially for  $g = 0.25$  we see at larger  $m$  that there are simulations in which the algorithm did not tunnel to the other ground state. Therefore there are points with a very small error at  $-0.5$  and at  $1$ . If the bare mass is decreased we start to tunnel between the two ground states which is what creates the scattered data points with large errors. If the simulation was run longer the algorithm would have tunnelled more frequently and the point where enter  $Z_{pp}(m) \simeq 0$  would be shifted to larger bare mass.

Let us also consider the ratio

$$W \propto \frac{Z_{pp}}{Z_{ap}}, \quad (3.81)$$

which serves as a pseudo order parameter for the supersymmetric phase transition. The reason why  $Z_{pp}$  is divided by  $Z_{ap}$  is that the two minima then correspond to  $Z_{pp}/Z_{ap} = \pm 1$ . In the right panel of fig. 3.8  $Z_{pp}/Z_{ap}(m)$  is shown at fixed physical volume  $gL = 4$  for various couplings. Note that when decreasing the coupling we are decreasing the lattice spacing and approaching the continuum limit. We can therefore already state that the

value of the critical bare mass  $m_c$  is decreasing when going to the continuum. This is obvious since  $[m] = a^{-1}$ . In the simulation that generated the data in fig. 3.8 on the right, the initial value of the bosonic field was chosen to be positive.

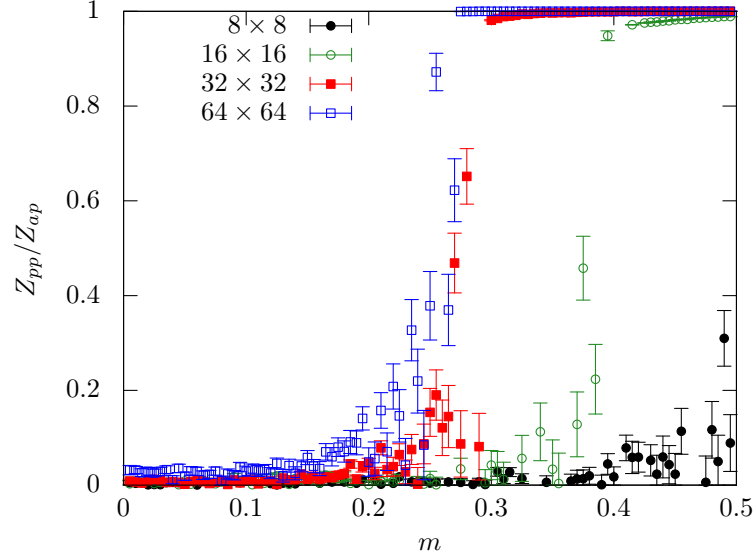


Figure 3.9.: Showing the  $Z_{pp}/Z_{ap}$  ratio at fixed coupling  $g = 0.125$  for various lattice extents.

Since the ratio  $Z_{pp}/Z_{ap}(m)$  is proportional to the Witten index we can already argue, based on what is shown in fig. 3.8 in the right panel, that for masses larger than  $m_c$  one ground state will be selected and we presumably find ourselves in what becomes the supersymmetric phase in the continuum and thermodynamic limit.

In fig. 3.9 we can observe the behaviour of  $Z_{pp}/Z_{ap}(m)$  at fixed lattice spacing for different volumes. The finite volume effects of the estimated critical bare mass  $m_c$  seem rather strong when going from an  $8 \times 8$  volume to a  $16 \times 16$  volume, whereas from  $32 \times 32$  to  $64 \times 64$  the critical point  $m_c$  varies less.

### 3.6.6. Determination of the critical coupling

In this section we determine the numerical value of the critical point  $f_c$  in the thermodynamic continuum limit. We will use two different techniques for this determination in order to handle the systematic errors. The lattice spacing is fixed by choosing a fixed bare coupling  $g$  and we then vary  $m$  in order to find the critical mass  $m_c$  at which the  $\mathbb{Z}_2$  symmetry breaks down spontaneously. With these values we can then determine the critical dimensionless coupling  $f_c = g/m_c$ . The critical value in the thermodynamic limit can be found by considering simulations at fixed lattice spacings, i.e. fixed coupling  $g$ , and vary the extent of the lattice and therefore the physical volume  $gL$ . The continuum limit is then found by sending the coupling to zero. If not stated differently we will use  $L = L_x$  and will always label the time direction as such, i.e.  $L_t$ .

### Susceptibility of the Ising-spin projection

To find the critical point we need an order parameter for the phase transition. For  $m > m_c$  the two classical minima of the potential are at  $\langle \phi \rangle = \pm m/(2g)$ . It is of advantage to introduce an observable which is not distinguishing between fermionic and bosonic minimum but can tell us if the ground state is  $\mathbb{Z}_2$ -symmetric or not, i.e. an order parameter for the  $\mathbb{Z}_2$  symmetry breaking. We will use the absolute value of the Ising-spin projection of the field  $\phi$ , defined by

$$I = \frac{1}{V} \left| \sum_x \text{sign}(\phi_x) \right|. \quad (3.82)$$

This choice is made because  $I$  maps both minima to the identical value. The spontaneous  $\mathbb{Z}_2$  symmetry breaking then amounts to the following conjectured behaviour in the thermodynamic and continuum limit

$$I(f) = \begin{cases} 1, & \text{if } f < f_c \\ 0, & \text{if } f > f_c, \end{cases} \quad (3.83)$$

whereas on the lattice we should also see the same in the thermodynamic limit since the Ising-spin projection does not distinguish between the two minima, i.e. hiding the explicit  $\mathbb{Z}_2$  symmetry breaking at finite lattice spacings. In order to have a peak around the critical point we are considering the susceptibility of  $I$ , using the common definition

$$\chi = \langle I^2 \rangle - \langle I \rangle^2. \quad (3.84)$$

The susceptibility of a system with twice periodic b.c. and a system with anti-periodic b.c. in time and periodic in space can be expressed in terms of the topological sectors as

$$\langle \chi \rangle_{pp} = \langle I^2 \rangle_{pp} - \langle I \rangle_{pp}^2 \quad \text{and} \quad \langle \chi \rangle_{ap} = \langle I^2 \rangle_{ap} - \langle I \rangle_{ap}^2. \quad (3.85)$$

The pseudo critical point  $m_c$  is then identified with the location of the peak of the susceptibility curve. When  $g$  is getting smaller we are approaching the continuum limit and the value of  $m_c$  is also decreasing and will eventually be zero in the continuum. This can be observed in fig. 3.10 on the left. When staying at a fixed lattice spacing and letting the volume increase, as shown on the right of fig. 3.10, we see that the susceptibility signal is getting stronger since the peak of the susceptibility curve is peaked more sharply. Larger lattices are generally desired in order to decrease the error of the determined  $m_c$ . Note that at fixed lattice volume and decreasing coupling the physical volume  $gL$  is decreasing as well.



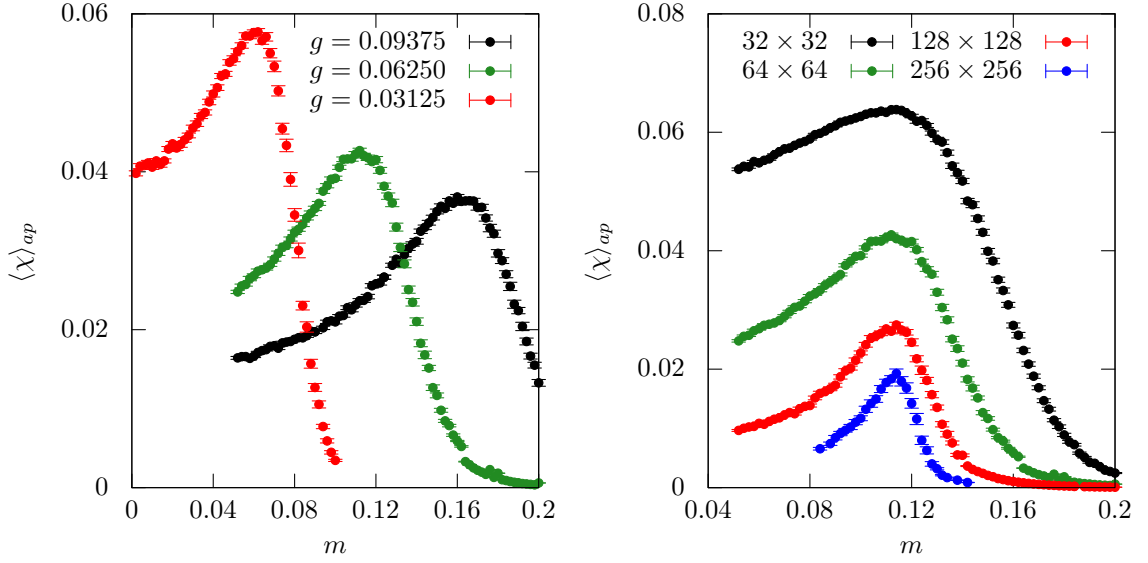


Figure 3.10.: This figure is illustrating the behaviour of the susceptibility of the Ising-spin variable. On the left  $I$  is shown for a fixed lattice volume of  $V = 64 \times 64$  for three different couplings. On the right the coupling is fixed at  $g = 0.0625$  and the volume is varied. Each data point is created with statistics from  $10^7$  runs.

For large couplings our signal is already reasonably good on small lattice volumes, whereas at small  $g$  one needs a correspondingly larger lattice volume in order to stay at the same physical volume  $gL$  and to get the same signal strength. In order to have a mathematical criterion for finding the critical mass  $m_c$  we fit the susceptibility curve at fixed coupling  $g$  with a Gaussian function

$$f(m) = A \exp \left[ -(m - m_c)^2 / (2\sigma^2) \right] \quad (3.86)$$

and extract  $m_c$  from the fit. The fit range is chosen such that it includes only several points around the peak of the susceptibility curve. In fig. 3.11 we see the fit performed to the curve  $\langle \chi \rangle_{ap}(m)$  for a lattice of volume  $32 \times 32$  at  $g = 0.125$ . The statistical error of  $m_c$  is determined by the standard jackknife method explained in the appendix C. On top of this the systematic error of choosing an appropriate fit range in  $m$  is considered. This is done by varying the fit range and accepting all fit results  $m_c$  coming from fits with a reasonable  $\chi^2/\text{dof}$ . The result  $m_c$  is chosen for which the most other values of  $m_c$ , obtained by varying the fit-range, lie in between of one standard deviation of the former  $m_c$ <sup>5</sup>. Doing this fitting procedure for different lattice volumes  $V$  and different couplings  $g$  lets us build up the data set shown in table A.1. The errors of  $m_c$  which we denote with  $\delta m_c$  are mainly bigger for small lattices than the errors from larger lattices due to a less incisive peak in the susceptibility curve.

The statistics, computer-time essentially, limits us in taking very large lattices. This is the reason for the lower bound of simulations at  $g = 0.03125$  for the determination of the

<sup>5</sup>Note that this is in general a poor estimate of the systematic error. If we were using only one method to determine the critical bare mass a more conservative approach would surely be needed. However, since we will additionally use a completely different method to determine  $m_c$ , we will use the results from the two different methods in order to estimate the systematic error.

### 3. $\mathcal{N} = 1$ $D = 2$ WESS-ZUMINO MODEL

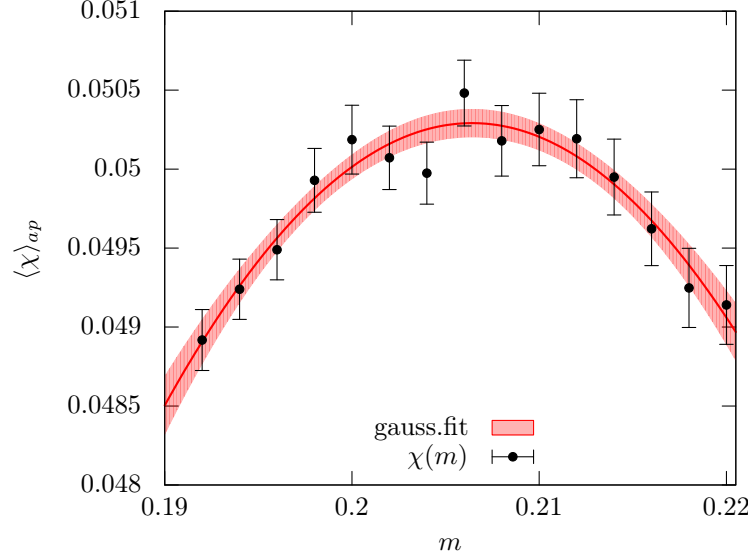


Figure 3.11.: Illustrating a Gaussian function fitted to  $\chi$  for a  $32 \times 32$  lattice at fixed coupling  $g = 0.125$  with a one sigma error band.

critical point. All simulations shown in this section consist of  $10^7$  complete sweeps. It is of course arguable if  $\chi$  and a Gaussian fit function is a good choice for the determination of  $m_c$ . This is why another method should be used to determine the critical mass in order to estimate the systematic error of the procedures. Note that two different methods are clearly not expected to yield identical values for  $m_c$  at finite volume. However, they must be identical in the infinite volume at zero lattice spacing. In the next section we will discuss the Binder cumulant, which forms our second method to determine  $m_c$  at fixed  $g$ .

#### Binder cumulant

The Binder cumulant [65] forms another standard method that can be used to find the critical point of a spontaneous  $\mathbb{Z}_2$  symmetry breaking. Let us define

$$U = 1 - \frac{\langle \phi^4 \rangle}{3\langle \phi^2 \rangle^2}. \quad (3.87)$$

The theoretical behaviour of  $U$  tells us that for  $m \ll m_c$  the cumulant decreases towards zero like  $U \propto (V^{-1})$  whereas for  $m \gg m_c$  it is approaching a constant value  $U = 2/3 + \mathcal{O}(V^{-1})$ . At  $m = m_c$  all  $U$  from different volumes should intersect. As previously discussed we can choose physical boundary conditions for our system and write the Binder cumulant as

$$\langle U \rangle_{pp} = 1 - \frac{\langle \phi^4 \rangle_{pp}}{3\langle \phi^2 \rangle_{pp}^2} \quad \text{and} \quad \langle U \rangle_{ap} = 1 - \frac{\langle \phi^4 \rangle_{ap}}{3\langle \phi^2 \rangle_{ap}^2}. \quad (3.88)$$

In fig. 3.12 the Binder cumulant is shown for various lattice volumes at a fixed coupling of  $g = 0.0625$ . In order to have a mathematical criterion to find the critical mass, a linear fit is performed in the region of the function where the Binder cumulants of different volumes intersect. Only fit ranges that yield a good  $\chi^2/\text{dof}$  are considered. One thus has a straight line for each different volume and can estimate  $m_c$  by considering the intersection

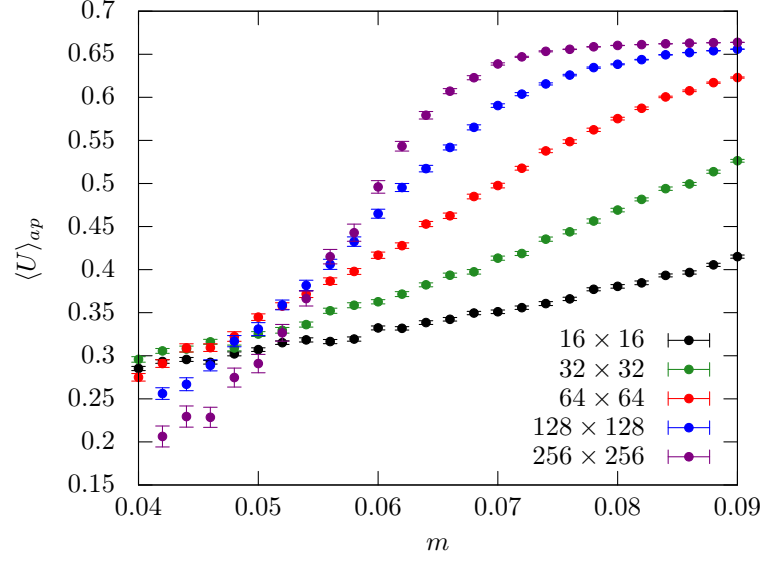


Figure 3.12.: Here we show the Binder cumulant for anti-periodic boundary conditions in time and periodic in space for several lattice volumes at fixed coupling  $g = 0.0625$ .

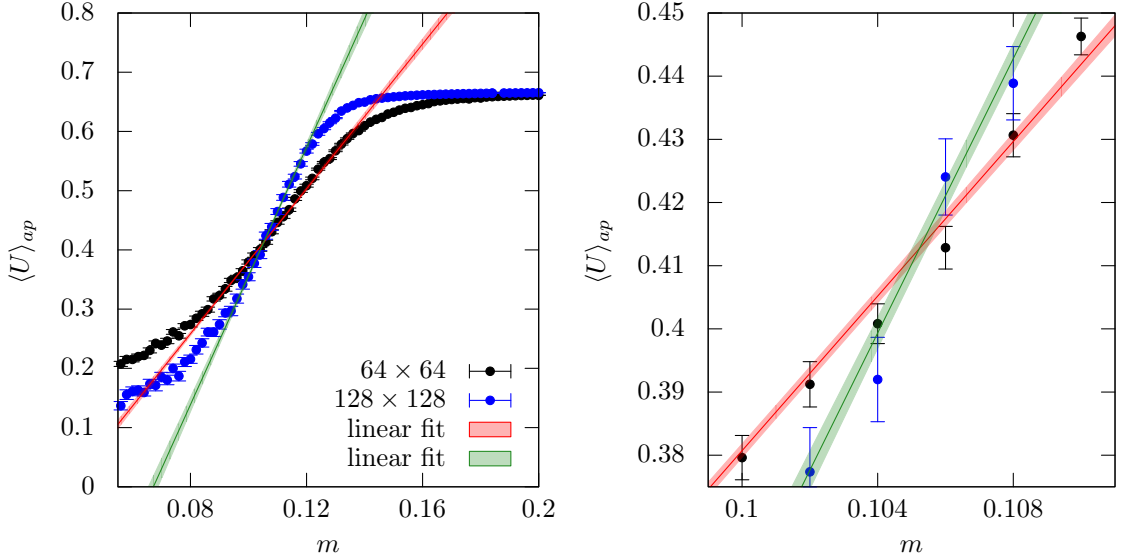


Figure 3.13.: In this figures we plot the Binder cumulant at fixed coupling  $g = 0.0625$  for two different volumes  $64 \times 64$  and  $128 \times 128$ . On the right a close up is chosen in which one can see the linear fits with their one sigma error bands. The point where those lines intersect then corresponds to the critical value  $m_c$ .

points. This is illustrated in fig. 3.13. We keep the coupling  $g$  fixed and vary the volume of the system in order to simulate at fixed lattice spacings. For each volume we scan the parameter space in  $m$  and obtain the corresponding values of  $U(m)$ . Each Binder cumulant slope at a certain volume  $V = L_t \times L_x$  then gets compared with one that has a volume which is four times larger, i.e. with  $V' = 2L_t \times 2L_x$ . A linear fit is then performed for both curves close to the point of intersection. The value of  $m$  where the two linear fits intersect is then identified with  $m_c(L_x)$ . Note that this choice is arbitrary, one could

### 3. $\mathcal{N} = 1$ $D = 2$ WESS-ZUMINO MODEL

just as well use  $m_c(L'_x)$ . In fig. 3.13 we illustrate this method. On the left we show two curves at fixed coupling  $g = 0.0625$  corresponding to the volumes  $64 \times 64$  and  $128 \times 128$ . In this figures we also include the performed linear fits. In table A.2 the results obtained with this procedure are listed. In order to estimate the systematic error we can again vary the fit range and consider fits with reasonable  $\chi^2/\text{dof}$  values. We again use the value  $m_c$  for which most other fit results, obtained by varying the fit range, lie in between of one standard deviation.

#### 3.6.7. Thermodynamic limit

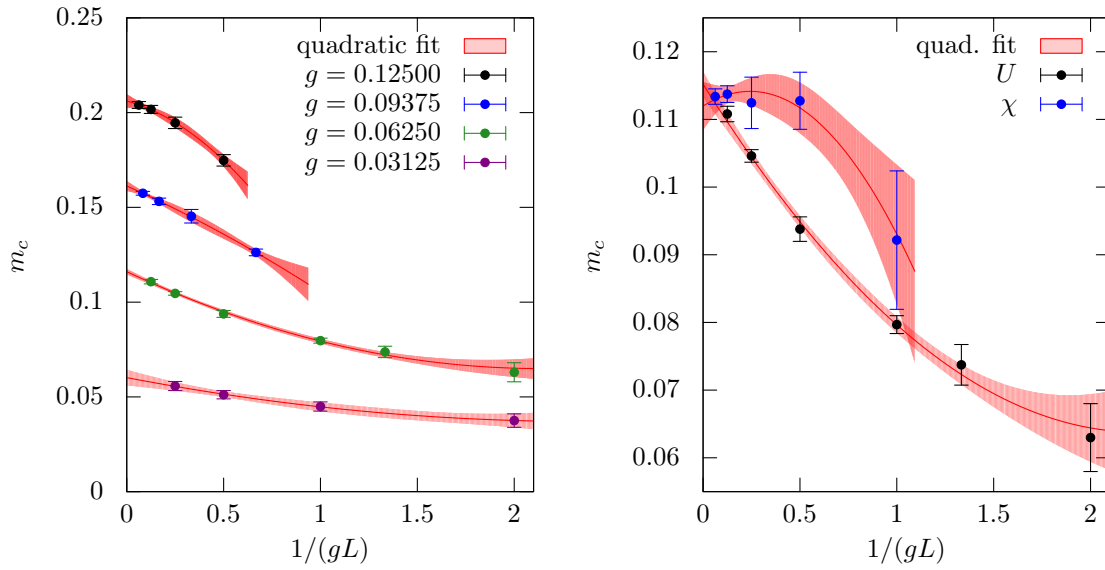


Figure 3.14.: On the left  $m_c$  determined with the Binder cumulant method is shown for various lattice extents at different fixed couplings. A quadratic fit through all data points is performed for each  $g$ . On the right the extrapolation to the thermodynamic limit at fixed  $g = 0.0625$  is shown for  $m_c$  from both techniques, the susceptibility and the Binder cumulant.

For all the mentioned couplings in table A.1 and A.2 we are taking the thermodynamic limit of  $m_c$ . The points  $m_c$  are fitted with a quadratic and a linear function in order to perform an extrapolation into the thermodynamic limit. In fig. 3.14 on the left panel we show data obtained by the Binder cumulant method for various lattice extents at different fixed couplings including a quadratic fit with a one sigma error band. On the right side of fig. 3.14 we compare the two different methods, the Binder cumulant ( $U$ ) and the Ising-spin susceptibility ( $\chi$ ) at fixed coupling  $g = 0.0625$ . Both extrapolations yield values of  $m_c$  in the thermodynamic limit that agree nicely. This can be seen by considering the two one sigma error bands of the extrapolations that largely overlap at  $1/(gL) = 0$ . The finite size effects seem to be rather strong for the critical point determined by the Ising-spin susceptibility up to a certain volume where they start to diminish drastically.

In the following fig. 3.15 the same data is plotted but a linear fit is performed for data points closer to the infinite volume limit. We clearly see that there are quadratic corrections for small lattice volumes, but if the linear fit is restricted to the data corresponding to the

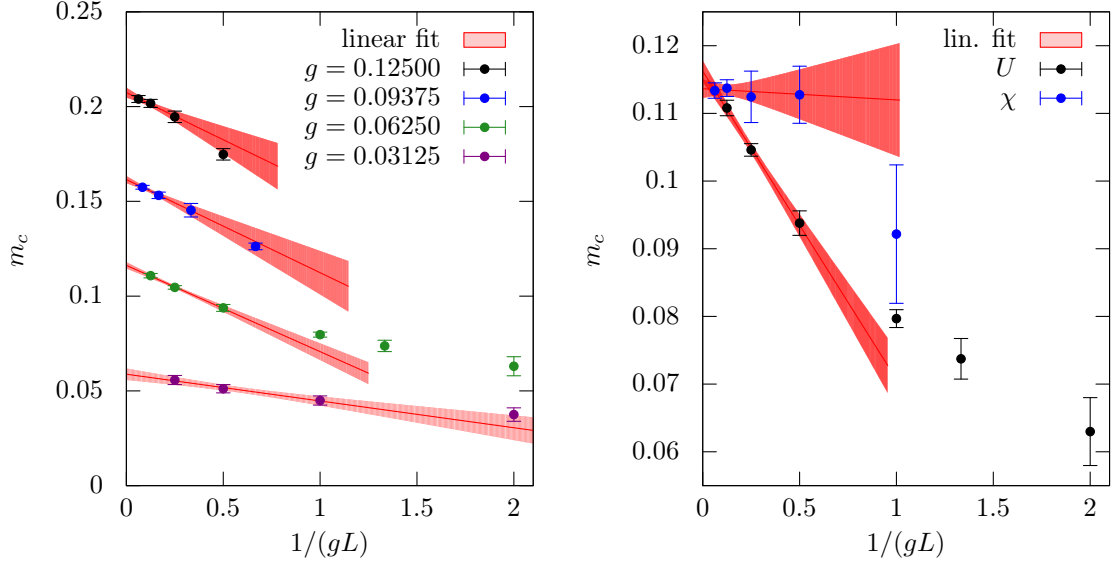


Figure 3.15.: The identical data are plotted as in fig. 3.14. The extrapolation here is performed by linear fits for data closer to the thermodynamic limit.

larger volumes, the thermodynamic limits of both fits are compatible with one another. This can for example be observed in fig. 3.15 on the right where the two one sigma error bands of the fits again overlap.

method	$g$	$m_c^{V \rightarrow \infty}$	$\delta m_c^{V \rightarrow \infty}$
$\chi$	0.18750	0.29844	0.00425
$U$	0.18750	0.28601	0.00238
$\chi$	0.15850	0.26059	0.00354
$U$	0.15850	0.24907	0.00282
$\chi$	0.12500	0.20826	0.00160
$U$	0.12500	0.21109	0.00284
$\chi$	0.09375	0.16413	0.00163
$U$	0.09375	0.16197	0.00208
$\chi$	0.06250	0.11364	0.00135
$U$	0.06250	0.11387	0.00196
$\chi$	0.03125	0.06212	0.00293
$U$	0.03125	0.05696	0.00217

Table 3.1.: List of  $m_c$  values in the thermodynamic limit for various couplings  $g$  from the two different techniques.

Performing a linear and a quadratic fit as a possible extrapolation in to the thermodynamic limit we take the larger error from both fits at  $g = 0$  in order to estimate the error  $\delta m_c^{V \rightarrow \infty}$  of the critical bare mass  $m_c^{V \rightarrow \infty}$ . The results obtained with this procedure are listed in table 3.1. Note that the critical value of the bare mass at fixed coupling in

### 3. $\mathcal{N} = 1$ $D = 2$ WESS-ZUMINO MODEL

the thermodynamic limit does not have to agree among both methods, it is only in the continuum limit where they must coincide. However, the results show that they agree with one another at already rather coarse lattice spacings.

One should note that for very small couplings, i.e. smaller lattice spacings, we are limited by statistics since our lattice volumes need to be very large in order to have a reasonably large physical volume  $gL$ . For very large  $g$  the problem arises that there is less of a phase transition present because the lattice spacing is getting larger.

In the following we will refrain from using the notation  $m_c^{V \rightarrow \infty}$  since it should always be clear if we consider the system at finite or infinite volume.

#### 3.6.8. Continuum limit

The goal of this section is to carry out the extrapolation of  $m_c$  to the continuum limit, i.e.  $a \rightarrow 0$ . This can be done in a rather simple fashion by following the obtained critical masses for decreasing couplings. However, we will need to renormalise the mass parameter because, as we have seen in section 3.4, the boson one loop self energy correction of the bare mass is diverging when sending the lattice spacing to zero. By logarithmic renormalisation the mass parameter can be made finite and therefore also the dimensionless coupling will be a renormalised quantity, i.e.  $f^R = g/m^R$ .

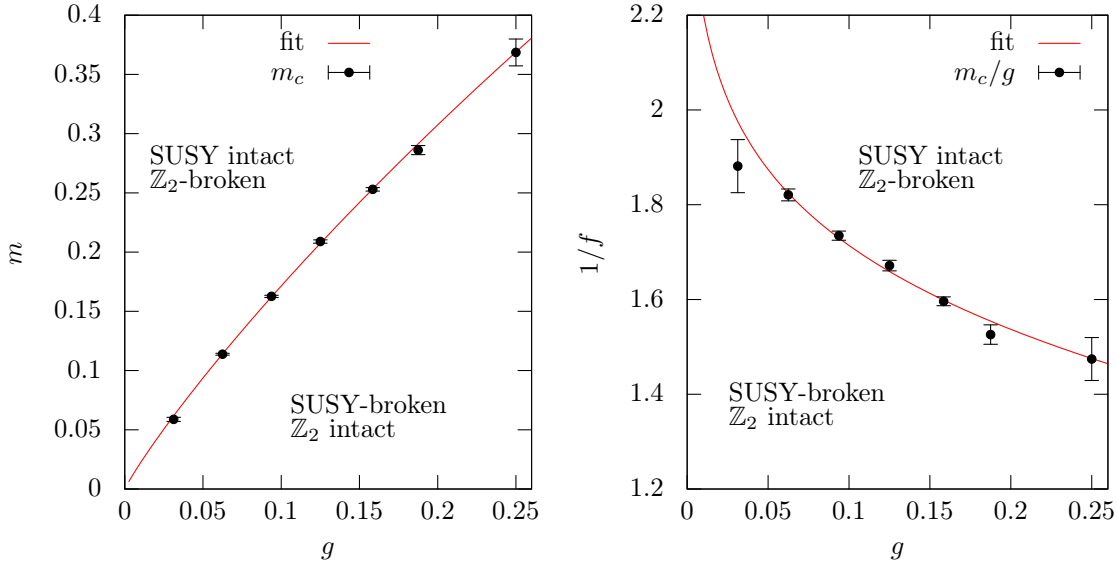


Figure 3.16.: Illustrating the bare phase diagram separating the supersymmetric and  $\mathbb{Z}_2$ -broken phase from the supersymmetry-broken and  $\mathbb{Z}_2$ -symmetric phase. On the left the critical mass is plotted against the coupling. On the right we show the inverse dimensionless coupling  $m/g$ . The data points  $m_c^2(g)$  are fitted with a linear term and an additional logarithmic term accounting for the expected divergence in the self energy.

In fig. 3.16 on the left we present the bare phase diagram separating the supersymmetric and  $\mathbb{Z}_2$ -broken phase from the supersymmetry-broken and  $\mathbb{Z}_2$ -symmetric phase. Note that

all points display the critical bare mass in the thermodynamic limit. When now decreasing the coupling  $g$  we send the lattice spacing to zero. A fit is performed with a linear minus a logarithmic term  $\mu g - \lambda g \log(g)$  accounting for the expected corrections [36], yielding  $\mu = 1.1533 \pm 0.0407$  and  $\lambda = 0.2424 \pm 0.0184$ . On the right side of fig. 3.16 we present the critical inverse dimensionless coupling  $m_c/g$  for various lattice spacings. Additionally we can again fit a function  $\mu - \lambda \log(g)$  and obtain the exact same values for  $\mu$  and  $\lambda$  as previously on the left of fig. 3.16. Even though the logarithmic corrections can be fitted acceptably well it is notable that the data points  $m_c/g$  alone do not show strong evidence of divergence. Admittedly it is only the insight into the structure of the one loop Feynmann diagrams that provide us with a logarithmic fitting Ansatz. Nevertheless, this agrees with the data very well.

In fig. 3.17 the same is shown as in fig. 3.16 but with the renormalised quantities. On the left a quadratic plus linear correction is fitted with a  $\chi^2/\text{dof} = 0.38$ , illustrating the behaviour of the renormalised critical mass at different lattice spacings. On the right an additional linear fit is performed besides the quadratic one in order to estimate the continuum extrapolated value of the renormalised critical dimensionless inverse coupling  $1/f^R$ . We obtain the numerical value by considering the mean of the extrapolated value at  $g = 0$  from the quadratic and the linear fit and find

$$1/f_c^R = 2.2859^{+0.073}_{-0.055}, \quad (3.89)$$

where we used the upper limit from the upper bound of the one sigma error bound of the quadratic fit and the lower limit from the lower bound of the one sigma error bound of the linear fit.

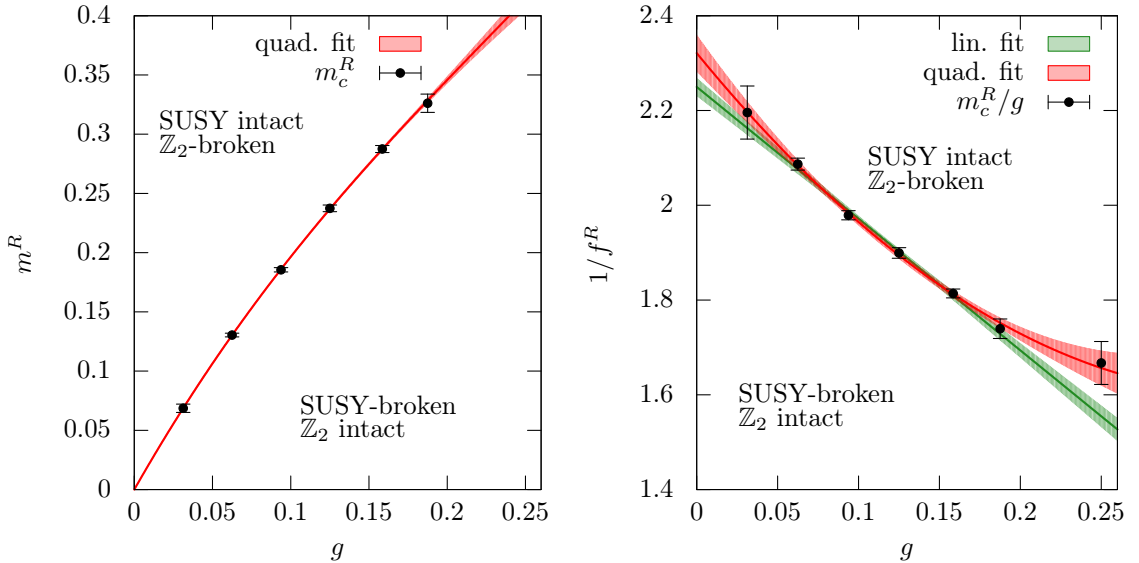


Figure 3.17.: Showing the renormalised phase diagram of the two phases analogously to fig. 3.16. A quadratic fit is performed in order to describe the behaviour of the data. Additionally a linear fit is performed in the right panel, illustrating another continuum extrapolation in which the point at the largest lattice spacing is not used for the fit.

### 3.6.9. Chiral condensate

Let us briefly look at the chiral condensate  $\langle \psi^T \mathcal{C} \psi \rangle$  when crossing the critical point on the bare mass scale. In fig. 3.18 we can observe the condensate for anti-periodic boundary conditions in time and periodic boundary conditions in space for various lattice extents at fixed coupling  $g = 0.125$ . Note that since we formulated our fermionic degrees of freedom in terms of occupation numbers, the condensate is an easily measurable quantity since it is proportional to the number of occupation numbers  $m(x)$  that are set to one, i.e. the fermion monomer term density.

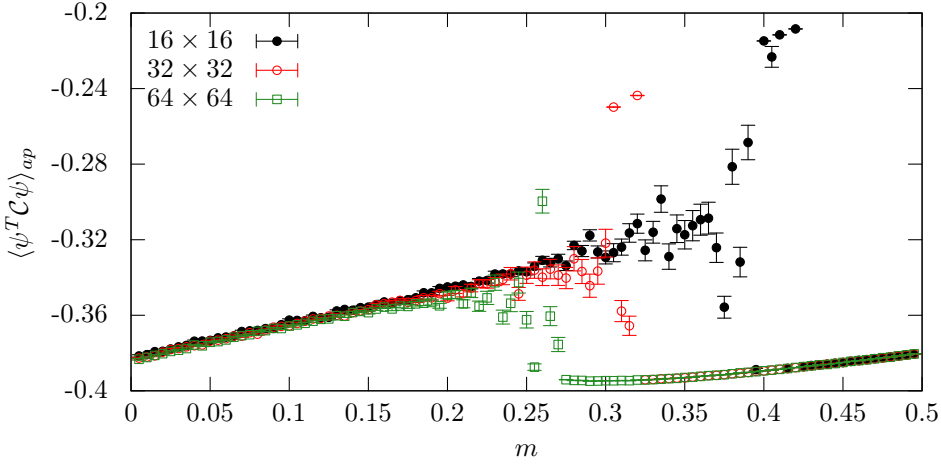


Figure 3.18.: In this figure we show the chiral condensate  $\langle \psi^T \mathcal{C} \psi \rangle_{ap}$  for various lattice volumes at fixed coupling  $g$ .

### 3.6.10. A Ward identity of supersymmetry

A way how to check if a theory is supersymmetric is to consider a Ward identity created with the supersymmetry transformation. Ward identities in general form a rather huge topic on their own and more details can be found in almost any textbook on quantum field theory. A Ward identity of supersymmetry can serve us to investigate whether supersymmetry is spontaneously broken or not. The basic idea in the construction of a Ward identity is to consider a desired observable  $\mathcal{O}$  and some symmetry transformation  $\delta$ , under which the action is invariant. If we perform a transformation with  $\phi' = \phi + \delta\phi$  and  $\psi' = \psi + \delta\psi$ , e.g. the supersymmetry transformation listed in eq.(3.4), an observable can be written as

$$\langle \mathcal{O} \rangle = \frac{1}{Z} \int \mathcal{D}\phi' \mathcal{D}\psi' \mathcal{O}(\phi', \psi') e^{-S(\phi', \psi')} \quad (3.90)$$

$$= \frac{1}{Z} \int \mathcal{D}\phi' \mathcal{D}\psi' [\mathcal{O}(\phi, \psi) + \delta\mathcal{O}(\phi, \psi)] e^{-S(\phi, \psi)} [1 - \delta S(\phi, \psi)]. \quad (3.91)$$

We focus on the anomaly free case, where the measure is invariant under the symmetry, i.e.  $\mathcal{D}\phi' \mathcal{D}\psi' = \mathcal{D}\phi \mathcal{D}\psi$ . So we can simplify

$$\langle \mathcal{O} \rangle = \frac{1}{Z} \int \mathcal{D}\phi \mathcal{D}\psi [\mathcal{O}(\phi, \psi) + \delta\mathcal{O}(\phi, \psi)] e^{-S(\phi, \psi)} [1 - \delta S(\phi, \psi)] \quad (3.92)$$

$$= \langle \mathcal{O} \rangle + \langle \delta\mathcal{O} \rangle - \langle \mathcal{O} \delta S \rangle, \quad (3.93)$$



which implies that for any observable

$$\langle \delta \mathcal{O} \rangle = \langle \mathcal{O} \delta S \rangle. \quad (3.94)$$

If the action and the ground state are invariant under  $\delta$ , the term  $\langle \mathcal{O} \delta S \rangle$  is zero and we are left with  $\langle \delta \mathcal{O} \rangle = 0$ . If though the ground state is not annihilated by  $\delta$ , then  $\langle \delta \mathcal{O} \rangle = 0$  is not true in general. We construct, analogously to [35, 48], the Ward identity

$$\langle - \int d^2x \delta \psi \rangle = - \int d^2x \langle \not{\partial} \phi - P' \rangle \epsilon = 0 \quad \Leftrightarrow \quad \langle P' \rangle = 0 \quad (3.95)$$

where

$$\langle P' \rangle = -\frac{m^2}{4g} + g \langle \phi^2 \rangle. \quad (3.96)$$

If  $\langle P' \rangle = 0$ , the Ward identity holds and supersymmetry is intact. However, if  $\langle P' \rangle \neq 0$  supersymmetry is broken. At finite lattice size and finite volume the symmetry is broken explicitly, which is why the statements above are only valid in the thermodynamic and continuum limit. Note that  $\langle P' \rangle$  has the dimension of a lattice spacing and it is  $\langle P'/m \rangle$  or  $\langle P'/g \rangle$  that can serve as a dimensionless Ward identity. Further the bosonic field  $\phi$  needs to be renormalised in the continuum limit in order to render the Ward identity finite as well. As was already mentioned this is closer explained in [36].

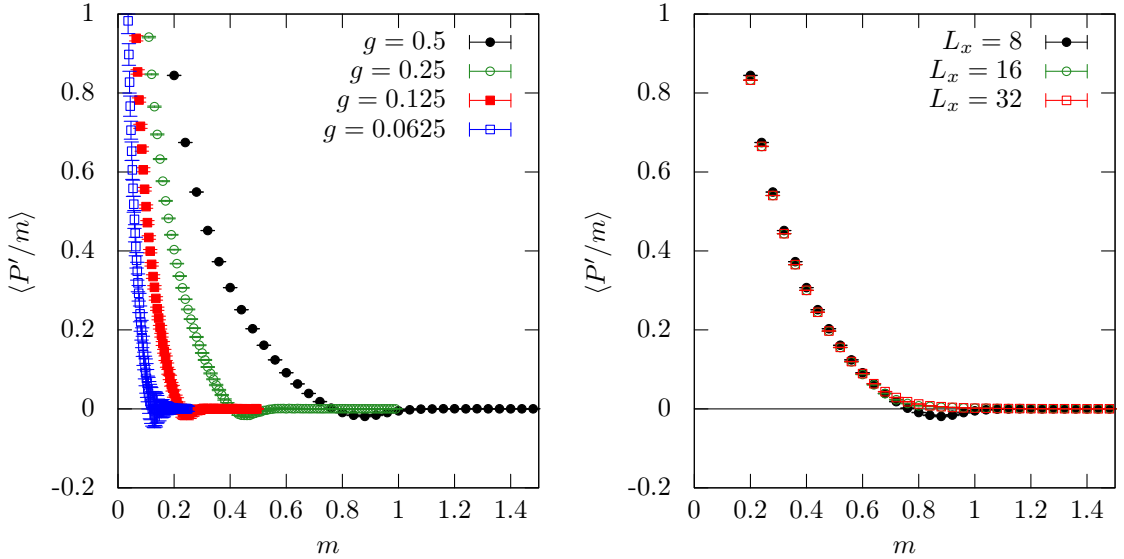


Figure 3.19.: On the left the Ward identity  $\langle P'/m \rangle$  is plotted at fixed physical volume  $gL = 4$  and  $g$  is varied. In the phase where  $\langle P'/m \rangle = 0$ , supersymmetry is intact (in the continuum). On the right we illustrate the finite size effects of  $\langle P'/m \rangle$  at fixed lattice spacing  $g = 0.5$ . The temporal extent of the system is fixed at  $L_t = 128$ .

On the left of fig. 3.19 the Ward identity  $\langle P'/m \rangle$  is shown for different couplings, i.e. lattice spacings, at fixed physical volume  $gL = 4$ . The critical bare mass  $m_c$  marks the point on the bare mass scale at which we enter the supersymmetric phase where  $\langle P'/m \rangle = 0$ . We can already roughly read off the value of  $m_c$ , above which the symmetry is

### 3. $\mathcal{N} = 1$ $D = 2$ WESS-ZUMINO MODEL

intact. Even though our discretisation breaks supersymmetry explicitly, we already observe  $\langle P'/m \rangle$  being zero at non-zero lattice spacings. This is surprising because  $\langle P'/m \rangle$  was only expected to be compatible with zero in the continuum limit.

On the right of fig. 3.19 the finite size effects of  $\langle P'/m \rangle$  at fixed coupling  $g = 0.5$  can be studied. For this coupling we can state that at  $gL = 16$  ( $L_x = 32$ ) we are already fairly close to the thermodynamic limit and only see diminishing finite size effects in the critical region when comparing with a smaller volume like  $gL = 8$  ( $L_x = 16$ ). For  $gL = 4$  ( $L_x = 8$ ) the Ward identity suddenly seems to feel stronger finite size effects near  $m_c$ .

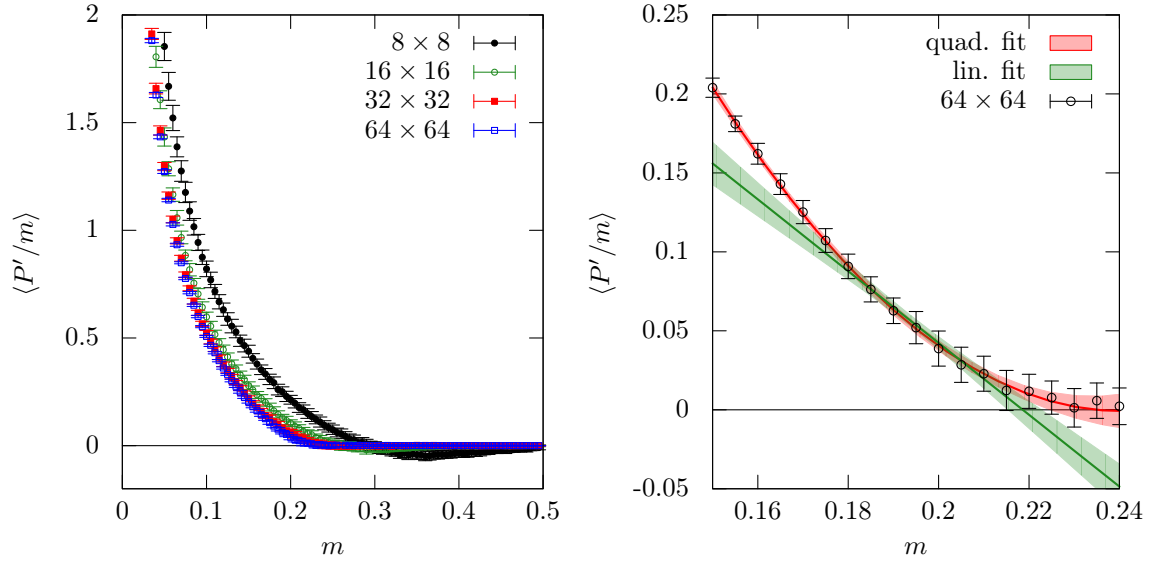


Figure 3.20.: On the left side the Ward identity is shown at fixed coupling  $g = 0.125$  for various lattice extents. On the right we show a quadratic plus linear function fitted to  $\langle P'/m \rangle$  in the critical region at fixed lattice volume  $64 \times 64$ . On the right we additionally show a linear function, fitted to the Ward identity through all points with  $m \in [0.18, 0.215]$ .

In fig. 3.20 on the left we illustrate the behaviour of the Ward identity at fixed lattice spacing for different square lattice volumes. In the critical parameter regime of  $m$ , close to the point  $m_c$  where we enter the supersymmetric phase, the Ward identity  $\langle P'/m \rangle$  can be nicely described by a quadratic plus linear function. Such a fit is shown in fig. 3.20 on the right at fixed coupling  $g = 0.125$  and lattice volume  $64 \times 64$ .

Let us define the critical bare mass  $m_c$  to be the value on the bare mass scale where we enter the regime in which  $\langle P'/m \rangle = 0$ . In order to have a mathematical criterion for the determination of  $m_c$  we perform a linear fit in the critical region and determine the intersection point with the zero axis. Such a fit is shown in fig. 3.20 on the right. The statistical error of  $m_c$ , determined by the jackknife estimated standard deviation of the intersection point from the linear fit with the zero axis, is smaller than the systematic error obtained by varying the fit range. We estimate the systematic error by the following procedure. First we naively choose a fit range by hand that has a good  $\chi^2/\text{dof}$ -value, we then start varying the fit range in  $m$  by two to three data points, considering only fits with  $\chi^2/\text{dof}$ -values that are comparable with the one coming from the fit in the initially picked fit range. The maximum and minimum of the intersection points of the one sigma

error bounds of all those fits with the zero axis are used in order to give us a systematic error for  $m_c$ <sup>6</sup>.

In fig. 3.21 we show the values of the critical bare mass, obtained by the just described fitting procedure to the Ward identity curve, for various physical volumes  $gL$  at fixed coupling  $g = 0.125$ . A linear fit is describing the extrapolation into the thermodynamic limit. We can compare the value of the critical point  $m_c$  with the one determined by the Ising-spin susceptibility variable. In the infinite volume they seem to agree with one another already at non-zero lattice spacing, as we can also see in fig. 3.21 on the left. Note though that we incorporated the systematic error coming from the choice of the fit range, but another fit function could have given us a different value of  $m_c$  that might only be compatible with the critical point of the spontaneous  $\mathbb{Z}_2$  symmetry breakdown in the continuum limit.

In fig. 3.21 on the right we further show the two (pseudo) order parameters  $Z_{pp}/Z_{ap}$  and  $\langle P'/m \rangle$  in the interesting bare mass regime. It is already at this large coupling  $g = 0.5$ , where we see that the critical point of the spontaneous  $\mathbb{Z}_2$  symmetry breaking as well as the critical point of the spontaneous supersymmetry breaking seem to lie close, which is not necessary a priori, due to both techniques of determining the critical point may suffer differently from finite volume and discretisation effects.

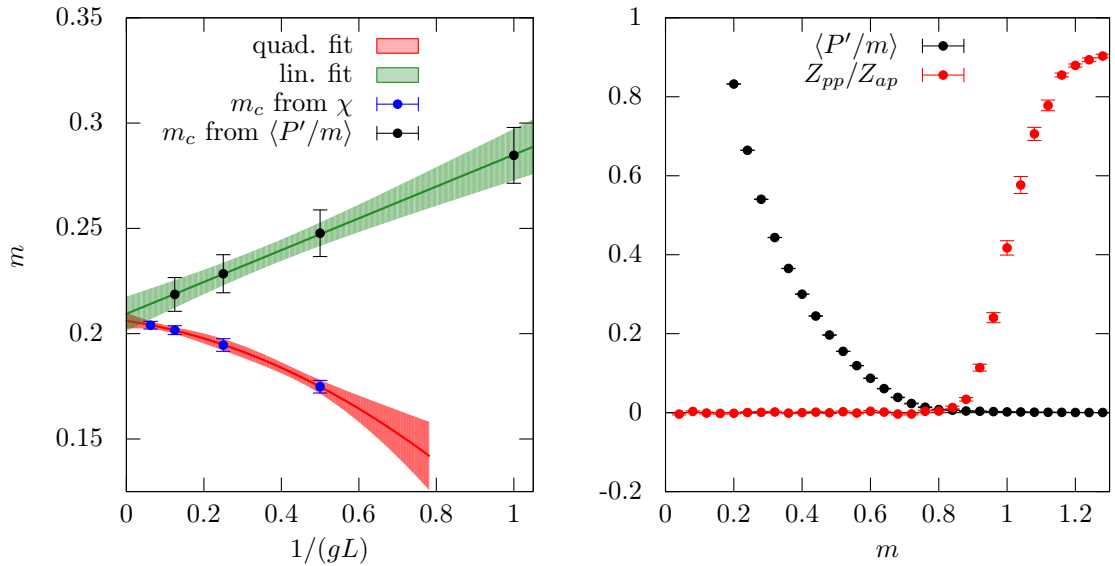


Figure 3.21.: On the left side the Ward identity is shown at fixed coupling  $g = 0.125$  for various lattice extents. On the right we show the extrapolation of  $m_c$  into the thermodynamic limit also at  $g = 0.125$ . Further the values for  $m_c$  obtained by the susceptibility method are added in order to compare with  $m_c$  determined with the Ward identity.

This brief cross check with the Ward identity gives us certainty that the critical point of the spontaneously broken  $\mathbb{Z}_2$  symmetry can already at finite lattice spacings in the

<sup>6</sup>Note that this is obviously not the most elaborate way to estimate the real error of the critical bare mass. However, we are simply interested in a cross-check between the value of the critical point of the spontaneous  $\mathbb{Z}_2$  symmetry breaking and the critical point of the spontaneous supersymmetry breaking.

infinite volume limit be identified with the critical point of the spontaneous supersymmetry breaking.

### 3.7. Masses in the system

In this section we examine the bosonic and fermionic masses of the system. Since we can measure both correlation functions in both phases we present the mass spectrum in the supersymmetric phase as well as in the phase where supersymmetry is spontaneously broken. In section 1.5 we discussed the correlation function in the fermion loop formulation. The bosonic correlation function is obtained by simply measuring the field value on every site and calculate the correlator for all times. When talking about a correlator we refer to the correlation of the field in time and consider the correlators projected to zero spatial momentum which we denote by  $\langle C_{\mathcal{O}}(t) \rangle = \langle \mathcal{O}(0) \mathcal{O}^T(t) \rangle$ . We are specially interested in the lowest mass states of the system and their behaviour when crossing the critical point. In the phase where supersymmetry is broken we expect to see the Goldstino arising as a almost massless state in the fermion correlator. After removing the lattice spacing and taking the system to the infinite volume limit we expect a completely massless Goldstino. The mass of an observable is denoted by  $m_{\mathcal{O}}^{(i)}$  and the observables that we are considering are  $\phi$  and  $\psi$ , where  $i$  is the excitation number and  $i = 0$  is therefore marking the lowest mass state.

#### 3.7.1. Supersymmetric phase

What we expect in the supersymmetric phase are mass states which are degenerate, i.e.  $m_{\phi}^{(i)} = m_{\psi}^{(i)}$ . Note that the expected degeneracy does not need to be present at non-zero lattice spacings since the discretisation breaks supersymmetry explicitly. However, when sending the lattice spacing to zero our data must show the same mass spectrum for both fields.

In this phase the correlators can be well described by a single exponential term and for the bosonic correlator with an additional constant. We therefore choose

$$h(t) = \cosh[-m_{\mathcal{O}}^{(0)}(t - L_t/2)] + k \quad (3.97)$$

as a fit function in order to extract the mass. In fig. 3.22 we show what happens with the correlator  $\langle C_{\phi} \rangle$ , where we subtracted the constant contribution, on a  $L_t \times L_x = 128 \times 48$  lattice at fixed coupling  $g = 0.25$  when approaching the critical point  $m_c = 0.38$  from the  $\mathbb{Z}_2$ -broken and supersymmetric phase. We observe that the correlation in time drops off slower when approaching the critical point, therefore the mass  $m_{\phi}^{(0)}$  must be decreasing when approaching  $m_c$ . This can be also seen by considering the same data on a logarithmic scale, as it is shown in fig. 3.22 on the right. When fitting the two correlators  $\langle C_{\phi}(t) \rangle$  and  $\langle C_{\psi}(t) \rangle$  in the supersymmetric phase, only the first few time steps are used for the fit since the correlator drops off quickly and nothing but noise remains for large  $t$ . If we look at the fermion correlator  $\langle C_{\psi}(t) \rangle_{\mathcal{L}_{00}}$  in the same region the exact same behaviour as for the boson is found. The only difference is that the fermion correlator does not need the extra constant in  $h(t)$ . The fit results show that for various bare masses in the supersymmetric

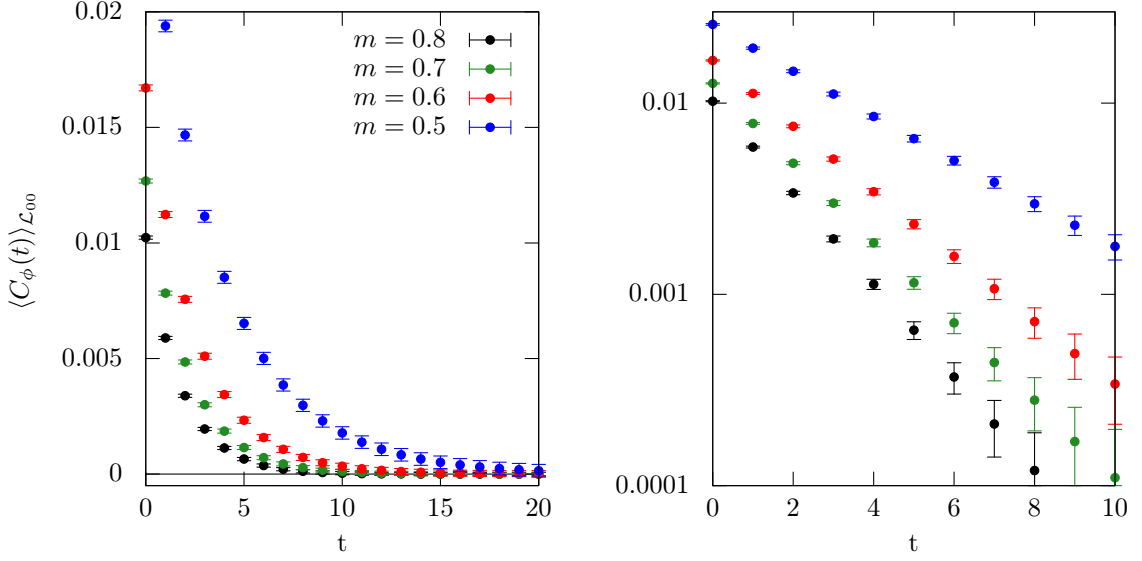


Figure 3.22.: On the left side we plot the bosonic correlation function  $\langle C_\phi(t) \rangle_{\mathcal{L}_{00}}$  in the bosonic vacuum for various bare masses  $m$  where the constant contribution is subtracted. On the right the same is shown on a logarithmic scale.

phase, the fermion mass is identical to the boson mass, i.e.  $m_\phi^{(0)} = m_\psi^{(0)}$ . This is illustrated in fig. 3.23, where one can see that in the supersymmetric phase,  $m > 0.38$ , the two masses are identical for large enough bare mass  $m$ . The line separating the supersymmetric phase and the broken one is drawn by using the value of the bare critical mass in the thermodynamic limit. The observed mass degeneracy is highly surprising since supersymmetry is only restored in the continuum limit. It is only in the region close to the critical point where we see the two mass states splitting off. This is triggered by the fact that the system at finite volume allows for tunnelling between the two vacuum states.

The estimation of the statistical error of the masses follows the ordinary Jack-knife method explained in appendix C.3 whereas the systematic error is estimated by varying the fit range, which is discussed in detail in appendix C.5. The algorithm showed itself to work with a very high efficiency in the supersymmetric phase. Low statistics already allow for very accurate determinations of the masses, strongly supporting our choice of discretisation. The area below  $m_c$  is the parameter regime in which supersymmetry is spontaneously broken. The behaviour of the masses in the supersymmetry broken phase is discussed in the next section.

### 3. $\mathcal{N} = 1$ $D = 2$ WESS-ZUMINO MODEL

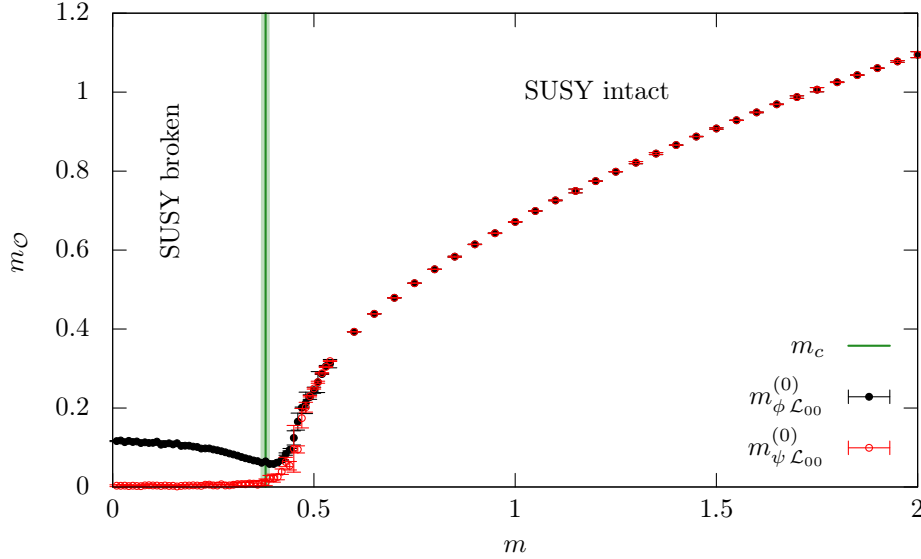


Figure 3.23.: In this plot we show the degeneracy of the groundstates  $m_\phi$  and  $m_\psi$  in the bosonic vacuum for various bare masses  $m$  in the supersymmetric phase. This is for  $L_t = 128$ ,  $L_x = 48$  and  $g = 0.25$ . The vertical line indicates the value of the critical bare mass in the thermodynamic limit for  $g = 0.25$ . The results look identical for the fermionic sector.

#### 3.7.2. Supersymmetry broken phase

Let us first consider the measured correlators in the  $\mathbb{Z}_2$ -symmetric supersymmetry-broken phase and then discuss the extracted masses.

In fig. 3.24 we plot the correlators  $\langle C_\psi(t) \rangle$  (top),  $\langle C_\phi(t) \rangle$  (bottom) for a system with  $L_t = 128$ ,  $L_x = 48$ ,  $g = 0.25$  and  $m = 0.13$ . In the fermionic correlator  $C_\psi(t)$  a very light mass is contributing at larger times, showing that the temporal extent  $L_t$  will need to be large enough in order to properly extract the light fermionic mass. The bosonic correlator  $\langle C_\phi(t) \rangle$  is now different from the fermionic one, the signal is falling off quicker and we can expect a larger mass than for the fermion. In this phase the correlators allow for a fit with a double exponential. So the fit function is chosen to be

$$g(t) = A_0 \cosh \left[ m_O^{(0)} (t - L_t/2) \right] + A_1 \cosh \left[ m_O^{(1)} (t - L_t/2) \right] + k. \quad (3.98)$$

for the fermion and boson correlator, where  $m_O^{(0)} < m_O^{(1)}$ . A constant  $k$  can be added in order to account for the small explicit  $\mathbb{Z}_2$  symmetry breaking. In fig. 3.25 we consider  $\langle C_{\psi\phi}(t) \rangle$  (top), which is the correlator of the  $\mathbb{Z}_2$ -odd observable  $\psi\phi$ , which can still be fitted with a single cosh. Likewise the correlator  $\langle C_{\phi^2}(t) \rangle$  which is shown in fig. 3.25 at the bottom.

In fig. 3.26 we show the two lowest masses found in the supersymmetry-broken phase for the boson and the fermion at  $g = 0.25$  for a lattice of extent  $L_t \times L_x = 128 \times 48$ . The data show that the masses are clearly no longer degenerate which agrees with the expected picture in the supersymmetry-broken phase. It is in the region of  $m \simeq m_c$  where

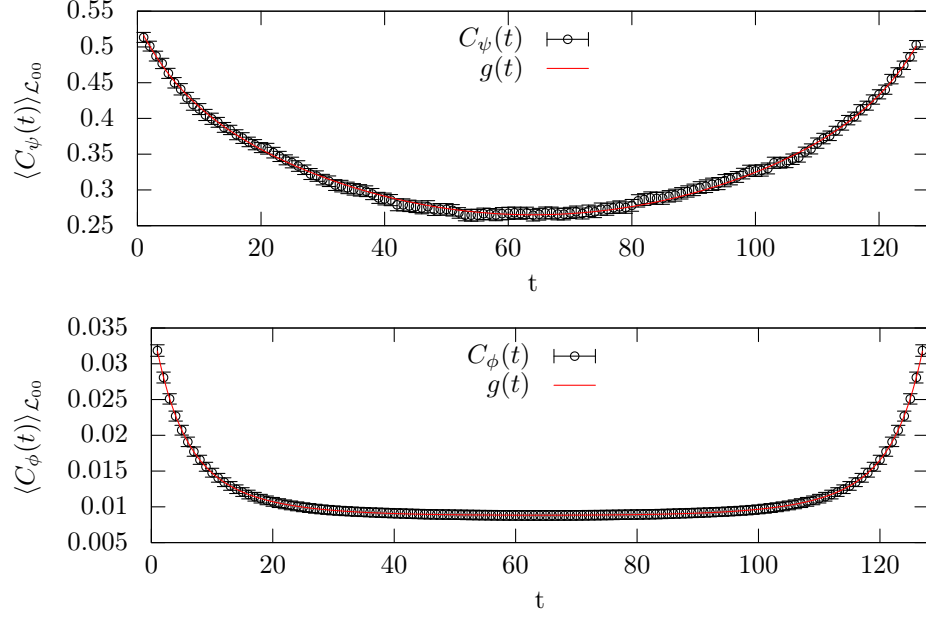


Figure 3.24.: For a system with  $L_t = 128$ ,  $L_x = 48$  and  $g = 0.25$  in the  $\mathbb{Z}_2$ -symmetric supersymmetry-broken phase at bare mass  $m = 0.13$  we show the correlators  $\langle C_\psi(t) \rangle$ (top) and  $\langle C_\phi(t) \rangle$ (bottom) in the bosonic vacuum.

supersymmetry is getting restored and we can see the bosonic and fermionic masses starting to match up again. The smallest masses  $m_\phi^{(0)}$  and  $m_\psi^{(0)}$  are accurately determinable, whereas the excited states already suffer from larger errors. In appendix C.5 we discuss the exact procedure how the systematic error is estimated. Let us now consider the lowest and first excited states in more detail.

In fig. 3.27 on the left we plot the two lowest mass states  $m_\phi^{(0)}$  and  $m_\psi^{(0)}$  and on the right we see the two excited states  $m_\phi^{(1)}$  and  $m_\psi^{(1)}$ . In the region close to the critical point we clearly see that the fermionic and bosonic mass states merge together. This is true for both the lowest states and the first excited states. Note though that around the critical point the error bars are pretty large. This comes from the uncertainty in the fit range and the fact that we enter a regime in which also a single cosh can be fitted well, this is therefore creating an ambiguity in what fit function to choose in the critical region.

In fig. 3.28 on the left we additionally show the measured  $m_{\phi\psi}$  in the same parameter setup as the already discussed data. The corresponding correlator was fitted with a single cosh. It turns out that the mass state of this observable is not measurable as accurately as the others and we will in the following neglect further investigations of it. On the right of fig. 3.28 we compare  $m_\phi^{(0)}$  with the mass  $m_{\phi^2}$ , obtained by fitting a single cosh plus a constant to the correlator  $\langle C_{\phi^2}(t) \rangle$ .

Up until now we only considered the bosonic vacuum in the  $\mathbb{Z}_2$ -symmetric supersymmetry-broken phase. Let us consider the difference between the masses in the bosonic vacuum

### 3. $\mathcal{N} = 1$ $D = 2$ WESS-ZUMINO MODEL

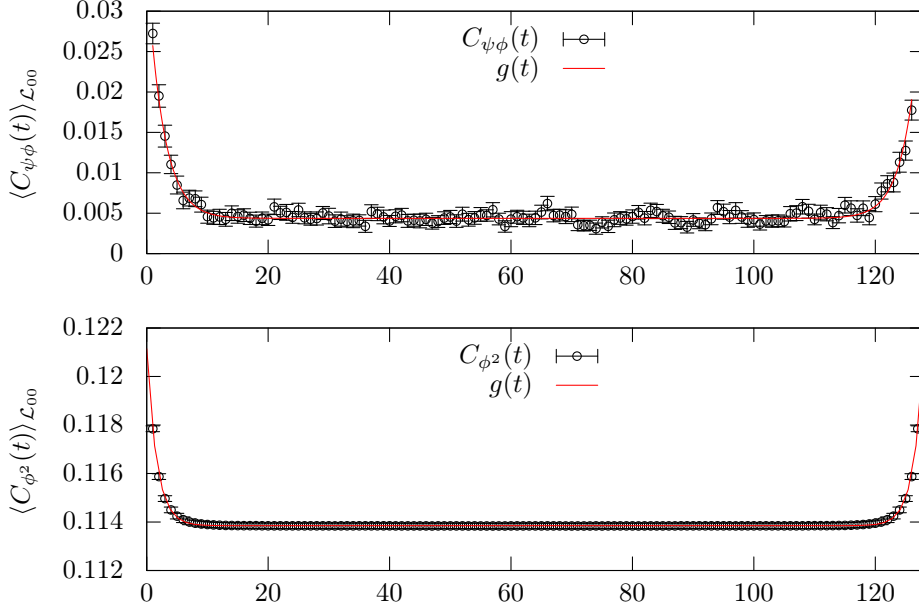


Figure 3.25.: For a system with  $L_t = 128$ ,  $L_x = 48$  and  $g = 0.25$  in the  $\mathbb{Z}_2$ -symmetric supersymmetry-broken phase we show the correlators  $\langle C_{\psi\phi}(t) \rangle$  (top) at  $m = 0.13$  and  $\langle C_{\phi^2}(t) \rangle$  (bottom) at  $m = 0.01$  in the bosonic vacuum.

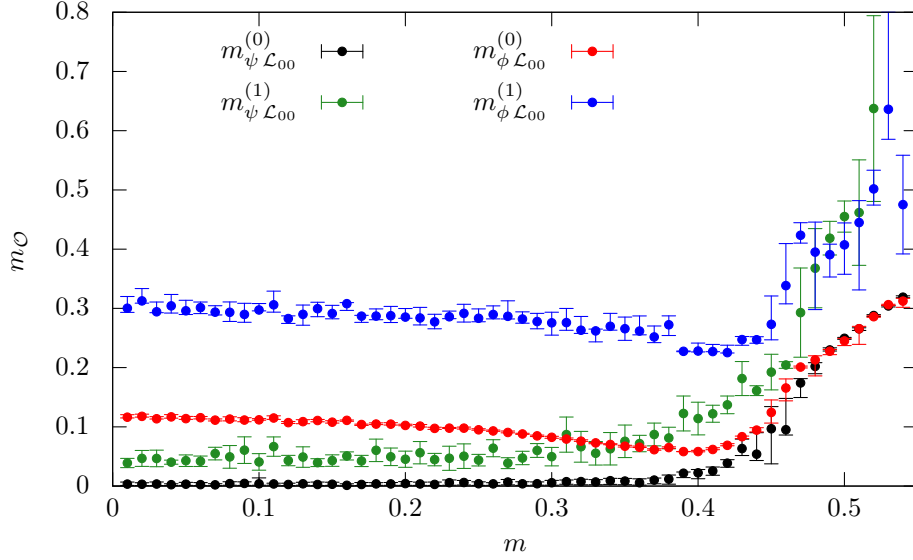


Figure 3.26.: This plot shows the first excited states and the two lowest states of the observables  $m_{\phi}$  and  $m_{\psi}$  for various bare mass  $m$  in the supersymmetry-broken phase. At larger bare mass the masses start to become degenerate and we enter the supersymmetric phase. This is again for a system with  $L_t = 128$ ,  $L_x = 48$  and  $g = 0.25$ . The statistics consist of  $6 \cdot 10^7$  complete sweeps for each data point.

and those obtained in the fermionic vacuum. In fig. 3.29 we illustrate the lowest masses of the fermion and the boson in both vacua, i.e.  $m_{\phi\mathcal{L}_{00}}^{(0)}$ ,  $m_{\phi\mathcal{L}_{01}+\mathcal{L}_{10}+\mathcal{L}_{11}}^{(0)}$ ,  $m_{\psi\mathcal{L}_{00}}^{(0)}$  and



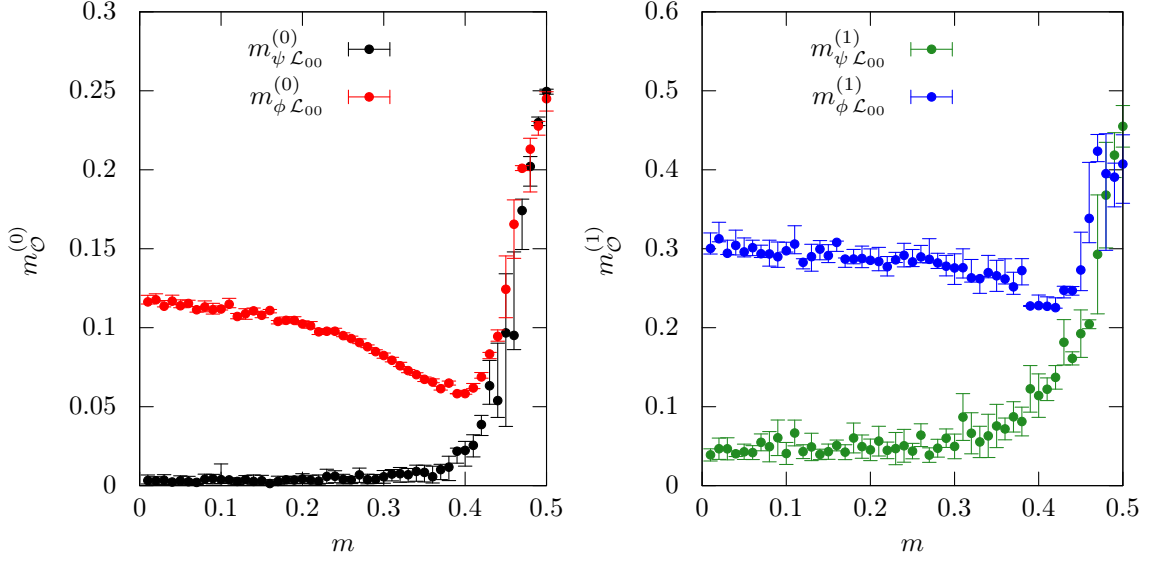


Figure 3.27.: This plot shows the two lowest mass states (left) and the first excited states (right) of the observables  $m_\phi$  and  $m_\psi$  for various bare masses  $m$  in the supersymmetry-broken phase. At larger bare mass the measured mass states start to become degenerate and we enter the supersymmetric phase. This is again for a system with  $L_t = 128$ ,  $L_x = 48$  and  $g = 0.25$ .

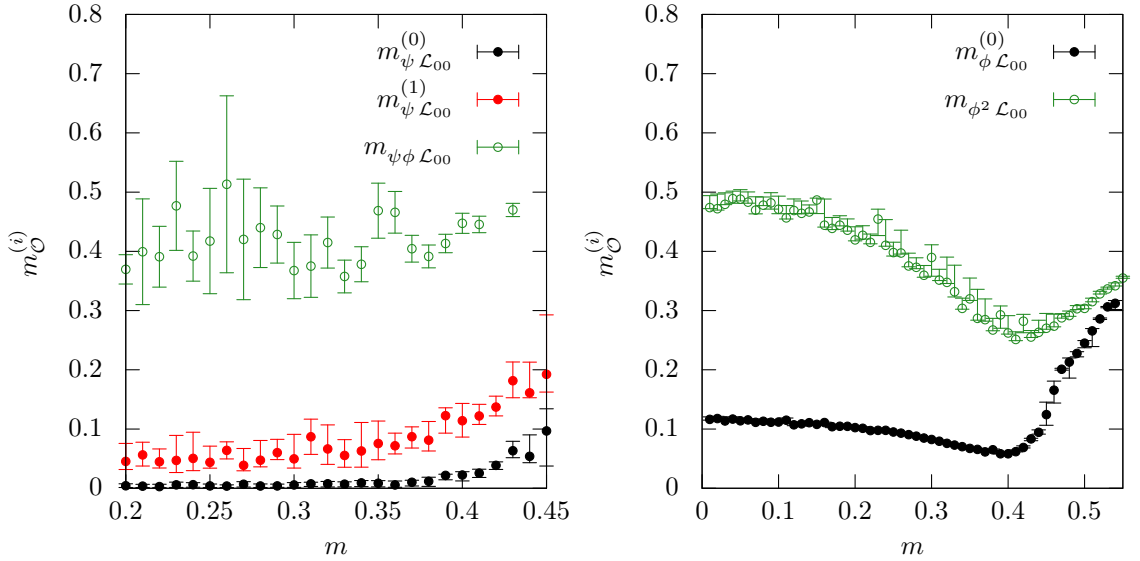


Figure 3.28.: On the left we show the ground state and the first excited state of the fermion mass and additionally add  $m_{\psi\phi}$ . On the right we consider the ground state and the first excited state of the boson mass and additionally add  $m_{\phi^2}$ . Both plots correspond to a system with fixed  $g = 0.25$  and  $L_t \times L_x = 128 \times 48$ .

$m_\psi^{(0)} \mathcal{L}_{01+\mathcal{L}_{10}+\mathcal{L}_{11}}$ . This is for a system with  $L_t \times L_x = 128 \times 32$  and  $g = 0.25$ . The bosonic mass seems to be identical in both vacua for small enough bare mass. When approaching the critical point from smaller bare mass we see that this is no longer the case and the mass obtained in the fermionic vacuum becomes smaller than the one in the bosonic vacuum.

### 3. $\mathcal{N} = 1$ $D = 2$ WESS-ZUMINO MODEL

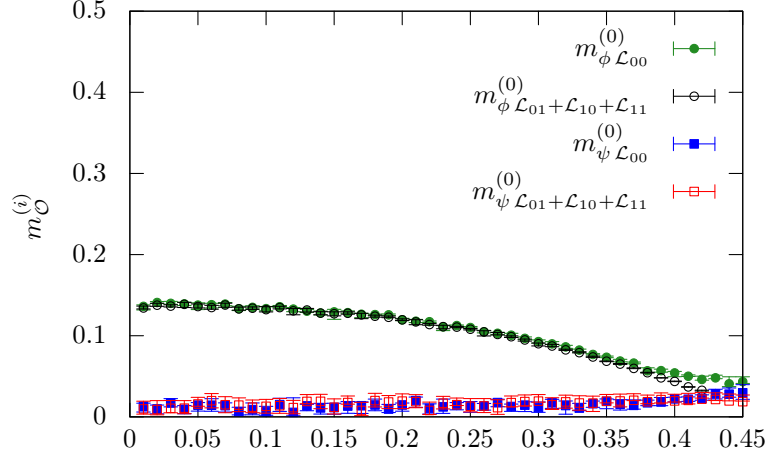


Figure 3.29.: In this plot we illustrate the lowest bosonic and fermionic mass in the supersymmetry-broken phase in the two different vacua. This is on a lattice of volume  $L_t \times L_x = 128 \times 32$  at fixed  $g = 0.25$ .

What creates this effect is the fact that in the supersymmetric phase we will remain in the bosonic vacuum and will not tunnel to the fermionic one because we are already on a considerably large lattice. As also shown in fig. 3.29, we can see that the fermion mass is behaving similarly. We claim that with more statistics and a probably more accurate determination of the fitted masses we would see a small difference between the values in the two different vacua at any bare mass. However, this effect should diminish when sending the lattice spacing to zero and can be neglected already at  $g = 0.25$  and small enough  $m$  since the difference of the masses in the two vacua is smaller than the precision of the determination of masses.

The lowest mass state of the fermion can be identified with the expected Goldstino. Let us consider the Goldstino mass and amplitude in the next section before performing extrapolations of the different masses into the thermodynamic limit.

#### 3.7.3. Goldstino and Goldstino-amplitude

The lowest fermion mass  $m_\psi^{(0)}$  in the supersymmetry-broken phase can be identified with the expected Goldstino. Since we are still at finite lattice spacings and at finite volume, the Goldstino is only approximately massless. The contribution of the Goldstino to the full fermion correlation function can be investigated by considering the amplitude of that state. In fig. 3.30 on the left we plot the Goldstino amplitude  $A_0$  from eq.(3.98). When approaching the critical point  $m_c$  from smaller bare mass, the Goldstino amplitude decreases and vanishes at the critical point, i.e. the Goldstino decouples from the system when entering the supersymmetric phase. If we set the Goldstino mass to zero and keep it fixed during the fitting procedure we still get an acceptable  $\chi^2/\text{dof}$  value if the volume is large enough.

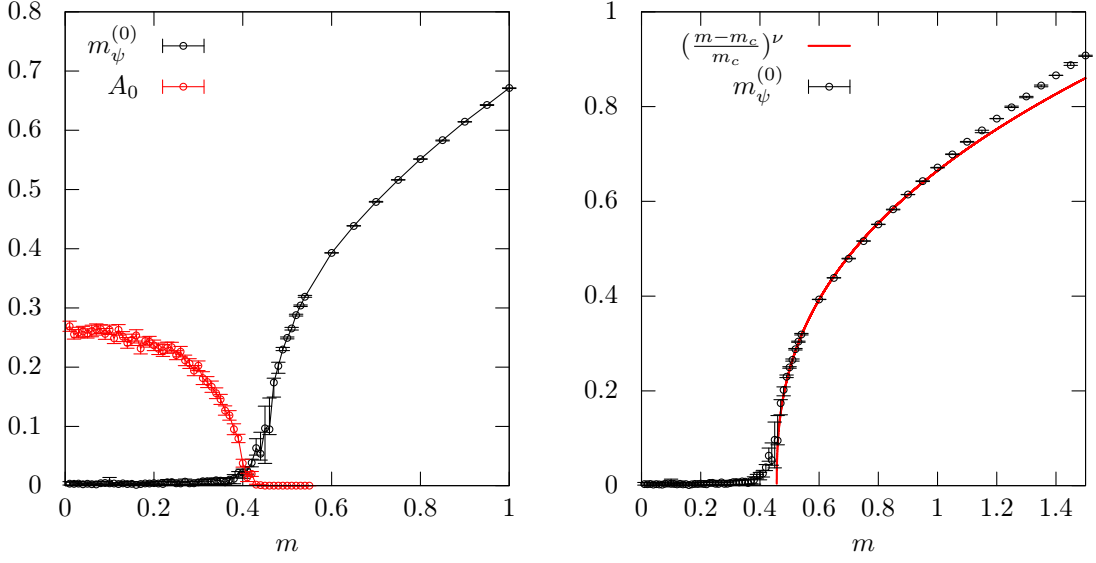


Figure 3.30.: On the left we plot the Goldstino amplitude  $A_0$  and the Goldstino mass  $m_\psi^{(0)}$  for a  $L_t \times L_x = 128 \times 48$  lattice. In the right panel we show fit to the data points  $m_\psi^{(0)}$  with  $((m - m_c)/m_c)^\nu$  in the region of  $m \in [0.45, 1]$ . A total  $6 \cdot 10^7$  complete sweeps are performed for each data point.

On the right side of fig. 3.30 we investigate the critical behaviour of  $m_\psi^{(0)}$  when approaching the critical point from  $m > m_c$ . When  $m \rightarrow m_c$  the fermion mass should behave according to

$$m_\psi^{(0)} \propto \left( \frac{m - m_c}{m_c} \right)^\nu. \quad (3.99)$$

We perform a fit of this function to the data points  $m_\psi^{(0)}$  in the critical region, i.e.  $m \in [0.45, 1.0]$ . The critical index  $\nu$  is telling us in which universality class the phase transition falls. In our fit we obtain a value of  $\nu = 0.395 \pm 0.003$ . Note that only the statistical error is respected here and an estimation of the systematic error is neglected. Further the critical point  $m_c$ , determined by the fit, is  $0.457 \pm 0.002$ , which does not agree with the value we obtained via the Ising-spin susceptibility or the Binder cumulant method. However, this is not expected since we are still at relatively large lattice spacings, i.e.  $g = 0.25$ , and at finite volume.

### 3.7.4. Thermodynamic limit of lowest the mass states

Let us in this section consider the measured masses in the supersymmetric phase and in the supersymmetry-broken phase at fixed lattice spacing and investigate the thermodynamic limit.

#### Supersymmetry-broken phase

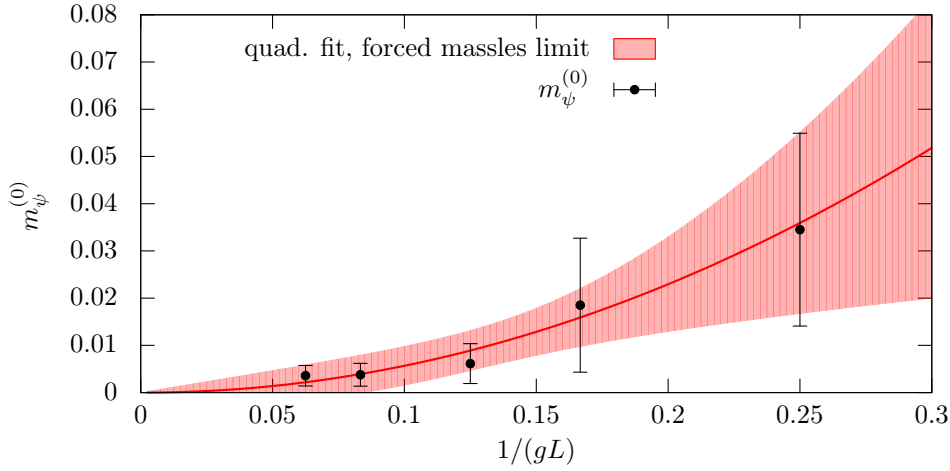


Figure 3.31.: In this plot we show the Goldstino mass  $m_\psi^{(0)}$  for various physical volumes  $gL$ . Additionally a quadratic fit is performed in which the parameter  $m_\psi^{(0)}$  was fixed to zero.

Our data is compatible with the assumption that  $m_\psi^{(0)} = 0$  in the thermodynamic limit in the supersymmetry-broken phase. This is illustrated in fig. 3.31 by a quadratic fit through all data points, enforcing a vanishing mass at  $1/(gL) = 0$ . Such a fit is shown in fig. 3.31 with a  $\chi^2/\text{dof}$  value of 0.29. Note that also a linear fit could be performed with an acceptable  $\chi^2/\text{dof}$  value.

In fig. 3.32 in the left panel we perform a linear extrapolation of the measured bosonic mass  $m_\phi^{(0)}$  into the thermodynamic limit at fixed  $g = 0.25$  for three different bare masses  $m = 0.3$ ,  $m = 0.18$  and  $m = 0.02$ , corresponding to different points in the  $\mathbb{Z}_2$  symmetry and supersymmetry-broken phase. A linear fit is possible for all four data points at  $m = 0.3$ , whereas for smaller bare mass the finite volume effects seem to be stronger and a linear fit is only possible when including the data from the three largest volumes. This extrapolation indicates that the value of  $m_\phi^{(0)}$  in the infinite volume limit does not depend on  $m$ , at least in the inspected region. A quadratic fit would indicate a slightly decreasing mass  $m_\phi^{(0)}$  in the thermodynamic when decreasing the bare mass parameter. Such a scenario is illustrated on the right of fig. 3.32, where we used all data points for  $m = 0.18$  and  $m = 0.02$  in a quadratic fit.

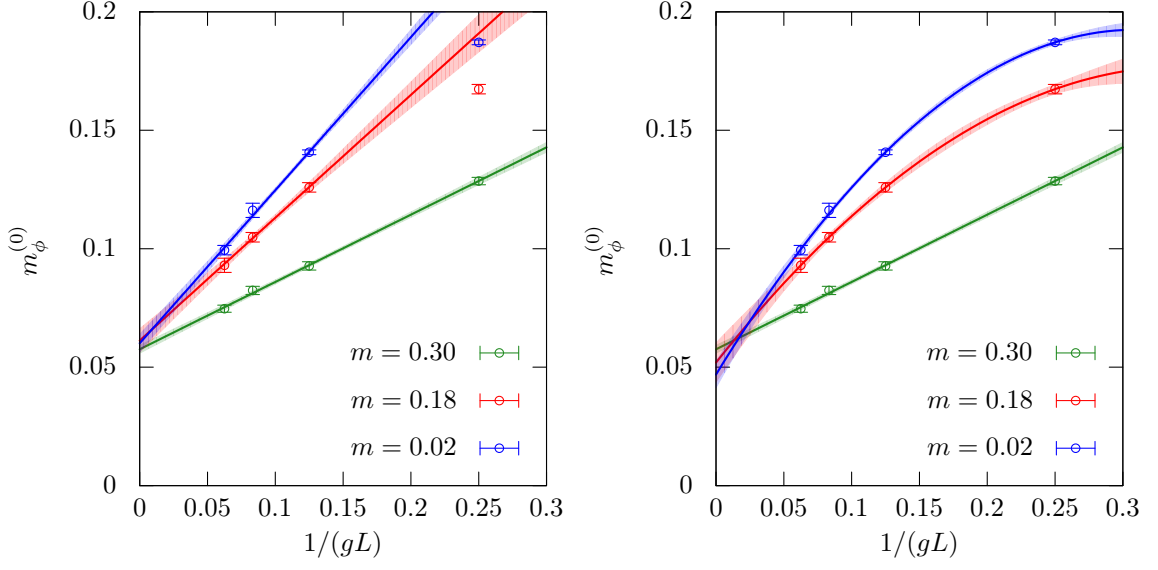


Figure 3.32.: On the left we show we show linear extrapolations into the thermodynamic limit of  $m_\phi^{(0)}$  at fixed coupling  $g = 0.25$  for various bare masses  $m = 0.3$ ,  $m = 0.18$  and  $m = 0.02$  ( $\mathbb{Z}_2$ -symmetric and supersymmetry-broken phase). For the data at the two smaller bare masses only the three points closest to the infinite volume are fitted. On the right the same data is shown but the data points corresponding to the two smaller bare masses are fitted with a quadratic function.

### Supersymmetric phase

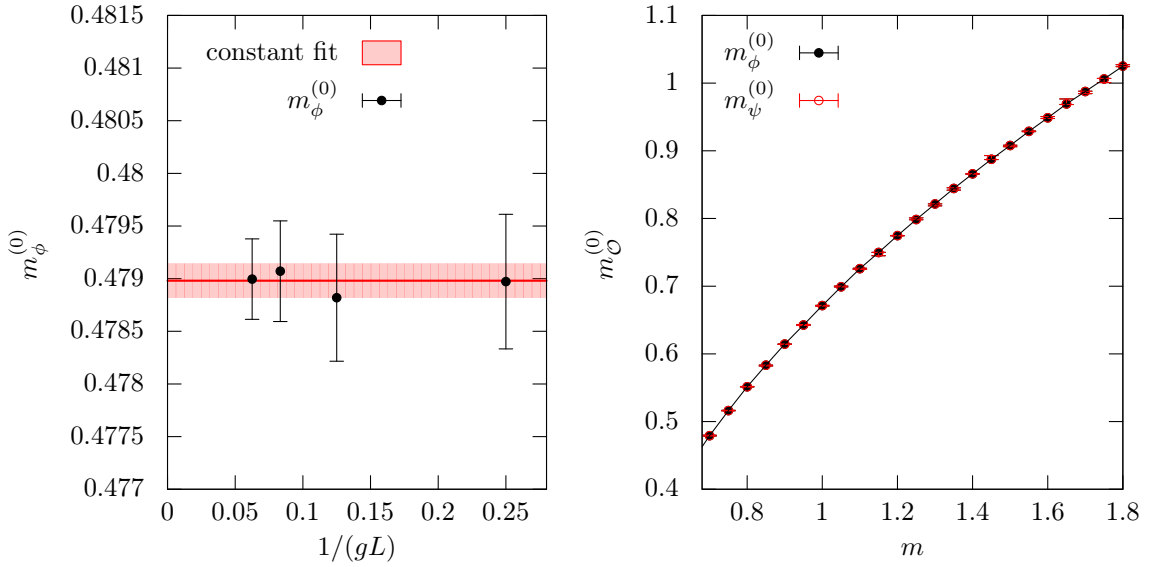


Figure 3.33.: On the right we show the extrapolation of  $m_\phi^{(0)}$  at  $m = 0.7$ , which corresponds to the  $\mathbb{Z}_2$ -broken and supersymmetric phase, with a constant fit. The same can be done for  $m_\psi^{(0)}$ , creating the identical picture. On the left we then show both, the boson and fermion lowest mass state in the thermodynamic limit in the supersymmetric phase. All data points are at fixed lattice spacing and on the right a black line is drawn connecting all the data points.

### 3. $\mathcal{N} = 1$ $D = 2$ WESS-ZUMINO MODEL

We saw that in the supersymmetric phase the fermion and boson masses are degenerate at the already investigated lattice spacing and volume used in fig.3.23. This picture also seems to be unaffected from any finite volume effects, as it is shown in fig. 3.33 where the observed masses at different physical volume  $gL$  can be fitted by a constant. Note that this is also true for the fermion mass. In the right panel of fig. 3.33 we then plot the lowest boson and fermion mass in the thermodynamic limit in the supersymmetric phase. The data shown in fig. 3.33 is at fixed coupling  $g = 0.25$  which means that we consider a system with fixed lattice spacing. We conclude that in the supersymmetric phase the masses are degenerate in the thermodynamic limit.

#### 3.7.5. Continuum limit of masses at constant renormalised coupling $f^R$

Let us investigate how the masses behave at fixed physical volume and constant renormalised coupling  $f^R$ , when varying the lattice spacing. This can be achieved by setting  $f^R$  to a fixed value, choosing  $g$ , and then adjust  $L$  such that  $gL$  stays fixed and calculate  $m$  for which  $f^R = g/m^R$  is the initially fixed value. We do this for a renormalised coupling corresponding to a coupling in the supersymmetric phase and one in the supersymmetry-broken phase. All data points in this section are based on statistics corresponding to with  $10^6$  complete sweeps.

#### Supersymmetric phase

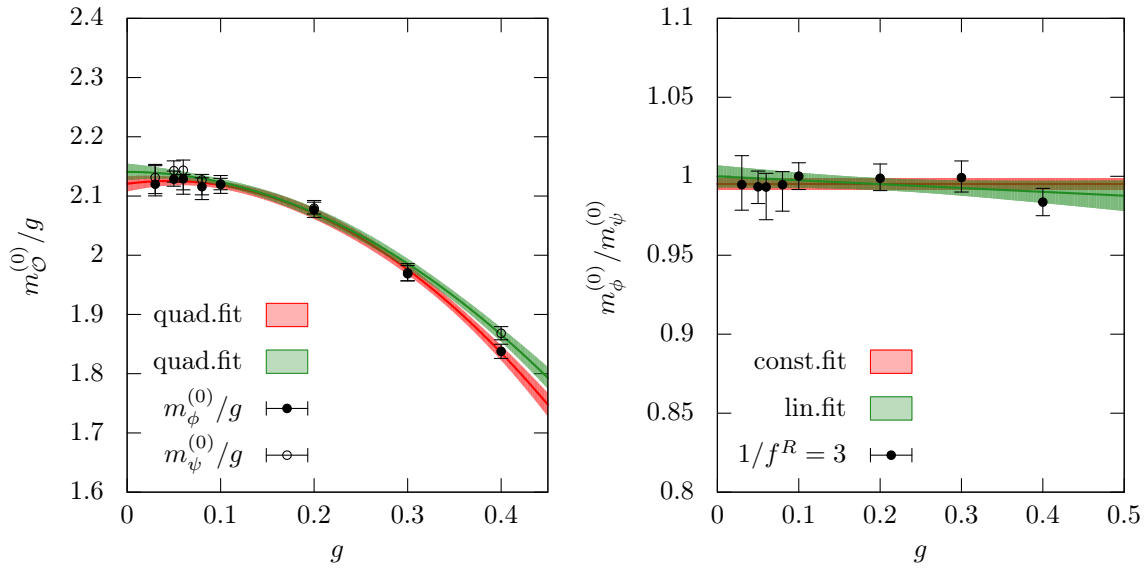


Figure 3.34.: Showing  $m_\phi^{(0)}/g$  and  $m_\psi^{(0)}/g$  with a quadratic plus linear continuum extrapolation on the left at fixed dimensionless renormalised coupling  $1/f^R = 3$ . On the right the mass ratio  $m_\phi^{(0)}/m_\psi^{(0)}$  is shown for various lattice spacings and a constant and linear fit illustrates the extrapolation to the continuum. The system is at fixed physical volume  $gL = 8$ .

In a first step we consider  $1/f^R = 3$  which corresponds to the supersymmetric phase. It is in this phase where we can fit the correlators with a single cosh function, as done

in the previous section, and determine the masses  $m_\phi^{(0)}$  and  $m_\psi^{(0)}$ . In fig. 3.34 we illustrate the dimensionless ratios  $m_\phi^{(0)}/g$  and  $m_\psi^{(0)}/g$  on the left at different couplings, i.e. lattice spacings. The extrapolation to the continuum limit can in both cases be done by a quadratic plus linear fit through all shown data points. Note that the physical volume is  $gL = 8$ , however, we can argue that what is shown in fig. 3.34 on the left is most likely corresponding to the actual picture in the thermodynamic limit as well. This statement can be made because there, at least at the investigated couplings, no finite volume effects can be seen like it was previously shown in fig. 3.33. As also already observed in fig. 3.23 it is astonishing to see the mass degeneracy already at finite lattice spacings despite the fact that the lattice artefacts on  $m_\phi^{(0)}$  are of order 10% at  $g = 0.4$ . It is only for very large  $g$  where we start to see a small deviation between the two masses. On the right of fig. 3.34 the ratio  $m_\phi^{(0)}/m_\psi^{(0)}$  is shown for various couplings and additionally a constant and a linear fit serve as valid extrapolations to the continuum limit, both leading to the same statement that the masses are degenerate at  $a = 0$ . This plot specially shows the quality of the data in the supersymmetric phase leaving no ambiguity in the fact that in the thermodynamic and continuum limit the data show that the lowest mass of the fermion and the boson are degenerate. This is in perfect agreement from what is expected in the supersymmetric phase. Note that this behaviour is only observed for dimensionless couplings  $f^R$  which are far away from the point of spontaneous break down of the supersymmetry, i.e.  $f^R \ll f_c^R$ .

### Supersymmetry-broken phase

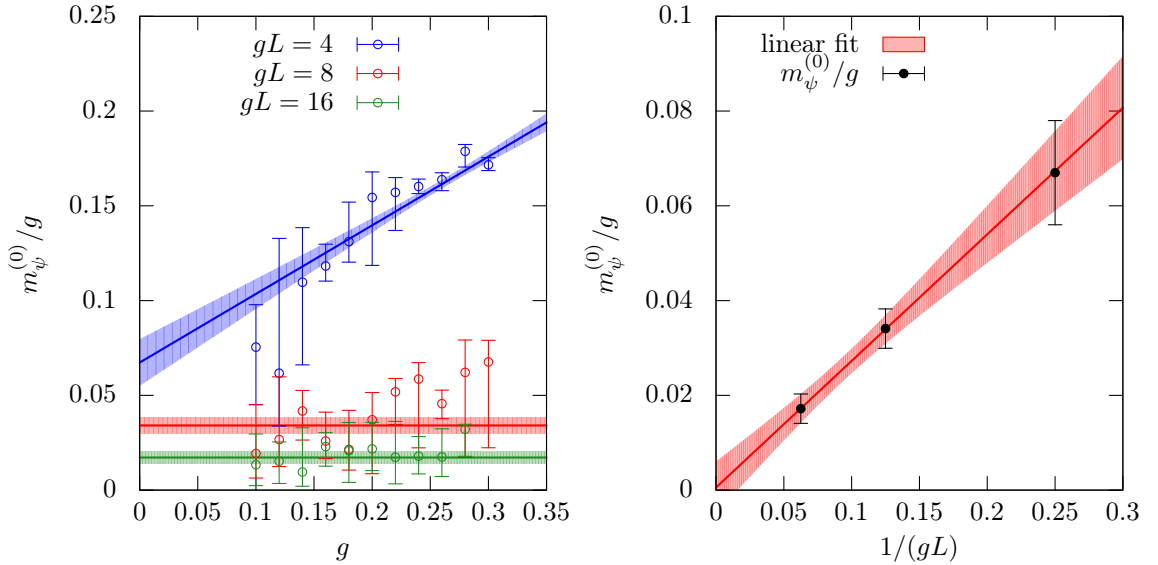


Figure 3.35.: On the left we show the dimensionless quantities  $m_\psi^{(0)}/g$  at fixed renormalised dimensionless coupling  $1/f^R = 1.2$ , which corresponds to the  $\mathbb{Z}_2$ -symmetric supersymmetry-broken phase, at different couplings, i.e. lattice spacings. This is done for three physical volumes 4, 8 and 16. A possible extrapolation to the continuum is done with a linear fit through all data points from the volume  $gL = 4$  and with a constant for  $gL = 8$  and  $gL = 16$ . On the right we show a linear extrapolation of the ratio  $m_\psi^{(0)}/g$  to the thermodynamic limit at zero lattice spacing.

### 3. $\mathcal{N} = 1$ $D = 2$ WESS-ZUMINO MODEL

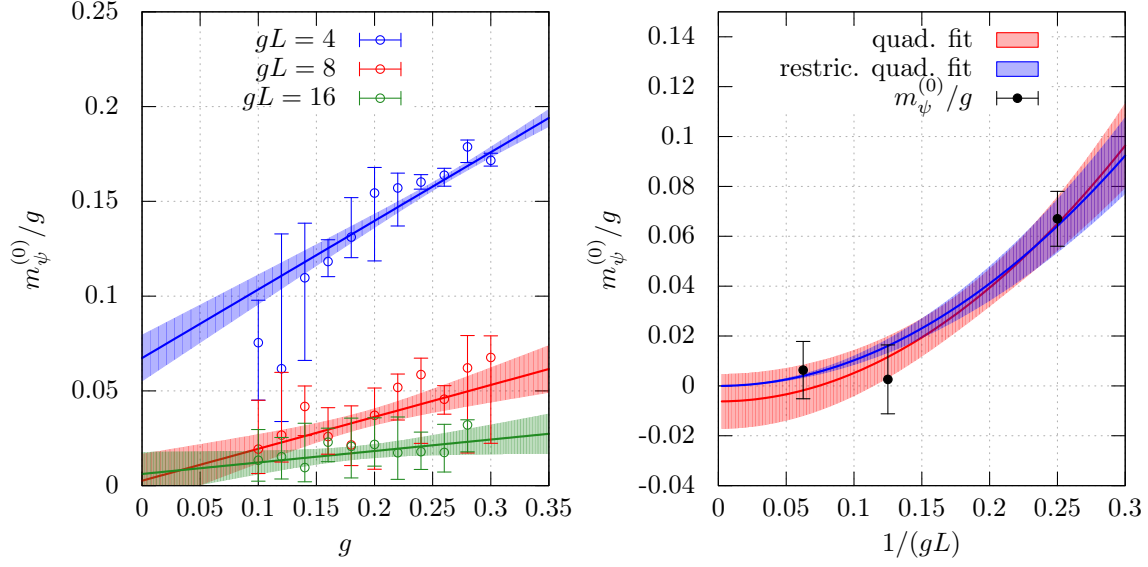


Figure 3.36.: On the left we show the dimensionless quantities  $m_\psi^{(0)}/g$  at fixed renormalised dimensionless coupling  $1/f^R = 1.2$  at different couplings, i.e. lattice spacings. A linear extrapolation to the continuum is done for all data from all volumes. On the right we show a quadratic fit with a constant  $\mu \cdot (gL)^{-2} + k$ . This fit gives us a value in the thermodynamic limit that is compatible with zero. On the right we additionally show a single quadratic term  $\mu \cdot (gL)^{-2}$  (blue) fitted ( $\mu = 1.02 \pm 0.17$ ) to the ratio  $m_\psi^{(0)}/g$  at zero lattice spacings. This thermodynamic limit enforcing  $m_\psi^{(0)}((gL)^{-1} \rightarrow 0) = 0$  is also compatible with the observed data.

In a next step we consider  $1/f^R = 1.2$ , which is corresponding to the supersymmetry-broken phase according to the symmetry phase diagram in fig. 3.17 on the right. In fig. 3.35 on the left we show the behaviour of the dimensionless quantity  $m_\psi^{(0)}/g$  when sending the lattice spacing to zero. This is done for three different physical volumes 4, 8 and 16. For larger physical volumes  $gL$  the ratio  $m_\psi^{(0)}/g$  seems to be almost constant when varying the lattice spacing. A linear fit is performed for the data from the smallest volume whereas the data from the two larger volumes are fitted with a constant, these fits serve as continuum extrapolations. On the right of fig. 3.35 we then perform a linear extrapolation to the thermodynamic limit of the data points at zero lattice spacing. Our results agree with the expected picture of a Goldstino mass  $m_\psi^{(0)}$  that must vanish in the thermodynamic continuum limit. However, the data shown in fig. 3.35 on the left would also allow for different continuum extrapolations with even larger error bars. If the data from  $gL = 8$  and  $gL = 16$  were fitted with a linear function they would already indicate a vanishing Goldstino mass at finite volume. This is illustrated in fig. 3.36 on the left. On the right side of fig. 3.36 we then show the thermodynamic limit of the data at zero lattice spacings. A quadratic function plus a constant  $\mu \cdot (gL)^{-2} + k$  can be fitted and gives us a mass compatible with zero in the thermodynamic limit, i.e.  $k = -0.006 \pm 0.01$ . Let us perform also another fit using a single quadratic function  $\mu \cdot (gL)^{-2}$  through the three data points, forcing  $m_\psi^{(0)}$  to be zero in the thermodynamic limit. The  $\chi^2/\text{dof}$  value is 0.58, making our data compatible with an imposed zero mass in the thermodynamic and continuum limit. Note that the volume is rather small for the fermion mass, i.e.  $m_\psi^{(0)} L \leq 0.5$ .



At the same fixed  $1/f^R = 1.2$  we now investigate the lowest mass state of the boson to coupling ratio  $m_\phi^{(0)}/g$ . In fig. 3.37 on the left we show  $m_\phi^{(0)}/g$  at different couplings for three different physical volumes 4, 8 and 16 as it was done before with the fermionic mass. A linear extrapolation to the continuum limit is shown for each fixed  $gL$ . On the right of fig. 3.37 a linear extrapolation into the thermodynamic limit is shown for  $m_\phi^{(0)}/g$  at zero lattice spacing. The value in the thermodynamic continuum limit of  $m_\phi^{(0)}/g$ , obtained with this procedure, is  $0.563 \pm 0.019$ . It seems that for large  $gL$  the ratio  $m_\phi^{(0)}/g$  might have a slight trend of becoming a plateau for very small lattice spacings. However, with the present data no distinct statement can be made about this. More data at smaller lattice spacings would resolve this and would allow an estimate on the systematic error.

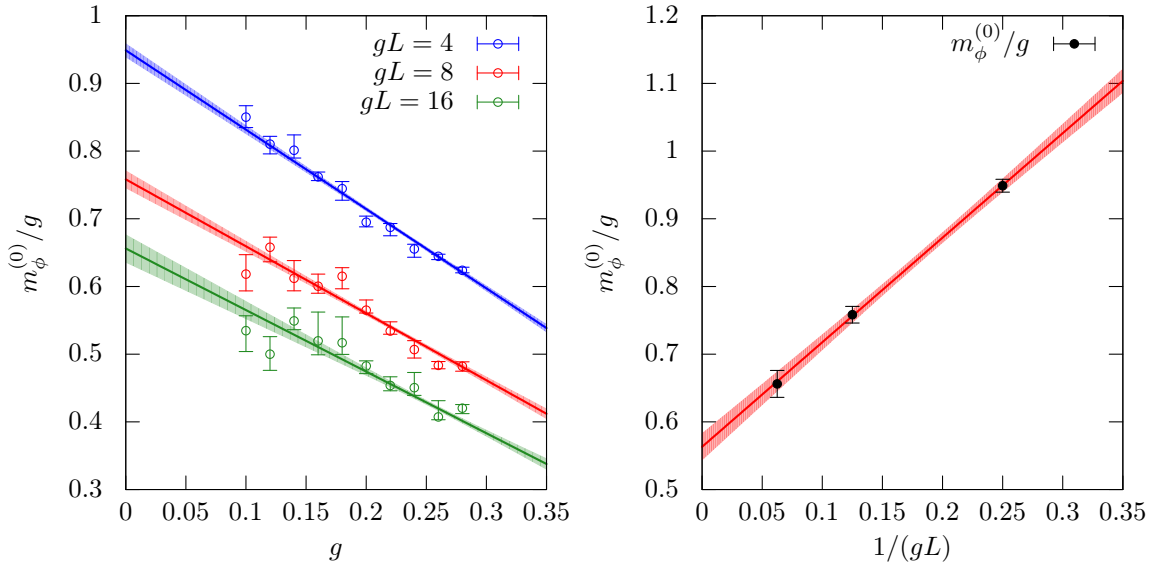


Figure 3.37.: On the left we show the dimensionless quantity  $m_\phi^{(0)}/g$  at fixed renormalised dimensionless coupling  $1/f^R = 1.2$ , which corresponds to the  $\mathbb{Z}_2$ -symmetric supersymmetry-broken phase, at different couplings, i.e. lattice spacings. This is done for three physical volumes 4, 8 and 16. The linear fit serves as a continuum limit extrapolation for all  $gL$ . On the right we show a linear extrapolation of the ratio  $m_\phi^{(0)}/g$  to the thermodynamic limit at zero lattice spacing.

### 3.8. Conclusion and outlook

We have established the fermion loop formulation for the  $\mathcal{N} = 1$  Wess Zumino model that allowed a sign problem free and efficient simulation with a worm algorithm even in the supersymmetry-broken phase. Two phases are observed, a  $\mathbb{Z}_2$ -symmetric supersymmetry-broken phase where the two vacua are degenerate and a  $\mathbb{Z}_2$ -broken supersymmetric phase where one ground state is removed in the infinite volume limit. The value of the critical coupling, separating those two phases, has been analysed with two techniques, the Binder cumulant and what we called the susceptibility of the Ising spin projection of the bosonic field variable. Proper extrapolations of the bare critical parameter into the thermodynamic and continuum limit were possible, which after renormalisation gave the value of the renormalised dimensionless critical coupling in the continuum. The observation of the Witten index and a Ward identity of supersymmetry give a clear sign of the intact and broken supersymmetry in the two different phases. In a second step we investigated the boson and fermion masses in both phases, confirming the mass degeneracy in the  $\mathbb{Z}_2$ -broken supersymmetric phase. Our data also agrees with the expected massless Goldstino arising in the  $\mathbb{Z}_2$ -symmetric supersymmetry-broken phase. The phase diagram of the two-dimensional  $\mathcal{N} = 1$  Wess-Zumino model, including the masses, has been presented with a quite remarkable precision. Let us in the following discuss some of these points in more detail.

The worm algorithm, as expected, works highly efficient in updating the closed fermion loop configurations. Specially in the supersymmetric phase very fast simulations are possible, creating accurate measurements of the masses in the system. It is the update of the bosonic field that forms the current limitations on the accuracy specially at the critical point. This is because the bosonic degrees of freedom are updated with an ordinary local Metropolis algorithm suffering from critical slowing down at the critical point. The established bosonic bond formulation would allow to update the so called bond occupation numbers with a worm algorithm, but the Wilson derivative for the bosonic field creates a diagonal hop term in the bosonic action contributing with a negative weight. This negative weight is a source of a possibly globally fluctuating sign, spoiling the efficient use of the worm algorithm. If however a symmetric derivative would be used, the bosonic field could be simulated in a very efficient way, analogous to the results seen for the  $\phi^4$ -theory [53, 55]. The formulation without Wilson derivative would also be amenable to a cluster algorithm [66]. Note though that in the  $\mathcal{N} = 1$  Wess-Zumino model we introduced the Wilson derivative for the boson in order to recover supersymmetry in the continuum without fine tuning, this nice feature would be lost if the boson fields were discretised differently. Our attempts to create an efficient cluster algorithm for the discretisation with a Wilson term for the boson failed due to the opposite signs of bosonic interactions that led to small acceptance rates of global  $\mathbb{Z}_2$  transformations.

C. Wozar and A. Wipf already provide numerical results [35] for the critical coupling in the two-dimensional  $\mathcal{N} = 1$  Wess-Zumino model. They studied the model using the SLAC derivative, which respects the  $\mathbb{Z}_2$  symmetry at non-zero lattice spacings by giving up locality. The critical dimensionless coupling of the  $\mathbb{Z}_2$  symmetry breaking is determined

with the Binder cumulant method and the supersymmetry breaking is investigated with a Ward identity. In order to renormalise the mass parameter the divergent one loop self energy contribution is subtracted, making our critical coupling in the continuum comparable. Our results though seem to disagree, they find a critical coupling of  $f = 21.1(1.1)$ . Translating our critical coupling to their convention gives us  $f = 0.765(0.04)$ . A third independent method would be desirable in order to clarify this mismatch. Our formulation suffers from the fact that the action is not manifestly  $\mathbb{Z}_2$ -invariant. The action used in [35] on the other hand is non-local. As a third method a  $\mathbb{Z}_2$ -symmetric and local action would form the ultimate solution. Introducing an extra dimension and using domain-wall fermions [60] could most likely be used in order to simulate the fermions with a worm-like algorithm while avoiding the explicit  $\mathbb{Z}_2$  symmetry breaking of the lattice action.

Despite the fact that our action explicitly breaks the  $\mathbb{Z}_2$  symmetry, we have seen that the effects are marginal and quickly diminish when sending the lattice spacing to zero. However, strictly speaking we only observe a pseudo phase transition in the current setup if the system is not at zero lattice spacing. This initially posed a possible drawback of the formulation but did not show to be a problematic factor at all.

The measured boson and fermion masses in the  $\mathbb{Z}_2$ -broken supersymmetric phase are degenerate as expected. What is amazing is the fact that we actually would expect supersymmetry to restore fully only in the continuum but our observations show that the degeneracy holds even up to very coarse lattice spacings. Understanding this observation of an intact supersymmetry with a lattice action that breaks supersymmetry explicitly is of great interest.

In the  $\mathbb{Z}_2$ -symmetric supersymmetry-broken phase the lowest mass states of both fields can be resolved and it is possible to gain also information about the first excited states. The lowest fermion mass state is compatible with zero in the thermodynamic and continuum limit, allowing us to identify this with the expected Goldstino. The bosonic mass ground state in the  $\mathbb{Z}_2$ -symmetric supersymmetry-broken phase was expected [33] to be independent of the bare mass  $m$  in the thermodynamic limit. We can confirm this scenario with our data, however we do not observe the bosonic mass ground state being compatible with zero in the continuum limit.



## 4. Supersymmetric Nonlinear $O(N)$ sigma Model

### 4.1. Motivation

There are certain key features of supersymmetric nonlinear  $O(N)$  sigma models which make them very interesting to investigate. The non-supersymmetric version has served as an important model due to its parallels to quantum chromodynamics, short QCD. Even though having only one dimensionless coupling the model shows a mass gap and is asymptotically free (at least for  $N > 2$ ). It is highly interesting to non-perturbatively investigate how a supersymmetric version of this model is behaving. Can we observe the same scenarios of exhibiting massive states as in the non-supersymmetric model? Is supersymmetry spontaneously broken? When putting supersymmetric theories on the lattice the question arises if the chosen discretisation, which in general explicitly breaks supersymmetry (or at least partially), restores the correct symmetric model in the continuum? It is then very interesting to check features like mass degeneracy and Ward-identities and how these properties behave on the lattice.

The non-supersymmetric model has been investigated and used in various ways [67–73], some already using the formulation of Prokof'ev and Svistunov [26] to simulate bosonic degrees of freedom in this reformulated way with the so called worm algorithm. The supersymmetric version of the model [37, 38] has been studied analytically by [39, 40], showing the spontaneous breakdown of the discrete chiral symmetry that leads to mass generation and the appearance of a supersymmetric pair of bound states. Further work [74] provided even a formula for the mass gap for  $N > 4$ . Numerical results have been performed, investigating the symmetry and mass phase diagram [41] with different discretisation methods for the  $N = 3$  case, where also results from twisted forms of the continuum action exist [75].

In this chapter we lay focus on creating a loop formulation for the supersymmetric version of the model. We are motivated to do so in order to use a worm-like algorithm that showed itself being very efficient [28], as also seen in the previous chapter when being used to simulate the Majorana fermion in the  $2d \mathcal{N} = 1$  Wess Zumino. We will therefore calculate the hopping expansion of the Boltzmann factor of both, the fermionic and the bosonic part of the action. In this reformulated model we will then simulate the fermionic degrees of freedom with a worm algorithm and the bosonic degrees of freedom with a standard Monte-Carlo technique. This is because in the bond formulation of the bosonic degrees of freedom there is a possible source of a locally fluctuating sign. In general it is our goal to deliver a proof of concept and start answering some of the motivational questions listed above by showing some first results for the special case of  $N = 2$ . We

#### 4. Supersymmetric Nonlinear $O(N)$ sigma Model

will see that the formulation can serve to numerically investigate also models with  $N > 2$ . However, all models with  $N > 2$  are suffering from an additional source of a possible sign fluctuation in the loop formulation. Representatively for all  $N > 2$  we will investigate the case where  $N = 3$  in more detail.

### 4.2. Continuum model

Following the concept of [37, 38] we can construct a nonlinear  $O(N)$  sigma model in two-dimensional Euclidean spacetime with a super field

$$\Phi = \phi + i\bar{\theta}\psi + \frac{i}{2}\bar{\theta}\theta f, \quad (4.1)$$

where we demand the constraint  $\Phi\Phi = 1$ . Since we consider a two-dimensional spacetime there is only one two-component real Majorana spinor  $\theta$ . The superfield is written in terms of  $\phi$  and  $f$ , which are real  $N$ -tuples of scalar fields, whereas  $\psi$  is an  $N$ -tuple of Majorana fields. The constraints in component space

$$\phi^2 = 1, \quad \phi\psi = 0, \quad \text{and} \quad \phi f = \frac{i}{2}\bar{\psi}\psi \quad (4.2)$$

are equivalent to the superfield constraint  $\Phi\Phi = 1$  in superspace. We can write down the supersymmetric  $O(N)$ -invariant Lagrangian density

$$\mathcal{L} = \frac{1}{2g^2} \bar{D}\Phi D\Phi|_{\bar{\theta}\theta}, \quad (4.3)$$

where  $D_\alpha$  is the covariant derivative  $\partial_{\bar{\theta}\alpha} + i(\gamma^\mu\theta)_\alpha\partial_\mu$ . This can then be written in component fields as

$$\mathcal{L} = \frac{1}{2g^2} (\partial_\mu\phi\partial^\mu\phi + i\bar{\psi}\not{\partial}\psi - f^2). \quad (4.4)$$

The equations of motion imply that  $f$  and  $\phi$  must be parallel, therefore the on-shell Lagrangian density contains a four Fermi term coming from

$$f^2 = \left[ \frac{i}{2}(\bar{\psi}\psi) \right]^2 = -\frac{1}{4}(\bar{\psi}\psi)^2. \quad (4.5)$$

Hence we can write

$$\mathcal{L} = \frac{1}{2g^2} \left( \partial_\mu\phi\partial^\mu\phi + i\bar{\psi}\not{\partial}\psi + \frac{1}{4}(\bar{\psi}\psi)^2 \right), \quad (4.6)$$

with the two remaining constraints

$$\phi^2 = 1 \quad \text{and} \quad \phi\psi = 0. \quad (4.7)$$

For the individual components of the scalar and fermionic fields we will use the notation

$$\phi = (\phi_0, \phi_1, \dots, \phi_{N-1}) \quad \text{and} \quad \psi = (\psi_0, \psi_1, \dots, \psi_{N-1}), \quad (4.8)$$

where  $\psi_i^T = (\psi_i^1, \psi_i^2)$ . So the superscript is the Dirac index and the subscript is the flavour index. The charge conjugation matrix  $\mathcal{C}$  arising in  $\bar{\psi} = \psi^T\mathcal{C}$  has the properties

$$\mathcal{C}\gamma_\mu\mathcal{C}^{-1} = -\gamma_\mu^T = -\gamma_\mu^*, \quad \mathcal{C}^\dagger = -\mathcal{C}^{-1} \quad \text{and} \quad \mathcal{C} = -\mathcal{C}^T. \quad (4.9)$$

The model described by eq.(4.6) and the constraints in eq.(4.2) are both invariant under the  $\mathcal{N} = 1$  supersymmetry transformations

$$\delta\phi = i\bar{\epsilon}\psi \quad \text{and} \quad \delta\psi = (\not{\epsilon} + \frac{i}{2}\bar{\psi}\psi)\phi\epsilon, \quad (4.10)$$

where  $\epsilon$  is a constant Majorana spinor. The action and the constraints satisfy the global  $O(N)$ -symmetry of which we can think of as a flavour symmetry, if we identify the  $i$ -th entry of an  $N$ -tuple with a flavour  $i$ . There is an additional chiral  $\mathbb{Z}_2$ -symmetry which is realised by  $\psi \rightarrow i\gamma_5\psi$  with  $\gamma_5 = i\gamma_0\gamma_1$ . The convention we choose is  $\gamma_0 = \sigma_3$ ,  $\gamma_1 = -\sigma_1$ , and  $\mathcal{C} = -i\sigma_2$ , where the pauli matrices are

$$\sigma_1 = \begin{pmatrix} 0 & 1 \\ 1 & 0 \end{pmatrix}, \quad \sigma_2 = \begin{pmatrix} 0 & -i \\ i & 0 \end{pmatrix} \quad \text{and} \quad \sigma_3 = \begin{pmatrix} 1 & 0 \\ 0 & -1 \end{pmatrix}. \quad (4.11)$$

As stated in [37] the one-loop  $\beta$  function coincides with the one calculated for the non-supersymmetric model. This already tells us that the  $O(2)$  model is not asymptotically free, whereas the model with  $N > 2$  show asymptotic freedom. As pointed out in [76] there exists an  $\mathcal{N} = 2$  extension for nonlinear sigma models which have a Kähler target manifold. For the  $O(3)$  model the target manifold is Kähler and therefore an additional supersymmetry can be created. This can be seen in [41], where this additional symmetry is worked out properly. For deeper understanding and more extensive explanation the original work [37, 38] should be consulted. In order to obtain the action we will need to perform the integral over the Lagrangian density in both dimensions

$$S(\phi, \psi) = \int dx_0 \int dx_1 \mathcal{L}[\phi(x), \psi(x)], \quad (4.12)$$

where we use  $x = (x_0, x_1)$ . When talking about the system at a finite temperature we refer to a finite temporal extent  $\beta$  of the first dimension, i.e. where  $\beta = 1/T$ . We will deal with the boundary conditions later on in this section.

### 4.3. Partition function and constraints

The partition function of our system is defined by

$$Z = \int \mathcal{D}\phi \mathcal{D}\psi e^{-S(\phi, \psi)} = \prod_{i, \alpha} \int_{-\infty}^{\infty} d\phi_i \int d\psi_i^\alpha e^{-S(\phi, \psi)}, \quad (4.13)$$

where  $i$  is the flavour index and  $\alpha$  the Dirac index. The  $\psi_i^\alpha$  are real Grassmann numbers as explained closer in [D.1]. In the following we omit writing the bosonic integration boundaries and make use of a subscript  $S_B$  and  $S_F$ , with  $S(\phi, \psi) = S_B(\phi) + S_F(\psi)$ , in order to talk about the bosonic and the fermionic action separately. Every field configuration appearing in the partition function needs to satisfy the two constraints  $\phi^2 = 1$  and  $\phi\psi = 0$ . This can be realised by inserting an adequate Dirac delta function just after the measure, analogously to [41],

$$Z = \int \mathcal{D}\phi \delta(\phi^2 - 1) \int \mathcal{D}\psi \delta(\phi\psi) e^{-S(\phi, \psi)}, \quad (4.14)$$

#### 4. Supersymmetric Nonlinear $O(N)$ sigma Model

and since the bosonic action is independent of the fermionic action, the Boltzmann factor can be split up

$$Z = \int \mathcal{D}\phi \delta(\phi^2 - 1) e^{-S_B(\phi)} \int \mathcal{D}\psi \delta(\phi\psi) e^{-S_F(\psi)}. \quad (4.15)$$

The bosonic constraint ( $\phi^2 = 1$ ) essentially reduces the number of degrees of freedom by one, whereas the fermionic constraint ( $\phi\psi = 0$ ) is the source of interaction between the bosonic and fermionic fields. Writing  $\phi\psi$  in flavour and Dirac components we find

$$\begin{aligned} Z &= \int \mathcal{D}\phi \delta(\phi^2 - 1) e^{-S_B(\phi)} \int \mathcal{D}\psi \delta(\phi\psi) e^{-S_F(\psi)} \\ &= \int \mathcal{D}\phi \delta(\phi^2 - 1) e^{-S_B(\phi)} \left( \prod_i \int d\psi_i \right) \delta \left( \sum_{l=0}^{N-1} \phi_l \psi_l \right) e^{-S_F(\psi)} \\ &= \int \mathcal{D}\phi \delta(\phi^2 - 1) e^{-S_B(\phi)} \left( \prod_{i,\alpha} \int d\psi_i^\alpha \right) \prod_{\beta=1}^2 \delta \left( \sum_{l=0}^{N-1} \phi_l \psi_l^\beta \right) e^{-S_F(\psi)}, \end{aligned} \quad (4.16)$$

where  $\alpha$  and  $\beta$  are the Dirac indices. Note that we omitted writing the spacetime dependence of the fields in  $\phi(x)\psi(x) = 0$ , it is a constraint which must hold at any point in spacetime. In a Grassmann Integral over a Grassmann variable  $\eta$  we can use the following relation for an occurring delta function

$$\int d\eta \delta(\eta - \eta') f(\eta) = \int d\eta (\eta - \eta') f(\eta) = f(\eta'), \quad (4.17)$$

which is explained in more detail in the appendix D.2. Using this relation we get

$$\begin{aligned} Z &= \int \mathcal{D}\phi \delta(\phi^2 - 1) e^{-S_B(\phi)} \prod_{i,\alpha} \int d\psi_i^\alpha \prod_{\beta=1}^2 \delta \left( \sum_{l=0}^{N-1} \phi_l \psi_l^\beta \right) e^{-S_F(\psi)} \\ &= \int \mathcal{D}\phi \delta(\phi^2 - 1) e^{-S_B(\phi)} \prod_{i,\alpha} \int d\psi_i^\alpha \left( \sum_{l,k} \phi_l \phi_k \psi_l^1 \psi_k^2 \right) e^{-S_F(\psi)}, \end{aligned} \quad (4.18)$$

in which the terms  $\phi_l \phi_k \psi_l^1 \psi_k^2$  are functioning as constraints for the Grassmann integral due to their nilpotency. Note that those constraints are the only coupling between the fermionic and the bosonic fields in the theory. We now derived what the constraint  $\phi\psi = 0$  looks like on component level, it is the multiplication of

$$\sum_{l,k} \phi_l \phi_k \psi_l^1 \psi_k^2 \quad (4.19)$$

in the Grassmann integral of the fermion fields, where  $l, k = 0, 1, \dots, N-1$ . It shows itself useful to formulate those constraints in terms of Majorana spinors. For any term in the product in eq.(4.19) we can do the following

$$\phi_i \phi_j \psi_i^1 \psi_j^2 + \phi_j \phi_i \psi_j^1 \psi_i^2 = \phi_i \phi_j (\psi_i^1 \psi_j^2 + \psi_j^1 \psi_i^2) = \phi_i \phi_j \bar{\psi}_i \psi_j, \quad (4.20)$$

which we can use to rewrite

$$\sum_{i,j} \phi_i \phi_j \psi_i^1 \psi_j^2 = \sum_{i,j} \frac{1}{2} \phi_i \phi_j \bar{\psi}_i \psi_j. \quad (4.21)$$



A flavour diagonal constraint with  $i = j$ , i.e.  $\bar{\psi}_i \psi_i$ , looks like a mass term for flavour  $i$  and a flavour off-diagonal constraint  $i \neq j$  like a point in space-time (or on the lattice a site), at which the fermion flavour can change. This last point will be worked out properly in a following section when considering actual fermionic loops on the lattice. Written in terms of Majorana spinors the partition function then becomes

$$Z = \int \mathcal{D}\phi \delta(\phi^2 - 1) e^{-S_B(\phi)} \int \mathcal{D}\psi \left( \sum_{i,j=0}^{N-1} \frac{1}{2} \phi_i \phi_j \bar{\psi}_i \psi_j \right) e^{-S_F(\psi)}. \quad (4.22)$$

and in individual components

$$Z = \int \mathcal{D}\phi \delta(\phi^2 - 1) e^{-S_B(\phi)} \int \mathcal{D}\psi \left( \sum_{\substack{i,j=0 \\ i \leq j}}^{N-1} \phi_i \phi_j (\psi_i^1 \psi_j^2 + \psi_j^1 \psi_i^2) \right) e^{-S_F(\psi)}. \quad (4.23)$$

In the following section we will discretise the system and work out the exact form of the partition function with the just discussed constraints, as well as the boson and fermion lattice action.

## 4.4. Discretisation

At this point we skip the definition of the lattice since it was already introduced in section 1.2.1. The notational conventions chosen there apply here in the exact same way.

### 4.4.1. Partition function and constraints on the lattice

We consider the partition function of our system, as derived in eq.(4.22), and define it on the lattice to be

$$\begin{aligned} Z &= \int \mathcal{D}\phi \delta(\phi^2 - 1) e^{-S_B(\phi)} \int \mathcal{D}\psi \left( \sum_{i,j=0}^{N-1} \frac{1}{2} \phi_i \phi_j \bar{\psi}_i \psi_j \right) e^{-S_F(\psi)} \\ &= \int \mathcal{D}\phi \left[ \prod_x \delta \left( \sum_{j=0}^{N-1} \phi_{j,x}^2 - 1 \right) \right] e^{-\hat{S}_B(\phi)} \end{aligned} \quad (4.24)$$

$$\times \int \mathcal{D}\psi \left[ \prod_x \left( \sum_{l,k=0}^{N-1} \frac{1}{2} \phi_{l,x} \phi_{k,x} \bar{\psi}_{l,x} \psi_{k,x} \right) \right] e^{-\hat{S}_F(\psi)}, \quad (4.25)$$

with

$$\int \mathcal{D}\phi = \prod_{x,i} \int d\phi_{i,x} \quad \text{and} \quad \int \mathcal{D}\psi = \prod_{x,i,\alpha} \int d\psi_{i,x}^\alpha, \quad (4.26)$$

where  $i$  is the flavour and  $\alpha$  the Dirac index.

### 4.4.2. Lattice derivative

The fact that we have a supersymmetric theory in the continuum motivates us to treat fermionic and bosonic fields identical, therefore we choose to replace both derivatives with the Wilson derivative, which we would have normally only introduced in the fermion action

#### 4. Supersymmetric Nonlinear $O(N)$ sigma Model

in order to handle the fermion doubling problem. This way of discretisation shows itself to reproduce the correct continuum limit of the two-dimensional  $\mathcal{N} = 1$  Wess-Zumino model [36]. Note that this does not mean that this discretisation must reproduce the correct continuum limit in this  $O(N)$ -model at all. However, numerical results [41] showed strong indications that exactly this discretisation is reaching a proper continuum limit of the supersymmetric nonlinear  $O(3)$  model, which is another motivation to stick to the introduction of the Wilson derivative also for the bosonic field.

##### 4.4.3. Bosonic lattice action

Consider the bosonic part of the continuum action

$$S_B = \int d^2x \frac{1}{2g^2} (\partial_\mu \phi \partial^\mu \phi) , \quad (4.27)$$

where, when discretising, the  $\phi$  will get replaced by  $\phi_x$  and analogously  $\phi_i$  by  $\phi_{i,x}$ . Recapitulate that the Wilson derivative is

$$[\hat{\partial}_\mu^{\mathcal{W}}]_{xy} = [\hat{\partial}_\mu^S]_{xy} - \frac{ra}{2} [\Delta^{\mathcal{W}}]_{xy} , \quad (4.28)$$

where from now on we set  $r$  and  $a$  to one for convenience and will only write them if instructively helpful. We have the symmetric derivative

$$[\hat{\partial}_\mu^S]_{xy} = \frac{1}{2a} (\delta_{x+\hat{\mu},y} - \delta_{x-\hat{\mu},y}) \quad (4.29)$$

and the additional Wilson term

$$[\Delta^{\mathcal{W}}]_{xy} = \frac{ra}{2} \sum_{\nu=0}^{d-1} [\hat{\partial}_\nu^+]_{xz} [\hat{\partial}_\nu^-]_{zy} , \quad (4.30)$$

where  $\hat{\partial}_\nu^+$  is the forward derivative and  $\hat{\partial}_\nu^-$  is the backward derivative

$$[\hat{\partial}_\nu^+]_{xy} = \frac{1}{a} (\delta_{x+\hat{\nu},y} - \delta_{x,y}) \quad (4.31)$$

$$[\hat{\partial}_\nu^-]_{xy} = \frac{1}{a} (\delta_{x,y} - \delta_{x-\hat{\nu},y}) . \quad (4.32)$$

Since the derivative operator is diagonal in flavour space we can perform the calculation for only one  $\phi_i$  and drop the index  $i$  for the sake of a more neat calculation. If we write down the pure bosonic action, after performing a partial integration, the bosonic lattice action reads

$$\hat{S}_B = \sum_x \phi_x K_{xy} \phi_y , \quad (4.33)$$

where

$$\begin{aligned} K_{xy} &= - \sum_\mu [(\hat{\partial}_\mu^S)^2]_{xy} + [(\Delta^{\mathcal{W}})^2]_{xy} \\ &= - \sum_\mu [(\hat{\partial}_\mu^S)^2]_{xy} + \left[ \left( \frac{ra}{2} \sum_{\nu=0}^{d-1} \hat{\partial}_\nu^+ \hat{\partial}_\nu^- \right)^2 \right]_{xy} . \end{aligned} \quad (4.34)$$

The first term, sandwiched between the fields, is simply

$$-\phi_x[(\hat{\partial}^S)^2]_{xy}\phi_y = -\phi_x[\hat{\partial}_\mu^S]_{xz}[\hat{\partial}_\mu^S]_{zy}\phi_y \quad (4.35)$$

$$= -\phi_x \frac{1}{4} \sum_\mu (\delta_{x+\hat{\mu},z} - \delta_{x-\hat{\mu},z})(\delta_{z+\hat{\mu},y} - \delta_{z-\hat{\mu},y})\phi_y \quad (4.36)$$

$$= -\phi_x \frac{1}{4} \sum_\mu (\delta_{x+2\hat{\mu},y} + \delta_{x-2\hat{\mu},y} - 2\delta_{xy})\phi_y \quad (4.37)$$

$$= \phi_x^2 - \frac{1}{4} \phi_x \sum_\mu (\phi_{x+2\hat{\mu}} + \phi_{x-2\hat{\mu}}). \quad (4.38)$$

The second term in eq.(4.34), also sandwiched between the fields, has already been calculated in eq.(3.35), where we obtained

$$\begin{aligned} \phi_x (\Delta^{\mathcal{W}})_{xy}^2 \phi_y &= 5\phi_x^2 + \frac{1}{2}\phi_{x-\hat{0}}\phi_{x+\hat{0}} + \frac{1}{2}\phi_{x-\hat{1}}\phi_{x+\hat{1}} \\ &\quad + \frac{1}{2}\phi_{x+\hat{0}}\phi_{x+\hat{1}} + \frac{1}{2}\phi_{x+\hat{1}}\phi_{x-\hat{0}} + \frac{1}{2}\phi_{x-\hat{0}}\phi_{x-\hat{1}} + \frac{1}{2}\phi_{x+\hat{0}}\phi_{x-\hat{1}} \\ &\quad - 2\phi_x \sum_\mu (\phi_{x+\hat{\mu}} + \phi_{x-\hat{\mu}}). \end{aligned} \quad (4.39)$$

Due to the fact that we are summing over all sites in the action, we can rewrite the expression as

$$\phi_x (\Delta^{\mathcal{W}})_{xy}^2 \phi_y = 5\phi_x^2 + \frac{1}{4}\phi_x \sum_\mu (\phi_{x+2\hat{\mu}} + \phi_{x-2\hat{\mu}}) + \frac{1}{2}\phi_x \sum_{ij} \phi_{x+\kappa_{ij}} - 2\phi_x \sum_\mu (\phi_{x+\hat{\mu}} + \phi_{x-\hat{\mu}}), \quad (4.40)$$

in which we just introduced  $\kappa_{ij} = (-1)^i\hat{0} + (-1)^j\hat{1}$ , with  $i, j \in [0, 1]$ . Even though this is a rather trivial reformulation the factor of  $1/2$  is crucial to put in front of the now symmetrised terms. The complete action can now be constructed by simply adding the two terms derived above, respecting also the prefactor  $1/(2g^2)$  in eq.(4.6), one obtains the symmetrised bosonic lattice action

$$\hat{S}_B = \frac{1}{g^2} \sum_x \left[ 3\phi_x^2 + \frac{1}{4}\phi_x \sum_{i,j=0}^1 \phi_{x+\kappa_{ij}} - \phi_x \sum_{\mu=0}^1 (\phi_{x+\hat{\mu}} + \phi_{x-\hat{\mu}}) \right]. \quad (4.41)$$

Note that the terms connecting next to nearest neighbours of the form  $\phi_{x+\hat{\mu}}\phi_{x-\hat{\mu}}$  cancel out exactly. When considering the bond formulation it shows itself to be more useful to write the action in a way such that each interaction corresponding to a bond is occurring only once in the sum over all sites. Like that we can easily read off the weight of a bond by considering its prefactor in the non symmetrised bosonic lattice action

$$\hat{S}_B = \frac{1}{g^2} \sum_x \left[ 3\phi_x^2 + \frac{1}{2}\phi_x \sum_j \phi_{x+\kappa_{0j}} - 2\phi_x \sum_{\mu=0}^1 \phi_{x+\hat{\mu}} \right]. \quad (4.42)$$

Let us now turn to the fermion lattice action.

#### 4.4.4. Fermionic lattice action

The fermionic term of the action is

$$S_F = \int d^2x \frac{1}{2g^2} \left( i\bar{\psi}\not{\partial}\psi + \frac{1}{4}(\bar{\psi}\psi)^2 \right). \quad (4.43)$$

#### 4. Supersymmetric Nonlinear $O(N)$ sigma Model

When we put the model on the lattice we replace  $\psi_i^\alpha$  with  $\psi_{i,x}^\alpha$  and introduce the lattice Wilson derivative  $\hat{\partial}_\mu^\mathcal{W}$  in order to handle the fermion doubler problem. Let us now consider the fermionic action and focus first on the kinetic term which is

$$S_{F,kin} = \frac{1}{2g^2} \int d^2x \psi^T \mathcal{C} \gamma^\mu \partial_\mu \psi, \quad (4.44)$$

where  $\mathcal{C}$  is the charge conjugation matrix, such that  $\bar{\psi} = \psi^T \mathcal{C}$ . Note that this action is identical for any flavour, this is why we dropped the flavour index here. When putting this expression on the lattice we obtain

$$\hat{S}_{F,kin} = \frac{1}{2g^2} \sum_x \psi_x^T \mathcal{C} D_{xy} \psi_y = \frac{1}{2g^2} \sum_x \psi_x^T \mathcal{C} (\hat{\partial}^S - \Delta^\mathcal{W})_{xy} \psi_y, \quad (4.45)$$

in which we have, when setting  $a$  and  $r$  to one,

$$\begin{aligned} (\hat{\partial}^S - \Delta^\mathcal{W})_{xy} &= \gamma^\mu [\hat{\partial}_\mu^S]_{xy} - \frac{1}{2} \sum_{\nu=0}^{d-1} [\hat{\partial}_\nu^+]_{xz} [\hat{\partial}_\nu^-]_{zy} \\ &= \frac{1}{2} \sum_\mu \gamma^\mu (\delta_{x+\mu,y} - \delta_{x-\mu,y}) - \frac{1}{2} \sum_\nu (\delta_{x+\nu,y} + \delta_{x-\nu,y} - 2\delta_{x,y}) \\ &= 2\delta_{x,y} - \frac{1}{2} \sum_\mu [(1 - \gamma^\mu) \delta_{x+\mu,y} + (1 + \gamma^\mu) \delta_{x-\mu,y}]. \end{aligned} \quad (4.46)$$

Note that here we omitted writing the Dirac indices  $D_{xy}^{\alpha\beta}$ , which give rise to the Dirac structure via  $\gamma_\mu^{\alpha\beta}$ . Writing down the full fermion action on the lattice gives

$$\begin{aligned} \hat{S}_F &= \frac{1}{2g^2} \sum_x \left\{ M_x \psi_x^T \mathcal{C} \psi_x - \psi_x^T \mathcal{C} \sum_\mu \left[ \frac{1}{2} (1 - \gamma^\mu) \delta_{x+\mu,y} + \frac{1}{2} (1 + \gamma^\mu) \delta_{x-\mu,y} \right] \psi_y \right. \\ &\quad \left. + \frac{1}{4} (\psi_x^T \mathcal{C} \psi_x)^2 \right\}, \end{aligned} \quad (4.47)$$

where the mass monomer term is  $M_x = (m + 2)$  which is obviously not site dependent but we will keep this dependence for the ongoing calculations in order to illustrate that the following works just fine with a site dependent weight, as for instance in the two-dimensional  $\mathcal{N} = 1$  Wess-Zumino model discussed in section 3.3.3. One should exercise caution when writing down the action for every flavour, since they are not connected in the kinetic term but, there are terms involving every possible pair of flavour coming from the four Fermi potential. The sum over all flavours can therefore be written in front of the action, except for the four Fermi term where we have

$$\frac{1}{2g^2} \sum_x \frac{1}{4} (\psi_x^T \mathcal{C} \psi_x)^2 = \frac{1}{8g^2} \sum_x \left( \sum_{i=0}^{N-1} \psi_{i,x}^T \mathcal{C} \psi_{i,x} \right)^2. \quad (4.48)$$

#### 4.5. Hopping expansion

In this section we perform a hopping expansion for the bosonic and the fermionic variables in order to establish a bosonic bond and fermion loop formulation. This has already been done for a free Majorana fermion in section 1.3 and for a bosonic field theory in 2.1. The constraint  $\phi\psi = 0$ , which we discussed earlier on, needs to be reformulated as well in order to obtain a complete reformulation of the model in terms of the new degrees of freedom, the so called occupation numbers.

### 4.5.1. The constraint $\phi\psi = 0$

The constraint  $\phi\psi = 0$  can be built into the partition function, as seen in eq.(4.24), as a sum of the form

$$\sum_{i,j} \left( \frac{1}{2} \phi_{i,x} \phi_{j,x} \bar{\psi}_{i,x} \psi_{j,x} \right)^{c_{ij}(x)} = \sum_{i \neq j} \left( \frac{1}{2} \phi_{i,x} \phi_{j,x} \bar{\psi}_{i,x} \psi_{j,x} \right)^{c_{ij}(x)} + \sum_i \left( \frac{1}{2} \phi_{i,x}^2 \bar{\psi}_{i,x} \psi_{i,x} \right)^{c_{ii}(x)}, \quad (4.49)$$

where  $c_{ij}(x)$  are the occupation numbers  $\in \{0, 1\}$ , telling us if a constraint term is present on a given site or not. Every factor in the product over all lattice sites in the partition function gets multiplied with the sum in eq.(4.49), creating configurations in which every contribution only contains one term of the form  $\phi_{i,x} \phi_{j,x} \bar{\psi}_{i,x} \psi_{j,x}$  for every site. The fact that exactly one constraint needs to be picked per lattice sites, i.e.  $c_{ij}(x) = 1$ , can formally be expressed by

$$\sum_{i,j} c_{ij}(x) = \sum_{i \neq j} c_{ij}(x) + \sum_i c_{ii}(x) = 1 \quad \forall x. \quad (4.50)$$

However, note that if we want to write this expression in the path integral, all possible configurations need to be considered, essentially meaning that

$$Z = \int \mathcal{D}\phi \delta(\phi^2 - 1) e^{-\hat{S}_B} \int \mathcal{D}\psi \left[ \prod_x \sum_{i,j} \left( \frac{1}{2} \phi_{i,x} \phi_{j,x} \bar{\psi}_{i,x} \psi_{j,x} \right)^{c_{ij}(x)=1} \right] e^{-\hat{S}_F}, \quad (4.51)$$

where  $c_{ij}(x) = 1 \quad \forall x, i, j$ . But when considering one specific contribution to the partition function, we will need the prescription in eq.(4.50).

### 4.5.2. Bosonic bond formulation

When talking about a bond we refer to a bond between two sites. In the action from eq.(4.42) there are only two kinds of bonds, the one corresponding to the nearest neighbour interaction  $\phi_x \phi_{x+\hat{\mu}}$  and the diagonal bond corresponding to  $\phi_x \phi_{x+\kappa_{0j}}$ . Those are graphically illustrated in fig. 4.1

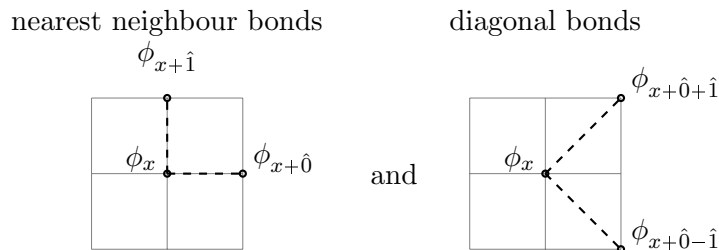


Figure 4.1.: This plot illustrates the two different interactions between bosonic field variables and therefore also characterises the two different bonds.

#### 4. Supersymmetric Nonlinear $O(N)$ sigma Model

We can now expand the bosonic Boltzmann factors and get

$$e^{-\hat{S}_B} = \prod_x \prod_\mu \left[ \sum_{n(x,\mu)=0}^{\infty} \left( \frac{2}{g^2} \right)^{n(x,\mu)} \frac{(\phi_x \phi_{x+\hat{\mu}})^{n(x,\mu)}}{n(x,\mu)!} \right] \prod_x \prod_\mu \left[ \sum_{d(x,\kappa_{0\mu})=0}^{\infty} \left( \frac{-1}{2g^2} \right)^{d(x,\kappa_{0\mu})} \frac{(\phi_x \phi_{x+\kappa_{0\mu}})^{d(x,\kappa_{0\mu})}}{d(x,\kappa_{0\mu})!} \right] \prod_x e^{-V(\phi_x)}, \quad (4.52)$$

where  $V(\phi_x) = 3\phi_x^2/g^2$ . The occupation number  $n(x, \mu)$  stands for the number of powers of the nearest neighbour bond between the site  $x$  and  $x + \hat{\mu}$  and  $d(x, \kappa_{0\mu})$  for the diagonal neighbour bond between  $x$  and  $x + \kappa_{0\mu}$ . When talking about a specific configuration of the system we refer to a fixed number of  $n(x, \mu)$  and  $d(x, \kappa_{0\mu}) \forall x$ . The contribution to the partition function from each bond can be easily read off from eq.(4.52), which is  $w(n(x, \mu)) = 2/g^2$  and  $w(d(x, \kappa_{0\mu})) = -1/(2g^2)$ , latter of which can be a local source of a globally fluctuating sign. Note that these diagonal bonds would not be present if we chose only a symmetric derivative for the boson instead of also introducing a Wilson term.

In this calculation we left out the constraints the model has in order to be supersymmetric (in the continuum). We have to consider both constraints in the bond formulation since they both include bosonic field variables. The constraints are  $\phi^2 = 1$  and  $\phi\psi = 0$ , which enter just after the measure in the path integral. For any given bosonic background configuration, i.e. fixed values of the occupation numbers  $n(x, \mu)$  and  $d(x, \kappa_{0\mu})$ , we have to perform the multiplication with the sum in (4.21) due to the constraint  $\phi\psi = 0$ . We already introduced the occupation number  $c_{ij}(x) \in \{0, 1\}$  which obey eq.(4.50), telling us that on every site there is exactly one term of eq.(4.21) that is picked. For our bosonic field this means that either a diagonal term  $\phi_{i,x}\phi_{i,x}$  is picked ( $c_{ii}(x) = 1$ ) and the power of the scalar field  $\phi_i$  at site  $x$  is increased by two or an off-diagonal term,  $\phi_{i,x}\phi_{j,x}$  with  $i \neq j$ , is picked ( $c_{ij}(x) = 1$ ) and the powers of the scalar field  $\phi_i$  and  $\phi_j$  are each increased by one. With this fact in mind let us write down the complete bosonic site occupation number for the flavour  $i$ , which is

$$N_i^B(x) = \sum_\mu [n_i(x, \mu) + n_i(x - \mu, \mu) + d_i(x, \kappa_{0\mu}) + d_i(x + \kappa_{1\mu}, \kappa_{0\mu})] + \sum_{j \neq i} c_{ij}(x) + 2c_{ii}(x). \quad (4.53)$$

This now corresponds to the total bond occupation number of flavour  $i$ , consisting of all bonds of flavour  $i$  which are connected to site  $x$  and the power of the bosonic field of same flavour arising in the terms from the constraints on that site. We can now write down the weight of the bosonic contribution to the partition function for a given set of occupation numbers in the following form

$$W_{tot}^B = \prod_{x=0}^{L_t-1} W^B(N^B(x)) \quad (4.54)$$

$$= \left[ \prod_x Q(N^B(x)) \right] \prod_i \left[ \prod_x \prod_{\mu, l} \frac{\left( \frac{2}{g^2} \right)^{n_i(x, \mu)}}{n_i(x, \mu)!} \frac{\left( \frac{-1}{2g^2} \right)^{d_i(x, \kappa_{0l})}}{d_i(x, \kappa_{0l})!} \right], \quad (4.55)$$

where the weight coming from one site is

$$W^B(N^B(x)) = Q(N^B(x)) \prod_i \prod_{\mu, l} \frac{\left(\frac{2}{g^2}\right)^{n_i(x, \mu)}}{n_i(x, \mu)!} \frac{\left(\frac{-1}{2g^2}\right)^{d_i(x, \kappa_{0l})}}{d_i(x, \kappa_{0l})!}. \quad (4.56)$$

The site dependent weight is the site weight depending on all flavours, i.e.  $Q(N^B(x)) = Q(N_0^B(x), \dots, N_{N-1}^B(x))$ . Including the constraint  $\phi^2 = 1$  which arises in the integral in form of a delta function, we get

$$Q(N^B(x)) = \int_{-\infty}^{\infty} \prod_i d\phi_{i,x} \delta\left(\sum_{j=0}^{N-1} \phi_{j,x}^2 - 1\right) \prod_{k=0}^{N-1} \phi_k^{N_k^B(x)} e^{-V(\phi_{k,x})}. \quad (4.57)$$

The term  $\exp[-V(\phi_{i,x})] = \exp[-3\phi_{i,x}^2/g^2]$  can be simplified with  $\phi^2 = 1$  to just a number, such that

$$Q(N^B(x)) = \int_{-\infty}^{\infty} \prod_i d\phi_{i,x} \delta\left(\sum_{j=0}^{N-1} \phi_{j,x}^2 - 1\right) \prod_{k=0}^{N-1} \phi_k^{N_k^B(x)}, \quad (4.58)$$

in which  $Q(N^B(x)) \neq 0$  for  $N_k^B(x) \bmod 2 = 0 \forall k$ . We can now simply obtain the contribution to the partition function coming from the bosonic action and the constraints by calculating  $Q(N^B(x))$  on every site and use eq.(4.54). There exists a closed analytic expression for these integrals

$$Q(N^B(x)) = \frac{\prod_{i=0}^{N-1} \left[1 + (-1)^{N_i^B(x)}\right] \Gamma\left(\frac{1+N_i^B(x)}{2}\right)}{2^{N-2} \left[\frac{1}{2} \left(N + \sum_{l=0}^{N-1} N_l^B(x)\right)\right]}, \quad (4.59)$$

such that we have a bosonic contribution to the weight in the partition function completely depending on the occupation numbers  $N_i^B$  and of course on the choice of  $O(N)$ . The formula above can be shown to hold by using the induction method and the appearing  $\Gamma$  is the well known Gamma function. We now integrated out the bosonic field in the partition function up to the bosonic occupation numbers  $N_i^B(x)$ . Those occupation numbers can be generally integrated out following the worm algorithm in section 2.2. In the following sections it will make more sense to leave the constraints out of the initial definition of  $N^B$ . This amounts to redefining

$$N_i^B(x) = \sum_{\mu} [n_i(x, \mu) + n_i(x - \mu, \mu) + d_i(x, \kappa_{0\mu}) + d_i(x + \kappa_{1\mu}, \kappa_{0\mu})]. \quad (4.60)$$

We will shortly see that this has its particular use when talking about a bosonic configuration on top of which we then pick the terms from the constraint  $\phi\psi = 0$  and the fermionic configuration. When picking the constraint terms we will have to increase the bond number explicitly on that site since it is now not anymore included in  $N^B$ .

### 4.5.3. Fermion loop formulation

We will follow the exact same steps as performed in section 1.3 by introducing Wilson projectors

$$\mathcal{P}_{\pm\mu} = \frac{1}{2} (1 \mp \gamma_{\mu}), \quad (4.61)$$

#### 4. Supersymmetric Nonlinear $O(N)$ sigma Model

which satisfy the relations

$$\mathcal{P}_{\pm\mu}\mathcal{P}_{\pm\mu} = \mathcal{P}_{\pm\mu} \quad (4.62)$$

$$\mathcal{P}_{+\mu}\mathcal{P}_{-\mu} = \mathcal{P}_{-\mu}\mathcal{P}_{+\mu} = 0. \quad (4.63)$$

Using those introduced projectors we can rewrite the action from eq.(4.47) like

$$\hat{S}_F = \frac{1}{2g^2} \sum_x \left\{ M_x \psi_x^T \mathcal{C} \psi_x - \psi_x^T \mathcal{C} \sum_{\mu} (\mathcal{P}_{+\mu} \psi_{x+\hat{\mu}} + \mathcal{P}_{-\mu} \psi_{x-\hat{\mu}}) + \frac{1}{4} (\psi_x^T \mathcal{C} \psi_x)^2 \right\}. \quad (4.64)$$

In the following we will quickly recapitulate that the orientation of the hop is not important for Majorana fermions. This can be seen by considering

$$\psi_x^T \mathcal{C} \mathcal{P}_{+\mu} \psi_{x+\mu} = - (\psi_x^T \mathcal{C} \mathcal{P}_{+\mu} \psi_{x+\mu})^T \quad (4.65)$$

$$= -\psi_{x+\hat{\mu}}^T (\mathcal{C} \mathcal{P}_{+\mu})^T \psi_x. \quad (4.66)$$

By the use of the appropriate relations of the Wilson projector

$$\mathcal{P}_{+\mu}^T = \mathcal{P}_{+\mu}, \quad \text{since } \gamma_{\mu}^T = \gamma_{\mu} \quad (4.67)$$

$$\mathcal{C}^T = -\mathcal{C}, \quad (4.68)$$

$$\mathcal{P}_{+\mu} \mathcal{C} = \mathcal{C} \mathcal{P}_{-\mu}, \quad \text{since } \gamma_{\mu} \mathcal{C} = -\mathcal{C} \gamma_{\mu}, \quad (4.69)$$

one can see that

$$(\mathcal{C} \mathcal{P}_{\pm\mu})^T = \mathcal{P}_{\pm\mu}^T \mathcal{C}^T = -\mathcal{P}_{\pm\mu} \mathcal{C} = -\mathcal{C} \mathcal{P}_{\mp\mu}. \quad (4.70)$$

This relation can now be used to simplify eq.(4.66) further

$$-\psi_{x+\hat{\mu}}^T (\mathcal{C} \mathcal{P}_{+\mu})^T \psi_x = -\psi_{x+\hat{\mu}}^T \mathcal{P}_{+\mu}^T \mathcal{C}^T \psi_x \quad (4.71)$$

$$= \psi_{x+\hat{\mu}}^T \mathcal{C} \mathcal{P}_{-\mu} \psi_x, \quad (4.72)$$

which shows that the direction of the so called hops is irrelevant for a Majorana fermion. The just derived fact, that  $\psi_{x+\hat{\mu}}^T \mathcal{C} \mathcal{P}_{\mu} \psi_x = \psi_{x+\hat{\mu}}^T \mathcal{C} \mathcal{P}_{-\mu} \psi_x$  can now be used in eq.(4.64) to combine the identical hops, giving rise to a factor of two which gets canceled by the overall prefactor appearing in  $1/(2g^2)$ . Working this out properly yields

$$\hat{S}_F = \frac{1}{2g^2} \sum_x \psi_x^T \mathcal{C} M_x \psi_x - \frac{1}{g^2} \sum_{x,\mu} \psi_x^T \mathcal{C} \mathcal{P}_{+\mu} \psi_{x+\hat{\mu}} + \frac{1}{8g^2} \sum_x (\psi_x^T \mathcal{C} \psi_x)^2. \quad (4.73)$$

In order to keep things readable we will look at each term of the above action individually. Since it is useful to consider some expressions also written out in Dirac components explicitly, we recall that

$$\bar{\psi} \psi = \psi^T \mathcal{C} \psi = (\psi^1, \psi^2) \mathcal{C} \begin{pmatrix} \psi^1 \\ \psi^2 \end{pmatrix} \quad (4.74)$$

$$= (-\psi^2, \psi^1) \begin{pmatrix} \psi^1 \\ \psi^2 \end{pmatrix} \quad (4.75)$$

$$= -\psi^2 \psi^1 + \psi^1 \psi^2 = 2\psi^1 \psi^2. \quad (4.76)$$



Let's consider the expansion of the exponential function for the first term (which we call A) in eq.(4.73)

$$\begin{aligned}
\exp(-\hat{S}_A) &= \exp\left(-\frac{1}{2g^2} \sum_{x,i} M_x \bar{\psi}_{i,x} \psi_{i,x}\right) \\
&= \prod_x \prod_{i=0} \exp\left(-\frac{M_x}{2g^2} \bar{\psi}_{i,x} \psi_{i,x}\right) \\
&= \prod_{x,i} \left(1 - \frac{M_x}{2g^2} \bar{\psi}_{i,x} \psi_{i,x}\right) = \prod_{x,i} \left(1 - \frac{M_x}{g^2} \psi_{i,x}^1 \psi_{i,x}^2\right). \quad (4.77)
\end{aligned}$$

The expansion of the second term B in eq.(4.73) is

$$\begin{aligned}
\exp(-\hat{S}_B) &= \exp\left(\frac{1}{g^2} \sum_{x,i} \sum_{\mu} \bar{\psi}_{i,x} \mathcal{P}_{\mu} \psi_{i,x+\mu}\right) \\
&= \prod_{x,\mu} \prod_{i=0} \left(1 + \frac{1}{g^2} \bar{\psi}_{i,x} \mathcal{P}_{\mu} \psi_{i,x+\mu}\right). \quad (4.78)
\end{aligned}$$

Finally we will investigate the last term C in eq.(4.73), which is

$$\begin{aligned}
\exp(-\hat{S}_C) &= \exp\left(-\frac{1}{8g^2} \sum_x (\bar{\psi}_{i,x} \psi_{i,x})^2\right) \\
&= \exp\left(-\frac{1}{8g^2} \sum_x \left(\sum_i \bar{\psi}_{i,x} \psi_{i,x}\right)^2\right) \\
&= \exp\left(-\frac{1}{4g^2} \sum_x \sum_{i < j} \bar{\psi}_{i,x} \psi_{i,x} \bar{\psi}_{j,x} \psi_{j,x}\right) \quad (4.79)
\end{aligned}$$

$$= \prod_{x,i < j} \left(1 - \frac{1}{4g^2} \bar{\psi}_{i,x} \psi_{i,x} \bar{\psi}_{j,x} \psi_{j,x}\right) \quad (4.80)$$

$$= \prod_{x,i < j} \left(1 - \frac{1}{g^2} \psi_{i,x}^1 \psi_{i,x}^2 \psi_{j,x}^1 \psi_{j,x}^2\right). \quad (4.81)$$

The terms  $\psi_{i,x}^1 \psi_{i,x}^2 \psi_{i,x}^1 \psi_{i,x}^2$  give zero anyway due to their nilpotency, that is why we can restrict the sum over  $i$  to be strictly smaller than  $j$ . Let us now collect all terms that we calculated from expanding eq.(4.73) and add the already derived constraint from eq.(4.20) in the following way

$$\begin{aligned}
\exp(-\hat{S}_F) &= \prod_x \left(\sum_{i,j} \frac{1}{2} \phi_{i,x} \phi_{j,x} \bar{\psi}_{i,x} \psi_{j,x}\right) \\
&\times \prod_{x,i} \left(1 - \frac{M_x}{2g^2} \bar{\psi}_{i,x} \psi_{i,x}\right) \\
&\times \prod_{x,\mu,i} \left(1 + \frac{1}{g^2} \bar{\psi}_{i,x} \mathcal{P}_{\mu} \psi_{i,x+\mu}\right) \\
&\times \prod_{x,i < j} \left(1 - \frac{1}{4g^2} \bar{\psi}_{i,x} \psi_{i,x} \bar{\psi}_{j,x} \psi_{j,x}\right). \quad (4.82)
\end{aligned}$$

#### 4. Supersymmetric Nonlinear $O(N)$ sigma Model

We can write the whole expanded action as

$$\begin{aligned}
\exp(-\hat{S}_F) &= \prod_x \sum_{i,j} \left( \frac{1}{2} \phi_{i,x} \phi_{j,x} \bar{\psi}_{i,x} \psi_{j,x} \right)^{c_{ij}(x)=1} \\
&\times \prod_{x,i} \left[ \sum_{m_i(x)=0}^1 \left( -\frac{M_x}{2g^2} \bar{\psi}_{i,x} \psi_{i,x} \right)^{m_i(x)} \right] \\
&\times \prod_{x,\mu,i} \left[ \sum_{h_i(x,\mu)=0}^1 \left( \frac{1}{g^2} \bar{\psi}_{i,x} \mathcal{P}_\mu \psi_{i,x+\mu} \right)^{h_i(x,\mu)} \right] \\
&\times \prod_{x,i < j} \left[ \sum_{q_{ij}(x)=0}^1 \left( -\frac{1}{4g^2} \bar{\psi}_{i,x} \psi_{i,x} \bar{\psi}_{j,x} \psi_{j,x} \right)^{q_{ij}(x)} \right] \quad (4.83)
\end{aligned}$$

where we use the occupation numbers which are  $\in \{0, 1\}$ . These are  $c_{ij}(x)$  for the constraint terms,  $m_i(x)$  for the mass monomer terms,  $q_{ij}(x)$  for the monomer terms generated by the four Fermi potential and  $h_i(x, \mu)$  for the fermion hopping terms from site  $x$  to  $x + \hat{\mu}$ .

A specific configuration of the partition function is now described by setting certain occupation numbers to one and others to zero. Note that there is a large amount of combinations that will not create a configuration that contributes to the partition function because of the nilpotency of the Grassmann fields. It is our goal to find a set of rules in form of an equation that constrains the occupation numbers, such that any combination of fixed occupation number not fulfilling this equation is not contribution to the partition function. A contributing configuration corresponds to a set of fixed occupation numbers, such that when multiplying the terms in eq.(4.83) we obtain a configuration in which every  $\psi_{i,x}^\alpha$  is appearing exactly once.

Let us analyse what kind of possibilities arise to saturate a flavour  $i$  on a site  $x$ . We start off by performing the mandatory step of choosing a fermionic constraint of which there are flavour diagonal constraints and flavour changing constraints. Assuming we chose  $c_{ii}(x) = 1$ , this means that the Grassmann field  $\bar{\psi}_{i,x} \psi_{i,x}$  is saturated and we need to deal with the other  $N - 1$  flavours. There could for instance be another flavour  $j$  propagating through that same site and saturate the fermion of flavour  $j$ , i.e.  $h_j(x, \mu) = h_j(x - \mu, \mu) = 1$ . Another flavour could be saturated by a mass monomer term, e.g.  $m_l(x) = 1$ , and so on. We quickly see that the number of options, which are possible to create a non-vanishing contribution, depend strongly on the number of flavours, i.e. on the choice of  $O(N)$ . The constraining equation for the occupation numbers of a flavour  $i$  is

$$\sum_{\pm\mu} h_i(x, \mu) \left( \frac{1}{2} \left[ 1 - \sum_j c_{ij}(x) \right] + \sum_j c_{ij}(x) \sum_{\pm\mu} h_j(x, \mu) \right) + \sum_j q_{ij}(x) + c_{ii}(x) + m_i(x) = 1 \quad \forall x. \quad (4.84)$$

This formula is not very instructive, therefore we will turn to an explicit choice of  $N = 2$  and  $N = 3$  for which we analyse the loop structures separately.

### Loop formulation for O(2)

When dealing with  $N = 2$ , the expansion from eq.(4.83) breaks down to a very reduced form. The possibilities on how to saturate the Grassmann integral on an arbitrary site are so limited that we can put them into words. We call the two flavours  $r$  and  $g$  for *red* and *green*.

In a first scenario the red flavour is saturated by a flavour diagonal constraint  $c_{rr}(x) = 1$ . The options which are left for the green flavour are two. Either the green flavour is saturated by the mass monomer term  $m_{gg}(x) = 1$  or there is a fermion of green flavour hopping through that site, i.e.  $h_g(x - \mu, \mu) = h_g(x, \nu) = 1$ . Those two options are illustrated below in fig.4.2

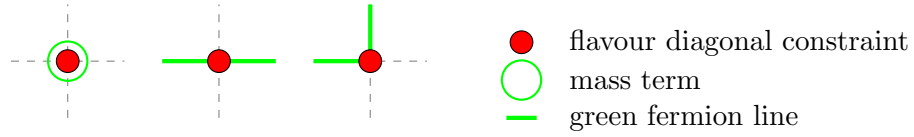


Figure 4.2.: Showing all non-vanishing contributions for  $c_{rr}(x) = 1$ , besides rotations of  $\pi/2$  and flavour interchange.

In a second and already last possible scenario the flavour changing constraint  $c_{rg}(x) = 1$  is picked. This means that this site can only be saturated if exactly one hop term of the red flavour and one of the green flavour is connected to that site, e.g.  $h_r(x - \mu, \mu) = h_g(x, \nu) = 1$ . In fig.4.3 those possibilities are illustrated.

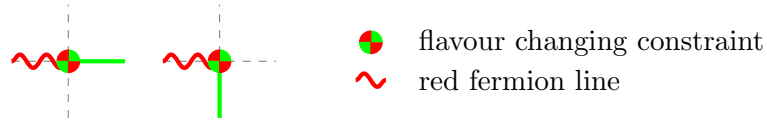


Figure 4.3.: Showing all non-vanishing contributions for  $c_{rg}(x) = 1$ , besides rotations of  $\pi/2$  and flavour interchange.

Formally this can be understood by considering two hop terms

$$\dots \psi_{r,x-\hat{\mu}}^T \mathcal{C} \mathcal{P}_{\mu} \underbrace{\psi_{r,x} \psi_{g,x}^T}_{\text{on site } x} \mathcal{C} \mathcal{P}_{\nu} \psi_{g,x+\hat{\nu}} \dots, \quad (4.85)$$

which are part of a fermion loop that is visiting site  $x$ . Note that we chose the hop from  $x - \hat{\mu}$  to  $x$  to be of red flavour and the one from  $x$  to  $x + \hat{\nu}$  to be the green one, but these can of course be interchanged. So the above situation described in eq.(4.85) can be shown to be the only one which is able to saturate the integral on site  $x$  if  $c_{rg}(x) = 1$ . This can be checked by performing, leaving away bosonic contributions, the Grassmann integral on

#### 4. Supersymmetric Nonlinear $O(N)$ sigma Model

that site with the added contribution of the constraint term, i.e.

$$\begin{aligned}
& \int d\psi_{r,x}^1 d\psi_{r,x}^2 d\psi_{g,x}^1 d\psi_{g,x}^2 \psi_{r,x} \psi_{g,x}^T \mathcal{C}(\overbrace{\psi_{r,x}^1 \psi_{g,x}^2 + \psi_{g,x}^1 \psi_{r,x}^2}^{c_{rg}(x)=1}) \\
&= \int d\psi_{r,x}^1 d\psi_{r,x}^2 d\psi_{g,x}^1 d\psi_{g,x}^2 \begin{pmatrix} \psi_{r,x}^1 \\ \psi_{r,x}^2 \end{pmatrix} \begin{pmatrix} -\psi_{g,x}^2 & \psi_{g,x}^1 \end{pmatrix} (\psi_{r,x}^1 \psi_{g,x}^2 + \psi_{g,x}^1 \psi_{r,x}^2) \\
&= \int d\psi_{r,x}^1 d\psi_{r,x}^2 d\psi_{g,x}^1 d\psi_{g,x}^2 \begin{pmatrix} -\psi_{r,x}^1 \psi_{g,x}^2 \psi_{g,x}^1 \psi_{r,x}^2 & 0 \\ 0 & \psi_{r,x}^2 \psi_{g,x}^1 \psi_{r,x}^1 \psi_{g,x}^2 \end{pmatrix} \quad (4.86) \\
&= \mathbb{1}_{2 \times 2}.
\end{aligned}$$

Any other term from the hopping expansion than the two hop terms would have generated zero. We now illustrated the possibilities how to create a non-vanishing contribution from a single site for the case of  $N = 2$ . From these considerations and those already made in section 1.3.2 for the free Majorana fermion, it becomes clear that for  $N = 2$  there are only self-avoiding, closed and non-backtracking loops and the occupation numbers  $q_{ij}(x)$  need to be always zero.

#### Loop formulation for $O(3)$

In order to talk about three different flavours we will add a *blue* flavour which we will denote with  $b$ . Let us state the key elements in the loop structures which are also true for arbitrary  $N$ :

- The term  $\psi_{i,x}^1 \psi_{i,x}^2 \psi_{j,x}^1 \psi_{j,x}^2$ , coming from the four Fermi potential, becomes relevant<sup>1</sup>. For  $N = 3$  we can for instance choose  $c_{rr}(x) = q_{gb}(x) = 1$ .
- The possibilities on how to saturate two fermion flavours on a site on which a flavour changing constraint is picked, i.e.  $c_{ij}(x) = 1$  with  $i \neq j$  still remains the discussed scenario seen in fig. 4.3. The contribution is only non-zero if the only other occupation numbers including  $i$  and  $j$  are  $h_i(x - \mu, x) = h_j(x, x + \nu) = 1$ , as shown in eq. (4.86).
- Having more flavours makes it possible to visit a site in a loop several times. This then allows non self-avoiding loops for all  $N > 2$ . This also leads to the fact that  $N - 1$  loops may visit the same site.

For  $N = 3$  the number of possible vertices that give a non-zero contribution to the partition function are listed in section 4.7.2 and can be easily generalised to arbitrary  $N$ .

### 4.6. Contributions to the partition function

In this section we calculate the contribution to the partition function coming from the Boltzmann factor of the fermion action. In order to understand the basic concepts it is wise to consider the calculations performed in 1.4, where the contributions of the fermion loops and the mass monomer terms were calculated in detail for a free Majorana fermion

<sup>1</sup>Not to be mistaken with *relevant* in the renormalisation group sense.

on a two-dimensional lattice. Recall that the partition function of a free Majorana fermion is

$$Z = \sum_{\{c\}} \prod_{x \in \{\Lambda \setminus \Omega\}} M_x \prod_{\Omega_i \in \{c\}} -(-1)^{\nu(\Omega_i)} 2^{-\frac{n_c(\Omega_i)}{2}}, \quad (4.87)$$

where the sum over  $\{c\}$  is the sum over all loop configurations and  $\Omega_i$  is the set of sites in a loop and  $n_c$  and  $\nu$  are the corresponding number of corners and rotations of that loop. We split up our partition function into topologically different sectors corresponding to the number of fermionic winding numbers in each dimension modulo 2. This showed itself being very useful because all configurations in a given topological sector contribute with weights that have the same sign. We will see that this concept can be applied to the fermion loop formulation of the supersymmetric nonlinear  $O(N)$  sigma model in the exact same fashion. However, we will see that these topologies are of less interest for  $N > 2$ .

#### 4.6.1. Fermionic contributions for $O(2)$

For  $N = 2$  the fermion loops are almost identical to the free Majorana fermion loops. They are closed, non-backtracking and self-avoiding. The difference is that there are sites on which the flavour of the fermion may change. This is because on every site we have either a flavour diagonal constraint ( $c_{rr} = 1$  or  $c_{gg} = 1$ ) or a flavour off-diagonal constraint ( $c_{rg} = 1$ ). These simply tell us if the flavour changes or not, but the contribution to the weight of the configuration from these terms is purely bosonic. Let us write the constraint, leaving away the bosonic fields, in the form  $\psi_i^T \mathcal{C} \psi_j$ . For  $N = 2$  the most general loop consists of consecutively appearing parts of the kind

$$\dots \mathcal{C} \mathcal{P} \psi_i \overbrace{\psi_k^T \mathcal{C} \psi_l}^{c_{kl}=1} \psi_j^T \mathcal{C} \mathcal{P} \dots \quad (4.88)$$

This only gives a contribution for

$$\int d\psi_r^1 d\psi_r^2 d\psi_g^1 d\psi_g^2 \psi_i \psi_k^T \mathcal{C} \psi_l \psi_j^T \mathcal{C} = (\delta_{ik} \delta_{lj} + \delta_{ij} \delta_{kl}) \mathbb{1}_{2 \times 2}, \quad (4.89)$$

which means that we either have

$$\dots \mathcal{C} \mathcal{P} \psi_r \psi_r^T \mathcal{C} \psi_g \psi_g^T \mathcal{C} \mathcal{P} \dots, \quad (4.90)$$

or

$$\dots \mathcal{C} \mathcal{P} \psi_r \psi_g^T \mathcal{C} \psi_g \psi_r^T \mathcal{C} \mathcal{P} \dots, \quad (4.91)$$

where of course red and green are interchangeable. The contribution from the Dirac algebra structure to the fermion loop is therefore the same for both of the above possibilities and we can write, like in eq.(1.65), again

$$W^F(\Omega_i) = -(-1)^{\nu(\Omega_i)} 2^{-\frac{n_c(\Omega_i)}{2}} \quad (4.92)$$

We did not write the factors of  $1/g^2$ , since every term in the hopping expansion of the fermionic Boltzmann factor contains a  $1/g^2$  and it can be pulled out in front, forming an overall factor of  $(1/g^2)^V$  for  $N = 2$ . Note that this only works for  $N = 2$  because we need to pick exactly  $V$  terms from the hopping expansion.

#### 4. Supersymmetric Nonlinear $O(N)$ sigma Model

The fermionic contribution from sites where no fermion loop is going through is also the same as for the free Majorana fermion calculated in eq.(1.66), i.e.

$$M_x = (m + 2). \quad (4.93)$$

This is because on a site on which no fermion is propagating through there must be a flavour diagonal fermionic constraint  $c_{ii}(x)$ , yielding a term  $\bar{\psi}_i \psi_i$ , that allows only for a mass monomer term of the other flavour, i.e.  $m_j(x) = 1$  yielding  $\bar{\psi}_j \psi_j$  with  $i \neq j$ .

##### 4.6.2. Fermionic contributions for $O(3)$

As we have seen already in the  $N = 2$  case, the contribution from the Dirac algebra structure is the same for all possible flavour combinations along the same fermion loop. What is now crucial for  $N = 3$  is the fact that a site can be visited twice. In the most general case, with a double-visit of site  $x$  in the same loop, we find

$$\dots \mathcal{CP} \underbrace{\psi_i \psi_k^T \mathcal{C} \psi_l \psi_j^T}_{\text{site } x} \mathcal{CP} \dots \mathcal{CP} \underbrace{\psi_h \psi_m^T}_{\text{site } x} \mathcal{CP} \dots, \quad (4.94)$$

where it is important that there is only one fermionic constraint on that site  $x$ . Performing the Grassmann integral we see that only some combinations survive, i.e.

$$\prod_{q=r,g,b} \int d\psi_q^1 d\psi_q^2 \psi_i \psi_k^T \mathcal{C} \psi_l \psi_j^T \psi_h \psi_m^T \mathcal{C} = (\delta_{ik} \delta_{lj} \delta_{hm} + \delta_{ij} \delta_{kl} \delta_{hm}) \mathbb{1}_{2 \times 2}, \quad (4.95)$$

where of course no flavour is exquisite and they can be interchanged. We see that also for non-self avoiding fermion loops the weight is still the trace of the product of all projectors along the fermion loop. This means that eq.(1.65) is still valid in order to determine the fermionic contribution to the partition function from a fermion loop. What changes for all  $N > 2$  is the fact that loops are now possible which have a rotation number of  $\nu \in \mathbb{Z}_{\{0\}}$ , this is obvious because they are no longer self-avoiding.

Topological sectors can nevertheless be introduced, but no longer form such a power concept. This is because for  $N > 2$  not all configurations in a given topological sector have a weight with the identical sign. In fig.(4.4) we illustrate the breakdown of this concept and consider two fermion loops (for simplification containing only two flavours *green* and *blue*) which would have fallen in our former class  $\mathcal{L}_{00}$ .

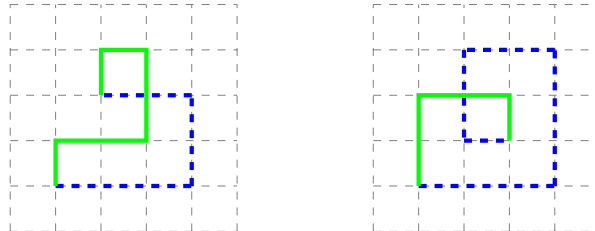


Figure 4.4.: Topological sectors do not hold any information about the number of rotations. This is shown here for the  $\mathcal{L}_{00}$  sector.

There seems to be no global feature to determine the sign of a contribution from a fermion loop configuration and we are forced to determine the sign of every single loop in a configuration in order to know the sign of the whole contribution.

On sites where neither a fermion of flavour  $i$  is hopping through nor arising in a constraint term we have the possibility of setting  $m_i(x) = 1$ . This yields the contribution

$$\frac{M_x}{g^2} = \frac{m+2}{g^2}. \quad (4.96)$$

There is now an additional term, coming from the last line of eq.(4.83), which is

$$\prod_{x,i < j} \left[ \sum_{q_{ij}(x)=0}^1 \left( -\frac{1}{4g^2} \bar{\psi}_{i,x} \psi_{i,x} \bar{\psi}_{j,x} \psi_{j,x} \right)^{q_{ij}(x)} \right]. \quad (4.97)$$

This term spoils the extraction of the factor  $1/g^2$  because we no longer need to pick  $V$  terms from the hopping expansion in order to saturate the Grassmann integral. It is now possible to saturate two flavours  $i$  and  $j$  at a site  $x$  with  $q_{ij}(x) = 1$ . This is in a sense identical to  $m_i(x) = m_j(x) = 1$ , but comes with a different weight. Let us integrate out the fermion fields on a given site  $x$  of eq.(4.97) with the assumption that the blue flavour is already saturated by  $c_{bb}(x) = 1$ . We can then use  $q_{rg}(x) = 1$  in order to get

$$\int d\psi_r^1 d\psi_r^2 d\psi_g^1 d\psi_g^2 \left( -\frac{1}{g^2} \psi_r^1 \psi_r^2 \psi_g^1 \psi_g^2 \right) = \frac{1}{g^2}. \quad (4.98)$$

We have the option to combine the scenario  $m_i(x) = m_j(x) = 1$  with  $q_{ij}(x) = 1$  by combining also the weights to

$$\left( \frac{M_x}{g^2} \right)^2 + \frac{1}{g^2} = \frac{(m+2)^2 + g^2}{g^4}. \quad (4.99)$$

We have now determined all weights contributing to the partition function coming from the Grassmann integral. Let us in the next sections consider the bosonic contribution.

### 4.6.3. Bosonic contribution from $\phi\psi = 0$ for $\mathbf{O}(2)$

Above we argued how the constraint terms from  $\phi\psi = 0$  effect the fermion loop flavour-structures but not their weight contributing to the partition function coming from the Dirac algebra structure. We will now consider the bosonic contribution for  $N = 2$ , which does get affected by the loop structure, i.e. the choice of diagonal or off-diagonal constraints.

Given a fixed bosonic background configuration, corresponding to a given set of bond occupation numbers  $N_i^B$ , we can ask, what is the total bosonic contribution if on top of the background we pick a fermion loop configuration which sets certain  $c_{ij}(x)$  to one. On each site we can have either a flavour diagonal constraint ( $c_{rr} = 1$  or  $c_{gg} = 1$ ) contributing with  $\phi_r^2$  or with  $\phi_g^2$ , or the off-diagonal constraint ( $c_{rg} = 1$ ) that contributes with  $\phi_r \phi_g$ . We can simply add the corresponding number of powers of  $\phi_r$  and  $\phi_g$  to the total bond

#### 4. Supersymmetric Nonlinear $O(N)$ sigma Model

occupation number of that flavour and evaluate  $Q(N^B)$  from eq.(4.59). At each site this can be summarised to

$$Q(N_r^B + 2, N_g^B) \quad \text{for } c_{rr} = 1, \quad (4.100)$$

$$Q(N_r^B, N_g^B + 2) \quad \text{for } c_{gg} = 1, \quad (4.101)$$

$$Q(N_r^B + 1, N_g^B + 1) \quad \text{for } c_{rg} = 1. \quad (4.102)$$

and we then have to perform the product over all sites in order to obtain the total bosonic contribution

$$\prod_x Q(N_x^B). \quad (4.103)$$

##### 4.6.4. Bosonic contribution from $\phi\psi = 0$ for $O(3)$

We can again ask what is the bosonic weight if we consider a fixed bosonic background configuration, i.e. initially fixed  $N_r^B, N_g^B$  and  $N_b^B$ , on top of which we add the bosonic contribution coming from the constraints  $\phi_i \phi_j \bar{\psi}_i \psi_j$ . Analogously to the previously discussed  $N = 2$ , we find

$$Q(N_r^B + 2, N_g^B, N_b^B) \quad \text{for } c_{rr} = 1, \quad (4.104)$$

$$Q(N_r^B, N_g^B + 2, N_b^B) \quad \text{for } c_{gg} = 1, \quad (4.105)$$

$$Q(N_r^B, N_g^B, N_b^B + 2) \quad \text{for } c_{bb} = 1, \quad (4.106)$$

$$Q(N_r^B + 1, N_g^B + 1, N_b^B) \quad \text{for } c_{rg} = 1, \quad (4.107)$$

$$Q(N_r^B, N_g^B + 1, N_b^B + 1) \quad \text{for } c_{gb} = 1, \quad (4.108)$$

$$Q(N_r^B + 1, N_g^B, N_b^B + 1) \quad \text{for } c_{rb} = 1. \quad (4.109)$$

and in order to get the contributions from all sites we simply have to perform the product over all sites

$$\prod_x Q(N_x^B). \quad (4.110)$$

Note that bosonic contribution from the constraint terms can easily be generalised to arbitrary  $N$ . We simply have to increase the corresponding occupation number

$$Q(\dots, N_i^B + 2, \dots) \quad \text{for } c_{ii} = 1, \quad (4.111)$$

$$Q(\dots, N_i^B + 1, \dots, N_j^B + 1, \dots) \quad \text{for } c_{ij} = 1. \quad (4.112)$$

##### 4.6.5. Z in the bond/loop formulation for $O(2)$

The complete partition function for  $N = 2$  constructed with the bosonic bond representation and the fermion loop formulation can be written in the following form

$$Z = \sum_{\{c\}} \left( \frac{1}{g^2} \right)^V \underbrace{\left[ \prod_x W^B(N^B(x)) \right]}_{\text{Bosonic bond contr.}} \underbrace{\left[ \prod_{x \in \Lambda/\Omega} M_x \right]}_{\text{Monomer contr.}} \underbrace{\left[ \prod_{\Omega_i \in \{c\}} W^F(\Omega_i) \right]}_{\text{Fermion loop contr.}}, \quad (4.113)$$

where  $W^B$  is the bosonic weight on site  $x$  from eq.(4.56),  $W^F$  the weight of a fermion loop from eq.(4.92) and  $M_x = m + 2$  are the mass monomer terms which live on all sites



that have no fermion propagating through. Note that since the factor  $1/g^2$  arises in every term of the fermionic hopping expansion it is pulled out of the fermionic contribution. It is interesting to see that the fermionic action does not directly feel the coupling  $g$  it is only connected to the coupling via interaction with the bosonic field. In the equation above the sum over all configurations  $\{c\}$  is a short hand notation for

$$\sum_{\{c\}} = \prod_x \prod_j \prod_i \sum_{c_{ij}(x)} \sum_{N_i^B(x)} \sum_{m_i(x)} \sum_{h_i(x)}, \quad (4.114)$$

where  $m_i(x)$ ,  $h_i(x)$  and  $c_{ij}(x)$  must fulfil eq.(4.84) in which  $q_{ij} = 0$  since  $N = 2$ . This can be reformulated in a more understandable way

$$\sum_{\{c\}} = \sum_{\{N^B\}} \sum_{\{\text{flavour}\}} \sum_{\{\text{loop conf.}\}}, \quad (4.115)$$

which means that we need to perform a sum over all possible configurations including closed loops, a sum over all possible flavour combinations and a sum over all possible bosonic occupation numbers.

#### 4.6.6. $Z$ in the bond/loop formulation for $O(3)$

The complete partition function for  $N = 3$  constructed with the bosonic bond representation and the fermion loop formulation can not be written down as nicely as for the  $N = 2$  case in eq.(4.113). This is due to the differences which we derived in the previous section 4.6.2. The most crucial difference lies in the sum over all configurations  $\{c\}$ , because for  $N > 2$  non self-avoiding and generally intersecting loops are now allowed structures that contribute to the partition function. An additional complication is that a site can, even though visited by a fermion loop, still contribute with a mass monomer term from another flavour. Further a double mass monomer term is now also allowed. The separation of monomer sites and loop sites is therefore no longer possible and we can only deliver a rather lengthy form of the partition function

$$\begin{aligned} Z = & \sum_{\{c\}} \underbrace{\left[ \prod_x W^B(N^B(x)) \right]}_{\text{Bosonic bond contr.}} \underbrace{\left[ \prod_{x \in \Lambda_M} \frac{(m+2)}{g^2} \right]}_{\text{Monomer contr.}} \\ & \times \underbrace{\left[ \prod_{x \in \Lambda_{M^2}} \frac{(m+2)^2 + g^2}{g^4} \right]}_{\text{Double Monomer contr.}} \underbrace{\left[ \prod_{\Omega_i \in \{c\}} W^F(\Omega_i) \right]}_{\text{Fermion loop contr.}}, \end{aligned} \quad (4.116)$$

where  $\Lambda_M$  and  $\Lambda_{M^2}$  are all the lattice sites holding a mass monomer or two mass monomer terms respectively. The sum over all loop configurations now also includes non self-avoiding and generally intersecting loops and the number of rotations of a loop is  $\nu \in \mathbb{Z}_{\{0\}}$ .

### 4.7. Graphical Representation for small $N$

In the following we will list all possible vertices for  $N = 2$  and  $N = 3$  on a fixed bosonic background configuration. A vertex illustrates one possible building block of a contributing configuration and below each we will add the corresponding weight it contributes to

#### 4. Supersymmetric Nonlinear $O(N)$ sigma Model

the partition function. The contribution from the Dirac algebra structure is depending on the rotation of the whole loop and can therefore not be encoded on a local level. However, the factor of  $1/\sqrt{2}$  that arises when a fermion loop is forming a corner, can be encoded in a local weight. The bosonic contribution to the weight is determined by the number of bosonic bonds which are connected to that site which we already assumed to be fix, but note that there are infinitely many bosonic configurations on top of which we can place these vertices.

Below we now show a graphical representation of all the possibilities up to those achieved by rotating the lattice by  $\pi/2$  or rotations in flavour space, this means that  $r$ ,  $g$  and  $b$  are interchangeable and of course  $r \neq g$ ,  $r \neq b$  and  $g \neq b$ . In the case of  $N = 2$  we still write the bosonic contribution coming from the  $\phi\psi = 0$  terms explicitly in component notation, whereas in the  $N = 3$  case we write down the modified site weight  $Q(N^B)$  in the bosonic bond formulation. Additionally we factor out all  $1/g^2$  factors in the  $N = 2$  case.

##### 4.7.1. $N = 2$

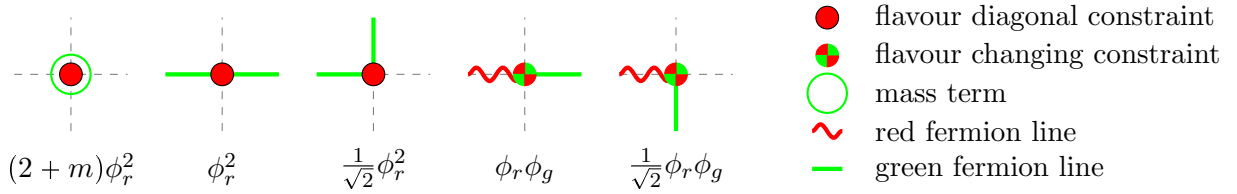
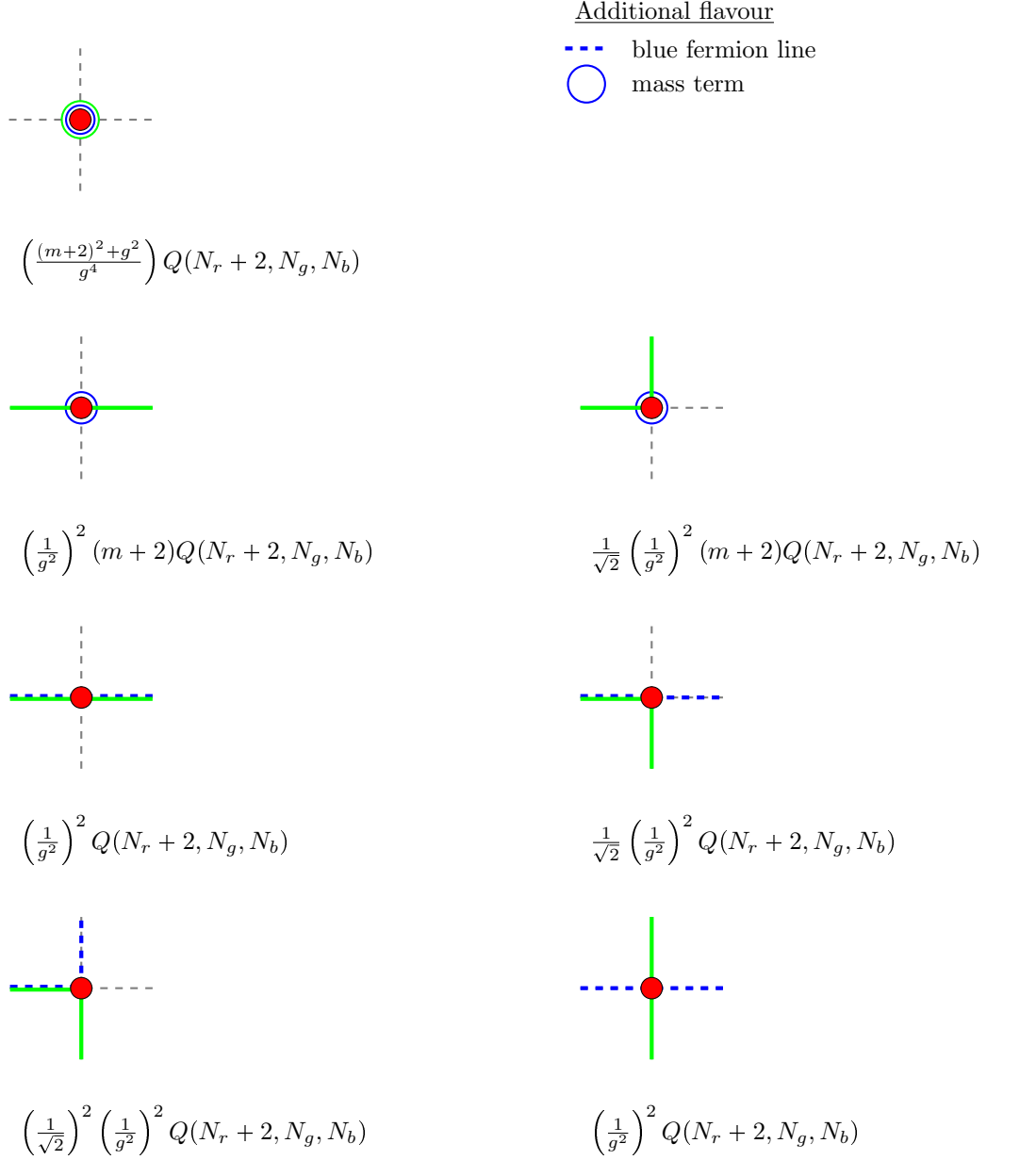


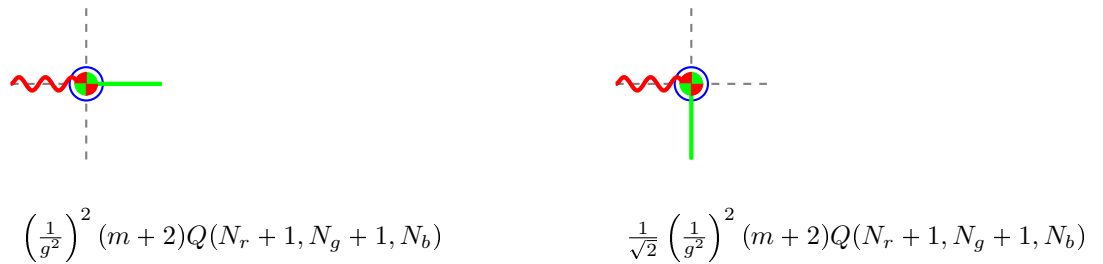
Figure 4.5.: All possible vertices for  $N = 2$  upon rotations of  $\pi/2$  and  $r \leftrightarrow g$ .

4.7.2.  $N = 3$ 

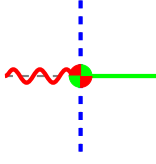
The possibilities with  $c_{rr} = 1$  are



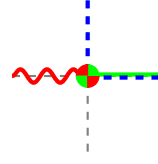
The possibilities with  $c_{rg} = 1$  are



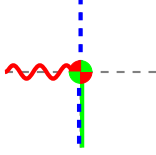
#### 4. Supersymmetric Nonlinear $O(N)$ sigma Model



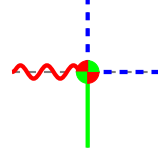
$$\left(\frac{1}{g^2}\right)^2 Q(N_r + 1, N_g + 1, N_b)$$



$$\frac{1}{\sqrt{2}} \left(\frac{1}{g^2}\right)^2 Q(N_r + 1, N_g + 1, N_b)$$

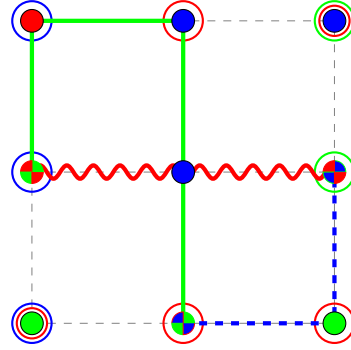


$$\frac{1}{\sqrt{2}} \left(\frac{1}{g^2}\right)^2 Q(N_r + 1, N_g + 1, N_b)$$



$$\left(\frac{1}{\sqrt{2}}\right)^2 \left(\frac{1}{g^2}\right)^2 Q(N_r + 1, N_g + 1, N_b)$$

Below we also illustrate a valid configuration that illustrates a non self-avoiding loop.



### 4.8. Partition function and boundary conditions

The following discussion only works for systems in which all contributions from configurations in the same topological sector come with the identical sign. This is not true in our current formulation for  $N > 2$ , since the loops are no longer self-avoiding. Even though we can use the following description only for  $N = 2$ , let us establish a formula for a system with  $N$  different self-avoiding fermions which tells us what sign a certain configuration has depending on the topological sector and boundary conditions, .

We previously introduced  $\alpha_\mu$  in eq.(1.9), which denotes if the boundary condition in direction of  $\mu$  is periodic  $\alpha_\mu = 0$  or anti-periodic  $\alpha_\mu = 1$ . In the case where more fermions are present in the system it is possible to set different boundary conditions for each of them, formally

$$\psi_{i,x+a\hat{\mu}L_\mu} = (-1)^{\alpha_\mu(i)} \psi_{i,x}, \quad (4.117)$$

where we introduced  $\alpha_\mu(i)$ , which denotes if the boundary condition of flavour  $i$  in direction of  $\mu$  is periodic ( $\alpha_\mu(i) = 0$ ) or anti-periodic ( $\alpha_\mu(i) = 1$ ). As already seen, we can divide the partition function into topological sectors. The number of different sectors depends

on the number of fermions and dimensions. If we have  $N$  different fermion flavours in two dimensions we can have up to  $4^N$  different topological sectors. In order to have a compact notation of the partition function as a sum of contributions from different topological sectors we introduce  $\epsilon = (\alpha_0(0), \alpha_1(0), \alpha_0(1), \alpha_1(1), \dots, \alpha_1(N-1))$ , which is a vector telling us which boundary condition each flavour has. Additionally we consider a vector  $n$  of extent  $2N$  which characterises the topological sector. If a fermion of flavour  $i$  is winding around the dimension  $\mu$  an odd amount of times, then the entry  $n(2i + \mu) = 1$ , if it is winding around that dimension an even amount of times or not at all, the entry is zero. Like this we can write down the partition function for a given set of boundary conditions  $\epsilon$  for  $N$  closed non-backtracking self-avoiding fermion loops to be

$$Z_\epsilon = \sum_{\{n\}} (-1)^{n^2 + \epsilon \cdot n} Z_{\mathcal{L}_n}, \quad (4.118)$$

where  $n$  and  $\epsilon$  are the vectors of length  $2N$  introduced above and the sum over  $\{n\}$  is the sum over all possible sectors. The signs coming from the Dirac algebra structure of the loops as well as the boundary conditions are both encoded in eq.(4.118).

In the following we will consider results obtained from the  $N = 2$  model, but will set the boundary conditions of both flavours identical, essentially setting  $\alpha_\mu(0) = \alpha_\mu(1)$  and reducing the topological sectors to four.  $Z_\epsilon$  is now identical to the already introduced case of one free Majorana fermion, where  $\epsilon = \alpha$ , and

$$Z_\alpha = Z_{(\alpha_0, \alpha_1)} = Z_{\mathcal{L}_{00}} + (-1)^{1+\alpha_0} Z_{\mathcal{L}_{10}} + (-1)^{1+\alpha_1} Z_{\mathcal{L}_{01}} + (-1)^{1+\alpha_0+\alpha_1} Z_{\mathcal{L}_{11}}. \quad (4.119)$$

We are again specially interested in the case of periodic-periodic boundary conditions

$$Z_{pp} = Z_{\mathcal{L}_{00}} - Z_{\mathcal{L}_{10}} - Z_{\mathcal{L}_{01}} - Z_{\mathcal{L}_{11}}, \quad (4.120)$$

where we used the notation  $Z_{pp} = Z_{(0,0)}$ . Another interesting set of boundary conditions is  $Z_{ap} = Z_{(1,0)}$ , referring to antiperiodic-periodic boundary conditions, which yields

$$Z_{ap} = Z_{\mathcal{L}_{00}} + Z_{\mathcal{L}_{10}} - Z_{\mathcal{L}_{01}} + Z_{\mathcal{L}_{11}}. \quad (4.121)$$

Note that in this discussion only the contribution from the Grassmann integral is considered. As we will shortly see there is an additional minus sign that can occur from the  $\phi\psi = 0$  constraint.

## 4.9. Observables

In general an observable is defined as

$$\langle \mathcal{O} \rangle = \frac{1}{Z} \int \mathcal{D}\phi \mathcal{D}\psi \mathcal{O} e^{-S(\phi, \psi)}, \quad (4.122)$$

and all equations already derived in section 1.7 can be used here with only small adaptations. In the following lines we want to investigate what happens if the weights of the configurations can be negative. We are motivated to do so, since the bosonic field can contribute with a negative sign due to the terms in  $\phi\psi = 0$ , in which fields can arise

#### 4. Supersymmetric Nonlinear $O(N)$ sigma Model

linearly. The non-normalised expectation value of an observable can then be written, as already done in eq.(1.81), like

$$\langle\langle\mathcal{O}\rangle\rangle_{\mathcal{L}_{ij}} = \sum_{\{c\}\in\mathcal{L}_{ij}} \mathcal{O}W_c = \sum_{\{c\}\in\mathcal{L}_{ij}} \mathcal{O}\sigma|W_c|, \quad (4.123)$$

where  $W_c$  simply denotes the Boltzmann weight of the configuration  $c$  and  $\sigma \in \{-1, 1\}$  is the sign of the corresponding weight. For a free Majorana fermion in two dimensions we showed that the formulation is free of any negative weights. Therefore  $Z = \langle\langle 1 \rangle\rangle_{\text{all sectors}}$ , since now in general there might be negative contributions,  $Z$  is the average sign  $\langle\langle\sigma\rangle\rangle_{\text{all sectors}}$ . This is important when norming an observable  $\langle\mathcal{O}\rangle$  with the adequate value of  $Z$  as in

$$\langle\mathcal{O}\rangle_{\mathcal{L}_{ij}} = \frac{\langle\langle\mathcal{O}\rangle\rangle_{\mathcal{L}_{ij}}}{\langle\langle\sigma\rangle\rangle_Z}. \quad (4.124)$$

If  $\langle\langle\sigma\rangle\rangle_Z \equiv Z \approx 0$  we suffer from a sign problem. It may though be that even if  $Z = 0$ , there are still sectors which contribute completely or merely with one fixed sign. Therefore it can be wise to look at ratios of observables. If we consider the ratio of two observables which were measured in the same ensemble  $Z$ , the normalisation obviously drops out

$$\frac{\langle\mathcal{O}\rangle_{\mathcal{L}_{ij}}}{\langle\mathcal{O}\rangle_{\mathcal{L}_{kl}}} = \frac{\langle\langle\mathcal{O}\rangle\rangle_{\mathcal{L}_{ij}}/Z}{\langle\langle\mathcal{O}\rangle\rangle_{\mathcal{L}_{kl}}/Z} = \frac{\langle\langle\mathcal{O}\rangle\rangle_{\mathcal{L}_{ij}}}{\langle\langle\mathcal{O}\rangle\rangle_{\mathcal{L}_{kl}}}. \quad (4.125)$$

A general observable  $\mathcal{O}$  in a system with boundary conditions  $\alpha$  still stays the same as in eq.(1.77)

$$\langle\mathcal{O}\rangle_\alpha = \frac{\langle\langle\mathcal{O}\rangle\rangle_{\mathcal{L}_{00}} + (-1)^{1+\alpha_0}\langle\langle\mathcal{O}\rangle\rangle_{\mathcal{L}_{10}} + (-1)^{1+\alpha_1}\langle\langle\mathcal{O}\rangle\rangle_{\mathcal{L}_{01}} + (-1)^{1+\alpha_0+\alpha_1}\langle\langle\mathcal{O}\rangle\rangle_{\mathcal{L}_{11}}}{Z_{\mathcal{L}_{00}} + (-1)^{1+\alpha_0}Z_{\mathcal{L}_{10}} + (-1)^{1+\alpha_1}Z_{\mathcal{L}_{01}} + (-1)^{1+\alpha_0+\alpha_1}Z_{\mathcal{L}_{11}}}, \quad (4.126)$$

but where

$$Z_{\mathcal{L}_{ij}} = \langle\langle\sigma\rangle\rangle_{\mathcal{L}_{ij}}. \quad (4.127)$$

What was done here was a rather trivial extension of the already derived concept of observables in the section 1.7 for the free Majorana.

### 4.10. Sign problem in the bond/loop formulation

In this section we give an overview of the possible sources of sign problems of the just derived formulation and also present some ideas on eventually more efficient formulations. Note that the following points are claimed to be possible sources of sign problems, if they actually produce one, can only be seen in the simulation.

#### In the fermion loop sector

The sign of the contributions to the partition function coming from fermion loops is depending on the number of rotations of the fermion loop. In the case where  $N = 2$  the fermion loops in the system are self-avoiding and the introduction of topologies with respect to the winding number is possible such that any configuration in a given topological sector comes with the same sign. Since the fermion loops are no longer self-avoiding for

$N > 2$ , these topologies hold no information about the rotation of loops and therefore their introduction is not such a powerful concept any more. In the current formulation for  $N > 2$ , every loop must be checked on the number of rotations and a local change could flip the sign of the configuration in just the next updating step. A priori at least, there seems to exist no reason why one of both, positive or negative loops, should appear more often.

#### From bosonic fields in $\phi\psi$

The second source of a possibly fluctuating sign comes from the fact that the bosonic fields may appear linearly in the fermionic constraints

$$\phi_i \phi_j \bar{\psi}_i \psi_j. \quad (4.128)$$

If  $i = j$  there is no problem at all, whereas if  $i \neq j$  there is the possibility of a negative contribution. This second possible source of sign fluctuation is appearing also for  $N = 2$ .

#### In the bosonic bond formulation

The last source of sign fluctuation comes from the Wilson derivative for the bosonic field variables. There exists an additional diagonal term with a negative prefactor. This term would not be present if we were using only a symmetric lattice derivative, as it is usually done in non-supersymmetric theories. When choosing to simulate the bosonic bond representation with a worm algorithm it is exactly this negative diagonal term which may also lead to a fluctuating sign in the boson sector. Note that this is again only a problem of our formulation. In the original formulation in which the exponential is not written as an infinite sum of hop terms, there are no negative contributions.

## 4.11. Flavour integration

The integration over flavour can be somewhat cumbersome. Specially in the case of large  $N$ , the number of combinations how a geometrically fixed loop can exist with subsections of different flavour, rises quickly. This gets only worse when approaching the chiral point of the theory, where the fermionic correlator is expected to diverge. Additionally the flavour changing constraints can contribute with a negative sign. We are motivated to perform the sum over all flavours with the goal in mind to create a formulation, in which all allowed combinatorial flavour possibilities are already included. This idea is pursued in more detail in appendix E where we consider the simple case of  $N = 2$ .

## 4.12. Numerical results for $N=2$

Here we present some first numerical results which help understand the structure of the phase diagram and the properties of the model for  $N = 2$ . The dynamics of the lattice system are essentially controlled by the two unitless bare couplings  $g$  and  $m$  and of course the lattice spacing  $a$  and the lattice extent  $L_t \times L_x$ . We update the bosonic field with an ordinary metropolis algorithm due to the sign problem in the bond formulation. The

#### 4. Supersymmetric Nonlinear $O(N)$ sigma Model

fermion is updated by a fermion worm algorithm, of which all building blocks have been derived in section 4.7.1 with their corresponding weights. We will make use of the term complete sweeps defined in section 3.6.2, in order to specify the statistics. If not stated differently we perform a thermalisation of one tenth of the total amount of complete sweeps and will use  $10^6$  complete sweeps per data point.

Note that the results obtained here are rather a proof of concept than a highly accurate determination of observables and their exact behaviour.

##### 4.12.1. Fermionic constraints and sings

In the derivation of the loop formulation of the fermionic degrees of freedom we saw that the constraint  $\phi\psi = 0$  plays a fundamental role of the flavour structure along closed fermion loops. It is also the only source of interaction between bosonic and fermionic degrees of freedom and forms the only source of negative signs in the  $N = 2$  model in the fermion loop formulation. We now want to investigate specially this constraint

$$\phi_r \phi_g \bar{\psi}_r \psi_g, \quad (4.129)$$

in a numerical simulation.

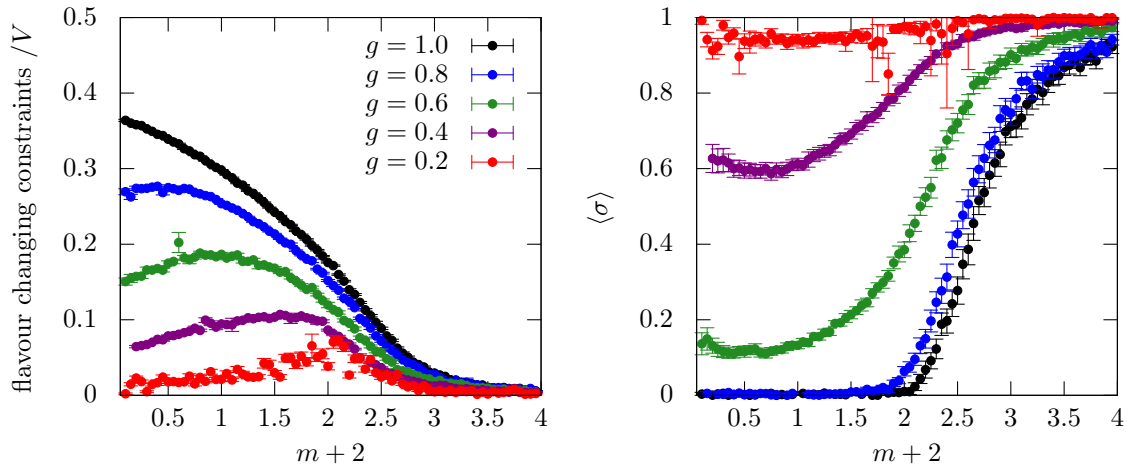


Figure 4.6.: These are plots showing data for a  $8 \times 8$  lattice for various couplings where each point was created with statistics containing of  $10^6$  complete sweeps. In the left panel we see the total amount of flavour changing constraints divided by the lattice volume at different bare masses. On the right the same is done for the average sign  $\langle \sigma \rangle$ .

In fig. 4.6 in the left panel we plot the number of flavour changing constraints divided by the lattice volume  $V = 8 \times 8$ . Each data point is created with  $10^6$  complete sweeps. Let us first focus on the behaviour of the constraints when varying the bare mass. It seems that for large enough  $m$  the flavour changing constraints disappear. This makes intuitively sense since the mass monomer terms, which have a weight of  $m + 2$ , become more favourable for larger masses and therefore all fermion loops will disappear. Since flavour changing constraints can only occur in a fermion loop, they must certainly disappear when



the loops do. We will shortly see that this dying out of fermion loops will refer to the transition between the fermion massless phase and the fermion massive phase. Consider now the behaviour of the constraints in fig. 4.6 on the left when changing the coupling  $g$ . We see that at any given point on the bare mass scale there are less flavour changing constraints if the coupling is decreased.

In order to see how the average sign behaves in the numerical simulation, consider the right panel of fig. 4.6. Here we show the average sign  $\langle\sigma\rangle$  for different bare masses and five different couplings. For small masses and large couplings we suffer from the fact that  $\langle\sigma\rangle = 0$ , there are as many positive as negative contributions. When increasing the mass, the number of negative contributions drops. Note that as we have just seen on the left, there are less possible sources of negative signs when decreasing the coupling. On the right we now observe the fact that  $\langle\sigma\rangle$  is also increasing if we go to smaller couplings. This was a priori not expected since it only takes one negative term to create an overall negative contribution. Our first conclusion is that at fixed lattice extent the numerical data shows that the sign problem seems to become milder for smaller  $g$  or larger  $m$ .

Since there has to be a fermionic constraint on every lattice site, we investigate the behaviour of the average sign when varying the volume. In fig. 4.7 we illustrate the behaviour of  $\langle\sigma\rangle$  at a fixed coupling  $g = 0.5$  for two different lattice extents  $8 \times 8$  and  $16 \times 16$ . In the very massive phase there seems to be no big difference, whereas for smaller mass we see a drastic aggravation of the sign problem. It shows that it is not only the coupling and the mass which influences the appearing of negative configurations, it is also strongly volume dependent.

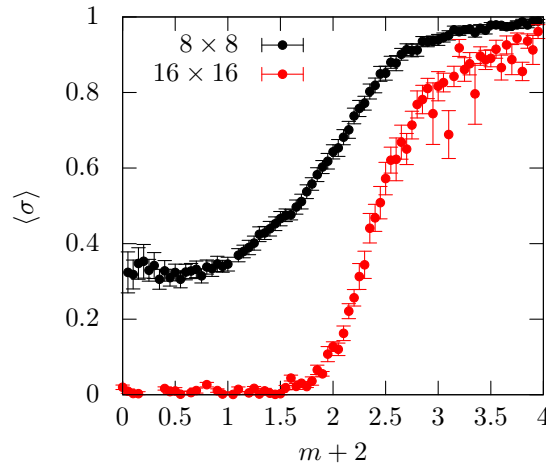


Figure 4.7.: Here we show the average sign  $\langle\sigma\rangle$  at fixed coupling  $g = 0.5$  for two different lattice volumes. This with statistics containing  $10^6$  complete sweeps per data point.

## 4.12.2. Critical point

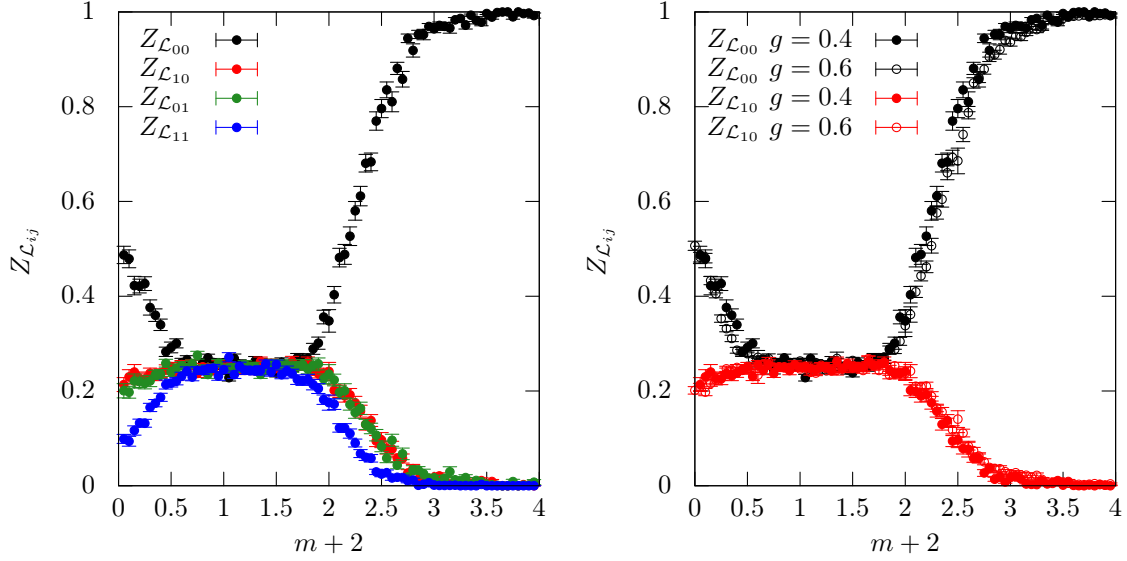


Figure 4.8.: In the right panel we show the partition functions in the different topological sectors at fixed coupling  $g = 0.4$  on a  $8 \times 8$  lattice. In the left panel we show the behaviour of two topological sectors for two different couplings.

The supersymmetric nonlinear  $O(N)$  sigma model is defined in the chiral limit where both the fermions and bosons are massless. However, since the Wilson term explicitly breaks chiral symmetry even at zero bare fermion mass, the chiral limit of the regularised theory is not defined simply by the vanishing of that mass. Instead, it needs to be tuned to the critical value  $m_c$  where the correlation length of the fermion diverges and the fermion develops a zero mode yielding  $Z_{pp}(m) = 0$  for the partition function with periodic boundary conditions in both directions [47, 77]. The fine tuned bare mass is denoted by  $m_c$ , referring to the critical point of the bare mass scale, and is defined as  $Z_{pp}(m_c) = 0$ . Let us in a first step investigate the behaviour of the partition functions in the topological sectors  $Z_{\mathcal{L}_{ij}}$  that appear in  $Z_{pp} = Z_{00} - Z_{10} - Z_{01} - Z_{11}$ .

In fig. 4.8 in the left panel we show data for a  $8 \times 8$  lattice at a coupling of  $g = 0.4$  from the phase quenched model. For larger  $m$  the  $Z_{\mathcal{L}_{00}}$  sector becomes the dominant one which is obvious since the mass monomer terms are favoured over the fermionic loops. It is exactly in this massive phase where we saw in the previous section that the sign problem vanishes. Note that specially at large couplings and small bare masses it is not known if this phase quenched results also describes the unquenched model. However, we have the possibility to approach the massless point from the massive phase in which the sign problem is mild for low couplings and small volumes. In fig. 4.8 on the right panel we see the  $Z$  ratios for two different couplings. If the coupling is increased, the fermion massive phase, where hardly any loops exist, is shifted slightly to larger bare masses.

We now investigate the behaviour of  $Z_{pp}/Z_{ap}$ . In fig. 4.9 on the left side, we show the

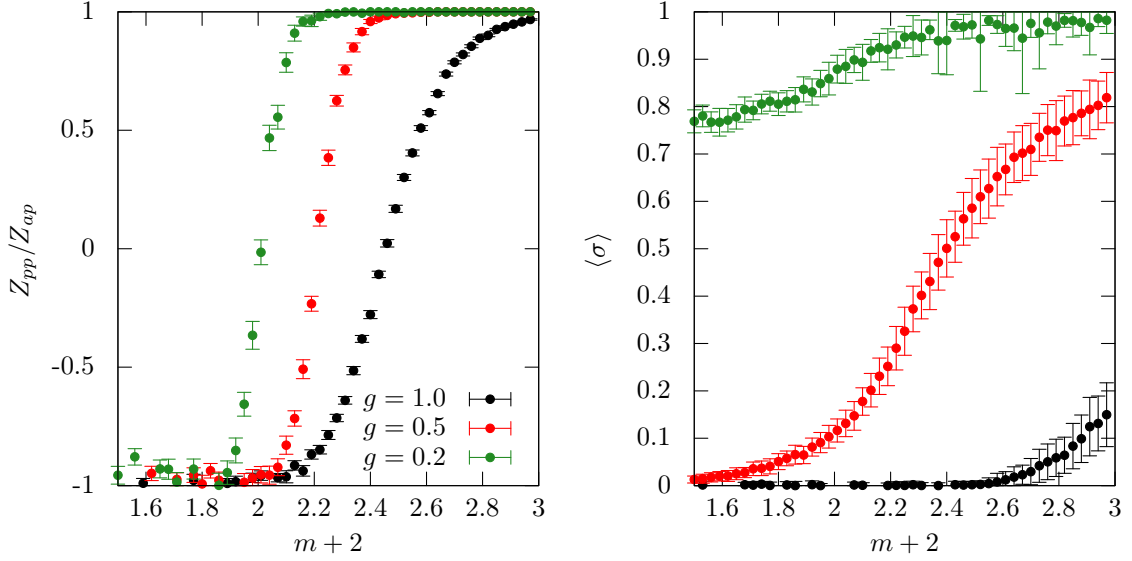


Figure 4.9.: On the left we plot the ratio  $Z_{pp}/Z_{ap}$  versus the bare mass  $M = m + 2$  for three different couplings. Here one can already get a first estimation of the critical point and the behaviour under the variation of  $g$ . On the right we see the corresponding average sign  $\langle\sigma\rangle$  for the same couplings. This is on a  $32 \times 32$  lattice with a statistics of  $10^7$  runs.

mass and coupling dependence of  $Z_{pp}/Z_{ap}$  for a lattice of extent  $32 \times 32$ . When increasing the coupling the point where  $Z_{pp} = 0$  is shifted to larger bare mass. We can therefore already anticipate the behaviour of the critical point, which follows the same behaviour. On the right side of fig. 4.9 the average sign  $\langle\sigma\rangle$  is shown for the same data. From this we see that at  $g = 1$ , even at high mass,  $\langle\sigma\rangle$  is close to zero. It is only at the smallest coupling and at larger  $m$  where the data can be considered to adequately represent the unquenched model.

In fig. 4.10 on the left side,  $Z_{pp}/Z_{ap}$  is plotted for various lattice volumes at fixed coupling  $g = 0.5$ . We perform a linear fit in the region where  $Z_{pp}/Z_{ap}$  is close to zero in order to obtain  $m_c$  which is defined as the point where the linear fit intersects with the zero axis. This is illustrated on the right of fig. 4.10 for a  $16 \times 16$  lattice. For all lattice extents good linear fits can be performed in the interesting regime.

The thermodynamic limit can be found by following the critical points on increasingly larger volumes. In fig. 4.11 we show a possible linear extrapolation to the thermodynamic limit of the obtained critical masses for two different couplings  $g = 0.5$  and  $g = 0.2$ . The linear fit is only using the three data points corresponding to the model at the three largest volumes. We observe different finite volume effects for the two couplings. At  $g = 0.5$ , the critical mass is shifted to larger bare mass, whereas at  $g = 0.2$ ,  $m_c$  is moving to lower bare mass. There is a coupling regime in between which seems less affected from finite volume effects.

In fig. 4.12 on the left we show the critical masses in the thermodynamic limit for five

#### 4. Supersymmetric Nonlinear $O(N)$ sigma Model

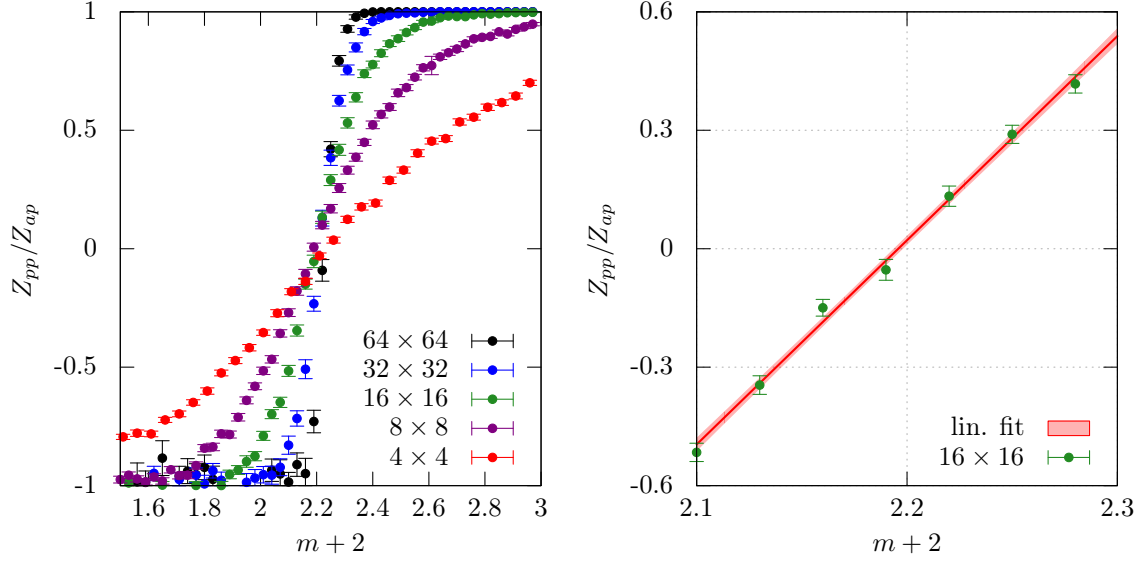


Figure 4.10.: On the left we plot  $Z_{pp}/Z_{ap}$  for fixed coupling  $g = 0.5$  for various lattice extents. At  $Z_{pp} = 0$  we obtain the critical bare mass  $m_c$ , which can be obtained by a linear fit in the region close to zero, as illustrated on the right with a one sigma error band. All data points come from statistics containing  $10^7$  complete sweeps.

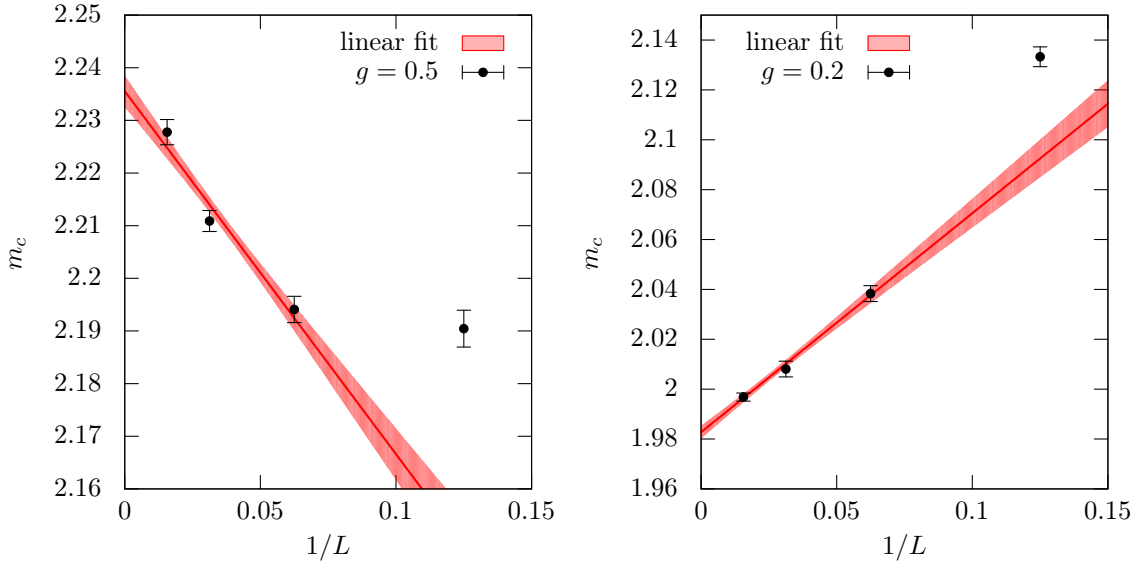


Figure 4.11.: We show the obtained, via linear fit of  $Z_{pp}/Z_{ap}$  in the region close to zero, critical masses  $m_c$  for various lattice extents. A linear fit, showing a one sigma error band, is performed in order to obtain a value of  $m_c$  in the thermodynamic limit. For these extrapolations only the three points corresponding to the simulations of the system with the largest lattice extents are used. On the left we show the situation for  $g = 0.5$  and on the right for  $g = 0.2$ .

different couplings. All points are obtained by fitting the critical mass from the three largest volumes  $16 \times 16$ ,  $32 \times 32$  and  $64 \times 64$  with a linear function. A quadratic plus linear function can be fitted through all data points in fig. 4.12 on the left and is describing the

behaviour of  $m_c(g)$  very well in the investigated regime of  $g \in [0.2, 1]$ . On the right side of fig. 4.12 we like to illustrate that also a tanh function can be used to characterise  $Z_{pp}/Z_{ap}$ , which showed to create identical critical masses as the procedure with the linear fit in the critical region.

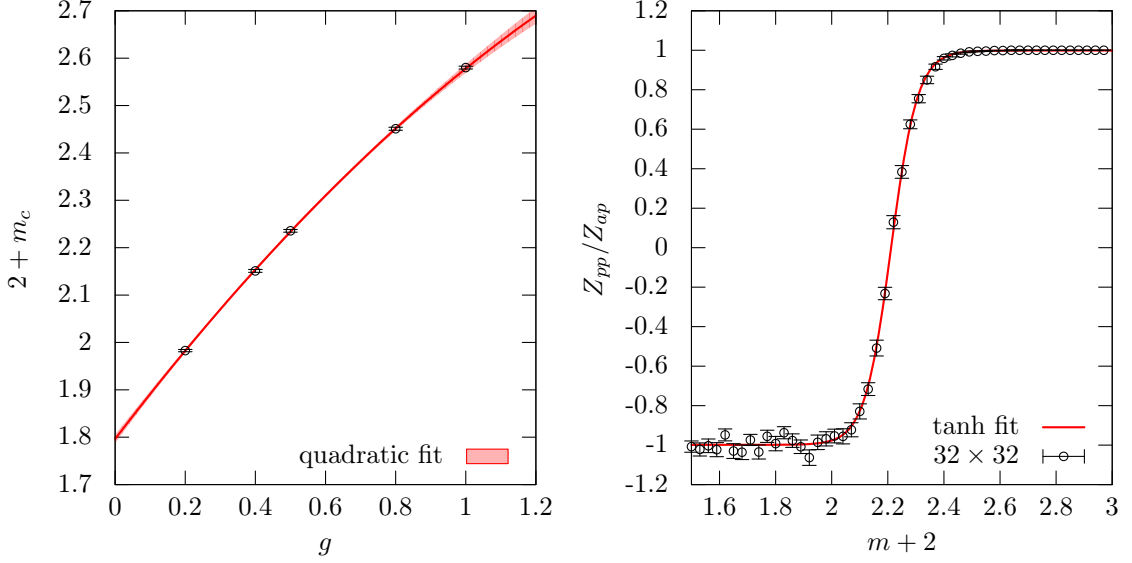


Figure 4.12.: On the left we illustrate the critical bare masses in the thermodynamic limit for various couplings. Additionally a quadratic fit is performed describing the behaviour of  $m_c$  in that regime of  $g$ . On the right side we show an alternative function, a tanh, which can also be used in order to determine the critical point where  $Z_{pp} = 0$ .

We have now tuned the bare mass such that our phase quenched system is at the chiral point where  $Z_{pp} = 0$ . This has been done for various couplings  $g$  and results in the thermodynamic limit are also obtained. Note that the numerical data from the phase quenched simulations can presumably only be considered to illustrate the physics of the full theory at extremely small couplings. In the next section we investigate how the fermionic and bosonic masses behave close to the critical point  $m_c$ .

### 4.12.3. Masses

In the following we analyse the mass spectrum of the phase quenched model. This is done by measuring the fermionic and bosonic correlator in time, considering the correlators projected to zero spatial momentum. Good fits where possible with  $A \cosh(m(t - L_t/2))$  for both the fermionic and the bosonic correlator. We will not distinguish the flavour of the fermionic loops and in the bosonic case use the correlator

$$C_\phi(t) = \phi(\tau)\phi(\tau+t) = \phi_r(\tau)\phi_r(\tau+t) + \phi_g(\tau)\phi_g(\tau+t). \quad (4.130)$$

In fig. 4.13 on the left side the fermionic masses  $m_\psi$  are plotted in the phase quenched scenario for the lattice extents  $16 \times 16$ ,  $32 \times 32$  and  $64 \times 64$  at fixed coupling  $g = 0.5$ . Starting at larger bare mass we observe a fermionic mass which is decreasing as we are

#### 4. Supersymmetric Nonlinear $O(N)$ sigma Model

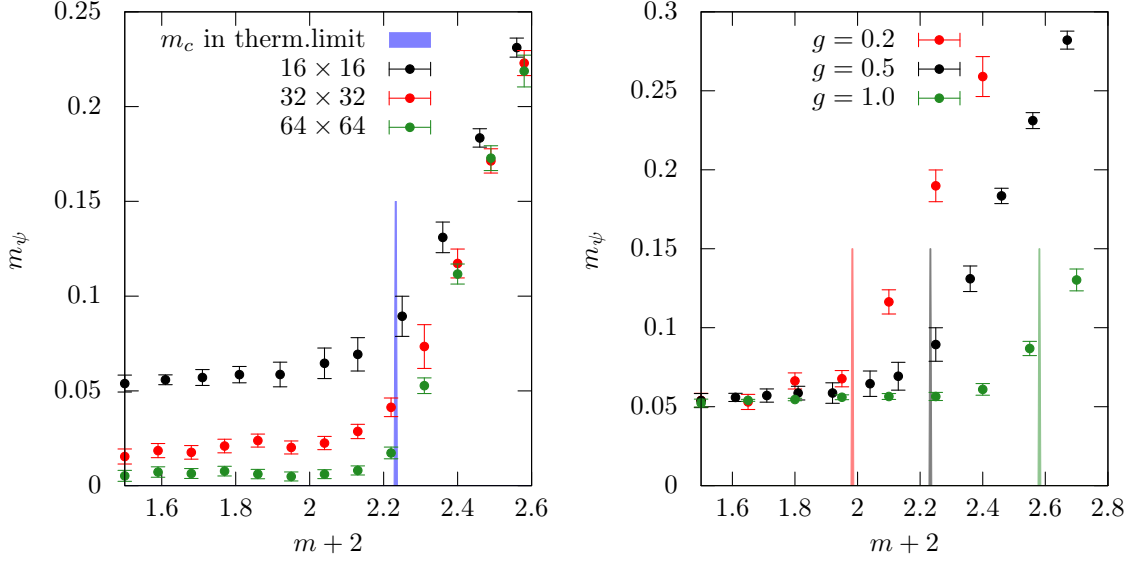


Figure 4.13.: On the left we plot the obtained fermionic masses for various lattice extents at fixed coupling  $g = 0.5$ . Additionally the value of  $m_c$  in the thermodynamic limit is shown. On the right the lattice extent is kept fixed at  $16 \times 16$  and the coupling is varied. We have again added the value of  $m_c$  in the thermodynamic limit in the according colour for each coupling. The statistics contain  $10^6$  complete sweeps.

approaching the critical regime from the right. Around the critical point of the bare mass scale the fermion obtains a very small mass which seems to become constant for  $m < m_c$ , this is specially true on larger lattices. When enlarging the volume the measured fermionic mass decreases around the critical point. This is an indication that  $m_\psi$  may zero in the thermodynamic limit in the regime of  $m < m_c$ . In the same figure we show the value of the critical mass  $m_c$  in the thermodynamic limit obtained by  $Z_{pp} = 0$ .

In fig. 4.13 on the right we consider a  $16 \times 16$  lattice for various couplings 0.2, 0.5 and 1.0. At low bare mass the fermionic mass  $m_\psi$  is identical for all the observed couplings. We also plot the three different critical masses  $m_c$  in the thermodynamic limit in fig. 4.13 on the right.

In fig. 4.14 on the left, we add the bosonic mass and illustrate both,  $m_\psi$  and  $m_\phi$  in the critical region at fixed coupling  $g = 0.5$  for two different lattice extents  $16 \times 16$  and  $32 \times 32$ . The two masses seem to meet in the vicinity of the critical point when going to larger volumes. On the right of fig. 4.14, we replot the data for the  $32 \times 32$  lattice and perform a linear fit for  $m_\psi$  in the declining region, i.e.  $m+2 \in [2.3, 3]$ . The boson mass  $m_\phi$  can be nicely fitted by a constant. If we consider the intersection of the linear fit describing the fermion mass with the constant value of the boson mass, we may argue that at this point the masses are degenerate. Even though still at finite volume this point already agrees with the critical value of  $m_c$  determined via  $Z_{pp}(m_c) = 0$ .

In fig. 4.15 on the left we show  $m_\psi$  and  $m_\phi$  for decreasing  $1/L$  at fixed coupling  $g$  at the critical point  $m_c$ . On the right of fig. 4.15 we take the continuum limit of the bosonic mass  $m_\phi$ . The bosonic mass at fixed coupling  $g = 0.5$  is obtained by fitting with the data

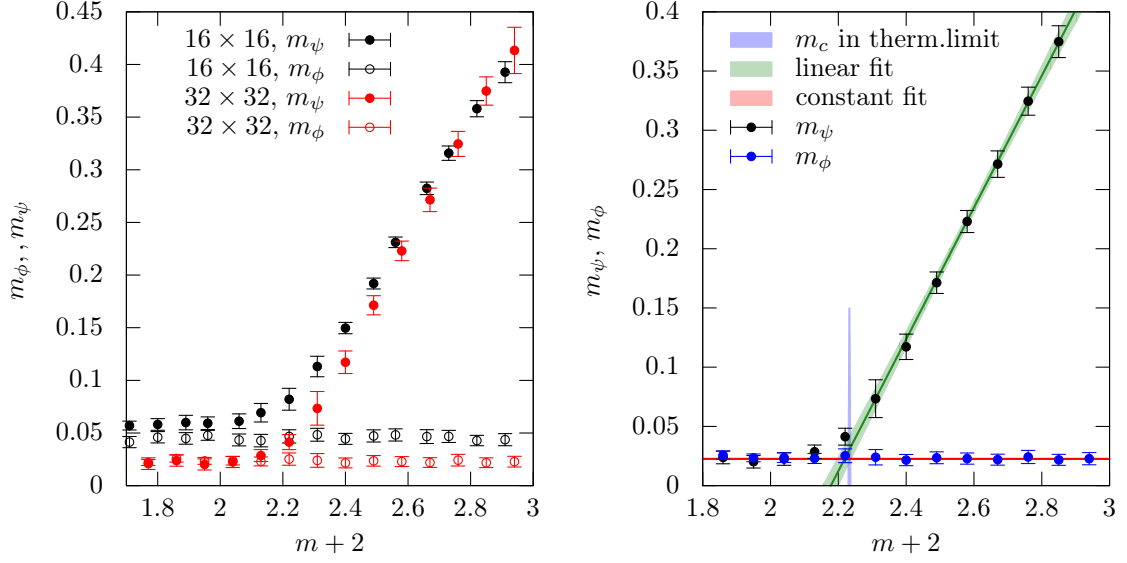


Figure 4.14.: On the left we show  $m_\psi$  and  $m_\phi$  are shown for two different lattice volumes at  $g = 0.5$ . On the right we perform a linear fit for  $m_\psi$  in the region  $m > m_\psi$  and a constant fit for  $m_\phi$ . Additionally  $m_c$  in the thermodynamic limit is shown. The statistics are again containing  $10^6$  complete sweeps.

points with a constant, as illustrated before in fig. 4.14 on the right. Keeping the physical length  $m_\psi L$  fixed and letting the lattice spacing  $a$  go to zero,  $m_\phi$  can be followed into the continuum limit. A linear extrapolation to the continuum limit is in agreement with a zero mass in the continuum. Note that this seems to hold for any fixed value of  $m_\psi L$  at fixed coupling.

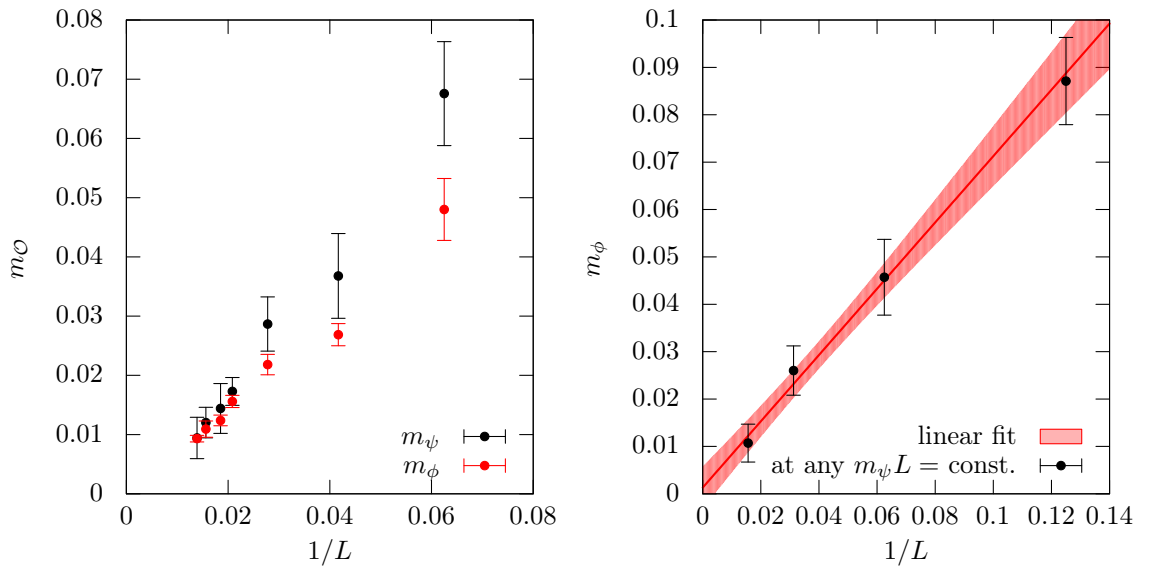


Figure 4.15.: On the left  $m_\psi$  and  $m_\phi$  are shown for various  $1/L$  at fixed  $g = 0.5$ . On the right  $m_\phi$  is plotted at fixed  $m_\psi L$  for various  $1/L$ .

#### 4.12.4. Uncertain phase diagram

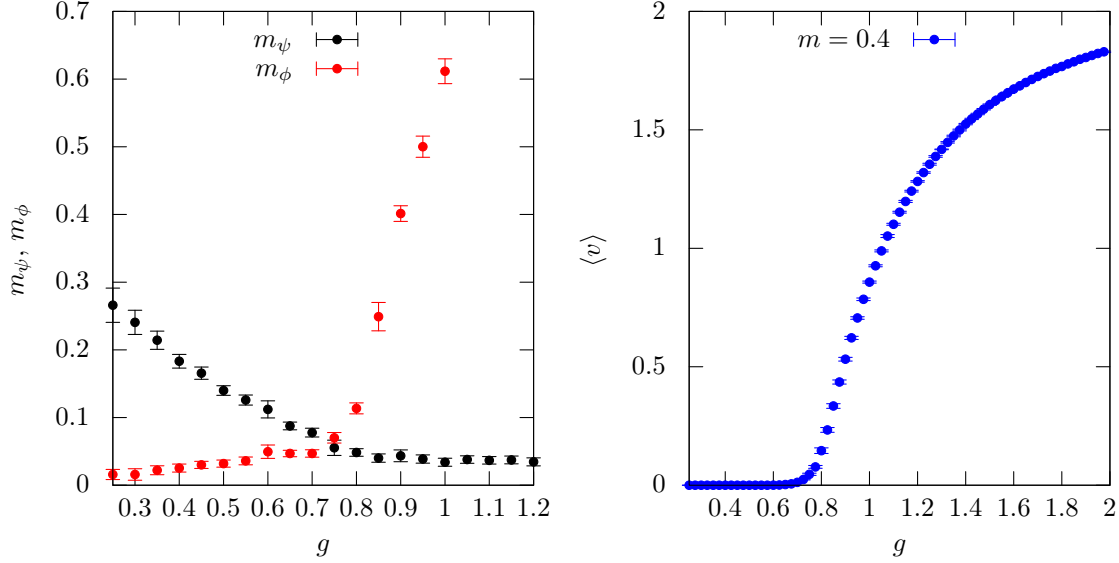


Figure 4.16.: In the left panel the fermionic and bosonic masses are plotted when varying the coupling. In the right panel we see how the vortex density suddenly obtains a non vanishing expectation value. We again only consider the phase quenched model. This is for a lattice of extent  $32 \times 16$ .

Before we investigated the system at couplings  $g \lesssim 1$ . We will now consider a system with fixed bare mass and vary the coupling. In fig. 4.16 on the left we show the behaviour of  $m_\psi$  and  $m_\phi$  for a lattice of size  $32 \times 16$  at fixed bare mass  $m = 0.4$  again in the phase quenched scenario. The critical point  $m_c$  is shifted to higher values when increasing the coupling. This means that at fixed bare mass  $m$  we should enter the fermion massless phase when enlarging the coupling. Exactly this can be observed on the left in fig. 4.16 where the fermionic mass is decreasing when the coupling is increased. In the non-supersymmetric nonlinear  $O(2)$  model we can observe a Kosterlitz-Thouless vortex unbinding transition [78] at a certain critical value of the coupling. We do not want to discuss this in detail here but state that we see such a vortex unbinding transition even in the supersymmetric version at some value of the coupling  $g_c$ . This is illustrated in fig. 4.16 on the right, where  $\langle v \rangle$  is the vortex density. It is interesting that around that critical coupling  $g_c$ , where this transition seems to occur, the bosonic mass, as seen on the left of the figure, suddenly rises quickly.

### 4.13. Conclusion and outlook

We established the fermion loop formulation and the bosonic bond formulation for the supersymmetric nonlinear  $O(N)$  model. The bosonic bond formulation showed to have a local source of a possibly fluctuating sign due to our choice of using also a Wilson derivative for the bosonic fields. In the case of a free Majorana fermion the partition function can be split up into topological sectors corresponding to the winding numbers of the fermion loops around the dimensions of the Euclidean torus. Those sectors hold all information about



the sign of the weight of any configuration in that sector. We encountered that this is no longer true for the supersymmetric version of the nonlinear sigma model if  $N > 2$ , since the closed fermion loops are no longer self-avoiding. Besides the possible sign problem in the loop formulation we encountered that the constraint  $\phi\psi = 0$ , which is needed to keep the continuum model supersymmetric, can contribute also with a negative sign.

For  $N = 2$  we only encounter the sign problem coming from the constraints. This however already spoils simulations in a large parameter region. We nevertheless presented numerical results for  $N = 2$  by considering the phase quenched model. In the quenched scenario we successfully determined the chiral point of the theory at which our data supports the expected picture of having a massless fermion and a massless boson in the continuum. First analysis also indicated that the phase diagram might be similar to the non-supersymmetric model which shows a Kosterlitz-Thouless vortex unbinding transition [78]. The drawback of the shown results is the fact that they describe the phase quenched model. Therefore one of the major future goals is to tackle the unquenched model by finding a reformulating without a sign problem. Another option is to stick to the current fermion loop formulation and perform a reweighting procedure in the parameter regions where the sign problem is mild. In a next step a Ward identity of supersymmetry should be numerically investigated and followed to the continuum limit in order to check if the chosen discretisation has the proper supersymmetric continuum limit. In prospect of using the bosonic bond formulation for a worm-like algorithm it would be interesting to check also the continuum limit of a lattice model with a symmetric boson derivative.

If the sign problem in the loop formulation can be solved for  $N > 2$ , we are specially motivated to create results for the very interesting case of  $N = 3$ , where already numerical results [41] exist.



## 5. Fermion sectors in Matrix-theory

Our goal is to provide a non-perturbative approach to investigate the phase structure of matrix quantum mechanics at finite temperature, as it is for example done in [79–84]. We investigate a one-dimensional matrix model which is obtained by dimensional reduction of a higher dimensional supersymmetric Yang-Mills theory and provide a formulation of the model that can be used to produce numerical data also including fermions. Trying to follow the common notational conventions in this field of research, we start by showing briefly how one obtains a one-dimensional matrix model by starting from a higher dimensional super Yang-Mills action and reducing the compact spatial dimensions. Afterwards the remaining time-like dimension will be discretised using Wilson fermions. After discretisation, we perform the hopping expansion of the fermion action and establish a fermion loop formulation. This enables us to express the partition function as a sum over all closed fermion loops which has been proven to be a well suited formulation for the use of a worm-like algorithm. In a second step we use a transfer matrix approach and deliver some results for the dimensionally reduced  $4d \mathcal{N} = 1$  super Yang-Mills model with symmetry group  $SU(2)$ . As will be seen, the generalisation of the loop and transfer matrix approach to arbitrary large  $N$  is trivial.

### 5.1. Motivation

String theorists became more interested in large  $N$  gauge theories due to the discoveries that  $U(N)$  gauge theories can be viewed as a low energy effective theory [42] of a stack of  $N$  D-branes [43]. A common conjecture following from this fact is that dimensionally reduced large- $N$   $10d U(N)$  super Yang Mills theory can serve as a non-perturbative formulation of superstring theories. If this former high dimensional gauge theory is reduced to one dimensions it is called a matrix theory [85]. If only reduced to two dimensions it is called matrix string theory [86] and if completely reduced to zero dimensions IIB matrix models [87]. Most of these models have been subject of various investigations, e.g. [79, 80, 88]. There are also other conjectured dualities between weakly coupled super gravity and strongly coupled large  $N$  gauge theories, via the AdS/CFT correspondence [44, 45], which was non-perturbatively investigated in [82].

Updating fermionic degrees of freedom with a worm-like algorithm, based on the idea of Prokof'ev and Svistunov [26], has shown to be a very efficient simulation method [27]. We are motivated to construct a fermion loop formulation for a dimensionally reduced super Yang Mills theory in order to create a tool, and in this field a yet unused formulation, to investigate non-perturbative physics in those models numerically.

## 5.2. Continuum model

In this section we highlight the main conceptual ideas on how a  $d$ -dimensional gauge theory is dimensionally compactified and reduced to one or zero dimensions. This section is strongly derived from [89] and is build up as follows. In a first subsection we define our model and the conventions. We then briefly explain the procedure of dimensional reduction and perform the complete dimensional reduction of all spatial dimensions. This leaves us with a matrix theory with one temporal dimension that we rotate to imaginary time.

### 5.2.1. Yang-Mills and adjoint fermion in $d$ dimensions

The Lagrangian of a Yang-Mills theory in  $d$  dimensions, of which one is time-like, can be written as

$$\mathcal{L} = \frac{1}{4} F_{\mu\nu}^a F^{\mu\nu a} - \frac{i}{2} \bar{\lambda}_\alpha^a (\gamma^\mu)_{\alpha\beta} (D_\mu \lambda_\beta)^a \quad (5.1)$$

where  $F_{\mu\nu}^a$  is the field strength tensor

$$F_{\mu\nu}^a = \partial_\mu X_\nu^a - \partial_\nu X_\mu^a + g f^{abc} X_\mu^b X_\nu^c \quad (5.2)$$

including the bosonic vector potentials  $X_\mu^a$  and fermions  $\lambda_\alpha^a$ . The index labelling the space time dimensions is  $\mu \in \{0, 1, \dots, d-1\}$ , where  $\mu = 0$  labels the time direction. The  $\gamma$  matrices correspond to the  $d$  Dirac matrices  $\gamma^\mu$  which satisfy the Clifford algebra  $\{\gamma^\mu, \gamma^\nu\} = 2\eta^{\mu\nu}$ , where  $\eta$  is the Minkowski metric. The subscript of  $\lambda_\alpha$  is the Dirac index  $\alpha$  and its range depends on the size of  $\gamma$  in  $d$ -dimensions, i.e the spinor nature. Further  $\bar{\lambda} = \lambda^\dagger \gamma^0$ . The bosonic and fermionic fields can be written as

$$X_\mu = X_\mu^a T^a \quad \text{and} \quad \lambda_\alpha = \lambda_\alpha^a T^a, \quad (5.3)$$

because they are elements of the Lie algebra of a compact semi-simple gauge group  $\mathcal{G}$ . The matrices  $T^a$  are the generators of the Lie algebra and they satisfy<sup>1</sup>

$$\text{Tr}\{T^a T^b\} = \frac{1}{2} \delta^{ab} \quad \text{and} \quad [T^a, T^b] = i f^{abc} T^c. \quad (5.4)$$

Let us already specify that we are dealing from now on only with  $SU(N)$  and therefore  $a = 1, \dots, N^2 - 1$ . The covariant derivative, involving the gauge field, is defined to be

$$(D_\mu \lambda)^a = \partial_\mu \lambda^a + g f^{abc} X_\mu^b \lambda^c, \quad (5.5)$$

where  $g$  stands for the coupling constant. The theory is invariant under the following gauge transformations

$$\lambda \rightarrow U \lambda U^{-1} \quad \text{and} \quad X_\mu \rightarrow U X_\mu U^{-1} - \frac{i}{g} (\partial_\mu U) U^{-1} \quad (5.6)$$

for  $U \in SU(N)$ . It will be convenient to drop indices sometimes and write eq.(5.1) as

$$\mathcal{L} = \text{Tr} \left\{ \frac{1}{2} F^2 - i \bar{\lambda} \not{D} \lambda \right\}. \quad (5.7)$$

---

<sup>1</sup>By this we set the generators to be  $T^a = \sigma^a/2$ , where  $\sigma^a$  are the generalised pauli matrices, e.g. the Pauli matrices for  $SU(2)$ , the Gellmann matrices for  $SU(3)$ .

### 5.2.2. Spin structure and SUSY

The nature of the spinor depends strongly on the number of spatial and time-like dimensions of the system. It is important to understand the spin structure in order to formulate a  $d$ -dimensional Yang-Mills action which is supersymmetric. Let us therefore quickly give an overview of the possible spin structures and conclude which models can be made supersymmetric. Here we are only considering systems with one time-like dimension.

In the dimensions  $d = 0, 1, 2, 3$  and 4 (modulo 8) there exists a Majorana condition. This means that there exists a basis such that all Dirac matrices are purely real or purely imaginary. In that case all spinors can be chosen to be purely real or purely imaginary while Lorentz symmetry can still be preserved. Essentially the Majorana condition is cutting the degrees of freedom in half. Weyl spinors are obviously realisable in any even dimension. In literature there exist many tables giving an overview on what bases are possible in which dimensions, also including additional time-like dimensions and supersymmetries. For more information on this we refer to [90]. The only thing that we want to stress here is that it is only possible to have supersymmetry in a model described by eq.(5.1) if the physical bosonic and fermionic degrees of freedom match. As explained in [89] and shown in [90] this is true in  $d = 10$  with Majorana Weyl spinors, in  $d = 6$  with Weyl spinors, in  $d = 4$  with Weyl or Majorana spinors and in  $d = 3$  with Majorana spinors. Note that the just made statements are only true if there is only one time-like dimension. If set up in one of these mentioned dimensions the model in eq.(5.1) is invariant under the supersymmetry

$$\delta X_\mu^a = \frac{i}{2} \bar{\epsilon} \gamma_\mu \lambda^a \quad \text{and} \quad \delta \lambda^a = -F_{\mu\nu}^a S^{\mu\nu} \epsilon, \quad (5.8)$$

where  $\epsilon$  is a constant Majorana spinor and

$$S^{\mu\nu} = \frac{1}{4} [\gamma^\mu, \gamma^\nu]. \quad (5.9)$$

Note that the supersymmetry only holds if the equation of motion is applied.

### 5.2.3. Dimensional reduction

Since the reduction of a dimension is identical for all spatial dimensions, we can illustrate the basic procedure with a two-dimensional space time  $x = (\tau, z)$  where  $z \equiv x_1$  is the spatial dimension we want to reduce and  $\tau$  labels the then remaining time direction, i.e.  $\tau \equiv x_0$ . We write the dependence on space and time of a field separately like  $X(\tau, z)$ . For simplification reasons we simply drop the spatial index  $\mu$  in the following. We expand in the compactified spatial dimensions and write

$$X(\tau, z) = \sum_n X_n(\tau) e^{inz}. \quad (5.10)$$

Note that writing the exponential amounts to the assumption of the dimension in question to have the geometry of a circle with radius  $R$ . If we consider the resulting Klein-Gordon equation

$$\square X_n(\tau) - \left(\frac{n}{R}\right)^2 X_n(\tau) = 0, \quad (5.11)$$

we can argue that we only keep the  $n = 0$  mode from the expansion and use the notation  $X(\tau) = X_{n=0}(\tau)$ . This is only valid if we assume that  $R$  is small enough, making all higher

## 5. Fermion sectors in Matrix-theory

modes incredibly heavy. Since we are interested in a low energy theory we can allow the heavy modes to be removed from the system.

Turning now back to our  $d$ -dimensional model we can perform exactly this reduction of all spatial dimensions for all fields  $X_\mu^a$  and  $\lambda_\alpha^a$ , assuming they are constant in space and only evolve in time. First we perform the dimensional reduction of the field strength tensor arising in eq.(5.1)

$$\begin{aligned}
F_{\mu\nu}^a F^{\mu\nu a} &= \left( \partial_\mu X_\nu^a - \partial_\nu X_\mu^a + g f^{abc} X_\mu^b X_\nu^c \right) \left( \partial^\mu X^{\nu a} - \partial^\nu X^{\mu a} + g f^{alm} X^{\mu l} X^{\nu m} \right) \\
&= \partial_\mu X_\nu^a \partial^\mu X^{\nu a} - \partial_\mu X_\nu^a \partial^\nu X^{\mu a} - \partial_\nu X_\mu^a \partial^\mu X^{\nu a} + \partial_\nu X_\mu^a \partial^\nu X^{\mu a} \\
&\quad + g f^{abc} X_\mu^b X_\nu^c \partial^\mu X^{\nu a} - g f^{abc} X_\mu^b X_\nu^c \partial^\nu X^{\mu a} \\
&\quad + \partial_\mu X_\nu^a g f^{alm} X^{\mu l} X^{\nu m} - \partial_\nu X_\mu^a g f^{alm} X^{\mu l} X^{\nu m} \\
&\quad + g^2 f^{abc} X_\mu^b X_\nu^c f^{alm} X^{\mu l} X^{\nu m}.
\end{aligned} \tag{5.12}$$

We can remove all spatial derivatives  $\partial_i = 0$  with  $i \in \{1, 2, \dots, d-1\}$  and the only derivative remaining will be  $\partial_0$ .

$$\begin{aligned}
(\partial_\mu X_\nu^a - \partial_\nu X_\mu^a) (\partial^\mu X^{\nu a} - \partial^\nu X^{\mu a}) &= \partial_\mu X_\nu^a \partial^\mu X^{\nu a} - \partial_\mu X_\nu^a \partial^\nu X^{\mu a} \\
&\quad - \partial_\nu X_\mu^a \partial^\mu X^{\nu a} + \partial_\nu X_\mu^a \partial^\nu X^{\mu a} \\
&= \partial_0 X_\nu^a \partial^0 X^{\nu a} - \partial_0 X_0^a \partial^0 X^{a0} \\
&\quad - \partial_0 X_0^a \partial^0 X^{a0} + \partial_0 X_\mu^a \partial^0 X^{a\mu} \\
&= 2\partial_0 X_i^a \partial^0 X^{ai}.
\end{aligned} \tag{5.13}$$

The terms in eq.(5.12) involving only one structure constant will cancel and we are left with

$$\begin{aligned}
g^2 f^{abc} X_\mu^b X_\nu^c f^{alm} X^{\mu l} X^{\nu m} &= g^2 f^{abc} f^{alm} X_\mu^b X_\nu^c X^{\mu l} X^{\nu m} \\
&= -2g^2 \text{Tr} \{ [X_\mu, X_\nu] [X_\mu, X_\nu] \},
\end{aligned} \tag{5.14}$$

where we introduced commutator brackets in order to write the expression in a more elegant way. Note that, since  $[T^a, T^b] = i f^{abc} T^c$  yields an  $i$ , as defined in eq.(5.4), we have to account for  $i^2$  with a minus sign. We now obtain, respecting the prefactor of  $1/4$  in eq.(5.1),

$$\text{Tr} \left\{ \frac{1}{2} F^2 \right\} = \frac{1}{g^2} \text{Tr} \left\{ (\partial_0 X_i)^2 - \frac{1}{2} [X_\mu, X_\nu] [X_\mu, X_\nu] \right\} \tag{5.15}$$

where  $g$  has been absorbed in a redefinition of the fields, i.e.  $X \rightarrow X/g$ . Using the covariant derivative

$$D_0 = \partial_0 - i[X_0, \cdot] \tag{5.16}$$

this can be rewritten as

$$\text{Tr} \left\{ \frac{1}{2} F^2 \right\} = \frac{1}{g^2} \text{Tr} \left\{ (D_0 X_i)^2 - \frac{1}{2} [X_i, X_j] [X_i, X_j] \right\}. \tag{5.17}$$

Let's now write out the fermionic term explicitly

$$\text{Tr} \{ -i \bar{\lambda} \gamma D \lambda \} = -\frac{i}{2} \bar{\lambda}_\alpha^a (\gamma^\mu)_{\alpha\beta} (\partial_\mu \lambda_\beta^a + g f^{abc} X_\mu^b \lambda_\beta^c). \tag{5.18}$$

Due to dimensional reduction of all spatial dimensions we can drop all non-temporal derivatives and obtain

$$-\frac{i}{2}\bar{\lambda}_\alpha(\gamma^0)_{\alpha\beta}\partial_0\lambda_\beta^a - \frac{i}{2}\bar{\lambda}_\alpha(\gamma^\mu)_{\alpha\beta}gf^{abc}X_\mu^b\lambda_\beta^c = \frac{1}{g^2}\text{Tr}\{-i\bar{\lambda}\gamma^0 D_0\lambda - \bar{\lambda}\gamma^i[X_i, \lambda]\}, \quad (5.19)$$

where the covariant derivative  $D_0$  is used again. In order to pull out the factor  $1/g^2$  we again rescaled the fields by  $1/g$ . As often seen, the gamma matrix appearing in  $\bar{\lambda} = \lambda^\dagger\gamma^0$ , can be pulled out and the whole expression can be rewritten in terms of new gamma matrices  $\Gamma^i = \gamma^0\gamma^i$  like

$$\text{Tr}\{-i\lambda^* D_0\lambda - \lambda^*\Gamma^i[X_i, \lambda]\}, \quad (5.20)$$

where we used that  $\gamma^0\gamma^0 = \mathbb{1}$ . If the system lived in a number of dimensions in which there exists a Majorana condition, we can drop the complex conjugation since all  $\lambda_\alpha^a$  are real. If there is no such condition we can double the length of  $\lambda_\alpha^a$  and rewrite it with real entries. The complete action can now be obtained by combining the bosonic and the fermionic parts to

$$S_M = \frac{1}{g^2} \int dx_0 \text{Tr} \left\{ (D_0 X_i)^2 - \frac{1}{2} [X_i, X_j] [X_i, X_j] - i\lambda D_0\lambda - \lambda_\alpha(\Gamma^i)_{\alpha\beta} [X_i, \lambda_\beta] \right\}. \quad (5.21)$$

Let us now move from our Minkowski metric  $\eta = \text{diag}\{-1, +1, +1, \dots, +1\}$  to the Euclidean one by performing an analytic continuation to “imaginary time”. We can achieve this by setting

$$X_0^a = iX_t^a \quad \text{and} \quad \gamma^0 = i\gamma^t. \quad (5.22)$$

The derivative with respect to time is then  $\partial_0 \rightarrow -i\partial_t$  and the measure  $dx_0 \rightarrow i dt$ . From now on we will only use the action in Euclidean space time

$$S = \frac{1}{g^2} \int_0^\beta dt \text{Tr} \left\{ (D_t X_i)^2 - \frac{1}{2} [X_i, X_j] [X_i, X_j] + \lambda D_t\lambda + \lambda_\alpha(\Gamma^i)_{\alpha\beta} [X_i, \lambda_\beta] \right\}, \quad (5.23)$$

where  $\beta \equiv 1/T$  and  $T$  can be interpreted as the temperature of the system if the fermionic degrees of freedom obey anti-periodic boundary conditions. Note that there is an overall factor of  $i$ , which in the Boltzmann weight forms a minus sign, i.e.  $\exp[-S]$ . We obtained a one-dimensional matrix model with a  $N \times N$  hermitian matrix  $X_t$ , corresponding to the gauge field in temporal direction. Additionally there are the bosonic matrices  $X_i$ , which of course are also  $N \times N$ , and come from the spatial components of the gauge field. The index  $i$  denotes these spatial components and runs from 1 to  $d-1$ . The  $\lambda_\alpha$  are  $N \times N$  fermionic matrices that come from the spinor living in the adjoint.

Additionally a system could be considered which has fields that are independent of space and time. This fact lets us drop also all the kinetic terms in temporal direction, i.e. “freezing” our system completely, giving<sup>2</sup>

$$S_{frozen} = \frac{1}{g^2} \text{Tr} \left\{ -\frac{1}{2} [X_\mu, X_\nu] [X_\mu, X_\nu] + \lambda_\alpha(\Gamma^\mu)_{\alpha\beta} [X_\mu, \lambda_\beta] \right\}. \quad (5.24)$$

<sup>2</sup>Note that in a lot of work the fields are rescaled  $X_\mu \rightarrow 2^{-\frac{1}{4}}X_\mu$  and  $\lambda_\alpha \rightarrow 2^{\frac{1}{8}}\lambda_\alpha$ . This changes the prefactors in the action, e.g. the potential term is then  $\frac{1}{4}[X_\mu, X_\nu][X_\mu, X_\nu]$ , further the measure is changed. See appendix of [89].

Note that the temporal derivatives have been dropped but not the interaction with the temporal component of the gauge field. Even though the fields are constant in all space time dimensions there are non-trivial constant configurations appearing in the partition function. It is astonishing that without any dynamics it is the non-abelian nature that gives rise to non-trivial structures even in a completely “frozen” system.

### 5.3. Discretised $4d \mathcal{N} = 1$ super Yang-Mills reduced to $1d$

In this section we consider a  $4d$  super Yang-Mills model with one supersymmetry that is dimensionally reduced to one temporal direction, accordingly to the description given in the previous section. This model is then discretised using a Wilson derivative for the fermions.

#### 5.3.1. Continuum model

Consider the action describing a model with four supercharges, as investigated in [80], which is defined in Euclidean space time by

$$S = \frac{1}{g^2} \int_0^\beta dt \text{Tr} \left\{ (D_t X_i)^2 - \frac{1}{2} [X_i, X_j]^2 + \bar{\lambda} D_t \lambda - \bar{\lambda} \sigma_i [X_i, \lambda] \right\}. \quad (5.25)$$

It is obtained by dimensionally reducing a  $4d \mathcal{N} = 1$   $SU(N)$  super Yang-Mills theory to one dimension. The covariant derivative  $D_t = \partial_t - i[A(t), \cdot]$  contains the hermitian  $N \times N$  matrix  $A(t)$ , which is the time component of the gauge field which was denoted by  $X_0(t)$  in the previous section. The bosonic hermitian  $N \times N$  matrices  $X_i(t)$  are corresponding to the three components of the gauge field in the compactified and reduced dimensions  $i = 1, 2, 3$ . The fermions are described by  $\bar{\lambda}_\alpha(t)$  and  $\lambda_\alpha(t)$ , which are  $N \times N$  matrices with complex Grassmann entries and  $\alpha = 0, 1$ . The Dirac structure is then given by the  $2 \times 2$  Pauli-matrices

$$\sigma_1 = \begin{pmatrix} 0 & 1 \\ 1 & 0 \end{pmatrix}, \quad \sigma_2 = \begin{pmatrix} 0 & -i \\ i & 0 \end{pmatrix} \quad \text{and} \quad \sigma_3 = \begin{pmatrix} 1 & 0 \\ 0 & -1 \end{pmatrix}. \quad (5.26)$$

Note that we could have chosen real Grassmann fields with  $4 \times 4$   $\gamma$  matrices replacing the Pauli matrices and  $\alpha = 0, 1, 2, 3$  due to the Majorana condition in  $4d$ . The fields live in the adjoint representation, we can write them as  $\lambda_\alpha = \lambda_\alpha^a T^a$ , where  $T^a$  are the generators of the symmetry group. The same of course applies for the bosonic fields. We take the symmetry group to be  $SU(N)$  and therefore  $a = 1, 2, \dots, N^2 - 1$ . The coupling parameter  $g^2$  can be absorbed by a rescaling of the matrices and the time coordinate  $t$  [80].

#### 5.3.2. Lattice

We will discretise our system by introducing a one-dimensional lattice in the temporal dimension. In one dimension the Wilson derivative we use for the fermions is reduced to a directed covariant derivative which is what we also use for the bosonic field. Analogous to [84, 88] we expect the lattice action then to be finite and will flow without fine tuning to the correct supersymmetric continuum theory when the lattice spacing is set to zero.



This was numerically tested in [83] for the model with 16 supercharges.

The temporal dimension is discretised in  $L_t$  time steps, labelled with  $t = 0, 1, \dots, L_t - 1$ , each separated by a lattice spacing  $a$ , which for convenience will mostly be set to one. Let us write  $\phi(t)$  for the field living on the lattice on a time-slice  $t$  for the corresponding field  $X(t)$  in the continuum, therefore also  $\phi_i^a(t)$  for  $X_i^a(t)$  in the component notation. For the fermionic fields  $\lambda(t)$  and  $\bar{\lambda}(t)$ , we simply use  $\psi(t)$  and  $\bar{\psi}(t)$ , respectively. The gauge field in temporal direction  $A(t)$  will be described by the gauge link fields  $U(t)$  from site  $t$  to the next  $t + a$ . The integral over time in the action  $S$  then becomes a sum over all discrete time-steps in the lattice action  $\hat{S}$ , i.e.

$$S = \int_0^\beta dt \mathcal{L}[A(t), X_i(t), \bar{\lambda}(t), \lambda(t)] \rightarrow \hat{S} = \sum_{t=0}^{L_t} \hat{\mathcal{L}}[U(t), \phi_i(t), \bar{\psi}(t), \psi(t)] . \quad (5.27)$$

The measure

$$\int \mathcal{D}U \mathcal{D}\phi \mathcal{D}\bar{\psi} \mathcal{D}\psi \quad (5.28)$$

of the path integral is defined by

$$\int \mathcal{D}U \mathcal{D}\phi \mathcal{D}\bar{\psi} \mathcal{D}\psi = \prod_{t=0}^{L_t-1} \prod_{i=1}^3 \prod_{\alpha=0}^1 \prod_{a=1}^{N^2-1} \int dU(t) d\phi_i^a(t) d\bar{\psi}_\alpha^a(t) d\psi_\alpha^a(t) , \quad (5.29)$$

where  $N^2 - 1$  is the number of generators of the  $SU(N)$  group. In the following we will construct the bosonic and fermionic lattice actions.

### 5.3.3. Boson lattice action

Let's consider the bosonic part of eq.(5.25), which is

$$S_B = \frac{1}{g^2} \int_0^\beta dt \text{Tr} \left\{ (D_t X_i)^2 - \frac{1}{2} [X_i, X_j]^2 \right\} , \quad (5.30)$$

with  $D_t = \partial_t - i[A(t), \cdot]$ . When written out in components, this reads

$$S_B = \frac{1}{g^2} \int_0^\beta dt \left\{ \frac{1}{2} D_t X_i^a(t) D_t X_i^a(t) + \frac{1}{4} f^{abc} f^{alm} X(t)_i^b X(t)_j^c X(t)_i^l X(t)_j^m \right\} , \quad (5.31)$$

Taking the model onto the lattice we find

$$\hat{S}_B = \frac{1}{g^2} \sum_{t=0}^{L_t-1} \text{Tr} \left\{ \hat{D}_t \phi_i(t) \hat{D}_t \phi_i(t) - \frac{1}{2} [\phi_i(t), \phi_j(t)]^2 \right\} , \quad (5.32)$$

where the covariant derivative is the covariant forward derivative

$$\hat{D}_t \phi_i(t) = U(t) \phi_i(t+1) U^\dagger(t) - \phi_i(t) , \quad (5.33)$$

which is identical to the choice made in [79]. Let us work out the kinetic term explicitly

$$\begin{aligned} \text{Tr} \left[ \hat{D}_t \phi_i(t) \right]^2 &= \text{Tr} \left[ (U(t) \phi_i(t+1) U^\dagger(t) - \phi_i(t)) (U(t) \phi_i(t+1) U^\dagger(t) - \phi_i(t)) \right] \\ &= \text{Tr} \left[ U(t) \phi_i(t+1)^2 U^\dagger(t) - U(t) \phi_i(t+1) U^\dagger(t) \phi_i(t) \right. \\ &\quad \left. - \phi_i(t) U(t) \phi_i(t+1) U^\dagger(t) + \phi_i(t)^2 \right] , \end{aligned} \quad (5.34)$$

## 5. Fermion sectors in Matrix-theory

where we used that  $U(t)U^\dagger(t) = \mathbb{1}$ . Since the fields live in the adjoint representation, we can write  $\phi_i(t) = \phi_i^a(t)T^a$ , in order to write the kinetic term of the lattice action in component fields

$$\begin{aligned} \text{Tr} \left[ \hat{D}_t \phi_i(t) \right]^2 &= \phi_i^a(t+1) \phi_i^b(t+1) \text{Tr} \left[ U(t) T^a T^b U^\dagger(t) \right] + \phi_i^a(t) \phi_i^b(t) \text{Tr} \left[ T^a T^b \right] \\ &\quad - \phi_i^a(t+1) \phi_i^b(t) \text{Tr} \left[ U(t) T^a U^\dagger(t) T^b \right] \\ &\quad - \phi_i^a(t) \phi_i^b(t+1) \text{Tr} \left[ U(t) T^a U^\dagger(t) T^b \right], \end{aligned} \quad (5.35)$$

Using  $\text{Tr}[T^a T^b] = \delta^{ab}/2$  and the cyclic property of the trace simplifies to

$$\text{Tr} \left[ \hat{D}_t \phi_i(t) \right]^2 = \frac{1}{2} \phi_i^a(t+1)^2 + \frac{1}{2} \phi_i^a(t)^2 - 2 \phi_i^a(t+1) \phi_i^b(t) \text{Tr} \left[ U(t) T^a U^\dagger(t) T^b \right]. \quad (5.36)$$

Note that due to the sum over all time steps in the action we can combine the squared terms. Plugging the derived expression back into eq.(5.32) we get the full bosonic lattice action of the form

$$\hat{S}_B = \frac{1}{g^2} \sum_{t=0}^{L_t-1} \left\{ -2 \phi_i^a(t+1) \phi_i^b(t) \text{Tr} \left[ U(t) T^a U^\dagger(t) T^b \right] + \phi_i^a(t)^2 + \frac{1}{4} V(t)^2 \right\} \quad (5.37)$$

where we introduced  $V^2 = V_{ij}^a V_{ij}^a$  with  $V_{ij}^a = f^{abc} \phi_i^b(t) \phi_j^c(t)$ . The boundary conditions for the bosonic fields are periodic, meaning that  $\phi_i^a(L_t) = \phi_i^a(0)$ . The static diagonal gauge is a simplification [91] that seems to be a common option [79, 80]. Nevertheless, let us consider the option of transforming every gauge link  $U'(t) = g_t U(t) g_{t+1}^{-1}$ , such that  $U'(t) = \mathbb{1}$ . This can be done up until the last link where  $U'(L_t - 1) = g_{L_t-1} U(L_t - 1) g_0^{-1}$  is a general  $SU(N)$  matrix. This is known as the temporal gauge. The action in temporal gauge can then be expressed by

$$\begin{aligned} \hat{S}_B &= \frac{1}{g^2} \sum_{t=0}^{L_t-2} \left\{ -\phi_i^a(t+1) \phi_i^a(t) + \phi_i^a(t)^2 + \frac{1}{4} V(t)^2 \right\} \\ &\quad + \frac{1}{g^2} \left\{ -2 \phi_i^a(0) \phi_i^b(L_t - 1) \text{Tr} \left[ U T^a U^\dagger T^b \right] + \phi_i^a(L_t - 1)^2 + \frac{1}{4} V(L_t - 1)^2 \right\}, \end{aligned} \quad (5.38)$$

where we use the notation  $U \equiv U(L_t - 1)$ , since there is only one dynamic gauge link left. We see that the temporal hops are diagonal in  $i$  and  $a$  up until the last link at which the gauge field allows non-diagonal hops in  $a$ .

### 5.3.4. Fermion lattice action

Consider the fermionic part of the action in eq.(5.25), which is

$$S_F = \frac{1}{g^2} \int_0^\beta dt \text{Tr} \left\{ \bar{\lambda} D_t \lambda - \bar{\lambda} \sigma_i [X_i, \lambda] \right\}. \quad (5.39)$$

In the lattice formulation this is

$$\hat{S}_F = \frac{1}{g^2} \sum_{t=0}^{L_t-1} \text{Tr} \left\{ \bar{\psi}(t) \partial^\mathcal{W} \psi(t) - \bar{\psi}(t) \sigma_i [\phi_i(t), \psi(t)] \right\}, \quad (5.40)$$

where we choose to use Wilson fermions. Leaving away the lattice gauge field  $U$  for now, the Wilson derivative is

$$\partial^{\mathcal{W}} = \hat{\partial}^S - \Delta^{\mathcal{W}}, \quad (5.41)$$

with  $\hat{\partial}^S$  being the symmetric lattice derivative  $\hat{\partial}^S \psi(t) = \frac{1}{2a}[\psi(t+1) - \psi(t-1)]$ . Note, that since we only have one dimension the Wilson term reduces to

$$\Delta^{\mathcal{W}} = \frac{ra}{2} \hat{\partial}_t^+ \hat{\partial}_t^-, \quad (5.42)$$

where  $\hat{\partial}_t^+$  is the forward derivative  $\hat{\partial}_t^+ \psi(t) = \frac{1}{a}[\psi(t+1) - \psi(t)]$  and  $\hat{\partial}_t^-$  is the backward derivative  $\hat{\partial}_t^- \psi(t) = \frac{1}{a}[\psi(t) - \psi(t-1)]$ . In the one-dimensional case, setting  $a = 1$  and  $r = 1$ , we get

$$\begin{aligned} \bar{\psi}(t) \left( \hat{\partial}^S - \frac{1}{2} \hat{\partial}_t^+ \hat{\partial}_t^- \right) \psi(t) &= \bar{\psi}(t) \frac{1}{2} [\psi(t+1) - \psi(t-1)] \\ &\quad - \frac{1}{2} \bar{\psi}(t) [\psi(t+1) - 2\psi(t) + \psi(t-1)] \end{aligned} \quad (5.43)$$

$$= \bar{\psi}(t) \psi(t) - \bar{\psi}(t) \psi(t-1) = \bar{\psi}(t) \hat{\partial}_t^- \psi(t), \quad (5.44)$$

which shows that only directed fermion hops are allowed. In the following we will use fermions hopping forward in time and stick to even lattice extents. Using this expression and adding the gauge link variables we obtain the fermionic lattice action

$$\hat{S}_F = \frac{1}{g^2} \sum_{t=0}^{L_t-1} \text{Tr} \left\{ (m+1) \bar{\psi}(t) \psi(t) - \bar{\psi}(t) U(t) \psi(t+1) U(t)^{-1} - \bar{\psi}(t) \sigma_i [\phi_i(t), \psi(t)] \right\}, \quad (5.45)$$

where we introduced the bare mass parameter  $m$ . In temporal gauge and component notation we find

$$\begin{aligned} \hat{S}_F &= \frac{1}{g^2} \sum_{t=0}^{L_t-2} \left[ -\frac{1}{2} \bar{\psi}_\alpha^a(t) \psi_\alpha^a(t+1) + \frac{(m+1)}{2} \bar{\psi}_\alpha^a(t) \psi_\alpha^a(t) - \frac{1}{2} \bar{\psi}_\alpha^a(t) (\sigma_i)_{\alpha\beta} i f^{abc} \phi_i^b \psi_\beta^c(t) \right] \\ &\quad + \frac{1}{g^2} \left[ -\bar{\psi}_\alpha^a(L_t-1) \psi_\alpha^b(0) \text{Tr} \left\{ T^a U T^b U^{-1} \right\} + \frac{(m+1)}{2} \bar{\psi}_\alpha^a(L_t-1) \psi_\alpha^a(L_t-1) \right. \\ &\quad \left. - \frac{1}{2} \bar{\psi}_\alpha^a(L_t-1) (\sigma_i)_{\alpha\beta} i f^{abc} \phi_i^b \psi_\beta^c(L_t-1) \right], \end{aligned} \quad (5.46)$$

where the first line corresponds to the first  $L_t - 1$  time steps and the second and third line to the last link of the system in which the gauge field dynamics enter.

## 5.4. Fermion loop formulation

In this section we will perform a hopping expansion of the fermionic lattice action and reformulate the fermion with new degrees of freedom called occupation numbers. In this formulation the Grassmann integral in the partition function is expressed as a sum over closed fermion loop configurations.

### 5.4.1. Hopping expansion

Consider the lattice action from eq.(5.46). Assuming for now that  $U = 1$  and dropping an overall prefactor of  $1/(2g^2)$ , we find in component notation

$$\hat{S}_F = \sum_{t=0}^{L_t-1} \left[ -\bar{\psi}_\alpha^a(t) \psi_\alpha^a(t+1) + \bar{\psi}_\alpha^a(t) \Phi_{\alpha\beta}^{ac}(t) \psi_\beta^c(t) \right], \quad (5.47)$$

where we defined

$$\Phi_{\alpha\beta}^{ac}(t) = (m+1)\delta^{ac}\delta_{\alpha\beta} - (\sigma_i)_{\alpha\beta} i f^{abc} \phi_i^b(t), \quad (5.48)$$

which is an interaction matrix living on the time slices connecting  $\bar{\psi}_\alpha^a(t)$  with  $\psi_\beta^c(t)$  and in which only the sum over  $b$  and  $i$  is implicit. The hopping expansion of the action in component notation then becomes

$$\exp(-\hat{S}_F) = \prod_{t,a,b,\alpha,\beta} \left[ 1 - \Phi_{\alpha\beta}^{ab}(t) \bar{\psi}_\alpha^a(t) \psi_\beta^b(t) \right] \prod_{t,a,\alpha} \left[ 1 + \bar{\psi}_\alpha^a(t) \psi_\alpha^a(t+1) \right], \quad (5.49)$$

where the Einstein sum convention for two identical indices is not implicit here. With the occupation numbers  $m_{\alpha\beta}^{ab}(t) \in \{0,1\}$  for terms interacting on a fixed time slice and  $h_\alpha^a(t) \in \{0,1\}$  for the hops in temporal direction from time slice  $t$  to the next  $t+1$ , we can rewrite the hopping expansion as

$$\begin{aligned} \exp(-\hat{S}_F) &= \prod_{t,a,b,\alpha,\beta} \left[ \sum_{m_{\alpha\beta}^{ab}(t)=0}^1 \left( -\Phi_{\alpha\beta}^{ab}(t) \bar{\psi}_\alpha^a(t) \psi_\beta^b(t) \right)^{m_{\alpha\beta}^{ab}(t)} \right] \\ &\times \prod_{t,a,\alpha} \left[ \sum_{h_\alpha^a(t)=0}^1 \left( \bar{\psi}_\alpha^a(t) \psi_\alpha^a(t+1) \right)^{h_\alpha^a(t)} \right]. \end{aligned} \quad (5.50)$$

The new degrees of freedom are the occupation numbers which function as dual variables in our theory. The sum over all possible occupation numbers is essentially generating all configurations. However, the number of non-vanishing contributions is highly restricted due to the nilpotency of the Grassmann fields. On each time slice  $t$  there are the same number of incoming as outgoing fermion hops. Mathematically this can be translated into

$$\sum_{a,\alpha} h_\alpha^a(t) = \sum_{a,\alpha} h_\alpha^a(t+1) \quad \forall t. \quad (5.51)$$

Since each Grassmann number needs to occur exactly once, we can state that for any non-vanishing contribution to the partition function

$$\sum_{b,\beta} m_{\beta\alpha}^{ba}(t) + h_\alpha^a(t-1) = 1 \quad \forall a, \alpha, t \quad (5.52)$$

$$\sum_{b,\beta} m_{\alpha\beta}^{ab}(t) + h_\alpha^a(t) = 1 \quad \forall a, \alpha, t \quad (5.53)$$

must hold. In a graphical language we can simply draw an arrow for every occupation number that is set to one. Each point in the graphical representation, corresponding to a fermion pair  $\bar{\psi}_\alpha^a \psi_\alpha^a$ , then needs to have an outgoing and incoming arrow. Let us in the following calculate the contributions to the partition function by performing the

Grassmann integral for a given fermion pair  $\bar{\psi}_\alpha^a \psi_\alpha^a$ . There are four scenarios that we distinguish. The pair could be saturated by an incoming and outgoing temporal hop, i.e.  $h_\alpha^a(t-1) = h_\alpha^a(t) = 1$ . This leads to a local weight of

$$\int d\bar{\psi}_\alpha^a(t) d\psi_\alpha^a(t) \underbrace{\left[ \bar{\psi}_\alpha^a(t-1) \psi_\alpha^a(t) \right]}_{h_\alpha^a(t-1)=1} \underbrace{\left[ \bar{\psi}_\alpha^a(t) \psi_\alpha^a(t+1) \right]}_{h_\alpha^a(t)=1} = \bar{\psi}_\alpha^a(t-1) (1) \psi_\alpha^a(t+1). \quad (5.54)$$

So the weight of the temporal hops is one. This scenario is graphically represented in fig. 5.1, where the fermion fields living on a fixed temporal slice are represented by dots on a horizontal line. The field for which we perform the integration is highlighted with a thick black dot. The other points fading away represent other fermionic fields on that time slice.

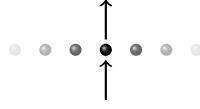


Figure 5.1.:  $h_\alpha^a(t-1) = h_\alpha^a(t) = 1$ , the Grassmann integral of this fermion pair yields a weight of 1.

In a second scenario we can imagine an incoming fermion line, via the temporal hop, which then propagates further on the time slice

$$\int d\bar{\psi}_\alpha^a(t) d\psi_\alpha^a(t) \underbrace{\left[ \bar{\psi}_\alpha^a(t-1) \psi_\alpha^a(t) \right]}_{h_\alpha^a(t-1)=1} \underbrace{\left[ -\Phi_{\alpha\beta}^{ab} \bar{\psi}_\alpha^a(t) \psi_\beta^b(t) \right]}_{m_{\alpha\beta}^{ab}(t)=1} = \bar{\psi}_\alpha^a(t-1) \left( -\Phi_{\alpha\beta}^{ab} \right) \psi_\beta^b(t). \quad (5.55)$$

This can of course easily be generalised to the situation where a fermion is saturated by an outgoing temporal hop instead of an incoming one. This is graphically illustrated in fig. 5.2.



Figure 5.2.: Left:  $h_\alpha^a(t-1) = m_{\alpha\beta}^{ab}(t) = 1$  with weight  $-\Phi_{\alpha\beta}^{ab}(t)$ . Right:  $m_{\rho\alpha}^{ra}(t) = h_\alpha^a(t) = 1$  with weight  $-\Phi_{\rho\alpha}^{ra}(t)$ . In this figure we additionally marked the two different fermion pairs with their group and Dirac index.

In a third scenario a fermion pair is saturated by

$$\int d\bar{\psi}_\alpha^a(t) d\psi_\alpha^a(t) \underbrace{\left[ -\Phi_{\alpha\beta}^{ab} \bar{\psi}_\alpha^a(t) \psi_\beta^b(t) \right]}_{m_{\alpha\beta}^{ab}(t)=1} \underbrace{\left[ -\Phi_{\gamma\alpha}^{ca} \bar{\psi}_\gamma^c(t) \psi_\alpha^a(t) \right]}_{m_{\gamma\alpha}^{ca}(t)=1} = -\bar{\psi}_\gamma^c(t) \psi_\beta^b(t) \left( \Phi_{\alpha\beta}^{ab} \Phi_{\gamma\alpha}^{ca} \right). \quad (5.56)$$

Two examples of this scenario are shown in fig. 5.3, one of which (the scenario on the right) would already saturate a second fermion pair since  $c = b$  and  $\gamma = \beta$ .

## 5. Fermion sectors in Matrix-theory



Figure 5.3.: Left:  $m_{\rho\alpha}^{ra}(t) = m_{\alpha\beta}^{ab}(t) = 1$  with weight  $\Phi_{\rho\alpha}^{ra}(t)\Phi_{\alpha\beta}^{ab}(t)$ . Right:  $m_{\alpha\beta}^{ab}(t) = m_{\beta\alpha}^{ba}(t) = 1$  with weight  $-\Phi_{\alpha\beta}^{ab}(t)\Phi_{\beta\alpha}^{ba}(t)$ .

At last we consider  $m_{\alpha\alpha}^{aa}(t) = 1$  which gives us

$$\int d\bar{\psi}_{\alpha}^a(t) d\psi_{\alpha}^a(t) \underbrace{\left[ -\Phi_{\alpha\alpha}^{aa} \bar{\psi}_{\alpha}^a(t) \psi_{\alpha}^a(t) \right]}_{m_{\alpha\alpha}^{aa}(t)=1} = \Phi_{\alpha\alpha}^{aa} = m + 1. \quad (5.57)$$

This can be graphically represented by a small loop connecting a point with itself. This is shown in fig. 5.4.



Figure 5.4.:  $m_{\alpha\alpha}^{aa}(t) = 1$  with weight  $\Phi_{\alpha\alpha}^{aa}(t) = m + 1$

Since there are no terms in the hopping expansion that have an odd number of fields only closed loops survive the Grassmann integral. Additionally, the temporal hops are directed, so the fermion can only hop in one direction in the temporal dimension. Let us summarise the above made considerations to a set of rules that tell us which loop configurations contribute to the partition function with the according weight coming from the Grassmann integral.

- Only closed loops survive the Grassmann integration, i.e. eq.(5.52) and eq.(5.53) must hold.
- The weight  $w$  of an interaction on a fixed time slice is simply

$$w(m_{\alpha\beta}^{ab}(t) = 1) = \Phi_{\alpha\beta}^{ab}(t) \quad (5.58)$$

- The number of fermions propagating forward in time is constant.
- All closed fermion loops come with a minus sign. This is true for loops winding around the temporal directions but also for loops on a fixed time slice.

We can now reformulate the partition function as

$$Z = \int \mathcal{D}\phi \exp[-S_B(\phi)] \sum_{\{c\}} (-1)^{n_l(c)} \prod_{a,b,\alpha,\beta,t} \left( \Phi_{\alpha\beta}^{ab}(t) \right)^{m_{\alpha\beta}^{ab}(t,c)}, \quad (5.59)$$

where the sum over all configurations  $\{c\}$  is meant to include all possible closed fermion loop configurations, i.e. possible occupation numbers that fulfil eq.(5.52) and eq.(5.53),

and  $n_l(c)$  is the total number of fermion loops in the given configuration. Note that we can break up the partition function into different sectors

$$Z = \sum_{|A|=0}^{2(N^2-1)} Z_{|A|} = \sum_{|A|=0}^{2(N^2-1)} \sum_{\{c\} \text{ with } |A|} (-1)^{n_l(c) + \epsilon|A|} \prod_{a,b,\alpha,\beta,t} \left( \Phi_{\alpha\beta}^{ab}(t) \right)^{m_{\alpha\beta}^{ab}(t,c)}, \quad (5.60)$$

where  $|A|$  is the number of fermions that are propagating forward in time. Note that in the current setup, in which we neglected the gauge field,  $|A|$  is equivalent to the number of fermions winding around the temporal dimension. The boundary conditions are periodic if  $\epsilon = 0$  and anti-periodic if  $\epsilon = 1$ . The total maximum number of fermions that can propagate in time are  $2(N^2 - 1)$ . Note that  $|A|$  is a conserved quantity due to the fact that we only have temporal hop terms that are oriented in one direction.

### 5.4.2. Gauge link

Up until now we considered  $U = \mathbb{1}$ . Let us include the gauge field living on the last link of our lattice

$$-\bar{\psi}_\alpha^a(L_t - 1) \psi_\alpha^b(0) \text{Tr} \left[ T^a U T^b U^{-1} \right], \quad (5.61)$$

which is a temporal hop from  $t = L_t - 1$  to  $t = 0$  being diagonal in the Dirac index  $\alpha$  but not in the colour index  $a$ . If we consider the hopping expansion of this term we get

$$\exp \left\{ \bar{\psi}_\alpha^a(L_t - 1) \psi_\alpha^b(0) \text{Tr} \left[ T^a U T^b U^{-1} \right] \right\} = \prod_{a,b,\alpha} \left[ \sum_{u_\alpha^{ab}=0}^1 \left( \bar{\psi}_\alpha^a(L_t - 1) \psi_\alpha^b(0) \text{Tr} \left[ T^a U T^b U^{-1} \right] \right)^{u_\alpha^{ab}} \right], \quad (5.62)$$

where in the latter term the Einstein sum convention is not implicit. The introduced occupation number  $u_\alpha^{ab} \in \{0, 1\}$  tells us if such a temporal hopping term is picked or not. In fig. 5.5 we graphically illustrate the effect of the gauge link in the fermion loop formulation. It allows us to draw an arrow from the last to the first time slice between two fermions with different group index  $a$ .

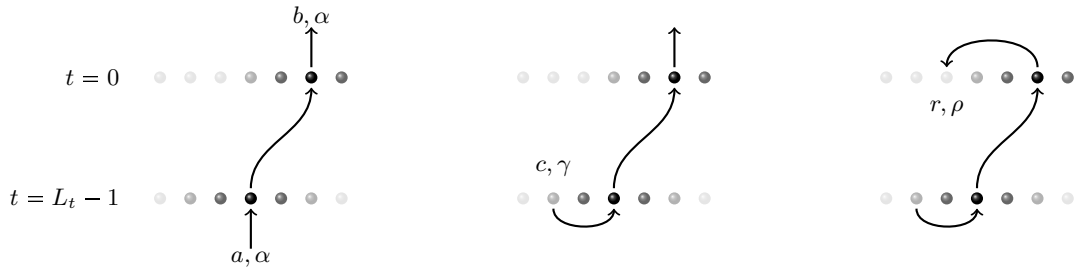


Figure 5.5.: Illustrating three scenarios how to saturate  $\bar{\psi}_\alpha^a \psi_\alpha^a$  on time slice  $t = L_t - 1$  (lower level) and  $\bar{\psi}_\alpha^b \psi_\alpha^b$  on slice  $t = 0$  (upper level). Left:  $h_\alpha^a(L_t - 2) = u_\alpha^{ab} = h_\alpha^b(0) = 1$ . Middle:  $m_{\gamma\alpha}^{ca}(L_t - 1) = u_\alpha^{ab} = h_\alpha^b(0) = 1$ . Right:  $m_{\gamma\alpha}^{ca}(L_t - 1) = u_\alpha^{ab} = m_{\alpha\rho}^{br}(0) = 1$ .

The set of rules on how to create a fermion loop configuration with a non-zero weight only needs the following extension:

## 5. Fermion sectors in Matrix-theory

- On the last link there exist temporal hops which are diagonal in Dirac space but mix fermions of different group index. The weight of such a link is

$$w(u_\alpha^{ab}(t) = 1) = \text{Tr} \left[ T^a U T^b U^{-1} \right] \quad (5.63)$$

and modify the constraints on the last and first slice

$$\sum_{b,\beta} m_{\beta\alpha}^{ba}(0) + h_\alpha^a(L_t - 1) + \sum_b u_\alpha^{ba} = 1 \quad \forall a, \alpha \quad (5.64)$$

$$\sum_{b,\beta} m_{\alpha\beta}^{ab}(L_t - 1) + h_\alpha^a(L_t - 1) + \sum_b u_\alpha^{ab} = 1 \quad \forall a, \alpha \quad (5.65)$$

With this we now know how to handle the gauge field, living on the last link of the system in the fermion loop formulation. The full partition function, including the boson, can then be expressed by

$$Z = \int \mathcal{D}\phi \mathcal{D}U \exp[-S_B(\phi, U)] \sum_{\{\mathbf{c}\}} (-1)^{n_l(\mathbf{c})} \left[ \prod_{a,b,\alpha,\beta,t} \left( \Phi_{\alpha\beta}^{ab}(t) \right)^{m_{\alpha\beta}^{ab}(t,\mathbf{c})} \right] \times \left[ \prod_{a,b,\alpha} \left( \text{Tr} \left[ T^a U T^b U^{-1} \right] \right)^{u_\alpha^{ab}(\mathbf{c})} \right], \quad (5.66)$$

where the sum over all configurations  $\{\mathbf{c}\}$  is the sum over all possible occupation numbers  $m_{\alpha\beta}^{ab}$ ,  $h_\alpha^a$  and  $u_\alpha^{ab}$  fulfilling eq.(5.52) and eq.(5.52) with the modification on the last link according to eq.(5.64) and eq.(5.53).

In this section we saw which configurations are in general giving non-zero contributions to the partition function. The goal of the next section is to consider a transfer matrix method based on the derived loop formulation. The transfer matrix will allow us to write the partition function as a trace over a product of matrices. We will see that it is possible to write down a transfer matrix for each sector  $|A|$  separately.

### 5.5. Fermion transfer matrix

In this section we establish a way on how to calculate the fermionic contribution to the partition function by means of a transfer matrix formulation. With the adequate transfer matrix  $T$  the fermionic part of the partition function can be written as

$$Z = \text{Tr} \left[ \prod_{t=0}^{L_t-1} T(t) \right], \quad (5.67)$$

where an entry  $T_{ij}$  describes the transition probability from state  $i$  to  $j$ . A state  $i$  is characterised by a given number of fermions of different Dirac and group index propagating forward in time. The transfer matrix  $T(t)$  is therefore defined on the dual lattice describing the transition probability of all sates  $i$  at  $t - a/2$  (all possible incoming fermion link configurations) to another sate  $j$  (all possible outgoing fermion link configurations) at  $t + a/2$ .



It is important to note that the transfer matrix displays a block structure since  $T_{ij} = 0$  if the amount of fermions in state  $i$  and state  $j$  are not identical. It is therefore possible to write down a transfer matrix separately for each fermion sector  $|A|$ , where  $|A|$  is the number of fermions propagating forward in time. The partition function then reads

$$Z = \sum_{|A|=0}^{2(N^2-1)} \text{Tr} \left[ \prod_{t=0}^{L_t-1} T_{|A|}(t) \right], \quad (5.68)$$

where we neglected the effect of boundary conditions.

Let us in a first attempt illustrate the basic ideas of this transfer matrix approach with a simple “non-physical” model. Afterwards we can then generalise to larger systems and finally discuss the transfer matrix in detail for the matrix model with four super charges described in eq.(5.46).

### 5.5.1. Basic idea

Consider a system living in one temporal dimension, identically to the Euclidean temporal direction described earlier. The action is defined as

$$S_{\text{toy}} = \sum_{t=0}^{L_t-1} \left[ \bar{\psi}^a(t) \Phi_{ab}(t) \psi^b(t) - \bar{\psi}^a(t) \psi^a(t+1) \right], \quad (5.69)$$

where  $\bar{\psi}^a$  and  $\psi^a$  are independent Grassmann variables which we will call fermions for convenience. The label  $a = 0, 1$  and the lattice is periodic, i.e.  $t + L_t = t$ .  $\Phi(t)$  is an interaction matrix connecting the fields on each time slice. The partition function is

$$Z = \prod_{a,t} \int d\bar{\psi}^a(t) d\psi^a(t) \exp[-S_{\text{toy}}]. \quad (5.70)$$

Expanding the Boltzmann factor yields

$$\exp[-S_{\text{toy}}] = \prod_{t=0}^{L_t-1} \left[ 1 + \bar{\psi}^0(t) \psi^0(t+1) \right] \left[ 1 + \bar{\psi}^1(t) \psi^1(t+1) \right] \quad (5.71)$$

$$\times \prod_{a,b} \left[ 1 - \bar{\psi}^a(t) \Phi_{ab}(t) \psi^b(t) \right], \quad (5.72)$$

where the product over time is meant to cover the whole expression and the Einstein sum convention is not implicit in the last term. Due to the Grassmann nature of  $\bar{\psi}$  and  $\psi$  only closed loops contribute to the partition function. We can split up the partition function into three different sectors  $Z_0$ ,  $Z_1$  and  $Z_2$ , where the subscript corresponds to the number of fermions winding around the temporal dimension. As an example we can consider a small system for which  $L_t = 2$ , in that case we can write draw all configurations that contribute with a non-zero weight to the partition function. This is done in fig. 5.7, 5.9 and 5.10, which correspond to the configurations in the sector where zero, one and two fermions are propagating in time. The fermion lines not corresponding to temporal hops are labelled with the adequate weight coming from the  $\Phi$  matrix.

## 5. Fermion sectors in Matrix-theory

### Zero fermions propagating in time

Let us first consider the  $|A| = 0$  sector and look at a single time slice  $t$ . There is no  $\psi^a(t)$  coming from a temporal hop into the time slice and there is also no  $\bar{\psi}^b(t)$  from a hop term that is going out. The complete Grassmann integration measure on that time slice is

$$\int d\bar{\psi}^0 d\psi^0 d\bar{\psi}^1 d\psi^1 \quad (5.73)$$

and can only be saturated by contributions coming from the  $\bar{\psi}\Phi\psi$  terms. The two possibilities are

$$\bar{\psi}^0 \psi^0 \Phi_{00} \bar{\psi}^1 \psi^1 \Phi_{11} + \bar{\psi}^1 \psi^0 \Phi_{10} \bar{\psi}^0 \psi^1 \Phi_{01}, \quad (5.74)$$

which are graphically illustrated in fig. 5.6.



Figure 5.6.: In this figure the two possibilities are shown how to create a contributing configuration on a time slice if no fermion is propagating in time.

When integrating over the Grassmann fields this yields

$$\begin{aligned} W_0 &= \int d\bar{\psi}^0 d\psi^0 d\bar{\psi}^1 d\psi^1 \left[ \bar{\psi}^0 \psi^0 \Phi_{00} \bar{\psi}^1 \psi^1 \Phi_{11} + \bar{\psi}^1 \psi^0 \Phi_{10} \bar{\psi}^0 \psi^1 \Phi_{01} \right] \\ &= \Phi_{00} \Phi_{11} - \Phi_{10} \Phi_{01} \end{aligned} \quad (5.75)$$

$$= \det[\Phi], \quad (5.76)$$

where the minus sign in the second line comes from the odd number of reordering steps of the Grassmann variables. The fact that  $W_0 = \det[\Phi]$  is clear due to the actual definition of the determinant of an  $N \times N$  matrix  $\Phi$

$$\det[\Phi] = \sum_{\sigma} \text{sgn}(\sigma) \prod_{i=0}^{N-1} \Phi_{i, \sigma_i}, \quad (5.77)$$

where the sum is performed over all permutations  $\sigma$  of the integer set  $\{0, 1, \dots, N-1\}$  and  $\text{sgn}(\sigma)$  is the signature of a given permutation. Every closed fermion loop will create a minus sign, due to the odd number of reordering steps in the Grassmann integral. Note that  $\bar{\psi}^a \psi^a$  alone represents a closed loop itself, i.e.

$$\int d\bar{\psi}^a d\psi^a \bar{\psi}^a \psi^a = -1. \quad (5.78)$$

The first term  $\Phi_{00}\Phi_{11}$  in eq.(5.75) then corresponds to two fermion loops, both contributing with an additional minus sign and in total forming an overall positive prefactor. The second term in eq.(5.75) is  $-\Phi_{10}\Phi_{01}$  and there is a minus sign because there is one closed

fermion loop. The determinant in this case gives us the correct sign for both contributions.

In a second step let us now construct the corresponding transfer matrix  $T_0(t)$ . The complete weight of all possible contributions to  $Z_0$  of a given time slice is  $\det[\Phi]$ , therefore  $T_0(t)$  is a scalar and the partition function can be expressed by

$$Z_0 = \text{Tr} \left[ \prod_t T_0(t) \right] = \prod_t \det [\Phi(t)] . \quad (5.79)$$

For our toy model, when setting  $L_t = 2$ , the find

$$\begin{aligned} Z_0 &= \det [\Phi(0)] \det [\Phi(1)] \\ &= \Phi_{00}(0)\Phi_{11}(0)\Phi_{00}(1)\Phi_{11}(1) - \Phi_{00}(0)\Phi_{11}(0)\Phi_{10}(1)\Phi_{01}(1) \\ &\quad - \Phi_{10}(0)\Phi_{01}(0)\Phi_{00}(1)\Phi_{11}(1) + \Phi_{10}(0)\Phi_{01}(0)\Phi_{10}(1)\Phi_{01}(1) , \end{aligned} \quad (5.80)$$

which corresponds exactly to the four solutions shown in fig.(5.7).

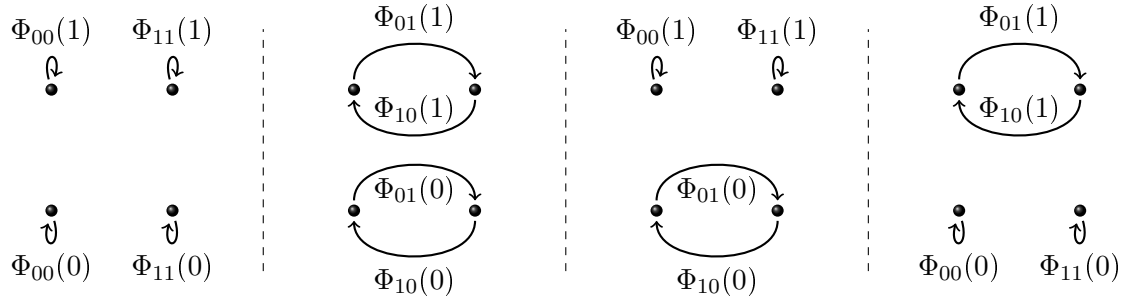


Figure 5.7.: In this figure we show all configurations contributing to  $Z_0$  if  $L_t = 2$ . The vertical dashed lines simply separate the configurations from one another and have no physical meaning.

### One fermion propagating in time

In the sector where one fermion is propagating in time  $|A| = 1$ . The options on a time slice to saturate the Grassmann integral are different. An incoming fermion hop with index  $b$  creates the constraint that on this time slice  $t$  no other term of the hopping expansion can be picked which also includes the fermion  $\psi^b(t)$ . Let us now assume that the  $\bar{\psi}^0(t-1)\psi^0(t)$  term is picked, this means that all terms including factors arising in the first column of  $\Phi(t)$  are generating zero because these are exactly those terms that come with an additional power of the same Grassmann variable. This means no term of  $\bar{\psi}^a\Phi_{a0}\psi^0$  can be picked. If the fermion hops further in time with the hop term  $\bar{\psi}^1(t)\psi^1(t+1)$ , we have no other option than to saturate the Grassmann integral with  $\bar{\psi}^0\Phi_{01}\psi^1$ . This scenario is illustrated in fig. 5.8 on the left. The scenario where the fermion propagates further with  $\bar{\psi}^0(t)\psi^0(t+1)$  is shown on the right.

## 5. Fermion sectors in Matrix-theory

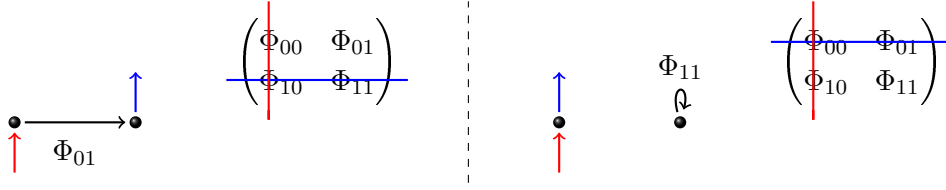


Figure 5.8.: We illustrate two possibilities on how to saturate the Grassmann integral on a time slice with an incoming fermion hop term  $\bar{\psi}^0(t-1)\psi^0(t)$ . In both scenarios the adequate matrix row and column are crossed out, leaving the resulting possible interaction.

An incoming fermion hop of kind  $b$  is essentially eliminating all options of column  $b$  in the matrix  $\Phi$  and an outgoing fermion hop of kind  $a$  is eliminating all options in row  $a$  respectively. Therefore we define  $W_1^{ab}(t)$  to be the weight corresponding to the transition probability to enter a time slice  $t$  with an incoming fermion hop of kind  $b$  and an outgoing one of kind  $a$ . Let us in a first attempt try to stick with the determinant method and use

$$W_1^{ab}(t) = \det \left[ \Phi^{\searrow \mathbb{k}}(t) \right], \quad (5.81)$$

where  $\Phi^{\searrow \mathbb{k}}$  is the matrix  $\Phi$ , in which row  $a$  and column  $b$  are cut out. In our toy model we know that these four possibilities should be  $W_1^{00} = -\Phi_{11}$ ,  $W_1^{10} = \Phi_{01}$ ,  $W_1^{01} = \Phi_{10}$  and  $W_1^{11} = -\Phi_{00}$ . The minus signs come from the fact that in certain configurations, e.g. fig. 5.8 on the right, we can have a closed loop. The determinant in this case does not give us the correct sign. We can correct this by adding a prefactor in the following way

$$W_1^{ab}(t) = (-1)^{\delta_{ab}} \det \left[ \Phi^{\searrow \mathbb{k}}(t) \right], \quad (5.82)$$

The transfer matrix is now a  $2 \times 2$  matrix of the form

$$T_1(t) = \begin{pmatrix} W_1^{00}(t) & W_1^{01}(t) \\ W_1^{10}(t) & W_1^{11}(t) \end{pmatrix} = \begin{pmatrix} -\Phi_{11}(t) & \Phi_{10}(t) \\ \Phi_{01}(t) & -\Phi_{00}(t) \end{pmatrix}. \quad (5.83)$$

In the case of  $L_t = 2$  we can again write down all the terms of the partition function

$$\begin{aligned} Z_1 &= \text{Tr} \left[ \prod_{t=0}^1 T_1(t) \right] \\ &= \text{Tr} \left[ \begin{pmatrix} -\Phi_{00}(0) & \Phi_{10}(0) \\ \Phi_{01}(0) & -\Phi_{11}(0) \end{pmatrix} \begin{pmatrix} -\Phi_{00}(1) & \Phi_{10}(1) \\ \Phi_{01}(1) & -\Phi_{11}(1) \end{pmatrix} \right] \\ &= \Phi_{11}(0)\Phi_{11}(1) + \Phi_{10}(0)\Phi_{01}(1) + \Phi_{01}(0)\Phi_{10}(1) + \Phi_{00}(0)\Phi_{00}(1), \end{aligned} \quad (5.84)$$

which are the four contributions shown in fig.(5.9).

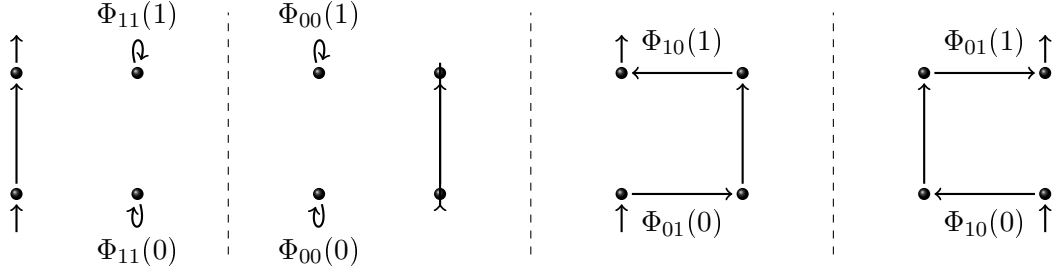


Figure 5.9.: In this figure we show all four configurations which contribute to  $Z_1$  if  $L_t = 2$ . The dashed lines are again only separating the configurations.

### Two fermions propagating in time

The last sector, where two fermions are propagating through the system, saturates every time slice already with the hop-terms  $\bar{\psi}^a(t)\psi^a(t+1)$ . There are no options left which contribute from  $\Phi$  and therefore

$$Z_2 = 1. \quad (5.85)$$

On each time slice there is only one configuration contributing, as it is illustrated in fig.(5.10) for the special case of  $L_t = 2$ . This is the same as to say that we eliminated all rows and all columns of  $\Phi$ , simply making no other interactions possible.

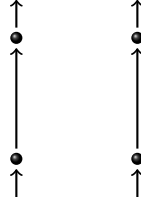


Figure 5.10.: This figure shows the only configuration contributing to  $Z_2$  if  $L_t = 2$ .

### Complete partition function

We now determined all contributions to  $Z = Z_0 + Z_1 + Z_2$  for the limited toy model with two different fermion pairs at each time slice. Until now neglected the contributions from the fermions winding around the temporal dimension. It can easily be checked that also these loops simply contribute with a  $-1$ . We can therefore write the complete partition function as

$$Z = Z_0 + (-1)^{1(\epsilon+1)} Z_1 + (-1)^{2(\epsilon+1)} Z_2 = Z_0 + (-1)^{\epsilon+1} Z_1 + Z_2, \quad (5.86)$$

which gives us for the partition function with periodic( $\epsilon = 0$ ) and anti-periodic( $\epsilon = 1$ ) boundary conditions

$$Z_p = Z_0 - Z_1 + Z_2 \quad \text{and} \quad Z_a = Z_0 + Z_1 + Z_2. \quad (5.87)$$

In a next section we generalise the discussed model to arbitrary many fermions.

### 5.5.2. Enlarging and generalising the toy model

We enlarge the toy model introduced in eq.(5.69) to a system with  $|F|$  different fermion pairs  $\bar{\psi}^a(t)\psi^a(t)$ , with  $a = 0, 1, \dots, |F| - 1$ , at every time slice  $t$ . The goal is to construct the adequate transfer matrix for a system where  $|A|$  fermions are propagating forward in time.

Let us define the set of integers

$$F = \{0, 1, \dots, |F| - 1\}, \quad (5.88)$$

which corresponds to the integers  $a$  labelling all the different fermion pairs  $\bar{\psi}^a(t)\psi^a(t)$ . The cardinality of the set is denoted by  $|F|$ , telling us how many elements are in the set, which in our case is exactly the total number of fermion pairs on each time slice. Further we define  $A_i$  that is  $\subseteq F$  and holds all integers labelling the kinds of fermion hops that are coming into a time slice, i.e.  $\bar{\psi}^a(t-1)\psi^a(t)$  with  $a \in A_i$ . Another set  $A_j$  which is also  $\subseteq F$  represents the kinds of fermion hops going out, i.e.  $\bar{\psi}^a(t)\psi^a(t+1)$  with  $a \in A_j$ . Since every interaction term from  $\bar{\psi}\Phi\psi$  holds an even number of Grassmann variables, the number of incoming and outgoing fermion lines must be the same, i.e.  $|A_i| = |A_j| \equiv |A|$ , but generally  $A_i \neq A_j$ .

An entry of the transfer matrix, bringing  $|A|$  fermions forward in time, is now depending on the exact choice of  $A_i$  and  $A_j$ . The transfer matrix  $T_{|A|}$  is of size

$$\binom{|F|}{|A|} \times \binom{|F|}{|A|}, \quad (5.89)$$

because we have  $|F|$  different fermions and can choose all possible unordered sets  $A_i$ , where  $i = 0, 1, \dots, \binom{|F|}{|A|}$ , to hop in and again all possibilities to hop out of a time slice. Let's try to construct an entry of the transfer matrix, almost analogously to the simple model from eq.(5.69), by eliminating all columns in  $\Phi$  corresponding to the entries in  $A_i$  and all rows corresponding to the entries in  $A_j$ . The transfer matrix is then

$$[T_{|A|}(t)]_{ij} = (-1)^{|F|-|A|+A_i+A_j} \det [\Phi^{\overline{A_j} A_i}(t)], \quad (5.90)$$

where  $|F| - |A| + A_i + A_j$  is the number of fermions in the system, minus the number of propagating fermions, plus all the entries from  $A_i$  and  $A_j$ . Note that  $|F| - |A|$  is constant in a given sector. This determinant method works in all scenarios in which one of the following properties is fulfilled

$$|F| < 3 \quad \text{or} \quad |F| - 1 \leq |A| \quad \text{or} \quad |A| \leq 1 \quad \text{or} \quad A_i = A_j. \quad (5.91)$$

Even though the use of the determinant method seems valid in only very limited setups, there are some first results that we can obtain with this formulation, as it will be discussed in section 5.8. We now proceed to create a formula for the transfer matrix for arbitrary  $|A|$ .

In order to write down an expression for arbitrary many fermions we reformulate our problem: we need to look for all possible bijective mappings  $f$  that map  $F \setminus A_i \rightarrow F \setminus A_j$  and determine the sign by counting the number of cycles. Let us therefore define

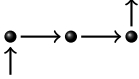

$$G(F, A_i, A_j) = \{f : F \setminus A_j \rightarrow F \setminus A_i \mid f \text{ bijective}\}. \quad (5.92)$$

Note that if  $A_i = A_j$ , then  $f$  is usually called a permutation. However, let us in the following stick to the term permutation even though in general  $A_i \neq A_j$ . We can now define a function  $P$  that gives us all possible permutations and adds the correct sign to each of those, i.e.

$$P[\Phi^{\overrightarrow{A_j A_i}}] = \sum_{f \in G(F, A_i, A_j)} (-1)^{N_{\text{cycles}}(f)} \prod_{k \in F \setminus A_j} \Phi_{k, f_k}. \quad (5.93)$$

The function  $N_{\text{cycles}}(f)$  is counting the number cycles and  $f_k$  denotes the  $k$ -th element of the permutation. After this formal mathematical definition let us in a short example illustrate how  $P[\Phi^{\overrightarrow{A_j A_i}}]$  actually works.



We consider a system where  $F = \{0, 1, 2\}$  and assume that the incoming fermion hop is  $A_i = \{0\}$  and the outgoing one is  $A_j = \{2\}$ . Let us in the following table summarise the two permutations  $f_1, f_2$ , list the cycles, the actual number of cycles and the corresponding graphical illustration:

$f:$	$f_1 = \begin{cases} 0 \rightarrow 1 \\ 1 \rightarrow 2 \end{cases}$	$f_2 = \begin{cases} 0 \rightarrow 2 \\ 1 \rightarrow 1 \end{cases}$
cycles:	—	(1)
$(-1)^{N_{\text{cycles}}(f)}:$	+1	-1
graphical:		

So the function  $P[\Phi^{\overrightarrow{A_j A_i}}]$  will in this scenario return

$$P[\Phi^{\overrightarrow{\{2\} \{0\}}}] = \Phi_{01} \Phi_{12} - \Phi_{11} \Phi_{02}. \quad (5.94)$$

In another example we consider at the scenario where the incoming and outgoing fermion is identical, let's say this is the first one and set  $A_i = A_j = \{0\}$ . This gives us the following

$f:$	$f_1 = \begin{cases} 1 \rightarrow 1 \\ 2 \rightarrow 2 \end{cases}$	$f_2 = \begin{cases} 1 \rightarrow 2 \\ 2 \rightarrow 1 \end{cases}$
cycles:	(1)(2)	(12)
$(-1)^{N_{\text{cycles}}(f)}:$	+1	-1
graphical:		

Therefore we find

$$P[\Phi^{\overrightarrow{\{0\} \{0\}}}] = \Phi_{11} \Phi_{22} - \Phi_{21} \Phi_{12}. \quad (5.95)$$

The transfer matrix can in general be calculated by

$$[T_{|A|}(t)]_{ij} = P[\Phi^{\overrightarrow{A_j A_i}}(t)], \quad (5.96)$$

## 5. Fermion sectors in Matrix-theory

and the partition function in a given sector  $|A|$  is then expressed by

$$Z_{|A|} = \text{Tr} \left[ \prod_{t=0}^{L_t-1} T_{|A|}(t) \right], \quad (5.97)$$

where the total partition function is

$$Z = \sum_{|A|=0}^{|F|} (-1)^{|A|(\epsilon+1)} Z_{|A|}, \quad (5.98)$$

where  $\epsilon$  again accounts for the boundary conditions.

A main achievement made with these simple considerations is the fact that we can now look at all different sectors  $|A|$  of the partition function separately by considering the product of the corresponding transfer matrices. This can now easily be translated to the dimensionally reduced  $4d \mathcal{N} = 1$  super Yang-Mills model, which forms the goal of the next section.

### 5.5.3. Transfer matrix of dimensionally reduced $4d \mathcal{N} = 1$ super Yang-Mills

Consider the lattice action from eq.(5.46), leaving away the gauge field for now, we find in component notation

$$\hat{S}_F = \frac{1}{2g^2} \sum_{t=0}^{L_t-1} \left[ -\bar{\psi}_\alpha^a(t) \psi_\alpha^a(t+1) + \bar{\psi}_\alpha^a(t) \Phi_{\alpha,\beta}^{ac}(t) \psi_\beta^c(t) \right], \quad (5.99)$$

where we defined

$$\Phi_{\alpha\beta}^{ac}(t) = (m+1)\delta^{ac}\delta_{\alpha\beta} - (\sigma_i)_{\alpha\beta} i f^{abc} \phi_i^b(t), \quad (5.100)$$

which is an interaction matrix living on the time slices connecting  $\bar{\psi}_\alpha^a(t)$  with  $\psi_\beta^c(t)$ . The matrix  $\Phi$  is a  $2(N^2-1) \times 2(N^2-1)$  matrix with entries in  $\mathbb{C}$ , where the factor of 2 comes from the fact that  $\alpha = 0, 1$ . It has the properties

$$\Phi_{\alpha\beta}^{ac} = -\Phi_{\alpha\beta}^{ca} \quad \text{and} \quad \Phi_{\alpha\beta}^{ac} = -\Phi_{\beta\alpha}^{ac*}, \quad (5.101)$$

which is due to the completely anti-symmetric structure constant and because  $\sigma_i^T = \sigma_i^*$ . Considering eq.(5.101) we know that for the case of  $SU(N)$  the interaction matrix is hermitian, i.e.

$$\Phi^\dagger = \Phi. \quad (5.102)$$

We want to add that the matrix size, for a former  $d$ -dimensional theory for  $SU(N)$ , is in general

$$2^{d/2}(N^2-1) \times 2^{d/2}(N^2-1), \quad (5.103)$$

which can be of course reduced in certain dimension, e.g. by a Majorana or Majorana-Weyl condition.



Let us organise the matrix  $\Phi$  in a particular way<sup>3</sup>, where the coordinates  $k$  of an entry  $\Phi_{kl}$  in the matrix correspond to  $k(a, \alpha) = 2a + \alpha$ . With this choice we simply say that

$$\psi_k \equiv \psi_{2a+\alpha} \equiv \psi_\alpha^a \quad (5.104)$$

are the individual Grassmann components and the interaction term can then be written as

$$\bar{\psi}_k \Phi_{kl} \psi_l. \quad (5.105)$$

A graphical representation of this ordering on a time slice is given in fig. 5.11 for the special case of  $SU(2)$ .

$$\begin{array}{cccccc} k = & 0 & 1 & 2 & 3 & 4 & 5 \\ & \bullet & \bullet & \bullet & \bullet & \bullet & \bullet \\ \alpha = & 0 & 1 & 0 & 1 & 0 & 1 \\ a = & \underbrace{\quad}_1 & & \underbrace{\quad}_2 & & \underbrace{\quad}_3 & \end{array}$$

Figure 5.11.: In this figure we show the arrangement of the Grassmann pairs ( $\bar{\psi}_\alpha^a \psi_\alpha^a$ =black dot) on a time slice. Note that this is for the special case of  $SU(2)$ , where we have 6 different fermion pairs.

Analogously to the previous section we now create the transfer matrix for a certain sector of the partition function. Note that the structure is identical to the one found in the action of the toy model in eq.(5.69). There are no terms in eq.(5.100) which would allow different kinds of fermion structures than closed loops. The only difference to our toy model is the actual number of different fermion pairs being now  $|F| = 2(N^2 - 1)$  and the fact that we know the explicit structure of the interaction matrix  $\Phi$ . The transfer matrix for a sector with a fixed number of fermions propagating forward in time is again

$$[T_{|A|}(t)]_{ij} = P[\Phi^{\overrightarrow{A}, \overleftarrow{A}}(t)], \quad (5.106)$$

where we have to cut out the columns and rows of the according kinds of incoming and outgoing fermion hops. The size of the transfer matrix is now

$$\binom{2(N^2 - 1)}{|A|} \times \binom{2(N^2 - 1)}{|A|}. \quad (5.107)$$

An entry of the transfer matrix can also be expressed in terms of the introduced occupation numbers in the fermion loop formulation. It is the Grassmann integral of the sum of all configurations that have  $m_{\alpha\beta}^{ab}(t)$  that fulfil eq.(5.52) where a given set of  $|A|$  different hop occupation numbers  $h_\alpha^a(t-1)$  and  $h_\beta^b(t)$  are set to one. The fermion partition function in that sector  $|A|$  is

$$Z_{|A|} = \text{Tr} \prod_{t=0}^{L_t-1} T_{|A|}(t), \quad (5.108)$$

<sup>3</sup>Note that this is simply a choice and has no physical motivation. However, since a fermion carries two labels  $a$  and  $\alpha$ , the introduction of  $k = 2a + \alpha$  simplifies writing  $F$  analogously to the previous section.

## 5. Fermion sectors in Matrix-theory

and the full partition function, including also the bosonic fields, must then be of the form

$$Z = \sum_{|A|=0}^{2(N^2-1)} \prod_{i,a,t} \int d\phi_i^a(t) \exp \left[ -\hat{S}_B(\phi) \right] \left( \frac{1}{2g^2} \right)^v (-1)^{|A|(\epsilon+1)} \text{Tr} \left[ \prod_{t=0}^{L_t-1} T_{|A|}(\phi(t)) \right], \quad (5.109)$$

where we wrote the bosonic fields as the argument of the transfer matrix in order to emphasise that its entries are built up by combinations of these fields. Further we added the factor  $(2g^2)^{-v}$  with  $v = 2(N^2-1)L_t$ , which is coming from the fact that we need to pick  $2(N^2-1)L_t$  terms from the hopping expansion that include the identical factor  $1/(2g^2)$  appearing in the action in eq.5.99. Up until now we set  $U = \mathbb{1}$ . In the next subsection we include the gauge field, which in the temporal gauge appears as one dynamic gauge link living between  $t = L_t - 1$  and  $t = 0$ .

### 5.5.4. Including the gauge link

In this section we discuss how to add an adequate transfer matrix in order to describe a system with a dynamic gauge link on the last link of the lattice.

The fermionic terms in the hopping expansion including the temporal gauge link are

$$\bar{\psi}_\alpha^a(L_t - 1) \psi_\alpha^b(0) \text{Tr} \left[ T^a U T^b U^{-1} \right], \quad (5.110)$$

which allow fermion hops on the last link that are mixing  $\bar{\psi}^a$  and  $\psi^b$ . If we think of an interaction matrix  $\tilde{\Phi}$ , defined on the last link between  $t = L_t - 1$  and  $t = 0$ , we can write the fermion terms interacting with the gauge fields as

$$\bar{\psi}_\alpha^a(L_t - 1) \tilde{\Phi}_{\alpha\beta}^{ab} \psi_\beta^b(0), \quad (5.111)$$

with

$$\tilde{\Phi}_{\alpha\beta}^{ab} = \delta_{\alpha\beta} \text{Tr} \left[ T^a U T^b U^{-1} \right], \quad (5.112)$$

If we again choose the basis where  $k = 2a + \alpha$  in order to write  $\bar{\psi}_k(L_t - 1) \tilde{\Phi}_{kl} \psi_l(0)$ , the interaction matrix has the form

$$\tilde{\Phi}_{kl} = \text{Tr} \left[ T^{[k/2]} U T^{[l/2]} U^{-1} \right], \quad (5.113)$$

where  $[k/2]$  denotes the smallest integer larger or equal  $k/2$ , where the factor of one half comes from the fact that the Dirac index runs from  $\alpha = 0, 1$ . An explicit form of this matrix is given in section 5.8 for the special case of  $SU(2)$ . It is also interesting to consider the interaction matrix  $\tilde{\Phi}$  using  $k = (N^2 - 1)\alpha + a$  because then  $\tilde{\Phi}$  is block diagonal, i.e.

$$\tilde{\Phi} = \begin{pmatrix} \tilde{\Phi}_{00} & 0 \\ 0 & \tilde{\Phi}_{11} \end{pmatrix}, \quad (5.114)$$

where  $\tilde{\Phi}_{\alpha\alpha}$  is a  $(N^2 - 1) \times (N^2 - 1)$  matrix. However, regardless of which basis we choose, the prescription on how to create a transfer matrix living on the last link of the system in order to account for the gauge field dynamics is

$$\left[ T_{|A|}^U \right]_{ij} = \det \left[ \tilde{\Phi}^{\cancel{F} \setminus A_i \setminus \cancel{F} A_j}(t) \right]. \quad (5.115)$$

In order to create the transfer matrix describing the interactions with the gauge link we have to cancel all rows and columns of  $\tilde{\Phi}$  corresponding to all fermion hops that are not incoming and outgoing, i.e. eliminating all rows  $F \setminus A_j$  and all columns  $F \setminus A_j$ . Due to the gauge field on the last link a single closed fermion loop might wind around the temporal direction several times. This means that  $|A|$  is generally not telling us how many closed fermion loops are winding around the temporal direction. This is illustrated in fig. 5.12 where we consider the last link of the system. On the left the number of fermions propagating forward in time is  $|A| = 2$  and the number of fermions winding around the temporal direction, i.e. closed loops winding around the temporal direction, is  $N_t = 2$ . On the right side of fig. 5.12 however,  $|A| = 2$  and  $N_t = 1$ , which tells us that the contributions to the partition function partition of those configurations in fig. 5.12 differ by a sign. The determinant is used in eq.(5.115) since it accounts for the relative sign among contributions from configurations with the same number of fermions hopping forward in time but with a different number of fermions winding around the temporal dimension.



Figure 5.12.: This figures shows two fermions propagating forward in time on the last link of the lattice where the gauge field allows also component mixing. On the left  $|A| = N_t = 2$  which is contributing a positive sign, on the right  $|A| = 2$  and  $N_t = 1$  is contributing with a negative sign.

The fermionic contribution of a given sector, including the gauge link, can then be written as

$$Z_{|A|} = \text{Tr} \left[ T_{|A|}(0) T_{|A|}(1) \dots T_{|A|}(L_t - 1) T_{|A|}^U \right] = \text{Tr} \left[ T_{|A|}^U \prod_{t=0}^{L_t-1} T_{|A|}(t) \right]. \quad (5.116)$$

Putting everything together we can write down the full partition function of the  $4d \mathcal{N} = 1$  super Yang Mills action dimensionally reduced to one temporal dimension with an  $SU(N)$  gauge group in terms of the fermion transfer matrix as

$$\begin{aligned} Z &= \sum_{|A|=0}^{2(N^2-1)} \prod_{i,a,t} \int d\phi_i^a(t) dU(t) \exp \left[ -\hat{S}_B(\phi, U) \right] \\ &\times \left( \frac{1}{2g^2} \right)^v (-1)^{|A|(\epsilon+1)} \text{Tr} \left[ T_{|A|}^U \prod_{t=0}^{L_t-1} T_{|A|}(\phi(t)) \right]. \end{aligned} \quad (5.117)$$

## 5.6. Boson bond formulation

Let us in this section derive a bond formulation for the bosonic degrees of freedom. The bosonic action, leaving away the gauge field, is

$$\hat{S}_B = \sum_{t=0}^{L_t-1} \left[ -\frac{1}{g^2} \phi_i^a(t+1) \phi_i^a(t) + W(t) \right], \quad (5.118)$$

with

$$W(t) = \frac{1}{g^2} \phi_i^a(t)^2 + \frac{1}{4g^2} f^{abc} f^{alm} \phi_i^b(t) \phi_j^c(t) \phi_i^l(t) \phi_j^m(t). \quad (5.119)$$

Using the bosonic bond occupation number for the temporal hops  $n_i^a(t)$ , we can write the hopping expansion for the bosonic action as

$$\exp(-\hat{S}_B) = \left[ \prod_t \exp[-W(t)] \right] \prod_{a,i,t} \sum_{n_i^a(t)=0}^{\infty} \left( \frac{1}{g^2} \right)^{n_i^a(t)} \frac{[\phi_i^a(t+1) \phi_i^a(t)]^{n_i^a(t)}}{n_i^a(t)!}. \quad (5.120)$$

We can define the total number of bosonic bonds

$$N_i^a(t) = n_i^a(t-1) + n_i^a(t), \quad (5.121)$$

which tells us how many factors of  $\phi_i^a(t)$  are added to this site. The bosonic contribution of a given configuration, i.e. fixed number of  $n_i^a$ , to the partition function, can now be encoded in a time slice dependent way like

$$W_B(t) = \left[ \prod_{i,a} \frac{1}{n_i^a(t)!} \left( \frac{1}{g^2} \right)^{n_i^a(t)} \right] \int_{-\infty}^{\infty} \prod_{i,a} d\phi_i^a(t) [\phi_i^a(t)]^{N_i^a(t)} \exp[-W(t)], \quad (5.122)$$

where the latter product is not meant to cover the last exponential term. The total weight of a given configuration can now be constructed by  $\prod_t W_B(t)$ . We perform the hopping expansion also of the bosonic term involving the gauge field and find

$$\exp \left( 2\phi_i^a(L_t-1) \phi_i^b(0) \text{Tr} [UT^a U^\dagger T^b] \right) = \prod_{i,a,b} \sum_{l_i^{ab}=0}^{\infty} \left( \frac{2 \text{Tr} [UT^a U^\dagger T^b]}{g^2} \right)^{l_i^a(t)} \frac{(\phi_i^a(L_t-1) \phi_i^b(0))^{l_i^{ab}}}{l_i^{ab}!}, \quad (5.123)$$

where  $l_i^{ab}$  are the occupation numbers for the temporal hops on the last link involving the gauge field. The additional terms coming from the gauge link can be simply added in the following form

$$\begin{aligned} W_B &= \left[ \prod_{t=1}^{L_t-2} W_B(t) \right] \left[ \prod_{i,a} \frac{1}{n_i^a(L_t-1)!} \frac{1}{n_i^a(0)!} \left( \frac{1}{g^2} \right)^{n_i^a(L_t-1)+n_i^a(0)} \right. \\ &\times \int d\phi_i^a(L_t-1) [\phi_i^a(L_t-1)]^{N_i^a(L_t-1)+\prod_b l_i^{ba}} \\ &\times \left. \int d\phi_i^a(0) [\phi_i^a(0)]^{N_i^a(0)+\prod_b l_i^{ba}} \right] \\ &\times \exp[-W(L_t-1)] \exp[-W(0)] \prod_{i,a,b} \frac{1}{l_i^{ab}!} \left( \frac{1}{g^2} \right)^{l_i^a(t)} \left( 2 \text{Tr} [UT^a U^\dagger T^b] \right)^{l_i^{ab}} \end{aligned} \quad (5.124)$$

The total contribution to the partition function from the purely bosonic part of the action, including the gauge field, can then be written as the sum over all bond configurations

$$Z_B = \int \mathcal{D}U \left[ \prod_{i,a,b} \sum_{l_i^{ab}=0}^{\infty} \right] \left[ \prod_{t,i,a} \sum_{n_i^a(t)=0}^{\infty} \right] W_B. \quad (5.125)$$

The drawback of the current formulation lies in the fact that there are component mixing terms in the potential  $W(t)$ , not allowing for the integration of  $d\phi_i^a$  without dependence on other bosonic fields. Nevertheless, the integrals can be performed separately for each time slice.

## 5.7. Bond-Loop formulation

In a second step let us combine the just derived bosonic bond formulation with the already established fermion loop formulation. In eq.(5.50) we introduced the occupation number  $m_{\alpha\beta}^{ab}(t)$  telling us if a term  $\bar{\psi}_\alpha^a(t)\psi_\beta^b(t)$  is picked from the hopping expansion or not. The corresponding weight of this interaction was shown to be

$$w(m_{\alpha\beta}^{ab}(t) = 1) = \Phi_{\alpha\beta}^{ab} = (m + 1)\delta_{\alpha\beta}^{ab} - if^{acb}(\sigma_i)_{\alpha\beta}\phi_i^c(t), \quad (5.126)$$

where only the sum over  $c$  and  $i$  are implicit. So in the weight of the  $\bar{\psi}_\alpha^a(t)\psi_\beta^b(t)$  interaction there are several bosonic fields contributing. This is a simplification that was made in order to have every interaction term, connecting  $\bar{\psi}_\alpha^a(t)$  with  $\psi_\beta^b(t)$ , arising exactly once in the hopping expansion of the fermion. However, if we are interested in combining the fermion loop formulation with the bond formulation we will need to split up the sum over  $c$  and  $i$  in eq.(5.126) into its elementary pieces such that every interaction only includes exactly one bosonic field component. For this purpose let us modify the fermion loop formulation by breaking up those terms. Mathematically this amounts only to a separation of the occupation number  $m_{\alpha\beta}^{ab}(t)$  into its individual components, which we will call  $m_{\alpha\beta i}^{abc}(t)$ . This occupation number follows the same rules as  $m_{\alpha\beta}^{ab}(t)$ , since those rules in eq.(5.52,5.53) do not depend on  $i$  and  $c$ . The corresponding weight is simply

$$w(m_{\alpha\beta i}^{abc}(t) = 1) = (m + 1)\delta_{\alpha\beta}^{ab} - if^{acb}(\sigma_i)_{\alpha\beta}\phi_i^c(t), \quad (5.127)$$

in which there is no sum over  $c$  and  $i$ . Graphically  $m_{\alpha\beta i}^{abc}(t)$  can be represented by an arrow from point  $\bar{\psi}_\alpha^a(t)$  to  $\psi_\beta^b(t)$  as already introduced, but now passing a different intermediate point  $\phi_i^c(t)$ . We use the same graphical notation as before but we are changing the perspective angle such that we look onto a time slice in time direction. Let us use a red point for a  $\bar{\psi}_\alpha^a(t)\psi_\alpha^a(t)$  term and a blue point for  $\phi_i^c(t)$ . In fig. 5.13 we graphically illustrate two different ways, corresponding to two different weights including different bosonic fields, which connect the same two fermion points  $\bar{\psi}_\alpha^a(t)$  and  $\psi_\beta^b(t)$ .

## 5. Fermion sectors in Matrix-theory



Figure 5.13.: This figure is showing two different ways on how to connect  $\bar{\psi}_\alpha^a(t)$  with  $\psi_\beta^b(t)$ . Both fermion pairs are represented by a red point. Each way corresponds to a different weight, i.e. boson(blue point).

If now on a given time slice  $m_{\alpha\beta i}^{bca}(t) = 1$  there is an additional factor of  $\phi_i^a(t)$  from the fermion hopping expansion. With this insight we can combine the bosonic bond formulation with the fermion loop formulation which yields additional factors of  $\phi_i^a$ , depending on the loop structure of the fermion configuration  $c$ . On every time slice we then need to modify the bosonic bond formulation in the following way

$$[\phi_i^a(t)]^{N_i^a(t) + \prod_{cd} m_{\alpha\beta i}^{cda}(t, c)} \left[ i f^{cda}(\sigma_i)_{\alpha\beta} \right]^{m_{\alpha\beta i}^{cda}(t, c)}, \quad (5.128)$$

in order to account for the additional bosonic contribution coming from the fermion interactions. Note that in the formula above the sum convention is again not implicit and that now the sum over all configurations in the combined formulation is also including the bosonic bond configurations and not only the fermionic loop configurations, i.e.

$$\sum_{\{c\}} = \sum_{\text{loop conf.}} \sum_{\text{bond conf.}} = \sum_{\text{loop conf.}} \left[ \prod_{a,b,i} \sum_{l_i^{ab}=0}^{\infty} \right] \left[ \prod_{t,a,i} \sum_{n_i^a(t)=0}^{\infty} \right]. \quad (5.129)$$

## 5.8. Explicit calculations

As explained in section 5.5.3 we can write the fermionic part of the action contributing to the partition function as a product over transfer matrices. In this section we want to explicitly calculate the transfer matrix for the  $d = 4$   $\mathcal{N} = 1$  super Yang Mills model that is dimensionally reduced to one-dimensional  $\mathcal{N} = 4$  quantum mechanics in one temporal direction. We have seen that the transfer matrix can be computed separately for each sector of the partition function which has a different number of fermions  $|A|$  propagating forward in time. For  $|F| - 1 \leq |A|$  or  $|A| \leq 1$  the entries of the transfer matrix can even be computed with the determinant of the adequate interaction matrix. In the following we will restrict ourselves to those scenarios. This might seem like a large restriction but is motivated by the following facts. The size of the transfer matrix is depending on  $N$  and on  $|A|$ , as it is shown in eq.5.107, and therefore grows specially fast for  $|A| \simeq |F|/2$ . However, if we stick to the sectors in which the determinant method works, the matrix size will only maximally increase quadratically with  $N$ . This means that, even tough restricted in the size of the sector, we are able to perform the fermion integration for large  $N$ . The second reason why we favour the determinant method is the fact that the determinant can be calculated in polynomial time<sup>4</sup>, which is specially important in prospect of performing a

<sup>4</sup>This can be achieved by Gaussian elimination. Note that the function  $P$ , used to calculate transfer matrix entries for arbitrary  $|A|$ , is  $\#P$ -complete.

simulation of the bosonic degrees of freedom for which transfer matrix elements need to be computed repetitively.

We will now calculate the explicit form of the interaction matrices living on the time slices and also the interaction matrix describing the gauge field interactions. Afterwards we discuss the transfer matrix and the partition function in the sectors where zero, one, all and all minus one fermions are propagating in time.

### 5.8.1. Explicit time slice interaction matrix for $SU(2)$

Here we give an explicit representation of the interaction matrix from eq.(5.100) with the explicit choice of  $SU(2)$  as the symmetry group. The group index is now  $a = 1, 2, 3$  and the structure constants are the Levi-Civita tensors  $\epsilon^{abc}$  and therefore

$$\Phi_{\alpha\beta}^{ac}(t) = (m+1)\delta^{ac}\delta_{\alpha\beta} - i\epsilon^{abc}(\sigma_i)_{\alpha\beta}\phi_i^b(t). \quad (5.130)$$

The explicit form, following the introduced ordering of indices from eq.(5.105), of the interaction matrix  $\Phi$  is

$$\Phi = \begin{array}{c} a \backslash c \\ \begin{matrix} 1 & 2 & 3 \end{matrix} \end{array} \begin{pmatrix} M & \Lambda^{12} & \Lambda^{13} \\ \Lambda^{21} & M & \Lambda^{23} \\ \Lambda^{31} & \Lambda^{32} & M \end{pmatrix} \quad \text{with} \quad M = \begin{array}{c} \alpha \backslash \beta \\ \begin{matrix} 0 & 1 \end{matrix} \end{array} \begin{pmatrix} m+1 & 0 \\ 0 & m+1 \end{pmatrix}, \quad (5.131)$$

and

$$\Lambda^{ac} = -i\epsilon^{abc} \cdot \begin{array}{c} \alpha \backslash \beta \\ \begin{matrix} 0 & 1 \end{matrix} \end{array} \begin{pmatrix} \phi_3^b & \phi_1^b - \phi_2^b i \\ \phi_1^b + \phi_2^b i & -\phi_3^b \end{pmatrix}, \quad (5.132)$$

where the rows and columns are labelled with the index  $a, b, \alpha$  and  $\beta$  in order to identify the correct interactions easier. The full matrix then has the form

$$\Phi = \begin{pmatrix} m+1 & 0 & \phi_3^3 i & \phi_2^3 + \phi_1^3 i & -\phi_3^2 i & -\phi_2^2 - \phi_1^2 i \\ 0 & m+1 & -\phi_2^3 + \phi_1^3 i & -\phi_3^3 i & \phi_2^2 - \phi_1^2 i & \phi_3^2 i \\ -\phi_3^3 i & -\phi_2^3 - \phi_1^3 i & m+1 & 0 & \phi_3^1 i & \phi_2^1 + \phi_1^1 i \\ \phi_2^3 - \phi_1^3 i & \phi_3^3 i & 0 & m+1 & -\phi_2^1 + \phi_1^1 i & -\phi_3^1 i \\ \phi_3^2 i & \phi_2^2 + \phi_1^2 i & -\phi_3^1 i & -\phi_2^1 - \phi_1^1 i & m+1 & 0 \\ -\phi_2^2 + \phi_1^2 i & -\phi_3^2 i & \phi_2^1 - \phi_1^1 i & \phi_3^1 i & 0 & m+1 \end{pmatrix}. \quad (5.133)$$

Analogously any  $SU(N)$  group can be used. In the same basis the matrix

$$\bar{\psi}_\alpha^a(L_t - 1) \tilde{\Phi}_{\alpha\beta}^{ab} \psi_\beta^b(0), \quad (5.134)$$

describing the interactions on the last link including the gauge field is

$$\tilde{\Phi} = \begin{array}{c} a \backslash b \\ \begin{matrix} 1 & 2 & 3 \end{matrix} \end{array} \begin{pmatrix} \tilde{\Phi}^{11} & \tilde{\Phi}^{12} & \tilde{\Phi}^{13} \\ \tilde{\Phi}^{21} & \tilde{\Phi}^{22} & \tilde{\Phi}^{23} \\ \tilde{\Phi}^{31} & \tilde{\Phi}^{32} & \tilde{\Phi}^{33} \end{pmatrix}, \quad (5.135)$$

## 5. Fermion sectors in Matrix-theory

with

$$\tilde{\Phi}^{ab} = \begin{array}{c} \alpha \backslash \beta \\ \begin{array}{cc} 0 & 1 \\ \text{Tr}[UT^a U^\dagger T^b] & 0 \\ 1 & 0 \end{array} \end{array} \begin{pmatrix} 0 & 1 \\ \text{Tr}[UT^a U^\dagger T^b] & 0 \end{pmatrix}. \quad (5.136)$$

### 5.8.2. Zero fermions propagating in time

Let us consider the sector where no fermion is winding around the temporal direction. The adequate transfer matrix is only a scalar at each time slice of the following form

$$T_0(t) = (-1)^{|F|} \det [\Phi^{\overline{A_j A_i}}(t)] = (-1)^{|F|} \det [\Phi(t)], \quad (5.137)$$

where no row and column of  $\Phi$  need to be erased, since  $A_i = A_j = \emptyset$ . We recall that the number of fermions is  $2(N^2 - 1)$ , therefore the sign in the equation above is redundant and we have

$$T_0(t) = \det [\Phi(t)]. \quad (5.138)$$

Using  $\Phi$  from eq.(5.130), which is the explicit form of the interaction matrix for the symmetry group  $SU(2)$ , we find a purely real and positive determinant

$$T_0(t) = \left[ (m+1)^3 - 2\epsilon_{ijk} \phi_i^1(t) \phi_j^2(t) \phi_k^3(t) - (m+1) \sum_{a,i} (\phi_i^a)^2 \right]^2, \quad (5.139)$$

where the  $\epsilon$ -tensor is used to simplify the sum over all spatial components of  $\phi$  which are  $i = 1, 2, 3$ . If we send  $m$  to zero we obtain

$$T_0(t) = \left[ 1 - 2\epsilon_{ijk} \phi_i^1(t) \phi_j^2(t) \phi_k^3(t) - \sum_{a,i} (\phi_i^a)^2 \right]^2. \quad (5.140)$$

This can be now used to write down the full partition function

$$Z_0 = \int dU \left( \prod_{i,\alpha} \int d\phi_\alpha^i \right) \exp \left[ -\hat{S}_B(\phi, U) \right] \left( \frac{1}{2g^2} \right)^{6L_t} \prod_{t=0}^{L_t-1} T_0(t), \quad (5.141)$$

where we do not need to insert a gauge link transfer matrix for the fermions, simply because there are no fermions propagating in temporal direction. The expression for the partition function can straightforwardly be generalised to any  $SU(N)$  by considering the matrix  $\Phi$  as shown in eq.(5.100) for the desired symmetry group. The factor  $(2g^2)^{-6L_t}$  which is specific for  $N = 2$  was generally denoted by  $(2g^2)^{-v}$  with  $v = 2(N^2 - 1)L_t$  and will drop out in any expectation value calculated in this formulation and will be therefore left out in the following formulas. Note that the size of the interaction matrix increases for larger  $N$  but the transfer matrix remains a scalar in this sector.

This result allows us to study the  $Z_0$  sector of the partition function independently from any other sector and makes the fermion integration, at least shown for  $SU(2)$ , free of any sign problem. Since there are zero fermions winding around the temporal dimension,  $Z_0$  is not sensitive to the choice of boundary conditions and always appears with a positive sign in

$$Z = Z_0 + \dots. \quad (5.142)$$



### 5.8.3. One fermion propagating in time

In the  $Z_1$  sector of the partition function only one fermion is propagating, i.e.  $|A| = 1$ . A transfer matrix element can therefore be calculated by

$$[T_1(t)]_{ij} = (-1)^{1+A_i+A_j} \det [\Phi^{\overline{A_j A_i}}(t)] . \quad (5.143)$$

Since  $A_i$  and  $A_j$  hold exactly one element we denote them with  $i$  and  $j$  in order to obtain the more elegant form

$$[T_1(t)]_{ij} = (-1)^{1+i+j} \det [\Phi^{\overline{j i}}(t)] . \quad (5.144)$$

This again works for any symmetry group  $SU(N)$  and is only growing quadratically with  $N$ . The transfer matrix size for  $N = 2$  is  $6 \times 6$ , for  $N = 8$  it is  $126 \times 126$  and for  $N = 32$  it is  $2046 \times 2046$ , making calculations for even large  $N$  possible. Note that since a fermion is propagating in time we will need to take into account the interactions of the fermion with the gauge field on the last link. This is done by inserting the transfer matrix  $T_1^U$  on the last link, which in the case of one propagating fermion is simply

$$[T_1^U]_{ij} = \tilde{\Phi}_{ij} . \quad (5.145)$$

The partition function, including also the gauge field and bosonic fields, is

$$Z_1 = \int dU \left( \prod_{i,\alpha} \int d\phi_\alpha^i \right) \exp \left[ -\hat{S}_B(\phi, U) \right] \text{Tr} \left\{ T_1^U \prod_{t=0}^{L_t-1} T_1(t) \right\} , \quad (5.146)$$

which appears in

$$Z = Z_0 + (-1)^{\epsilon+1} Z_1 + \dots , \quad (5.147)$$

where  $\epsilon = 0$  denotes periodic and  $\epsilon = 1$  anti-periodic boundary conditions.

### 5.8.4. All fermions are propagating in time

In the sector where all fermions are propagating in time there are no contributions from the interaction matrix living on the time slices. We simply get

$$Z_{|F|} = \int dU \left( \prod_{i,\alpha} \int d\phi_\alpha^i \right) \exp \left[ -\hat{S}_B(\phi, U) \right] \text{Tr} \left\{ T_{|F|}^U \right\} , \quad (5.148)$$

where the transfer matrix accounting for the gauge field is a scalar, i.e.

$$T_{|F|}^U = \det[\tilde{\Phi}] . \quad (5.149)$$

The contribution of the configurations with  $|A| = |F|$  appear in

$$Z = Z_0 + (-1)^{\epsilon+1} Z_1 + \dots + Z_{|F|} \quad (5.150)$$

with a positive sign, since  $|A| = |F|$  and  $|F|$  is even.

### 5.8.5. All but one fermions are propagating in time

In the sector where  $|F| - 1$  fermions are propagating, the transfer matrix is of size  $|F| \times |F|$  because there are exactly  $|F|$  ways how to cut  $|F| - 1$  columns or rows out of a  $|F| \times |F|$  matrix. The the transfer matrix size is identical to the size of the transfer matrix in the sector where only one fermion is propagating in time but taking the determinant in order to obtain the transfer matrix elements is trivial now since it is only a scalar. Therefore the determinant is redundant and we are left with

$$[T_{|F|-1}(t)]_{ij} = (-1)^{\delta_{ij}} [\Phi(t)]_{ij} , \quad (5.151)$$

where the partition function can be again obtained by

$$Z_{|F|-1} = \int dU \left( \prod_{i,\alpha} \int d\phi_\alpha^i \right) \exp \left[ -\hat{S}_B(\phi, U) \right] \text{Tr} \left\{ T_{|F|-1}^U \prod_{t=0}^{L_t-1} T_{|F|-1}(t) \right\} , \quad (5.152)$$

where  $|F| = 2(N^2 - 1)$ . The transfer matrix on the last link is

$$[T_{|F|-1}^U]_{ij} = \det[\tilde{\Phi}^{\cancel{F \setminus A_i} \setminus A_j}] \quad (5.153)$$

but since  $|A_i| = |F| - 1$  we can label the only fermion hop that is not incoming with  $i$  and the only one not hopping out with  $j$  and write

$$[T_{|F|-1}^U]_{ij} = \det[\tilde{\Phi}^{\cancel{i} \setminus j}] . \quad (5.154)$$

So we find

$$Z = Z_0 + (-1)^{\epsilon+1} Z_1 + \dots + (-1)^{\epsilon+1} Z_{|F|-1} + Z_{|F|} \quad (5.155)$$

## 5.9. Conclusion and Outlook

In this chapter we considered the  $4d \mathcal{N} = 1$  super Yang-Mills model that is dimensionally reduced to a one-dimensional  $\mathcal{N} = 4$  quantum mechanical matrix model. The lattice served as a regulator with the Wilson derivative for the fermionic fields and the symmetric derivative for the bosonic fields. Following Wilson's description, the gauge field was described by a dynamic link variable of the  $SU(N)$  group. In this setup the fermionic hop terms of the action are directed, only allowing the fermions to propagate in one direction. We then calculated the hopping expansion of the Boltzmann factor from the fermionic term of the action and established a fermion loop formulation. In the fermion loop formulation the configurations contributing to the partition function can be written as a sum over closed loop configuration. We then laid spacial focus on the construction of a transfer matrix approach in order to write the partition function as a trace of a product of time dependent transfer matrices that are defined on the dual lattice. The number of fermions propagating forward in time is constant and the transfer matrix therefore showed to have a block diagonal structure. This allows to split off the partition function into different sectors, where each sector corresponds to contributions from configurations with a fixed number of fermions propagating forward in time. After providing an explicit formula for the calculation of a transfer matrix element we showed how to deal with the gauge field. We chose the temporal gauge and described the gauge field by an additional matrix living

on the last link of our one-dimensional lattice. The formulation of the partition function in terms of a sum over closed fermion loop configurations described by a product of transfer matrices can be generalised to a wide range of one-dimensional models obtained by dimensional reduction of  $d$ -dimensional super Yang-Mills models.

The entries of a transfer matrix can in some sectors of the partition function be calculated by taking a determinant of a matrix, or a sub-part of it, that is describing the interactions of the fermions with the bosonic fields. In our last section we presented some explicit calculations of the transfer matrix for the sector where zero, one, all and all but one fermions are propagating forward in time for  $SU(2)$ . Most of these results can be trivially generalised to any  $SU(N)$  group.

In practice the transfer matrix approach seems to run into computational problems when investigating the large- $N$  behaviour due to extremely large transfer matrices. This however is not true for certain sectors of the partition function. If the number of fermions that are propagating in time is close to zero or close to the total number of possibly propagating fermions, the transfer matrices grow moderately, e.g. grow not at all for zero propagating fermions, grow quadratically for one propagating fermion. We therefore restricted ourselves to sectors where zero, one, all and all but one fermions are propagating forward in time and use the determinant to calculate transfer matrix elements. This assures the calculation of transfer matrix elements in polynomial time and makes calculations for larger  $N$  possible. Note that it may well be, as seen in the two-dimensional  $\mathcal{N} = 1$  Wess-Zumino model, that several physical properties, like for example the mass of a field, are identical in the sector where no fermions are winding around any dimension and the sectors where we have fermions winding around the extents of the system.

A numerical investigation with a standard Metropolis algorithm for the bosonic fields and gauge field, while calculating the contribution of the fermions with the transfer matrix, is currently ongoing. In a first step we will stick to the one-dimensional model with 4 supercharges and symmetry group  $SU(2)$ . In the case where  $N = 2$  we can access all sectors of the partition function since the transfer matrix size is still in a computable range. This will serve as a proof of concept and a first comparison can be made with already existing data. Afterwards we will restrict ourselves to the mentioned sectors where the determinant method works which allow us to exploit the large- $N$  limit. In a second step we plan on considering more interesting models like the one with 16 supercharges.

A different strategy to follow is the simulation of such models with a worm-like algorithm. In order to do such we have established a bond formulation for the bosonic degrees of freedom and a loop formulation for the fermionic fields for the model with 4 supercharges and symmetry group  $SU(2)$ . In the presented form this model can now be simulated with a worm-like algorithm. However, there are different sources of sign problems which most likely ruin a straightforward simulation in the bond/loop formulation. Nevertheless, some first ideas<sup>5</sup> exist which might eliminate the sign problem. Note that this might only work for the system with 4 supercharges since the fermion determinant should

---

<sup>5</sup>The basic idea is to use the fact that for every closed fermion loop (on a fixed bosonic background) there exists another loop with a  $\pm$  complex conjugated contribution.

## 5. *Fermion sectors in Matrix-theory*

be free [88] of any sign problem, for the model with 16 supercharges this is not the case.

# Acknowledgement

My most profound thanks go to Urs Wenger for his support during the last couple of years. He gave me the chance to conduct research in this interesting field of science and fostered my interests by being an inspiring and enthusiastic physicist and supervisor. I thank Andreas Wipf for reading my thesis and accepting the responsibility of being the co-referee for my thesis.

I also want to thank my physicist friends who helped me in various ways during my time as a PhD student. Thanks go to David Baumgartner and Vidushi Maillart for familiarising myself with many concepts of lattice field theory in the beginning of my thesis. For countless hours of discussions throughout the past years I want to thank Michael Bögli, Stefanie Marti, Peter Stoffer, Lukas Marti, Lorena Rothen, Ramon Stucki, Albert Deuzemann and Adolfo Guarino. Special thanks also go to my office mates Philippe Widmer and Pascal Stebler who besides discussing problems related to physics also educated me with valuable programming and computer knowledge.

My gratitude also goes to Ester Fiechter, the secretary of our institute, dealing with many administrative issues. I am much indebted to the Institute and Urs Wenger for making it possible to attend a summer school and a lattice conference, where I was able to meet other people from the community. I thank Peter Stoffer with whom I had the chance to maintain the cluster of the institute for the last three years. I would also like to thank Markus Moser for maintaining hardware and software of the computers at our institute and for his professional support in administrating the Institute's cluster.

Last but not least, I thank my family and friends for their support, encouragement and love.



## A. Numerical data

### A.1. Ising-suszeptibility

$g$	$V$	$m_c$	$\delta m_c$
0.25000	$16 \times 16$	0.38394	0.01224
0.25000	$32 \times 32$	0.38055	0.01238
0.25000	$64 \times 64$	0.37161	0.00828
0.18750	$16 \times 16$	0.28863	0.00402
0.18750	$32 \times 32$	0.30082	0.00397
0.18750	$64 \times 64$	0.29532	0.00405
0.18750	$128 \times 128$	0.29525	0.00386
0.15750	$16 \times 16$	0.24652	0.00531
0.15750	$32 \times 32$	0.25914	0.00466
0.15750	$64 \times 64$	0.25862	0.00441
0.15750	$128 \times 128$	0.25777	0.00301
0.12500	$16 \times 16$	0.19912	0.00160
0.12500	$32 \times 32$	0.20645	0.00099
0.12500	$64 \times 64$	0.21063	0.00176
0.12500	$128 \times 128$	0.20821	0.00227
0.12500	$256 \times 256$	0.20711	0.00184
0.09375	$16 \times 16$	0.14383	0.00213
0.09375	$32 \times 32$	0.15919	0.00151
0.09375	$64 \times 64$	0.16226	0.00160
0.09375	$128 \times 128$	0.16374	0.00240
0.09375	$256 \times 256$	0.16281	0.00179
0.06250	$16 \times 16$	0.09216	0.01022
0.06250	$32 \times 32$	0.11274	0.00422
0.06250	$64 \times 64$	0.11244	0.00379
0.06250	$128 \times 128$	0.11373	0.00123
0.06250	$256 \times 256$	0.11336	0.00114
0.03125	$16 \times 16$	0.02212	0.01116
0.03125	$32 \times 32$	0.05263	0.00472
0.03125	$64 \times 64$	0.06152	0.00300
0.03125	$128 \times 128$	0.06037	0.00299
0.03125	$256 \times 256$	0.05959	0.00321

Table A.1.: Critical mass  $m_c$  at various couplings and volumes with error  $\delta m_c$  obtained by fitting a Gaussian to the susceptibility of the Ising-spin projection of the scalar field variable  $\chi$ .

## A.2. Binder cummulant

g	V	$m_c$	$\delta m_c$
0.18750	16×16	0.27120	0.00559
0.18750	32×32	0.27899	0.00380
0.18750	64×64	0.29225	0.00293
0.15750	16×16	0.22397	0.00343
0.15750	32×32	0.23814	0.00306
0.15750	64×64	0.24228	0.00263
0.12500	16×16	0.17481	0.00302
0.12500	32×32	0.19459	0.00304
0.12500	64×64	0.20168	0.00215
0.12500	128×128	0.20401	0.00181
0.09375	16×16	0.12623	0.00175
0.09375	32×32	0.14532	0.00357
0.09375	64×64	0.15318	0.00168
0.09375	128×128	0.15743	0.00100
0.06250	16×16	0.07967	0.00131
0.06250	32×32	0.09378	0.00180
0.06250	64×64	0.10460	0.00093
0.06250	128×128	0.11079	0.00114
0.03125	16×16	0.03750	0.00353
0.03125	32×32	0.04492	0.00243
0.03125	64×64	0.05115	0.00218
0.03125	128×128	0.05574	0.00239

Table A.2.: Critical mass  $m_c$  at various couplings and volumes with error  $\delta m_c$  obtained by linear fits of intersecting Binder cummulants  $U$  of the scalar field.



## B. Monte Carlo

In this section we only highlight fundamental concepts of the Monte Carlo methods which were used in the numerical simulations in this thesis. In the following we closely follow [19].

### B.1. Markov Chain

Monte Carlo methods are used to numerically estimate the expectation value of an observable  $\mathcal{O}[x]$  depending on some variable  $x$ , which may also be a set of variables which we call configuration. An example of such a configuration is the field configuration  $x = \{\phi_1, \phi_2, \dots, \phi_V\}$  of some bosonic field defined on the lattice. The goal of the Monte Carlo algorithm is to generate a sample consisting of a large number of configurations  $x$  with the use of random numbers. This needs to be done in a way such that the distribution within a sample is converging to the desired distribution. The expectation value of an observable is approximated by the mean value

$$\overline{\mathcal{O}} = \sum_x \mathcal{O}[x] p(x), \quad (\text{B.1})$$

where  $p(x)$  is the probability to find the system in a state  $x$ . When considering systems that describe a canonical ensemble with an action  $S[x]$ , this probability is proportional to the Boltzmann factor, i.e.

$$p(x) = \frac{1}{Z} e^{-S[x]}, \quad (\text{B.2})$$

analogous to the case of statistical mechanics where we have  $S[x] \equiv \beta E[x]$ , where  $\beta$  is the inverse temperature and  $E[x]$  the energy.  $Z$  is the partition function defined as

$$Z = \sum_x w(x), \quad (\text{B.3})$$

where  $w(x)$  is the weight of a configuration  $x$ , generally the Boltzmann factor. The configurations in a sample are in numerical simulations generated by what is commonly referred to as updating. An update is a stochastic process going from one configuration  $x$  to the next  $x'$ . The probability that an update is performed is described by the transition probability  $p(x \rightarrow x')$ , which only depends on  $x$  and  $x'$ . We additionally have the normalisation conditions

$$\sum_{x'} p(x \rightarrow x') = 1 \quad \text{and} \quad \sum_x p(x) = 1. \quad (\text{B.4})$$

The chain of configurations created by this kind of stochastic updating steps is called Markov chain.

## B.2. Importance sampling

In already small statistical systems the configuration space can be very large. Consider for example an Ising-model with  $n$  different spins with possible values  $\pm 1$ . The number of total configurations is  $2^n$ , which already for small  $n$  makes it impossible to visit all possible configurations in a Markov Chain of reasonable length. The goal is to pick configurations which have more impact on the expectation value. In order to achieve this and therefore reduce the variance of the estimator in eq.(B.1), a subset of the configuration space is chosen in which the configurations that are generated are distributed accordingly to the Boltzmann factor  $\exp(-S[x])$ . This idea of generating the more probable configurations is called importance sampling. One way to create such samples is the Metropolis algorithm which we will discuss below.

## B.3. Metropolis algorithm

The goal of a Metropolis algorithm is to create a Markov chain by using importance sampling and by designing the update procedure in a way such that the transition probability is close to one. If the transition probability  $p(x \rightarrow x')$  is close to one it is likely that the new state  $x'$  becomes the next element of the Markov chain. The transition probability is set to fulfil two key features

### Ergodicity

Any configuration  $x'$  can be reached from any other configuration  $x$  in a finite number of updating steps.

### Detailed balance

The transition probabilities are set to satisfy

$$w(x)p(x \rightarrow x') = w(x')p(x' \rightarrow x), \quad (\text{B.5})$$

which is called detailed balance. This condition is set in order to ensure that the fixed point of the canonical ensemble is unique and therefore also the result of a numerical simulation.

It shows itself useful to divide the transition probability into

$$p(x \rightarrow x') = p_c(x \rightarrow x')p_a(x \rightarrow x'), \quad (\text{B.6})$$

where  $p_c(x \rightarrow x')$  is an arbitrary probability distribution for the proposed change of the configuration  $x$  to  $x'$  and  $p_a(x \rightarrow x')$  is called the acceptance probability. In an updating step the algorithm starts with a configuration  $x$  and proposes a new one  $x'$  according to the probability distribution  $p_c(x \rightarrow x')$ . The probability to accept the proposed update to become the next element of the Markov chain is then

$$p_a(x \rightarrow x') = \min \left\{ 1, \frac{p_c(x' \rightarrow x)w(x')}{p_c(x \rightarrow x')w(x)} \right\}. \quad (\text{B.7})$$

## C. Data and error analysis

An estimated value of an observable means nothing without a realistic error. Although data and error analysis is being covered in countless textbooks and forms a whole mathematical art on its own, we would like to pick and highlight the most important concepts which were of special importance for this thesis. When doing computer simulations in lattice field theory one is mainly faced with the following setup. A set of data is generated by a Monte Carlo Simulation (B) forming a sequence of data points in a Markov chain. Having created such data one is usually interested in an estimator for a desired observable which is a function of the measured data. Along with the estimator of the observable an adequate error is needed. Getting to realistic results amounts to deal with two main problems which are the correlation among the data and the possibly non-linear dependence of quantities on the mean value of the data. In the following we will show how these problems can be tackled in a rather simple way.

### C.1. Correlated data

Let's look at a sequence of configurations  $x_i$ , where  $i = 0, 2, \dots, N-1$  and  $N$  is the number of configurations produced by a Metropolis algorithm. The best estimator for the expectation value of an observable  $\langle \mathcal{O}[x] \rangle$  is the mean value

$$\overline{\mathcal{O}}[x] = \frac{1}{N} \sum_{i=0}^{N-1} \mathcal{O}[x_i]. \quad (\text{C.1})$$

In the limit where  $N \rightarrow \infty$  we have  $\overline{\mathcal{O}}[x] = \langle \mathcal{O}[x] \rangle$ . Following the notation and structure of [19] such quantities can be called primary quantities  $\mathcal{O}$  which are directly obtained by averaging. Secondary quantities  $\theta$  are those which are functions of averages e.g. the Binder cumulant  $U = 1 - \langle x^4 \rangle / (3\langle x^2 \rangle^2)$ . Since  $x_i$  is the  $i$ -th element of a Markov chain and depends on its preceding element  $x_{i-1}$ , they are generally not independent and there exists a correlation in the data. This correlation also has an effect on the level of the observable  $\mathcal{O}$ , the mean value will be calculated in the same manner but the error calculation is more delicate. If the data were independent the best estimator for the variance of  $\mathcal{O}$  would be given by

$$\sigma_{\mathcal{O}}^2 = \frac{1}{N-1} (\langle \mathcal{O}^2 \rangle - \langle \mathcal{O} \rangle^2), \quad (\text{C.2})$$

but since we are dealing with correlated data the formula above is underestimating the error of  $\mathcal{O}$ . We need a method to analyse the integrated autocorrelation time  $\tau_{\mathcal{O}}$  in order to be able to tell how many updating steps one has to perform until an uncorrelated element is found in the Markov chain. We will therefore consider a very simple method of binning.

## C.2. Binning analysis

A reliable way to estimate the integrated autocorrelation time is the binning method. Binning is the procedure of averaging consecutive entries of the data set  $x$  and then obtain a new less correlated data set  $y$ . One usually divides the  $N$  measurements into blocks of size  $l$ , averages over each of them to get  $y_i$  and calculates the standard deviation on this new “ binned ” data. The average over a certain bin  $i$  is

$$y_l = \frac{1}{s} \sum_{j=0}^{N_l-1} \mathcal{O}[x_{ls+j}] \quad \text{with} \quad l = 0, 2, \dots, N_l - 1, \quad (\text{C.3})$$

where  $N_l$  is the number of bins with size  $s$ , i.e.  $N_l = N/l$ . The standard deviation  $\sigma_y$  is growing with increasing bin size  $s_l$  and is asymptotically going to the correct error. In practice the function  $\sigma_{y(l)}$  is building a plateau and stops growing with increasing bin size when the bin size is much larger than the integrated autocorrelation time. This procedure gives us an estimate of  $\tau_{\mathcal{O}}$  and a correct  $\sigma_y$ . Another common procedure is to consider the autocorrelation function.

## C.3. Jackknife analysis

The error calculation needs to be addressed carefully for secondary quantities which are functions of averages i.e.  $\theta = \theta(\langle \mathcal{O}_0[x] \rangle, \dots, \langle \mathcal{O}_j[x] \rangle, \dots)$ . The Jackknife method is such a way of analysing the error of such quantities. Note that the best estimate of  $\bar{\theta}$  is  $\theta(\bar{\mathcal{O}})$  and that  $\bar{\theta}(\bar{\mathcal{O}})$  is generally an unusable estimator. When it comes to calculating the error  $\sigma_{\theta}$  the jackknife method comes into play. Consider a set of  $N$  independent primary quantities  $\mathcal{O}_i$ , we now create a so called Jackknife sample by removing one single measurement from the rest of the data and then average over those remaining  $N - 1$ . By removing the  $j$ -th measurement we create the  $j$ -th jackknife sample

$$\mathcal{O}_j^J = \frac{1}{N-1} \left( \sum_{i=0}^{N-1} \mathcal{O}_i - \mathcal{O}_j \right). \quad (\text{C.4})$$

Doing this for  $N_J$  different  $j$  in  $[0, N-1]$  gives us all the  $N_J$  Jackknife samples  $\mathcal{O}_j^J$ . If there exists a function  $\theta$  which is depending on a set of observables  $\mathcal{O}_l$ , we can now estimate the standard deviation of  $\theta(\bar{\mathcal{O}})$  by forming the Jackknife samples of all  $\mathcal{O}_l$  and compute the corresponding  $\theta_j^J(\mathcal{O}_j^J)$ . The jackknife estimator

$$\sigma_{\theta}^J = \sqrt{\frac{N_J - 1}{N_J} \sum_{i=0}^{N_J-1} (\mathcal{O}_i^J - \bar{\mathcal{O}}^J)^2}, \quad (\text{C.5})$$

where

$$\bar{\mathcal{O}}^J = \frac{1}{N_J} \sum_{i=0}^{N_J-1} \mathcal{O}_i^J, \quad (\text{C.6})$$

then gives us a reliable estimate for the standard deviation of  $\theta$ , i.e.  $\sigma_{\bar{\theta}} = \sigma_{\bar{\theta}}^J$ . Note that mostly a function  $\theta$  does not only depend on one observable, but the extension to multiple observables is trivial, since one just needs to perform the Jackknife sampling identically with all observables.

## C.4. Cumulative distribution

The cumulative distribution function  $F_x(y)$  is

$$F_x(y) = P(x \leq y), \quad (\text{C.7})$$

where  $P(x \leq y)$  is the probability to find the real random variable  $x$  being less or equal to  $y$ . If there exists a probability density function  $f_x(y)$  describing the likelihood of the random variable  $x$  to be the value  $y$ , then the cumulative distribution function is defined as

$$F_x(y) = \int_{-\infty}^y f_x(z) dz. \quad (\text{C.8})$$

More on this can be found in almost any literature on statistics and computational science, e.g. [92].

## C.5. Systematic error estimate

In this section we want to discuss how the systematic error of choosing a fitrange is estimated in the fitting procedure that was used to extract the masses in the  $d = 2$   $\mathcal{N} = 1$  Wess-Zumino model.

Since there are many fit-ranges which yield the similar quality of fit, i.e.  $\chi^2/\text{dof}$  and p-value, we fitted the function to the correlator in all possible and reasonable ( $\chi^2/\text{dof} < 1.4$ ) ranges by varying  $t_{\min}$  and  $t_{\max}$ , the starting and ending point of the fit range in  $t$ . We then calculate the cumulative distribution function (CDF), see C.4, for all the fit results weighted with their  $\chi^2/\text{dof}$  values. From the CDF we can then read off the estimated mean value of the observable and the corresponding standard deviation. As an example let us illustrate this procedure by fitting the fermion correlator in order to obtain the lowest mass state  $m_\psi^{(0)}$  in the supersymmetric phase. We vary the fit range and obtain various results for  $m_\psi^{(0)}$ . Let  $N$  be the number of fits performed and  $m_\psi^{(0)}(j)$  be the  $N$  different fit results, where  $j \in \{1, 2, \dots, N\}$ . A weight  $w(j) = 1/\chi^2(j)$  is now assigned to every measurement. If we use the total weight

$$W = \sum_{j=1}^N w(j) \quad (\text{C.9})$$

in order to norm the weights

$$\bar{w}(j) = \frac{1}{\chi^2(j)W}, \quad (\text{C.10})$$

we can then construct the approximate CDF by

$$\text{CDF} \left( m_\psi^{(0)}(j) \right) = \sum_{i=1}^{i \leq j} \bar{w}(i). \quad (\text{C.11})$$

Assuming that there are enough samples, i.e.  $N$  is large enough, the expected mean value

and its standard deviation  $\sigma$  can be calculated by

$$m_\psi^{(0)} \quad \text{where} \quad \text{CDF} = 0.5, \quad (\text{C.12})$$

$$m_\psi^{(0)} + \sigma \quad \text{where} \quad \text{CDF} = 0.5 + 34.1\%, \quad (\text{C.13})$$

$$m_\psi^{(0)} - \sigma \quad \text{where} \quad \text{CDF} = 0.5 - 34.1\%. \quad (\text{C.14})$$

$$(\text{C.15})$$

In fig.C.1 on the left the CDF of a normal distribution is shown with the one sigma confidence interval. In the centre of the same figure we illustrate this on a data set in the supersymmetric phase in order to obtain the fermion mass  $m_\psi^{(0)}$  with its corresponding errors. In that case the error in both directions is symmetric since the CDF is almost symmetric around  $m_\psi^{(0)}$ . On the right of fig.C.1 we are considering the fermionic ground state in the supersymmetric phase close to the spontaneous breakdown. We see that the CDF is not symmetric and therefore neither are the errors. This can nicely be seen in fig.3.26 around the critical point. What can be also already extracted from the plot on the right of fig.C.1 is that there seems to emerge a second region in which fits with low  $\chi^2/\text{dof}$  are possible. This comes from the fact that closer to the critical point the measured masses decrease and an excited state enters our correlators resolution. After the symmetry breakdown there exist two regions in the correlator in which a single exponential can be fitted nicely, one in a time window rather close to zero and one further away. We are therefore using the fit function from eq.(3.98) in the broken phase for the correlators that show a second contribution from another higher mass.

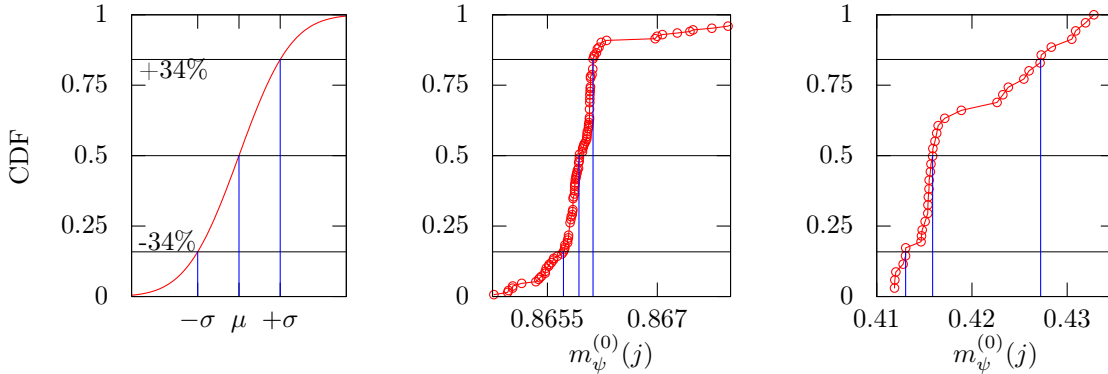


Figure C.1.: On the left we plot the cumulative distribution function of a normal distribution with the one sigma confidence interval. In the middle we look at fit results for  $m_\psi^{(0)}$  in the SUSY phase on a  $L_t \times L_x = 128 \times 48$  lattice at  $g = 0.25$  and bare mass  $m = 1.4$ . On the right we show the same but closer to the critical point. The blue vertical lines illustrate the expected mean value and the one sigma confidence interval of the observable  $m_\psi^{(0)}$

The correlator in the supersymmetric phase can be fitted very well with a single cosh function plus a constant and the fit range can be varied slightly in the region of small  $t$ . The  $\chi^2/\text{dof}$  and p-values of the fit give us realistic criteria to determine how good a fit is. It is the supersymmetric phase where fitting is a more delicate task. The errors of the correlator seem overestimated, therefore we need to perform a fit which respects

the fact that the data are correlated in time  $t$ . This can be achieved by using a proper covariance matrix in the fit procedure when minimising the residuals. The exact procedure is explained in detail in the next appendix C.6.

The lowest mass state can be extracted by following the signal over several orders of magnitude. The signals coming from the first excited states are not determinable as precisely as the lowest states. Increasing the precision of the first excited states or even accessing a second excited states were not possible. Efforts [93] showed that also methods like the diagonalisation of the correlator matrix hardly improve the situation.

## C.6. Fitting correlated data

Assume we have  $N$  samples of unbiased estimators of quantities  $\mathcal{O}^k$ . The data set  $\mathcal{O}_i^k$  with  $i = 0, 1, \dots, N-1$  are said to be independent of  $i$  for fixed  $k$  but can be correlated in  $k$ . In our case the observable of interest is the correlator  $\mathcal{O}_i^k = C(t)C(t + k \cdot dt)$ , where  $k$  stands for the number of lattice steps  $dt$  in the time direction and  $i$  stands for the  $i$ -th measurement. If we want to fit a function to the correlator in time, i.e. to  $\mathcal{O}_i^k$  at fixed  $i$  but various  $k$ , the straightforward  $\chi^2/\text{dof}$  value is not a realistic criterion of the fit quality. A covariance matrix needs to be incorporated in the fitting procedure to guarantee a proper estimate of the  $\chi^2/\text{dof}$ -value.

Let us introduce the covariance matrix

$$C_{kl} = \frac{1}{N-1} \sum_{i=0}^{N-1} (\mathcal{O}_i^k - \langle \mathcal{O}^k \rangle)(\mathcal{O}_i^l - \langle \mathcal{O}^l \rangle), \quad (\text{C.16})$$

where the expectation value  $\langle \mathcal{O}^k \rangle$  is the mean value of that observable. The next step is to invert the matrix  $M_{kl} = C_{kl}^{-1}$  and then the  $\chi^2$ -value can be written as

$$\chi^2 = \left( \langle \mathcal{O}^k \rangle - \mathcal{O}^k \right) M_{kl} \left( \langle \mathcal{O}^l \rangle - \mathcal{O}^l \right). \quad (\text{C.17})$$

We can now use the Cholesky decomposition in order to get a lower- and upper-triangular matrix  $L$  and  $L^T$  such that

$$M = LL^T, \quad (\text{C.18})$$

which can be used to calculate  $\chi^2$  in the following way

$$\chi^2 = \sum_{k=0}^{N_D-1} f_k^\dagger f_k, \quad (\text{C.19})$$

where

$$f_k = \sum_{l=0}^{N_D-1} L_{kl} \left( \langle \mathcal{O}^l \rangle - t_l \right), \quad (\text{C.20})$$

and where  $t_i$  is the fitted value and  $N_D$  the number of data points to be fitted. Concerning the weighted least square method one can use

$$f_k = \sum_{l=0}^{N_D-1} L_{kl} \frac{\langle \mathcal{O}^l \rangle - t_l}{\delta_l}. \quad (\text{C.21})$$

### *C. Data and error analysis*

From which one could create the correct error of a data point  $\mathcal{O}^k$  like

$$\delta_k^{\text{real}} = \left( \sum_{l=0}^{N_D-1} \frac{L_{kl}}{\delta_l} \right)^{-1}. \quad (\text{C.22})$$

This section is based on [94,95].



## D. Grassmann integrals

### D.1. Grassmann variables calculus

For every fermion a pair of Grassmann variables  $(\eta_i, \eta_j^*)$  is introduced [19]. They fulfil the anticommutation relation

$$\{\eta_i^*, \eta_j\} = \{\eta_i, \eta_j\} = \{\eta_i^*, \eta_j^*\} = 0, \quad (\text{D.1})$$

and the square of any Grassmann number is always zero, i.e.  $\eta_i \eta_i = 0$ . For a disquisition on Grassmann numbers and their description as degrees of freedom of fermionic fields in a path integral we refer again to [19]. Let us here simply list the trivial Grassmann integrals

$$\int d\eta = 0, \quad \int d\eta \eta = 1, \quad \int d\eta \eta \eta = 0, \quad (\text{D.2})$$

$$\int d\eta_i d\eta_j \eta_j \eta_i = 1 \quad \text{and} \quad \int d\eta_i d\eta_j \eta_i \eta_j = -1. \quad (\text{D.3})$$

### D.2. Delta function in a grassmann integral

Consider two anticommuting variables  $\eta$  and  $\eta_0 \in \mathcal{G}$ , where  $\mathcal{G}$  is the Grassmann algebra. Let's introduce a Grassmann-valued function  $f(\eta) = a + b\eta$  with  $a \in \mathcal{G}$  and  $b \in \mathbb{R}$ . If the function gets multiplied by a delta function in the Grassmann integral we find

$$\begin{aligned} \int d\eta f(\eta) \delta(\eta - \eta_0) &= \int d\eta (a + b\eta)(\eta - \eta_0) \\ &= -a - b\eta_0 \\ &= -f(\eta_0), \end{aligned} \quad (\text{D.4})$$

whereas

$$\begin{aligned} \int d\eta \delta(\eta - \eta_0) f(\eta) &= \int d\eta (\eta - \eta_0)(a + b\eta) \\ &= a + b\eta_0 \\ &= f(\eta_0). \end{aligned} \quad (\text{D.5})$$

In our fermion hopping expansion the  $\delta$ -function belongs to the integration measure, hence it is the second variant which is relevant for us.



## E. Flavour integration in the supersymmetric nonlinear $O(2)$ sigma model

In this appendix we illustrate the basic idea of establishing a fermion loop formulation of the supersymmetric nonlinear  $O(2)$  sigma model by including all flavour possibilities along a fermion loop in one combined loop.

### E.1. Flavour integrated partition function

The bosonic degrees of freedom  $\phi_r$  and  $\phi_g$  are reduced by  $\phi_r^2 + \phi_g^2 = 1$  to an angle on the unit circle which we call  $\theta \in [0, 2\pi]$ . Consider a geometrically fixed loop, which means that the contribution from the Grassmann integral, as calculated in eq.(1.65), is fixed for any possible flavour combination. We are left with the bosonic contribution which is depending on the flavour of the loop, i.e. the fermionic constraints from  $\phi\psi = 0$ . The bosonic contribution of a geometrically fixed loop including all possible flavour combinations can be written as

$$\text{Tr} \left[ \prod_{l \in \Omega} T(\theta_{x_l}) \right], \quad (\text{E.1})$$

where the loop passes through  $L$  sites which are in  $\Omega = \{x_0, x_1, \dots, x_{L-1}\}$ . The matrix

$$T(\theta_x) = \begin{pmatrix} \phi_{r,x}^2 & \phi_{r,x}\phi_{g,x} \\ \phi_{g,x}\phi_{r,x} & \phi_{g,x}^2 \end{pmatrix} = \begin{pmatrix} \cos^2(\theta_x) & \cos(\theta_x)\sin(\theta_x) \\ \sin(\theta_x)\cos(\theta_x) & \sin^2(\theta_x) \end{pmatrix} \quad (\text{E.2})$$

holds all distinguishable options that can occur on a site where a fermion loop is going through. The entries of the matrix  $T$  are the bosonic contributions of the chosen fermionic constraints, i.e.  $T_{ij}$  corresponds to the bosonic contribution of  $\phi_i\phi_j\bar{\psi}_i\psi_j$ . Performing a product along a fermion line of these matrices assures that all possible fermionic constraint combinations are being created. Closing the fermion line amounts to taking the trace, which projects out all allowed states. It guarantees that only contributions with an even number of flavour changing constraints survive. Let us think now of the matrix  $T$ , to be living on every site of the lattice, representing all available options from  $\phi\psi = 0$  and consider a geometrically fixed fermion loop passing through sites in  $\Omega$ . In the language of the newly introduced matrices we multiply all matrices along the fermion line  $\Omega$  and find it to have the following form

$$\prod_{l \in \Omega}^{L-1} T(\theta_{x_l}) = \begin{pmatrix} \cos(\theta_{x_0})\cos(\theta_{x_{L-1}}) \prod_{l \in \Omega}^{L-2} f(\theta_{x_l}, \theta_{x_{l+1}}) & \cos(\theta_{x_0})\sin(\theta_{x_{L-1}}) \prod_{l \in \Omega}^{L-2} f(\theta_{x_l}, \theta_{x_{l+1}}) \\ \sin(\theta_{x_0})\cos(\theta_{x_{L-1}}) \prod_{l \in \Omega}^{L-2} f(\theta_{x_l}, \theta_{x_{l+1}}) & \sin(\theta_{x_0})\sin(\theta_{x_{L-1}}) \prod_{l \in \Omega}^{L-2} f(\theta_{x_l}, \theta_{x_{l+1}}) \end{pmatrix}, \quad (\text{E.3})$$

### E. Flavour integration in the supersymmetric nonlinear $O(2)$ sigma model

where

$$f(\theta_{x_l}, \theta_{x_{l+1}}) = \cos(\theta_{x_l}) \cos(\theta_{x_{l+1}}) + \sin(\theta_{x_l}) \sin(\theta_{x_{l+1}}). \quad (\text{E.4})$$

The matrix in eq.(E.3) is obtained by simply considering the general form of a sequence of matrix multiplications. With the trigonometric relation  $\cos(\alpha) \cos(\beta) + \sin(\alpha) \sin(\beta) = \cos(\alpha - \beta)$  the function  $f$  can be simplified to

$$f(\theta_{x_l}, \theta_{x_{l+1}}) = \cos(\theta_{x_l} - \theta_{x_{l+1}}). \quad (\text{E.5})$$

Using this simplification in the product of all matrices along the fermion line and taking the trace we obtain

$$\text{Tr} \left[ \prod_{l \in \Omega}^{L-1} T(\theta_{x_l}) \right] = \prod_{l \in \Omega}^{L-2} \cos(\theta_{x_l} - \theta_{x_{l+1}}) [\cos(\theta_{x_0}) \cos(\theta_{x_{L-1}}) + \sin(\theta_{x_0}) \sin(\theta_{x_{L-1}})], \quad (\text{E.6})$$

in which again the already used trigonometric relation can be applied to get

$$\text{Tr} \left[ \prod_{l \in \Omega}^{L-1} T(\theta_{x_l}) \right] = \prod_{l \in \Omega}^{L-1} \cos(\theta_{x_l} - \theta_{x_{l+1}}), \quad \text{where } x_L = x_0. \quad (\text{E.7})$$

On sites where there is no fermion loop, no flavour changing constraints are allowed. There is either the saturation of the red flavour by the fermionic constraint, contributing with  $\phi_r^2$ , or equivalently for the green flavour, yielding  $\phi_g^2$ . In both cases the other flavour, since there is no fermion loop, must saturate the Grassmann integral by a mass monomer term with weight  $M = m + 2$ . The combined weight of both options then simplifies to

$$\phi_{r,x}^2 M + \phi_{g,x}^2 M = M [\cos^2(\theta_x) + \sin^2(\theta_x)] = M \quad \forall x \notin \{\Omega\}. \quad (\text{E.8})$$

Note that the bosonic contribution of the flavour integrated monomer site weight is simply the trace of  $T(\theta_x)$ . This is again emphasising the picture of having a matrix  $T$  on every site, even on the monomer sites, of which we can think of closed fermion lines of zero length. The partition function of the flavour integrated supersymmetric nonlinear  $O(2)$  sigma model can now be constructed, respecting also the factors of  $g$ , like

$$Z = \left( \prod_x \int_0^{2\pi} d\theta_x \right) e^{-S[\theta]} g^{-2V} \sum_{\{c\}} M^{k(c)} \prod_{\Omega_i \in \{c\}} W(\Omega_i) \prod_{l \in \Omega_i} \cos(\theta_{x_l} - \theta_{x_{l+1}}), \quad (\text{E.9})$$

where  $W(\Omega_i)$  is the contribution of the Dirac algebra structure of a closed fermion loop  $\Omega_i$  in a given configuration  $\{c\}$ , as derived in eq.(E.1), i.e.

$$W^F(\Omega_i) = -(-1)^\nu 2^{-\frac{n_c}{2}}. \quad (\text{E.10})$$

The integer  $k(c)$  is telling us how many sites in a configuration  $\{c\}$  are not part of a fermion loop, essentially counting the elements in  $\Lambda/\Omega$ . The bosonic action stays the same, we simply wrote it depending on the only degree of freedom  $\theta$ . It can also be completely rewritten in terms of trigonometric functions only depending on the difference of  $\theta$  between neighbouring sites. We now reformulated our theory and are left with the integration over  $\theta$  and the summation over all geometrically possible fermion loop configurations  $\{c\}$ . The integration over all possible flavour structures is now taken care of by the introduced

combined weights. Since there are only self-avoiding loops for  $N = 2$ , the sum over all configurations can, even now in the flavour integrated case, be simulated like a free Majorana fermion, although with a non-trivial bosonic contribution to the weights. Given a fixed  $\theta$ -field configuration any weight of a fermionic link, that can be set from point  $x$  to a neighbouring point  $y$ , is simply  $\cos(\theta_x - \theta_y)$ . If a corner is created there is an additional factor of  $1/\sqrt{2}$  that will appear due to the Dirac algebra structure. A site at which no fermion is hopping through must be occupied by a mass monomer term that comes with the weight  $M$ . Giving the constraint that only closed non-backtracking and self-avoiding loops are allowed, all rules on how to generate valid configurations are set, and all weights in  $Z$  are known. In a next step we want to investigate the space of two-point functions and discuss the actual realisation of a local update procedure as it can be used for example in a worm algorithm.

## E.2. Two-point function

The fermionic two-point function has the identical Dirac algebra structure as the two-point function of the free Majorana fermion. Since the Dirac algebra structure is known and independent of flavour, we can now discuss the bosonic contribution to the two-point functions separately.

Let  $\bar{\psi}_{i,x_0}$  be set on one end of the open string and  $\psi_{j,x_{L-1}}$  on the other, both partially saturating the Grassmann integral of a yet not assigned flavour  $i, j \in \{r, g\}$ . Due to the introduced form of  $T$  in eq.(E.2) the flavour projectors are vectors of the form

$$\bar{P}_i = (\delta_{gi} \quad \delta_{ri}) \quad \text{and} \quad P_i = \begin{pmatrix} \delta_{gi} \\ \delta_{ri} \end{pmatrix} \quad (\text{E.11})$$

Let us first consider the contribution to the two-point function of length zero, which we denote with  $C(0)_{ji}$ . This amounts to placing a  $\bar{\psi}_j$  and  $\psi_i$  onto the same site. Since only one site is considered we act on the same matrix with both of the just introduced projectors

$$\begin{aligned} C(0)_{ji} = \bar{P}_j T(\theta_x) P_i &= \delta_{gj} \delta_{gi} \cos(\theta_x)^2 + \delta_{rj} \delta_{gi} \sin(\theta_x) \cos(\theta_x) \\ &+ \delta_{gj} \delta_{ri} \cos(\theta_x) \sin(\theta_x) + \delta_{rj} \delta_{ri} \sin(\theta_x)^2. \end{aligned} \quad (\text{E.12})$$

If we set  $i = r$  and  $j = r$  we obtain  $\sin(\theta_x)^2$ , which is the bosonic contribution of the fermionic constraint  $\phi_g^2 \bar{\psi}_g \psi_g$  that needs to be picked on that site if the red flavour is already saturated. The projector  $\bar{P}_j$  acting from the left on the matrix  $T$  makes sure that on this site only constraints survive which do not include a  $\bar{\psi}_j$ . The same of course applies for  $P_i$  acting from the right, which assures that no contribution of a constraint containing  $\psi_i$  arises. In a longer fermionic open string the two projectors reduce the structure of the matrix at the two ends of the string. Let us consider some examples. For instance the correlator  $\bar{\psi}_r \psi_g$  for a fermion loop consisting of one link, i.e.  $L = 1$ , is

$$\begin{aligned} C(1)_{rr} &= \bar{P}_r T(\theta_{x_0}) T(\theta_{x_1}) P_g = \cos(\theta_{x_0}) \sin(\theta_{x_0}) \cos(\theta_{x_1}) \sin(\theta_{x_1}) + \sin(\theta_{x_0})^2 \sin(\theta_{x_1})^2 \\ &= \sin(\theta_{x_0}) \cos(\theta_{x_0} - \theta_{x_1}) \sin(\theta_{x_1}), \end{aligned} \quad (\text{E.13})$$

which represents the combined weight of the two possible solutions of flavour combinations between two neighbouring sites with  $\bar{\psi}_r$  on one and  $\psi_r$  on the other. Following the same concept, the other two-point functions with  $L = 1$  are

$$C(1)_{rg} = \sin(\theta_{x_0}) \cos(\theta_{x_0} - \theta_{x_1}) \cos(\theta_{x_1}) \quad (\text{E.14})$$

$$C(1)_{gr} = \cos(\theta_{x_0}) \cos(\theta_{x_0} - \theta_{x_1}) \sin(\theta_{x_1}) \quad (\text{E.15})$$

$$C(1)_{gg} = \cos(\theta_{x_0}) \cos(\theta_{x_0} - \theta_{x_1}) \cos(\theta_{x_1}). \quad (\text{E.16})$$

The bosonic contribution to the flavour integrated two-point function for a generic distance  $L$ , starting with flavour  $i$  and ending with  $j$ , can be written like

$$\bar{P}_j \left[ \prod_{l \in \Omega}^{L-1} T(\theta_{x_l}) \right] P_i, \quad (\text{E.17})$$

where here  $\Omega$  denotes the sites along the open fermionic string which is self avoiding and non-backtracking. Note that  $L$  is the length of the open string, i.e. the number of links along the path. In eq.(E.3), we already presented the general structure of the resulting matrix of consecutively following flavour integrated links. This formula can be applied here as well, but we have to act on both sides with the adequate projector, finding that

$$C(L)_{rr} = \sin(\theta_{x_0}) \left[ \prod_{l \in \Omega}^{L-2} \cos(\theta_{x_l} - \theta_{x_{l+1}}) \right] \sin(\theta_{x_{L-1}}) \quad (\text{E.18})$$

$$C(L)_{rg} = \sin(\theta_{x_0}) \left[ \prod_{l \in \Omega}^{L-2} \cos(\theta_{x_l} - \theta_{x_{l+1}}) \right] \cos(\theta_{x_{L-1}}) \quad (\text{E.19})$$

$$C(L)_{gr} = \cos(\theta_{x_0}) \left[ \prod_{l \in \Omega}^{L-2} \cos(\theta_{x_l} - \theta_{x_{l+1}}) \right] \sin(\theta_{x_{L-1}}) \quad (\text{E.20})$$

$$C(L)_{gg} = \cos(\theta_{x_0}) \left[ \prod_{l \in \Omega}^{L-2} \cos(\theta_{x_l} - \theta_{x_{l+1}}) \right] \cos(\theta_{x_{L-1}}), \quad (\text{E.21})$$

The product of cos functions is the resulting description of all possible ways to get from a certain site to another one. The trigonometric functions left and right of the product arise from the projectors which declare which correlator  $C(L)_{ij}$  is meant. Note that those contributions to the two-point function are obviously exactly the entries of the matrix  $\prod_{l \in \Omega}^{L-1} T(\theta_{x_l})$  in eq.(E.3). Note also that when closing a fermion loop and removing the projectors we leave the configuration space of two-point functions and enter again the configuration space of the partition function as shown in eq.(E.7).

We can now think of updating an open string of a given length  $L$ , by enlarging the length to  $L' = L + 1$  and moving one end of the open string from  $x_{L-1}$  to  $x_L$ . We can do this without caring about which flavours are at the end of the string. This can be achieved by simply enlarging the product of cos functions by another one, so the change in the weight, and therefore the Monte Carlo probability to enlarge the link, is

$$\frac{\prod_{l=0}^{L'-2} \cos(\theta_{x_l} - \theta_{x_{l+1}})}{\prod_{l=0}^{L'-3} \cos(\theta_{x_l} - \theta_{x_{l+1}})} = \cos(\theta_{x_{L-2}} - \theta_{x_{L-1}}). \quad (\text{E.22})$$

Recall that there is no exponential factor since this is the bosonic weight appearing in the measure of the integral in form of  $\delta(\phi\psi)$ . Note that we did not account for the Dirac structure here, but since it is identical to the free Majorana case it is trivial to add, the weight would simply get modified by  $m + 2$  for sites with a mass monomer term and a factor of  $1/\sqrt{2}$  for a corner in the fermion loop. After such an updating step we can perform a reweighting of the flavour combinations and obtain the desired correlator  $C_{ij}(L)$ .

An interesting reformulation of our model has been derived here which shows the interplay between boson dependent fermionic link weights and fermionic mass monomer terms. This formulation reduced the degrees of freedom by performing the sum over the two flavours already. However, there are still sources of possibly fluctuating sines because in this formulation a product of trigonometric functions appears in the partition function. Nevertheless, one might argue that when going to the continuum limit by sending the lattice spacing to zero, the  $\theta$ -field values of two neighbouring sites should differ less and less from one another. Since now the cos only depends on the difference of the fields of two neighbouring sites it seems likely that negative contributions vanish due to the predominantly smaller differences at smaller lattice spacing. Note that this statement is a possible scenario but yet remains to be numerically investigated.





# Bibliography

- [1] S. Glashow, *Partial Symmetries of Weak Interactions*, *Nucl.Phys.* **22** (1961) 579–588.
- [2] S. Weinberg, *A model of leptons*, *Phys. Rev. Lett.* **19** (Nov, 1967) 1264–1266.
- [3] A. Salam, *Elementary Particle Physics: Relativistic Groups and Analyticity*. Stockholm: Almqvist and Wiksell, 1968.
- [4] F. Jegerlehner and A. Nyffeler, *The Muon  $g-2$* , *Phys.Rept.* **477** (2009) 1–110, [[arXiv:0902.3360](#)].
- [5] V. Cirigliano and M. J. Ramsey-Musolf, *Low Energy Probes of Physics Beyond the Standard Model*, *Prog.Part.Nucl.Phys.* **71** (2013) 2–20, [[arXiv:1304.0017](#)].
- [6] E. Gildener, *Gauge-symmetry hierarchies*, *Phys. Rev. D* **14** (Sep, 1976) 1667–1672.
- [7] S. Weinberg, *Gauge Hierarchies*, *Phys.Lett.* **B82** (1979) 387.
- [8] **ATLAS Collaboration** Collaboration, G. Aad et. al., *Observation of a new particle in the search for the Standard Model Higgs boson with the ATLAS detector at the LHC*, *Phys.Lett.* **B716** (2012) 1–29, [[arXiv:1207.7214](#)].
- [9] **CMS Collaboration** Collaboration, S. Chatrchyan et. al., *Observation of a new boson at a mass of 125 GeV with the CMS experiment at the LHC*, *Phys.Lett.* **B716** (2012) 30–61, [[arXiv:1207.7235](#)].
- [10] S. Coleman and J. Mandula, *All possible symmetries of the  $s$  matrix*, *Phys. Rev.* **159** (Jul, 1967) 1251–1256.
- [11] H. Georgi and S. L. Glashow, *Unity of all elementary-particle forces*, *Phys. Rev. Lett.* **32** (Feb, 1974) 438–441.
- [12] J.-L. Gervais and B. Sakita, *Field Theory Interpretation of Supergauges in Dual Models*, *Nucl.Phys.* **B34** (1971) 632–639.
- [13] P. Ramond, *Dual theory for free fermions*, *Phys. Rev. D* **3** (May, 1971) 2415–2418.
- [14] A. Neveu and J. Schwarz, *Factorizable dual model of pions*, *Nucl.Phys.* **B31** (1971) 86–112.
- [15] L. Gof'land *JETP Letters* **13** (1971) 323.
- [16] J. Wess and B. Zumino, *A Lagrangian Model Invariant Under Supergauge Transformations*, *Phys.Lett.* **B49** (1974) 52.

- [17] A. I.J.R., *Supersymmetry in particle physics*. Cambridge University Press, New York, 2007.
- [18] L. O’Raifeartaigh, *Spontaneous Symmetry Breaking for Chiral Scalar Superfields*, *Nucl.Phys.* **B96** (1975) 331.
- [19] I. Montvay and G. Münster, *Quantum field on a lattice*. Cambridge Monographs on Mathematical Physics, 1994.
- [20] P. Dondi and H. Nicolai, *Lattice supersymmetry*, *Nuovo Cim.* **A41** (1977) 1.
- [21] K. Fujikawa, *Supersymmetry on the lattice and the Leibniz rule*, *Nucl.Phys.* **B636** (2002) 80–98, [[hep-th/0205095](#)].
- [22] F. Bruckmann and M. de Kok, *On the Noncommutativity Approach to Supersymmetry on the Lattice*, *AIP Conf.Proc.* **892** (2007) 163–165, [[hep-lat/0610120](#)].
- [23] J. Giedt, *Deconstruction and other approaches to supersymmetric lattice field theories*, *Int.J.Mod.Phys.* **A21** (2006) 3039–3094, [[hep-lat/0602007](#)].
- [24] D. Kaplan, *Supersymmetry on the lattice*, *Eur.Phys.J.ST* **152** (2007) 89–112.
- [25] A. Salam and J. A. Strathdee, *On goldstone fermions*, *Phys. Lett.* **B49** (1974) 465–467.
- [26] N. Prokof’ev and B. Svistunov, *Worm Algorithms for Classical Statistical Models*, *Phys.Rev.Lett.* **87** (2001) 160601.
- [27] U. Wenger, *Efficient simulation of relativistic fermions via vertex models*, *Phys.Rev.* **D80** (2009) 071503, [[arXiv:0812.3565](#)].
- [28] D. Baumgartner and U. Wenger, *Simulation of supersymmetric models on the lattice without a sign problem*, [arXiv:1104.0213](#).
- [29] E. Witten, *Constraints on Supersymmetry Breaking*, *Nucl.Phys.* **B202** (1982) 253.
- [30] J. Bartels and J. B. Bronzan, *Supersymmetry on a lattice*, *Phys. Rev.* **D28** (1983) 818.
- [31] J. Ranft and A. Schiller, *Hamiltonian Monte Carlo Study of (1+1)-dimensional Models With Restricted Supersymmetry on the Lattice*, *Phys.Lett.* **B138** (1984) 166.
- [32] M. Beccaria, G. F. De Angelis, M. Campostrini, and A. Feo, *Phase diagram of the lattice Wess-Zumino model from rigorous lower bounds on the energy*, *Phys.Rev.* **D70** (2004) 035011, [[hep-lat/0405016](#)].
- [33] F. Synatschke, H. Gies, and A. Wipf, *Phase Diagram and Fixed-Point Structure of two dimensional  $N=1$  Wess-Zumino Models*, *Phys.Rev.* **D80** (2009) 085007, [[arXiv:0907.4229](#)].

- [34] S. Catterall and S. Karamov, *A Lattice study of the two-dimensional Wess-Zumino model*, *Phys.Rev.* **D68** (2003) 014503, [[hep-lat/0305002](#)].
- [35] C. Wozar and A. Wipf, *Supersymmetry Breaking in Low Dimensional Models*, *Annals Phys.* **327** (2012) 774–807, [[arXiv:1107.3324](#)].
- [36] M. Golterman and D. Petcher, *A local interactive lattice model with supersymmetry*, *Nucl.Phys.* **B319** (1989) 307–341.
- [37] E. Witten, *A Supersymmetric Form of the Nonlinear Sigma Model in Two-Dimensions*, *Phys.Rev.* **D16** (1977) 2991.
- [38] P. Di Vecchia and S. Ferrara, *Classical Solutions in Two-Dimensional Supersymmetric Field Theories*, *Nucl.Phys.* **B130** (1977) 93.
- [39] O. Alvarez, *Dynamical Symmetry Breakdown in the Supersymmetric Nonlinear Sigma Model*, *Phys.Rev.* **D17** (1978) 1123.
- [40] R. Shankar and E. Witten, *s matrix of the supersymmetric nonlinear sigma model*, *Phys. Rev. D* **17** (Apr, 1978) 2134–2143.
- [41] R. Flore, D. Korner, A. Wipf, and C. Wozar, *Supersymmetric Nonlinear  $O(3)$  Sigma Model on the Lattice*, *JHEP* **1211** (2012) 159, [[arXiv:1207.6947](#)].
- [42] E. Witten, *Bound states of strings and p-branes*, *Nucl.Phys.* **B460** (1996) 335–350, [[hep-th/9510135](#)].
- [43] J. Polchinski, *Dirichlet Branes and Ramond-Ramond charges*, *Phys.Rev.Lett.* **75** (1995) 4724–4727, [[hep-th/9510017](#)].
- [44] J. M. Maldacena, *The Large  $N$  limit of superconformal field theories and supergravity*, *Adv.Theor.Math.Phys.* **2** (1998) 231–252, [[hep-th/9711200](#)].
- [45] E. Witten, *Anti-de Sitter space and holography*, *Adv.Theor.Math.Phys.* **2** (1998) 253–291, [[hep-th/9802150](#)].
- [46] D. Boss, K. Steinhauer, and U. Wenger, *Ongoing work*, to be presented at the lattice conference 2014, New York City.
- [47] U. Wolff, *Cluster simulation of relativistic fermions in two space-time dimensions*, *Nucl.Phys.* **B789** (2008) 258–276, [[arXiv:0707.2872](#)].
- [48] D. Baumgartner, *Supersymmetric Models in Low Dimensions on the Lattice*. PhD thesis, AEC for fundamental physics, University of Bern, 2012.
- [49] I. Stamatescu, *A Note on the Lattice Fermionic Determinant*, *Phys.Rev.* **D25** (1982) 1130.
- [50] C. Gattringer, *Loop representation for 2-D Wilson lattice fermions in a scalar background field*, *Nucl.Phys.* **B543** (1999) 533–542, [[hep-lat/9811014](#)].

- [51] C. Gattringer, V. Hermann, and M. Limmer, *Fermion loop simulation of the lattice Gross-Neveu model*, *Phys.Rev.* **D76** (2007) 014503, [[arXiv:0704.2277](#)].
- [52] W. Loinaz and R. Willey, *Monte Carlo simulation calculation of critical coupling constant for continuum  $\phi^4$  in two-dimensions*, *Phys.Rev.* **D58** (1998) 076003, [[hep-lat/9712008](#)].
- [53] T. Korzec, I. Vierhaus, and U. Wolff, *Performance of a worm algorithm in  $\phi^4$  theory at finite quartic coupling*, *Comput.Phys.Commun.* **182** (2011) 1477–1480, [[arXiv:1101.3452](#)].
- [54] I. Vierhaus, *Simulation of  $\phi^4$  theory in the strong coupling expansion beyond the ising limit*, *Diploma thesis, Humboldt University* (2010).
- [55] P. Leimer, *Simulating the hopping expansion of the 2-dimensional  $\phi^4$  theory*, *Master Thesis* (2014).
- [56] K. G. Wilson, *Quarks and Strings on a Lattice*, .
- [57] S. Ferrara, *Supersymmetric Gauge Theories in Two-Dimensions*, *Lett.Nuovo Cim.* **13** (1975) 629.
- [58] M. Beccaria, M. Campostrini, and A. Feo, *Supersymmetry breaking in two-dimensions: The Lattice  $N = 1$  Wess-Zumino model*, *Phys.Rev.* **D69** (2004) 095010, [[hep-lat/0402007](#)].
- [59] D. Baumgartner and U. Wenger, *Exact results for supersymmetric quantum mechanics on the lattice*, *PoS LATTICE2011* (2011) 239, [[arXiv:1201.1485](#)].
- [60] D. B. Kaplan, *A Method for simulating chiral fermions on the lattice*, *Phys.Lett.* **B288** (1992) 342–347, [[hep-lat/9206013](#)].
- [61] Y. Shamir, *Chiral fermions from lattice boundaries*, *Nucl.Phys.* **B406** (1993) 90–106, [[hep-lat/9303005](#)].
- [62] S.-J. Chang, *Existence of a second-order phase transition in a two-dimensional  $\phi^4$  to the fourth field theory*, *Phys. Rev. D* **16** (Sep, 1977) 1979–1979.
- [63] T. Reisz, *A Power Counting Theorem for Feynman Integrals on the Lattice*, *Commun.Math.Phys.* **116** (1988) 81.
- [64] J. Bartels and G. Kramer, *A Lattice Version of the Wess-Zumino Model*, *Z.Phys.* **C20** (1983) 159.
- [65] K. Binder, *Finite size scaling analysis of Ising model block distribution functions*, *Z.Phys.* **B43** (1981) 119–140.
- [66] R. H. Swendsen and J.-S. Wang, *Nonuniversal critical dynamics in Monte Carlo simulations*, *Phys.Rev.Lett.* **58** (1987) 86–88.

- [67] F. D. M. Haldane, *Nonlinear field theory of large-spin heisenberg antiferromagnets: Semiclassically quantized solitons of the one-dimensional easy-axis néel state*, *Phys. Rev. Lett.* **50** (Apr, 1983) 1153–1156.
- [68] R. Botet, R. Jullien, and M. Kolb, *Finite-size-scaling study of the spin-1 heisenberg-ising chain with uniaxial anisotropy*, *Phys. Rev. B* **28** (Oct, 1983) 3914–3921.
- [69] G. de Divitiis, R. Frezzotti, M. Guagnelli, and R. Petronzio, *Non-perturbative determination of the running coupling constant in quenched  $\{SU\}$  (2)*, *Nuclear Physics B* **433** (1995), no. 2 390 – 400.
- [70] J. Balog and A. Hegedus, *The finite size spectrum of the 2-dimensional  $O(3)$  nonlinear sigma-model*, *Nucl.Phys.* **B829** (2010) 425–446, [[arXiv:0907.1759](#)].
- [71] D. Banerjee and S. Chandrasekharan, *Finite size effects in the presence of a chemical potential: A study in the classical non-linear  $O(2)$  sigma-model*, *Phys.Rev.* **D81** (2010) 125007, [[arXiv:1001.3648](#)].
- [72] W. Bietenholz, M. Bögli, U. Gerber, F. Niedermayer, M. Pepe, et. al.,  *$O(N)$  Models with Topological Lattice Actions*, [arXiv:1309.6278](#).
- [73] U. Wolff, *Simulating the All-Order Strong Coupling Expansion III:  $O(N)$  sigma/loop models*, *Nucl.Phys.* **B824** (2010) 254–272, [[arXiv:0908.0284](#)].
- [74] J. M. Evans and T. J. Hollowood, *The Exact mass gap of the supersymmetric  $o(N)$  sigma model*, *Phys.Lett.* **B343** (1995) 189–197, [[hep-th/9409141](#)].
- [75] S. Catterall and S. Ghadab, *Twisted supersymmetric sigma model on the lattice*, *JHEP* **0610** (2006) 063, [[hep-lat/0607010](#)].
- [76] B. Zumino, *Supersymmetry and Kähler Manifolds*, *Phys.Lett.* **B87** (1979) 203.
- [77] O. Bar, W. Rath, and U. Wolff, *Anomalous discrete chiral symmetry in the Gross-Neveu model and loop gas simulations*, *Nucl.Phys.* **B822** (2009) 408–423, [[arXiv:0905.4417](#)].
- [78] J. M. Kosterlitz and D. J. Thouless, *Ordering, metastability and phase transitions in two-dimensional systems*, *J. Phys* **C6** (1973) 1181.
- [79] N. Kawahara, J. Nishimura, and S. Takeuchi, *Phase structure of matrix quantum mechanics at finite temperature*, *JHEP* **0710** (2007) 097, [[arXiv:0706.3517](#)].
- [80] M. Hanada, J. Nishimura, and S. Takeuchi, *Non-lattice simulation for supersymmetric gauge theories in one dimension*, *Phys.Rev.Lett.* **99** (2007) 161602, [[arXiv:0706.1647](#)].
- [81] M. Hanada, J. Nishimura, Y. Sekino, and T. Yoneya, *Direct test of the gauge-gravity correspondence for Matrix theory correlation functions*, *JHEP* **1112** (2011) 020, [[arXiv:1108.5153](#)].

- [82] M. Honda, G. Ishiki, S.-W. Kim, J. Nishimura, and A. Tsuchiya, *Direct test of the AdS/CFT correspondence by Monte Carlo studies of  $N=4$  super Yang-Mills theory*, *JHEP* **1311** (2013) 200, [[arXiv:1308.3525](#)].
- [83] S. Catterall and T. Wiseman, *Black hole thermodynamics from simulations of lattice Yang-Mills theory*, *Phys.Rev.* **D78** (2008) 041502, [[arXiv:0803.4273](#)].
- [84] S. Catterall and T. Wiseman, *Extracting black hole physics from the lattice*, *JHEP* **1004** (2010) 077, [[arXiv:0909.4947](#)].
- [85] T. Banks, W. Fischler, S. Shenker, and L. Susskind, *M theory as a matrix model: A Conjecture*, *Phys.Rev.* **D55** (1997) 5112–5128, [[hep-th/9610043](#)].
- [86] R. Dijkgraaf, E. P. Verlinde, and H. L. Verlinde, *Matrix string theory*, *Nucl.Phys.* **B500** (1997) 43–61, [[hep-th/9703030](#)].
- [87] N. Ishibashi, H. Kawai, Y. Kitazawa, and A. Tsuchiya, *A Large  $N$  reduced model as superstring*, *Nucl.Phys.* **B498** (1997) 467–491, [[hep-th/9612115](#)].
- [88] S. Catterall and T. Wiseman, *Towards lattice simulation of the gauge theory duals to black holes and hot strings*, *JHEP* **0712** (2007) 104, [[arXiv:0706.3518](#)].
- [89] P. Austing, *Yang-Mills matrix theory*, [hep-th/0108128](#).
- [90] A. Van Proeyen, *Tools for supersymmetry*, [hep-th/9910030](#).
- [91] T. Harmark and N. A. Obers, *New phases of near-extremal branes on a circle*, *JHEP* **0409** (2004) 022, [[hep-th/0407094](#)].
- [92] J. E. Gentle, *Computational statistics*. Springer, 2009.
- [93] U. Wenger, *Unpublished work*, .
- [94] C. Michael and A. McKerrell, *Fitting correlated hadron mass spectrum data*, *Phys.Rev.* **D51** (1995) 3745–3750, [[hep-lat/9412087](#)].
- [95] C. Michael, *Fitting correlated data*, *Phys. Rev. D* **49** (Mar, 1994) 2616–2619.

## **Erklärung**

gemäss Art. 28 Abs. 2 RSL 05

Name/Vorname: .....

Matrikelnummer: .....

Studiengang: .....

Bachelor ☐      Master ☐      Dissertation ☐

Titel der Arbeit: .....

.....

.....

LeiterIn der Arbeit: .....

.....

Ich erkläre hiermit, dass ich diese Arbeit selbständig verfasst und keine anderen als die angegebenen Quellen benutzt habe. Alle Stellen, die wörtlich oder sinngemäss aus Quellen entnommen wurden, habe ich als solche gekennzeichnet. Mir ist bekannt, dass andernfalls der Senat gemäss Artikel 36 Absatz 1 Buchstabe r des Gesetzes vom 5. September 1996 über die Universität zum Entzug des auf Grund dieser Arbeit verliehenen Titels berechtigt ist.

.....

Ort/Datum

.....

Unterschrift

# Kyle Steinhauer

## Curriculum Vitae

Kranichweg 20  
3074 Muri, Switzerland

☎ +41 79 748 96 35

☎ +41 31 352 94 73

✉ steinhauer@itp.unibe.ch

Swiss & British citizen

Place of origin: Riggisberg, BE

### Education

2010–2014 **Ph.D. in Theoretical Physics**, *University of Bern*.

2008–2010 **Master of Science in Theoretical Physics**, *University of Bern*.

2005–2008 **Bachelor of Science in Physics**, *University of Bern*.

### Theses

---

#### PhD-Thesis

Title *Loop Formulation in Low Dimensional Supersymmetric Models on the Lattice*

Supervisor Prof. Dr. Urs Wenger

---

#### Master-thesis

Title *Chrystal-phase in the 3D Gross-Neveu-model*

Supervisor Prof. Dr. Urs Wenger

---

#### Bachelor-thesis

Title *Universality of the critical index in the 2D Ising model*

Supervisor Prof. Dr. Peter Hasenfratz

---



